

DOCTORAL THESIS

Development of Solid
Lubricated Composites for
High-Temperature
Tribological Applications

Rahul Kumar

TALLINN UNIVERSITY OF TECHNOLOGY
DOCTORAL THESIS
75/2022

Development of Solid Lubricated Composites for High-Temperature Tribological Applications

RAHUL KUMAR



TALLINN UNIVERSITY OF TECHNOLOGY

School of Engineering

Department of Mechanical and Industrial Engineering

This dissertation was accepted for the defence of the degree 22/11/2022

Supervisor:

PhD Maksim Antonov
School of Engineering
Tallinn University of Technology
Tallinn, Estonia

Co-supervisor:

Prof. Irina Hussainova
School of Engineering
Tallinn University of Technology
Tallinn, Estonia

Opponents:

Prof. Ashish Ganvir
Department of Materials and Mechanical Engineering
University of Turku
Turku, Finland

PhD Arkadi Zikin
Head of Laser Center of Competence
Oerlikon Metco
Wohlen, Switzerland

Defence of the thesis: 22/12/2022, Tallinn

Declaration:

Hereby I declare that this doctoral thesis, my original investigation and achievement, submitted for the doctoral degree at Tallinn University of Technology has not been submitted for doctoral or equivalent academic degree.

Rahul Kumar

signature



European Union
European Regional
Development Fund



Investing
in your future

Copyright: Rahul Kumar, 2022

ISSN 2585-6898 (publication)

ISBN 978-9949-83-935-3 (publication)

ISSN 2585-6901 (PDF)

ISBN 978-9949-83-936-0 (PDF)

Printed by Koopia Niini & Rauam

TALLINNA TEHNIKAÜLIKOOL
DOKTORITÖÖ
75/2022

**Tahkmäärdega komposiitide
väljatöötamine kõrgtemperatuurseteks
triborakendusteks**

RAHUL KUMAR



Contents

List of publications	6
Author's contribution to the publications	7
Introduction	8
List of abbreviations and symbols	9
1 Review of literature.....	10
1.1 High temperature tribology	10
1.2 High-temperature solid lubricants.....	11
1.2.1 Soft metals	12
1.2.2 Laminar solids	13
1.2.3 Alkaline-earth fluorides.....	14
1.2.4 Lubricious oxides and Magneli phases.....	15
1.2.5 MAX phase and MXenes	15
1.2.6 Fabrication of solid-lubricating composites or composite-coatings	15
1.3 Research gaps	17
1.4 Objectives of the study	17
2 Materials and methods	19
2.1 Powder precursors.....	19
2.2 Mechanical mixing	20
2.3 Combustion synthesis (SHS) of Ni-W (-hBN).....	20
2.4 Spark plasma sintering (SPS).....	21
2.5 Laser surface melting and laser cladding	21
2.6 Characterization.....	22
2.7 Tribological tests.....	23
3 Results and discussion.....	26
3.1 System 1, Ti-TiB ₂ SPS-ed composite	26
3.2 System 2, Ni-Bi/ Ti-TiB ₂ laser modified composite.....	31
3.3 System 3, NiCrBSi/Metal sulfide laser claddings	37
3.4 System 4, Ni-40 wt.% W (-hBN) SPS-ed composite.....	44
4 Conclusions	48
5 Future work.....	50
References	51
Acknowledgements.....	55
Abstract.....	57
Lühikokkuvõte.....	59
List of publications not included in the thesis.....	61
Appendix	63
Curriculum vitae	134
Elulookirjeldus.....	136

List of publications

The list of author's publications, the thesis is based on:

- I **Kumar, R.**, Antonov, M., Liu, L., & Hussainova, I. (2021). Sliding wear performance of in-situ spark plasma sintered Ti-TiB_w composite at temperatures up to 900 °C. *Wear*, 476, 203663.
- II **Kumar, R.**, Torres, H., Aydinyan, S., Antonov, M., Varga, M., Rodriguez Ripoll, M., Hussainova, I. (2022). Microstructural and high temperature tribological behaviour of self-lubricating Ti-TiB_x composite doped with Ni-Bi. *Surface and Coatings Technology*, 128827.
- III **Kumar, R.**, Aydinyan, S., Ivanov, R., Liu, L., Antonov, M., & Hussainova, I. (2022). High-Temperature Wear Performance of hBN-Added Ni-W Composites Produced from Combustion-Synthesized Powders. *Materials*, 15(3), 1252.
- IV **Kumar, R.**, Hussainova, I., Rahmani, R., & Antonov, M. (2022). Solid Lubrication at High-Temperatures—A Review. *Materials*, 15(5), 1695.

Author's contribution to the publications

Contribution to the papers in this thesis are:

- I First author, Methodology, Design of experiments, Precursor preparation, Performing experiments, Formal analysis, Data curation, Writing original manuscript.
- II First and corresponding author, Conceptualisation, Methodology, Design of experiments, Precursor preparation, Performing experiments, Formal analysis, Data curation, Writing original manuscript, Review and editing.
- III First author, Design of experiments, Precursor preparation, Formal analysis, Data curation, Writing original manuscript.
- IV First and corresponding author, Conceptualisation, Methodology, Formal analysis, Data curation, Writing original manuscript, Review and editing.

Introduction

Significant energy losses are occurred to overcome friction. For example, it accounts for one-third of the fuel's energy in passenger cars and 40% of the energy in mineral mining (Holmberg, 2017). In engineering and technology, damage caused by wear is a common attribute in machinery (structures) and elements in relative motion sometimes resulting in a catastrophic failure, including process downtime, loss of mechanical performance, significant material wastage, and additional energy consumption. Such wear-led material damages are severely enhanced at high temperatures (HT) due to the complex transformation of physical, mechanical, and surface properties resulting in reduced material hardness and strength and thus, posing a substantial uncertainty in materials' reliability and performance (Pauschitz, 2008).

Minimizing friction and wear at HT by the use of liquid-based lubricants is a conventional practice. However, their volatilization or degradation at temperatures above 300 °C as well as the detrimental effects on the operator and environment limit their use in HT tribo-applications. In such scenarios, the use of solid lubricants (such as Ag, MoS₂, WS₂, etc.) to minimize friction and wear over a wide range of temperatures (up to 1000 °C) is seen as a promising solution. Besides, solid-based lubricants (SL) take over conventional-liquid ones to provide a clean working space, easy handling, and improved accuracy and precision. Nevertheless, frequently reported limitations of SLs includes their agglomeration (for soft metals- Ag, Bi) in the reinforced matrix (resulting in a compromised mechanical and lubrication property), the toxicity of lead (Pb) and a stricter rule to minimise its usage, and a poor flowability of widely used transition metal dichalcogenide WS₂ and MoS₂ (posing a problem to enlarge the production technology utilizing powder feeding system).

This Ph.D. work is a contribution to the exponentially advancing demands of high-temperature tribological materials to minimize friction and wear by using solid lubricant additives. The thesis is based on 4 publications and some additional unpublished work. The first publication [Publication I] reports on solving the extremely poor HT (up to 900 °C) mechanical and tribological characteristics of titanium through incorporation of high content of ceramic TiB₂. The second publication [Publication II] for the first time reports bismuth as an HT 'green' solid lubricant (up to 600 °C). Besides, novel synergetic use of Bi along with Ni is shown to overcome its reported agglomeration. Laser assisted incorporation of Ni-Bi as a solid lubricant was made into Ti-TiB₂ composite with the idea to enlarge the effective lubrication temperature and wear resistance. Publication three [Publication III], extends to microstructural and HT tribological (800 °C) study of hexagonal-boron nitride (hBN) reinforced Ni-W composites prepared using combustion synthesized powders. The fourth publication [Publication IV], reviews the state-of-art field of HT solid lubrication and details the wear reduction mechanisms behind existing and most used solid lubricants. The additional research work (Publication not included in the thesis V) reports the development of a HT self-lubricating NiCrBSi based laser claddings through incorporation of metal sulfides other than MoS₂ (due to its sticky nature, limitation for large scale production requiring powder feeding system). Besides, this study also extends to Bi₂S₃ as a newly reported solid-lubricant.

In the current works, the novel solid lubricated composites are designed, developed, and tested to ensure their HT tribological needs. The ways to extend the range of operating temperature of the wear-resistant composites are explored; revealing the wear reduction mechanisms of HT solid lubricants thereof.

List of abbreviations and symbols

AC2T	Austrian Center of Competence for Tribology
BE	Backscattered Electron
CALPHAD	CALculation of PHase Diagrams
CoF	Coefficient of Friction
CL	Conventional Lubricant (Liquid based)
CS	Combustion Synthesis
EDS	Energy Dispersive X-ray Spectroscopy
EP	Extreme Pressure
HAZ	Heat Affected Zone
hBN	Hexagonal Boron Nitride
HEBM	High Energy Ball Milling
HT	High Temperature
IFT	Indentation Fracture Toughness
LMD	Laser Metal Deposition
LM	Laser Melting/Melted
MML	Mechanically Mixed Layer
MS	Metal Sulfide
REF	Reference Sample
RT	Room Temperature
SEM	Scanning Electron Microscopy
SHS	Self-Propagating High-temperature Synthesis
SL	Solid Lubricant (Solid lubricating)
SPS	Spark Plasma Sintering
SS	Stainless Steel
TMD	Transition Metal Dichalcogenide
XRD	X-ray Diffraction
vol.%	Volumetric percentage
wt.%	Weight percentage
μm	Micrometer
mm	Millimeter
Ra	Average Surface Roughness
λ	Wavelength
∅	Diameter
ρ	Density

1 Review of literature

1.1 High temperature tribology

Wear (in tribology) can be stated as the removal or a displacement of material from one or both the surfaces in relative motion. The undesirable phenomenon of wear usually results in material damage and sometimes leading to a catastrophic failure. The major responsible mechanisms of wear are classified in several variants, of which few are frequently used in the current study namely: adhesive, abrasive, fatigue, or chemical (oxidation). Adhesive wear originates from the bonding of asperities between two mating (sliding) surfaces resulting in material transfer or detachment from either or both the surfaces. Abrasive wear occurs when asperities from a harder surface plough, cut (remove), or damage the softer counterpart (two-body abrasion). It is possible that during abrasion, a third body generates between the sliding-counterparts and intensifies wear, called as three-body abrasion. Fatigue wear generates as a result of repeated tribological stress cycles which further results in surface or sub-surface cracks, and even material detachment or removal. Chemical wear (corrosion or oxidation) usually accounts a chemical reaction (interaction) between mating or sliding counterparts or with environment resulting in material removal.

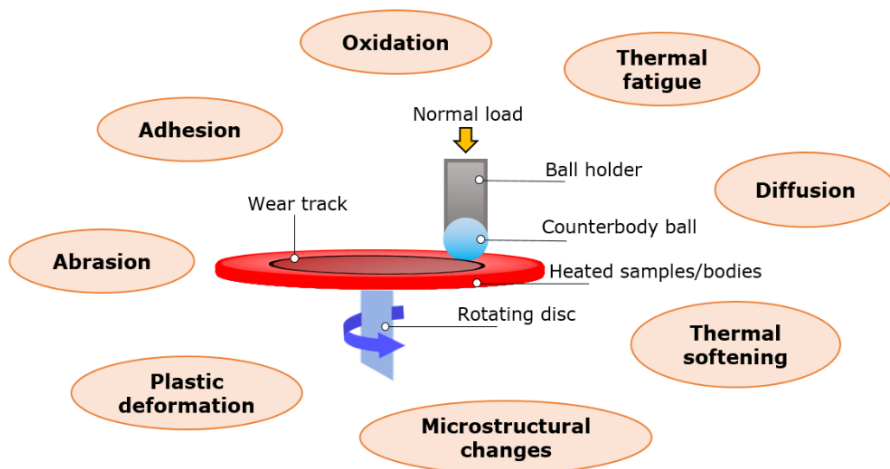


Figure 1: A scheme demonstrating the complexity of a sliding contact at elevated temperature.

With a significant number of operations carried out at high temperatures (>300°C) including metal processing (HT-forming, forging, stamping, etc), metal cutting, internal combustion engines, bearings, etc., there arises a need to fill the demand for high-temperature wear-resistant materials. Friction and wear at HT impose a serious concern. Nowadays the availability of test rigs capable of testing materials up to 1000 °C has aided in broadening the tribological understanding of materials at HT. In many cases, a significant difference in material behavior at ambient temperature in comparison to HT is seen (Antonov, 2012). At HT, the material response depends on a synergy of complex phenomena, which may include oxidation, adhesion, creep, fatigue, and tribological stress. Not to forget, that the principal characteristic of HT would include softening (possible strength, and hardness reduction; increase in ductility, etc) in an array of

metallic, ceramic and other materials. For example, most steels and ferrous alloys demonstrate a softening at $\geq 500^{\circ}\text{C}$. Figure 1 shows a general scheme illustrating the complexity of a sliding contact (acting wear mechanisms) at elevated temperature.

Concerning oxidation, unlike ambient conditions, operation at HT usually involves a fast developing tribolayer or mechanically mixed layers (consisting of debris material from tribo-bodies) which are rich in oxygen levels (due to oxidation) and at times cover the wear scar entirely (Antonov, 2012). During progressive sliding, these layers are compacted, retained, and adherent on the surface of the substrate material. This, in turn, protects the direct contact between original materials and is often reported to reduce wear by the orders of magnitude (Rynio, 2014). The developed layers can feature a smooth, glassy surface and are generally termed 'glaze-layers' (Pauschitz, 2008; Rynio, 2014). However, the extent of oxidation increases over time or at even higher temperatures, and the tribo-oxide layer develops thicker. Upon reaching a critical thickness, the layer may undergo spalling and loses its load-bearing nature (protective). Further, the spalled-off debris may remain on the wear zone and act as a third body rising friction and wear (Kumar, 2020). In another case of the composite where the material is a combination of several distinct phases, the tribolayer might feature a transition temperature to demonstrate its wear protective nature, beyond which due to its thin, brittle, or loosely adhered nature, remain unprotective or aid in wear increment (hard oxides can cause three body abrasion effect) (Lou, 2021; Munagala, 2021).

As for hot -forming, forging, rolling, or hot-working applications, the materials are shaped by plastic deformation at temperatures above recrystallization (usually around 0.4–0.6 times materials' melting point to increase its ductility and hence improve its formability (Prasad, 2015)) and involves an optimum degree of friction between the tool and the workpiece which might result in a change of dimensional tolerance of the tool and results in poor produced parts during successive operations. Moreover, the oxidation rates involved during these operations might differ from the general case where constant contact between the tribo-body is maintained. Here the contact between tool and workpiece is intermittent. Hence, it is necessary to reduce or optimize the functional friction during these operations utilizing a suitable lubrication mechanism. In this regards, solid lubricants are a solution.

1.2 High-temperature solid lubricants

Solids imparting reduced friction due to their low shear strength are known as solid lubricants (SL). Depending on their application and fabrication method, SLs are usually incorporated as (1) loose powders, embedded into material matrix as additives to form (2) composites, or (3) coating films between tribo-surface to reduce friction and wear. Besides, they also promote in reduction of surface energy on the sliding surface. Low sliding surface energy is reported to lower the wear-causing-mechanisms such as cutting, ploughing, adhesion, and plastic deformation (Bowden, 2001). Several benefits of SL over conventional-liquid-based (CL) include higher chemical, thermal and dimensional stability, a clean and healthier environment, and energy saving.

A comprehensive studies carried out by Kumar (Publication IV), Sliney (Sliney, 1982), Erdemir (Donnet, 2004), Torres (Torres, 2017) et al. present a detailed outlook on most known SLs, focusing on their HT behavior and a future outlook. Few others (Ayyagari, 2020; Efeoglu, 2008; Marian, 2020) illuminate the effect of humidity, and atmospheric gas on the tribology of SLs. Nevertheless, no individual SL is capable to demonstrate desired behavior under all the environmental conditions, different tribological needs,

operating from room temperature to $\sim 1000\text{ }^{\circ}\text{C}$, or compatible with most of the material matrices. Besides, the in-situ formation of solid-lubricating compounds (such as CrS, and boric acid) during fabrication (involving heat) or a tribo-chemical reaction is also a possibility and reported by a few (Torres, 2022). However, due to their unexpected formation, they are not purposely studied. Hence, the field of SL or self-lubricating materials (materials with embedded SL) is ever-growing. Figure 2 categorizes the widely accepted SLs based on their structure.

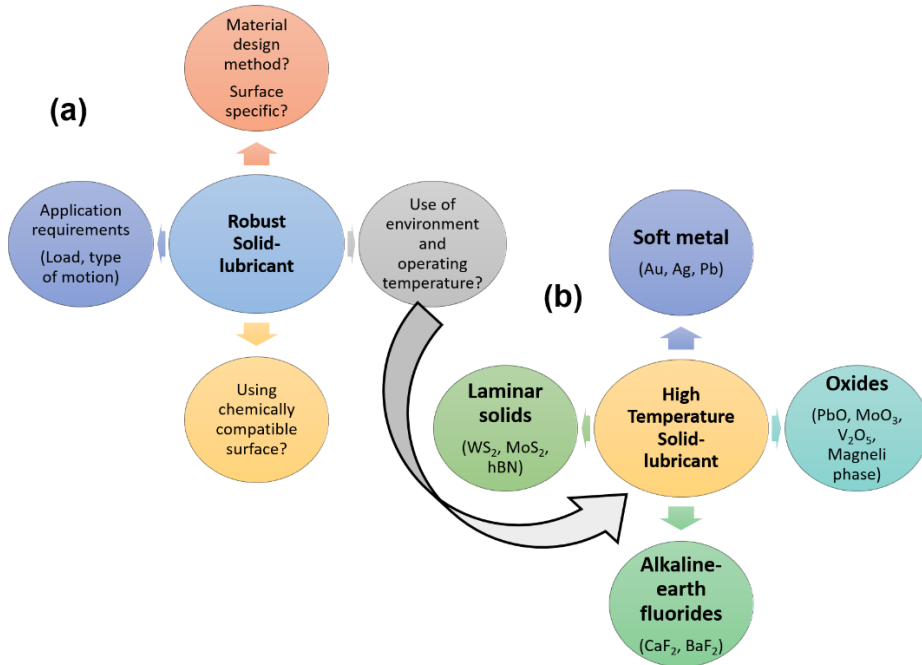


Figure 2: (a) General questionnaire for a solid-lubricant; and (b) Classification of HT solid-lubricants based on their chemical composition.

1.2.1 Soft metals

Soft metal family encompasses a range of metals with low melting point (in comparison to refractory metals) and hardness as low as 2.5–4 Mohs ($\sim 70\text{--}200\text{ HV}$) such as, silver, gold, bismuth, copper, lead, indium etc. The main mechanism behind their friction reduction is their impressive ductility and deformability under a low shearing force. Upon applied force during sliding, they usually show smearing or plastic deformation permitting a low CoF and wear rate. During HT operation (or frictional heating), soft metals are likely to spread (diffuse or squeeze out) easily to the sliding surface and act as a lubricating film between tribo-bodies mating as shown in Figure 3. Besides, heating tends to prohibits the defect potential and dislocation movement of soft metals resulting in their maintained low shear-ability even at HT operations (Torres, 2017). However, at certain range of HT, they undergo significant softening and might result in tribo-film (lubricious) extrusion or failure (Publication IV). Among all the soft metals, transition metals such as, silver (Ag) and copper (Cu) are widely used as HT SLs due to their cost effectiveness, ease of availability, environment friendly nature and an excellent thermal conductivity (Balachander, 2013).

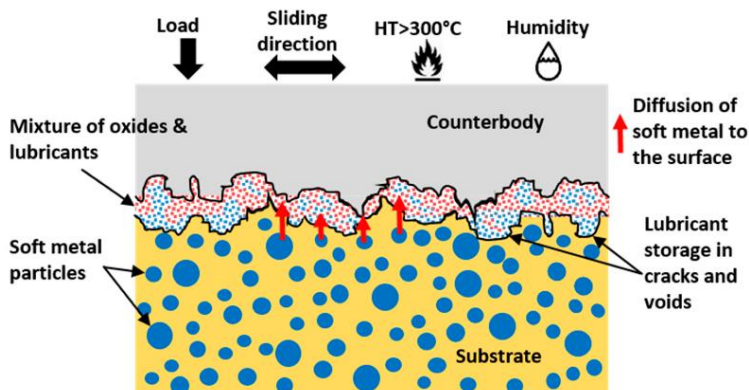


Figure 3: A scheme demonstrating soft metal diffusion to the tribo-surface during HT sliding (adapted from Publication IV).

Bismuth (Bi) is a member of soft metal and share a similar physical property as lead (Pb) or Indium (In). However, unlike lead (and all the heavy metals), bismuth benefits from its 'green and ecologically clean' nature and is alleged to possibly substitute Pb in lubrication industry (tribology). The maximum toxic intake level of bismuth lies around 15 g for a 70 kg human whereas, a high toxicity of lead was conveyed to be of 1 mg for a 70 kg human (Yang, 2011).

Very little is known on Bi as a SL material. Recently, a few tribological studies on Bi and its oxides has surfaced (Gonzalez-Rodriguez, 2016; Sun, 2021). However, most of them were carried out at RT condition. Due to its low melting point (270 °C), Bi is believed to easily spread between asperity contacts during tribo-condition (due to frictional heating) resulting in effective lubricated sliding. HT friction reducing role of Bi_2O_3 on Ni-Al composite coating was reported by (Sun, 2021). Contrariwise, in (Gonzalez-Rodriguez, 2016) an increase in CoF value of due to the formation of Bi_2O_3 beyond 200 °C sliding was reported.

One major limitation of bismuth (like silver, Ag) lies in its agglomeration or segregation in the matrix after sintering/coating process and further resulting in a poor mechanical property of the material (Liu, 2022b). Thus, there is a need to understand Bi lubrication at HT along with its possible ways of homogeneous distribution in the matrix material. Besides, a study towards the synergetic role of a 'non-toxic' bismuth-sulphur additive to replace lead-sulphur additives for extreme pressure (EP i.e. high load and high local temperatures) lubricants can be a useful approach (Rohr, 2002). Not to forget, the possibility of bismuth as a lubricant can open a new door (and replace Pb) for combination to copper and tin alloys which are greatly used in bearings and electrical components.

1.2.2 Lamellar solids

Lamellar solids, also known as layered lattice compounds, demonstrate a hexagonal layered structure with atoms in the layers/planes covalent bonded to each other as shown in Figure 4. The adjacent layers or basal planes are bonded by weak van der Waals forces; characterizing an easy shear along the planes (Akhtar, 2021). Therefore, this class of materials can result in outstanding anti-friction property. The commonly identified materials of this group comprise graphite (and graphene), hexagonal boron nitride (hBN),

TMDs, and particularly MoS₂ and WS₂ (Publication IV). Nevertheless, the use of MoS₂, WS₂, and graphite (also graphene) is limited until 450–500 °C due to their oxidation or degradation.

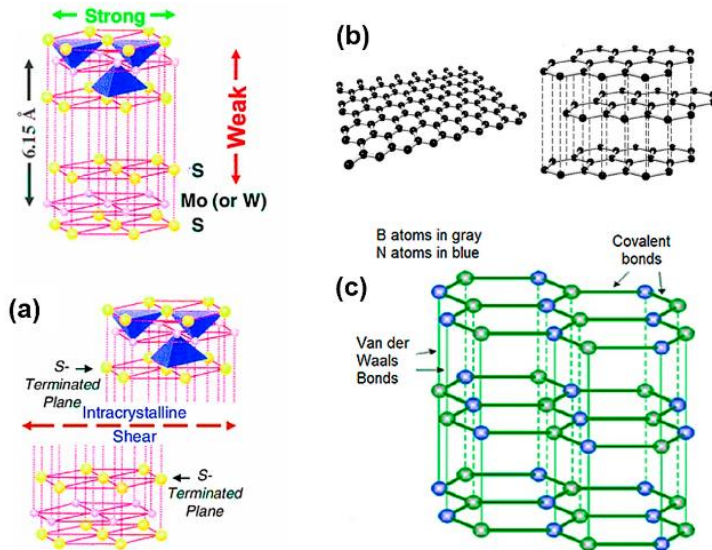


Figure 4: A scheme demonstrating crystal structure featuring an easy slip phenomenon between weakly held inter-lamellar layers/planers of (a) MoS₂ and WS₂; (b) layered graphene layers; and (c) hexagonal boron nitride (h-BN) (Akhtar, 2021).

An alternative to MoS₂, graphite and graphene is hexagonal boron nitride (hBN). Layered structured hBN is believed to effectively work at temperatures far beyond graphene and does not oxidize up to 1000 °C (Torres, 2022). A major limitation of hBN includes a poor sinterability, adhesiveness, and non-wettability resulting in low mechanical properties of the composites or coatings. Nevertheless, owing to its high thermal conductivity (~500 W/mK at RT), chemical and oxidation resistance is prospectively researched for HT tribological applications (Podgornik, 2015). In (Zhang, 2008), friction-reducing benefit of hBN/Ni-coating on stainless steel was reported up to 800 °C. Upon 600 °C sliding, the wear rate of the coating rises due to the fall in the strength of the coating at overly high-temperature (Zhang, 2008). Contrariwise, a drop in friction and wear properties with a rise in sliding temperature of NiCr/hBN composite was reported by Zhu et al. (Zhu, 2019). Besides, a satisfactory tribo-behavior was noticed with 10 wt% hBN content (S. Zhang, 2008; Zhu, 2019). Chen et al. (Chen, 2020) studied hBN/SiC composites from room temperature to 900 °C and reported friction-reducing but wear-deteriorating effects of hBN in the composite. Besides, few studies report negative effect of hBN on lubrication (Du, 2011; Torres, 2022; Zhu, 2019). Therefore, there is a need to verify hBN as HT SL through more studies.

1.2.3 Alkaline-earth fluorides

Fluorides of alkaline earth metals such as, CaF₂, LiF, and BaF₂ are recognized to impart lubrication in between 500–900 °C due to a reduced shear strength (Slinney, 2008). However, at low to moderate temperatures, they tend to behave like abrasive due to their brittle nature, and may escalate wear behaving as a third body on tribo-surface

(Kurzawa, 2020). It is reported that alkaline-earth fluorides undergo brittle to ductile transition around 500 °C resulting in their beneficial softening to offer lubricity (Lince, 2020). In general, CaF₂ is believed to be a SL at temperature lower in comparison to other fluorides counterpart and sometimes, used as in synergy (Slincy, 1982). Few studies describe the synergetic behavior of alkaline fluorides and Ag/Mo to enlarge the range of lubrication temperature (Cura, 2013; Kong, 2014).

1.2.4 Lubricious oxides and Magnéli phases

Lubricious oxides are compounds that demonstrate HT lubrication either by quick melting or a relatively lower shear strength in specific crystal orientations due to oxygen vacancies; also called a crystallographic shear planes (Wadsley, 2015). The latter has the propensity to offer low friction owing to their lattice structure and are termed Magnéli phase oxides (Cura, 2021). Besides, these oxides carry good chemical stability resulting in minimum tribo-oxidation and counterbody adhesion (Gassner, 2006). For more information about Magnéli phase oxides please refer to Publication IV.

1.2.5 MAX phase and MXenes

The MAX phase is the name of materials with a M_{n+1}AX_n chemistry, where M is a transition metal; A is a metal from group IIIA or IVA in the periodic table and X is C and/or N and n is mostly in the range of 1–3 (Zhen, 2005). Their feature to resist damage, oxidation, and corrosion, being thermal and electrically conductive, good machinability, and ductile nature (Vickers hardness of 2–8 GPa) has raised their interest as tribological material (Gupta, 2011; Zhen, 2005). Besides, MAX phases are reported to demonstrate a ductile to brittle transition at temperatures >1000 °C resulting in an efficient mechanical properties even above 1000 °C (Radovic, 2002; Zhen, 2005). Decomposition of MAX is reported to occur at temperatures between 1000–2000 °C (Gupta, 2011). Few of them particularly Ti₃SiC₂ and Ti₂AlC, are reported to form a protective tribo-oxide layer favoring wear reduction at HT (Li, 2003; Lin, 2007). The mechanism behind MAX phase friction reduction is linked to its layered structure resulting in a specific deformation mechanism via kink formation and thus, easy sliding (Emmerlich, 2008; Souchet, 2005). MXenes are a group of 2D inorganic compounds synthesized by chemical etching of the A element in MAX phases (Mohammadi, 2021). MXenes encompass a family of 2D transition metal carbides, carbonitrides, and nitrides that contain an odd number of layers in which metals (M) sandwich carbon or nitrogen (X) layers (such as Ti₂C, Ta₄C, Ti₃C₂) (Benchakar, 2020). It can be reported that only about 5% of studies is focused on mechanical and tribological needs of MXenes with almost no results obtained at HT. However, the trend seems to increase quickly in the coming years (Wyatt, 2021).

1.2.6 Fabrication of solid-lubricating composites or composite-coatings

Fabrication of SL composites/coatings through powder metallurgy way has already been understood and widely accepted (Kumar, 2020). Sintering is a method to transform powder precursors, or a green body (powder mixture held together by a low cohesive force), into a thermodynamically stable state due to a reduction in free surface energy of the existing pores or vacancies (Mamedov, 2013). Generally, during sintering, the loosely held powder mixture under the influence of either or simultaneous high temperature and pressure achieves coalescence to form a rigid, dense bulk. More than 80 % of sintered materials (especially with hard and refractory ceramics) are produced using a liquid phase sintering (German, 2009). Under which, spark plasma sintering (SPS)

has emerged as an energy-efficient, quick, and low-cost (for laboratory investigations) technique (Mamedov, 2013). On the other hand, a more efficient, faster, and a low-energy consuming technique known as microwave sintering is likewise gaining popularity (Kumar, 2021). The rapid heating progressing during microwave sintering due to the energy transformation instead of energy transfer (as in SPS) outcomes in volumetric heating resulting in a much finer and uniform microstructure. SPS utilizes a powder mixture to generate a sintered bulk. However, the preparation of powder mixture could be done either by manual mixing, ball, attritor, disintegrator and other milling techniques. The current study comprises powder preparation using ball milling as well as combustion synthesis by the self-propagating high-temperature synthesis (SHS) route. SHS utilizes a chemical reaction of constituents which is self-propagating in a manner as shown in Figure 5. The process can be carried out either in the air or inert atmosphere as per desire (Aydinyan, 2021). Since the SHS method harnesses the heat created during the reaction between reactants, it is labeled as 'green' or 'energy saving', the produced powders often result in a composite precursor with improved properties than individual constituents (Aydinyan, 2022). Besides, the reaction is extremely fast. SHS is termed to be a flexible, easy, cheap, and energy-saving approach to producing powders with extremely high purity and controlled phases (Aydinyan, 2021, 2022).

Apart from powder metallurgy, deposition of a coating comprising SL compounds using physical or chemical vapor deposition (PVD/CVD) has been broadly perceived (Publication IV). The development of thick coatings using the approach of laser cladding is highly undervalued regardless of its effectiveness (Vilar, 1999). Moreover, added advantages of laser cladding in the large-scale production, restoration, and repair of high-end components are constantly reported (Toyserkani, 2004). Since the 1970's when CO₂ lasers with an efficiency of about 20% and a low absorption by metals due to a very high wavelength in the range of ~10 μm resulted in a slower deposition with restrained energy efficiency. However, currently the advancement in diode lasers with efficiency as high as 40–50 % and an improved wavelength of 0.80 to 0.95 μm enables to a higher absorption rate (Torres, 2018). The use of diode lasers has widely encouraged the development of thick SL coatings within a varied range of materials. The advantages of developed coatings through laser cladding include:

- Deposition of a compact, dense structure with minimal coating defects such as pores or un-sintered area (Wang, 2020).
- A considerable reduction in coating dilution is achievable, results demonstrate dilution to be as low as 2–5% (Hemmati, 2012).
- Focused laser beam results in reduced HAZ and further better microstructure refinement (Torres, 2018).
- Possible restoration and repairing of large-scale industrial products (Torres, 2018).
- Laser clad demonstrates a strong adhesion to the substrate material (Lalas, 2006).
- High efficiency as close to 50% (Toyserkani, 2004).

1.3 Research gaps

With the development of new compounds, materials, their processing techniques, and widening their application areas, the pursuit for a potential solid lubricant or their combination to reduce friction and wear is continuously progressing. A non-uniform distribution of soft metals, such as Cu, Ag or Bi in coating/composite matrix (Liu, 2022a, 2022b; Torres, 2018) which might lead to a compromise in lubrication behavior along with other mechanical properties of coating/composite material is upsetting. In the case of laminar solids, during a laser deposition (cladding), sulfur-compounds such as MoS₂ tend to clog in the powder feeder due to its plate-like sticky structure. In order to enhance the powder flowability and maintain the sulfide-based source (for lubrication), it is necessary to search for a viable alternative. Besides, an unexpected lubrication imparted by some in-situ formed compounds, such as chromium sulfide, silver molybdates (Torres, 2018) has necessitated a focused study on the subject at HT. Recent studies of new solid lubricants, such as bismuth (Bi) or Bi₂S₃ or Bi₂O₃ has come into picture (Grützmacher, 2022; Prieto, 2022; Sun, 2022). However, none of them was performed at HT and thus, producing a need to explore them as HT solid lubricants, along with a detailed characterization of their addition/effect on host matrix. Conflicting results of hBN as HT solid lubricant need to be addressed (Podgornik, 2015; Torres, 2022; Zhang, 2008) in an effort to develop a homogeneous structure without compromising the mechanical property of the hBN-based material.

Scarcely reported study on solid lubricating materials produced using laser cladding in comparison to SPS, PVD/CVD techniques have to be taken up (Publication IV). Besides, use of self-propagating high-temperature synthesis (SHS) to produce powder precursors and sintering thereof also requires attention.

Most of the tribological studies regarding HT SL materials feature ceramic as a counterbody materials (Al₂O₃, Si₃N₄) due to their HT stability. However, certain hot-working operations like hot -forging or forming might involve steel or a counter material similar to a workpiece (Deng, 2018) and hence, completely different occurring mechanisms of wear. In addition, hard debris from ceramic counterbody has a high possibility to contribute to a higher degree of abrasive wear or act as a third body on the sliding surfaces. Above and beyond, there is a need to concisely choose the counterbody shape as a spherical (ball) one (most used due to easy alignment against the sliding body) may involve a high contact pressure (Hertzian contacts) and may not mimic the real operating conditions such as hot -forming or stamping (Deng, 2018; Mozgovoy, 2018).

1.4 Objectives of the study

A safe environment, workplace, and efficient tribological operation in a wide range of applications involving high temperatures (>300 °C i.e. degradation of conventional liquid-based lubricant) including machining, metal forming, internal combustion engines, etc. together with a strict EU directive to cut back on metalworking fluids (Boyde, 2002) have been the main motivation behind this PhD study.

The current research work takes on the designing, development, characterization, and HT tribological testing novel self-lubricating composite materials/coatings incorporated with various solid lubricants.

Based on this, the main objectives of this study are formulated as:

1. The design and development of a self-lubricating titanium-based ceramic composite (Ti-TiB₂) for temperatures up to 900 °C (System 1).
2. Development of technology for uniform distribution of soft metal (such as Ag or Bi) in the material through a combined use of secondary reinforcement.
3. Design, characterization, and tribological assessment of bismuth as a HT solid lubricant doped into a Ti-TiB₂ composite (System 2).
4. Optimization and subsequent preparation of sulfide-based (sulfides of nickel (Ni₃S₂) or copper (CuS) or bismuth (Bi₂S₃)) laser claddings and their microstructural and tribological characterization (System 3).
5. Design, development, and tribological study of hBN-based composites produced through SPS utilizing mechanically milled and SHS powder precursors (System 4).

Table 1.1 presents a correlation between the formed research objectives and the proposed solutions in the candidate's publications.

Table 1.1: Correlation between the objectives, materials' systems and solutions proposed in publications (Pub.).

Objectives	System	Pub. I	Pub. II	Pub. III	Pub. IV	Others (Pub. V)	Others (Pub. IX)
1	1	×			×		×
2	2		×			×	
3	2		×				
4	3					×	
5	4			×	×		

In the current PhD work, the tribological tests performed might not mimic exactly the field operations. However, the choice of tribo-bodies, testing conditions is made as per hot-metal forming or forging applications in mind. The study of model materials is intended to gather a deeper fundamental understanding of the designed solid-lubricating materials at high temperature tribological conditions, which can carry on to further optimization as per desired operational condition and reported thereof.

2 Materials and methods

The chapter deals with the materials and methods utilized to fabricate, characterize, and test the specimens.

2.1 Powder precursors

The used powder precursors utilized for the test specimens' fabrication along with their characteristics and procurement are listed in Table 2.1. The designed concentration of powder precursors and materials were selected (and optimized) based on experimental trials.

Table 2.1. Detailed characteristics of the powder precursors used.

Name	Composition	Particle size (μm)	Purity (%)	Supplier
Titanium	Ti	<44	99.5	Alfa Aesar
Titanium diboride	TiB ₂	<25	99.5	Alfa Aesar
Nickel oxide	NiO	<44	99	Alfa Aesar
Tungsten (VI) oxide	WO ₃	10-20	99	Alfa Aesar
Magnesium	Mg	150	>99	Alfa Aesar
Hexagonal-boron nitride	hBN	20	99	Alfa Aesar
Nickel	Ni	45–75	99.3	Oerlikon Metco
Bismuth	Bi	≤ 150	99	Sigma-Aldrich
Ni-based alloy	NiCrBSi (0.2 C, 4 Cr, 1 B, 2.5 Si, <2 Fe, 1 Al, and bal. Ni)	50–150	99	Castolin Eutectic
Nickel sulfide	Ni ₃ S ₂	≤ 100	99	Sigma-Aldrich
Copper sulfide	CuS	≤ 100	>99.8	Sigma-Aldrich
Bismuth sulfide	Bi ₂ S ₃	≤ 100	>99.5	Sigma-Aldrich

The following five powder mixtures were employed to prepare precursors for the consolidation processes:

- (i) Precursors 1: TiB₂ and Ti powder mixture with two different compositions i.e. 50 wt.%TiB₂-50 wt.% Ti and 10 wt.%TiB₂-90 wt.% Ti.
- (ii) Precursor 2: Ni and Bi powder mixture by 30 and 70 wt.% respectively.
- (iii) Precursor 3: Ni and W powder mixture in 60 and 40 wt% respectively.
- (iv) Precursor 4: NiO, WO₃, Mg, and graphite powder mixture (4NiO-WO₃-yMg-xC system designed as to obtain Ni-W alloys with a molar composition ratio of Ni:W = 4:1.).
- (v) Precursor 5: NiCrBSi alloy with 10 wt% Ni₃S₂ or Bi₂S₃ or CuS powder mixture.

Materials/material systems and their preparation techniques are listed in Table 2.3.

2.2 Mechanical mixing

Precursors 1, 2, and 5 were dry mixed using a 2 h of mechanical rotation mixing and subsequently, were dried in a heating oven at 60 °C for 20 min before the consolidation or laser cladding/deposition process for moisture elimination.

Precursor 3 (Ni-W) was produced using a high energy ball milling (HEBM) technique (Emax, Retch GmbH, Haan, Germany) in 125 mL jars. Metal powders (60 wt% of nickel and 40 wt% of tungsten) were initially dry mixed in a ceramic mortar. Wet milling in the existence of ethanol (75 vol.%) was achieved using 3 mm zirconia balls as a milling media with a powder-to-ball mass ratio of 1:1. The milling conditions were optimized as follows: 1000 rpm for 12 h using intervals of 15 min and a pause for 5 min. Afterward milling, the mixture was sieved to detach the balls and dried at 50 °C to eliminate the ethanol. hBN by 2 wt% (according to the mass of the final Ni-W product) was added to the milled Ni-W powder.

2.3 Combustion synthesis (SHS) of Ni-W (-hBN)

For SHS process (Figure 5), the raw powders as in precursor 4 as per two systems: (a) $4\text{NiO}\cdot\text{WO}_3\cdot 3.2\text{Mg}\cdot 3.2\text{C}$ and (b) $4\text{NiO}\cdot\text{WO}_3\cdot 3.2\text{Mg}\cdot 3.2\text{C}\cdot 2\text{ wt.}\% \text{ hBN}$ were homogeneously mixed using a pestle in a ceramic mortar for 20 min, and 23.4 mm in diameter and a cylinder-shaped green bodies of $1.7\text{--}1.8\text{ g/cm}^3$ density and 40–45 mm height were ready. Next, the green bodies were placed into a CPR-3.5l reaction compartment (Sapphire Co., Abovyan, Armenia) packed with argon gas of 99.98% purity at a pressure of 0.4 MPa. To start the combustion reaction, a tungsten coil buried in the igniting mixture was excited by electricity under 12 V for 5 sec. Two C-type tungsten-rhenium (W/Re-5 and W/Re-20, 100 μm in diameter) thermocouples were positioned at holes drilled in a green body to record the temperature-time development of the combustion wave progression manner. Subsequent to the SHS process, samples were cooled down in the compartment and the contrived samples were further crushed or milled into fine powders, sieved using a sieve with a mesh size of 100 microns, and put to acid leaching with a 10% HCl solution at 40 °C for 20 min to eradicate the magnesia by-product (for SPS).

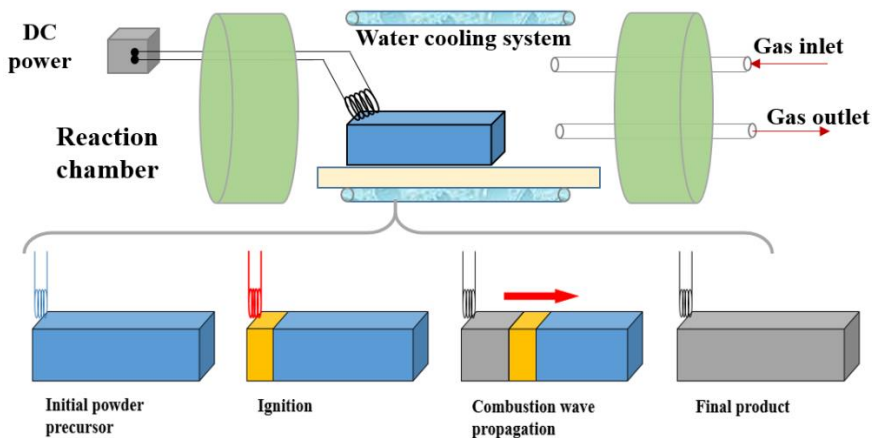


Figure 5: Scheme showing a typical SHS process.

To analyze, the systems (a) and (b) were designed as per thermodynamic prediction (using the 'ISMAN-THERMO' software package) to acquire Ni-W (-hBN) alloys with a molar composition ratio of Ni:W = 4:1.

2.4 Spark plasma sintering (SPS)

The produced powder precursors 1, 3, and 4 were consolidated using the approach of SPS (KCE-FCT HP D 10-GB, FCT Systeme GmbH, Frankenblick, Germany) under a simultaneous application of pressure and temperature in vacuum (<5 mbar) engaging a continuous electric current. The precursors (here, 20 g) are loaded into a graphite die of 20 or 25.4 mm diameter. Graphite sheets were positioned between the punch and the powder to avoid sticking between the sintered bulk and die/punch. The hBN spray was applied to hinder the graphite interaction with the bulk and their easy separation during subsequent sintering. Further, the loaded precursors are densified using a simultaneous application of pressure and temperature for a stipulated dwell time. A heating rate of 100 °C/min was applied during sintering, and afterwards cooled down by up to ~200 °C/min. The applied pressure, temperature, heating rate, dwell time for produced bulks were optimized so as to produce composite bulks with high relative density and are detailed in Table 2.2. The composites bulks achieve densification through solid-state sintering, which is a general approach for the production of high-temperature ceramics and composites.

Table 2.2. The process parameters of spark plasma sintering.

Powder precursor	Pressure (MPa)	Temperature (°C)	Dwell time (min)	Heating rate (°C/min)
50 wt.% TiB ₂ -50 wt.% Ti (Precursor 1)	35	1500	3	100
10 wt.% TiB ₂ -50 wt.% Ti (Precursor 1)	50	1050	5	100
Ni-40 wt.% W (-hBN) (HEBM-Precursor 3)	50	1300	5	100
Ni-40 wt.% W (-hBN) (SHSed-Precursor 4)	50	1100	5	100

2.5 Laser surface melting and laser cladding

Powder precursor 2 (Ni-70 wt% Bi) was spread over the SPS-ed bulk (10 wt.%TiB₂-Ti) for a subsequent laser surface incorporation (or laser melting) of Ni-Bi into the Ti-TiB₂ composite as to achieve a modified or transformed composite surface. Consequently, a heating step was accomplished in an oven at 100 °C for 1 h, to evaporate the ethanol binder (used during precursor mixing). The last stage of laser deposition (melting) was executed using a rectangular-shaped laser beam of 6 mm × 13 mm area under a shielding argon atmosphere to prevent any oxidation of the resulting coatings using a beam speed of 6 mm·s⁻¹ and laser power of 3500 W. The thickness of the as-melted modified surface was measured to lie between 1–1.5 mm. The dilution percentage calculated was <40%.

Powder precursor 5 (NiCrBSi alloy-10 wt% Ni₃S₂ or Bi₂S₃ or CuS) was dispersed over a 1.4301-grade stainless steel plate for subsequent laser cladding (generating a coating).

Prior to dispersal of the powder mixture, the SS plates were sandblasted by means of silica sand to improve the adhesion between the coating and substrate. Next, the plates with powders were heated in an oven at 100 °C for 1 h, to guarantee the evaporation of the ethanol binder. The subsequent step of laser cladding was performed utilizing a direct diode laser setup with a wavelength of 975 nm featuring a rectangular-shaped laser beam of 24 mm × 3 mm inside an inert argon shielding atmosphere to elude any oxidation of the resulting claddings. The clads were deposited using a beam speed of 4.3 mm·s⁻¹ and laser power of 6200 W. The thickness of the produced laser clad coatings was measured to be 2–2.5 mm with a dilution percentage as low as 5%. Figure 6 demonstrates a general view of the laser cladding process and the developed coating.

Further, the fabricated specimens were ground and polished to ~Ra 0.2 ±0.04 μm and later, cleaned with acetone for the next step of analysis.

Deposition parameters were optimized to achieve a good adhesion and minimum dilution to the substrate.

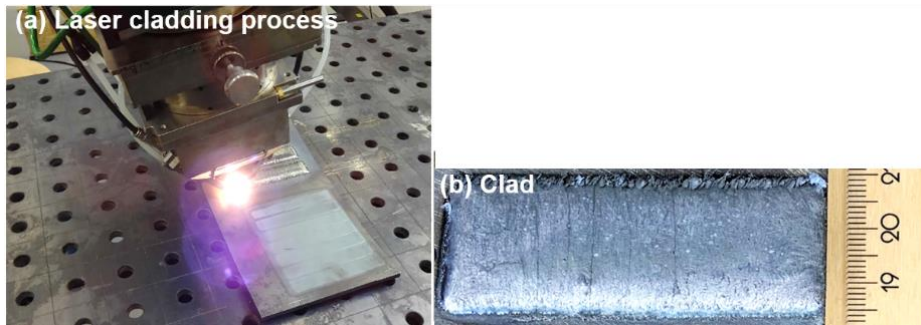


Figure 6: (a) Laser cladding in-progress; and (b) as-deposited top view of NiCrBSi+Bi₂S₃ coating (performed at AC2T research GmbH).

2.6 Characterization

Subsequent to the SPS process the graphite layers on the samples were detached by a grinding machine (80036, Cromag) and further, polished to 1 ±0.02 μm finish using a Phoenix 4000 (Buehler, USA) under water as a lubricating medium with the help of 8-inch diamond grinding discs (DGD Terra, Buehler, USA). The polishing was performed at a speed of 250 rev·min⁻¹ and held for 2 minutes for each disc. The discs were altered in a definite order (45, 25, 15, 9, 3 and 1 μm) and then cleaned with acetone and ethylene alcohol.

The laser surface melted and laser clad samples were ground to ensure parallelism and polished to achieve a Ra of 0.2 ±0.04 μm (measured using a Zygo New View 7300 3D optical profiler) for microstructural and tribological testing. All specimens were ultrasonically cleaned in petroleum ether and rinsed with acetone before testing.

The bulk density of samples was measured using Archimedes principle with a distilled water as the immersing medium using balance (Mettler Toledo ME204, Switzerland) with 0.1 mg accuracy. The density reported is the mean of at least 3 measurements.

The bulk Vickers hardness (HV) was measured using Indentec 5030 SKV (Brierley Hill, UK) unit with an indentation load X (X = 10, 30, 50 kg) for 10 s. The reported values are the average of at least 5 indentations.

The bulk microhardness (HV1) was measured using a standard Vickers hardness machine (Future-Tech FV-700; and Buehler Micromet) unit with an indentation load 1 kg for 10 s. The reported values are the mean of at least 3 indentations. The diagonals of the indents were investigated through optical microscopy (Zeiss Discovery.V20) equipped with AxioVision software.

The indentation fracture toughness (IFT) was calculated from the length of radial cracks originating from the corners of the indents following Palmqvist approach (Sergejev, 2006). The load of 50 kgf for 10 s on the indenter was used to develop measurable cracks on the sample's surface. The values reported are an average of five indents measured on a sample surface. The surface cracks initiated by the indenter were measured using optical microscopy.

The surface roughness (Ra) was measured in a contact mode using the Mahr perthometer, PGK 120 and a Zygo New View 7300 3D optical profiler.

The morphology, chemical composition, and SEM images of the initial powders, SHSed powders, SPSed bulks and laser deposited/cladded samples were investigated under scanning electron microscopes (HR-SEM Zeiss Merlin, Germany; and JSM-IT300 SEM, Jeol BV, Netherlands) equipped with energy dispersive x-ray spectroscopy (EDS) detectors.

Phase examination of the samples was accomplished using an X-ray diffractometer (XRD, Rigaku SmartLab SE using a D/teX Ultra 250 1D detector at RT) with radiation of 30 mA, 40 kV, $\lambda = 0.1542$ nm, a step size of 0.02° and a count time of 0.4 s.

2.7 Tribological tests

A universal materials test device (CETR/Bruker, UMT-2, USA) was engaged for SPS-ed materials' testing under a dry unidirectional circular sliding in ball-on-disc configuration as shown in Figure 7. The testing was performed at room and high temperatures (up to 900 °C). The heating rate was kept to $6^\circ\text{C}\cdot\text{min}^{-1}$. The coefficient of friction (CoF) during the sliding test was recorded. Each reported result comprises of average value from at least two repetitions of test. Further details of the tests are illustrated in Table 2.3. The choice of the load was made as per hot forming/stamping applications and also, upon an optimization to produce quantifiable wear.

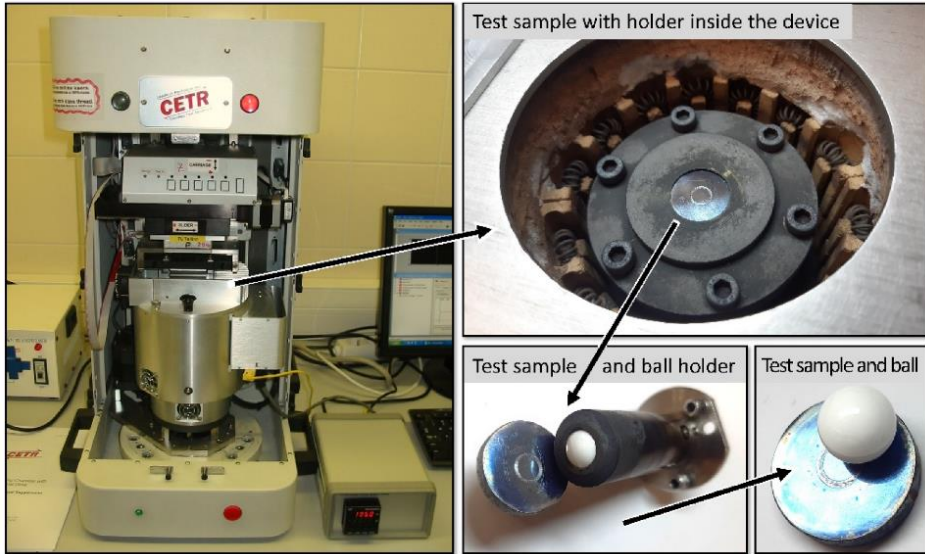


Figure 7: A universal tribo-test device (UMT-2) employed for the HT dry unidirectional sliding for system 1 and 4.

The sliding wear behavior of the laser surface melted and laser clad samples were performed using an Optimol SRV tribometer (Optimol Instruments Prüftechnik GmbH, Germany) under a reciprocating pin/or ball-on-flat configuration (performed at AC2T research GmbH). An upper counterbody sample was loaded against a stationary test specimen by means of a servo motor. The loaded upper sample oscillated using a spring deflection mechanism against the lower flat specimen, which could be heated resistively up to nominal temperatures of 900 °C. Actual temperatures on the sample surface were measured using a thermocouple. The test was performed at room temperature, 400, and 600 °C. The coefficient of friction (CoF) during the sliding test was recorded. Further details of the tests are illustrated in Table 2.3. Frequency of reciprocation and stroke length were attuned to give an average sliding speed of 0.1 m·s⁻¹ as in hot forming or forging or stamping operation.

3D wear topography measurements for the samples to determine the depth, shape, and volume of material removed (net missing volume) were executed using a 3D profilometer (Leica Microsystems; and Bruker Contour GT-K0 +). Counterbody pin wear (length of the pin lost) was evaluated using a Vernier caliper.

The wear rate, K , is calculated using Eq. (1), dividing the measured wear volume v_w by the normal load N and the total sliding distance d . Each reported result comprises of average value from at least two repetitions of test.

$$K = \frac{v_w}{N \cdot d} \quad (1)$$

Table 2.3. Details of material systems' evaluated under wear tests.

System	Material	Preparation	Sliding test	Reference
1	50wt.%TiB ₂ - 50wt.%Ti	SPS	Unidirectional circular ball-on-disc Counterbody: Ø10 mm Al ₂ O ₃ ball Contact pressure: 0.81 to 1.4 GPa Load: 5 to 26 N Speed of 0.1 ms ⁻¹ Distance 1000 m Temp.: RT to 900 °C	SPS-ed titanium
2	Ni-Bi laser surface doped 10wt.%TiB ₂ - 90wt.%Ti	SPS, Laser surface melting	Reciprocating pin-on- disc Counterbody: Ti6Al4V Load: 100 N Contact pressure: 30 MPa Speed: 0.1 ms ⁻¹ Frequency: 13 Hz Stroke length: 4 mm Duration: 200 s Temp.: RT, 400, 600 °C	Unmodified 10wt.%TiB ₂ - 90wt.%Ti
3	NiCrBSi-10wt% Ni ₃ S ₂	Laser cladding	Reciprocating ball-on- flat Counterbody: Ø10 mm AISI 52100 steel bearing ball Load: 50 N Contact pressure: 1.7 GPa Speed: 0.1 ms ⁻¹ Frequency: 25 Hz Stroke length: 2 mm Duration: 900 s Temp.: RT, 400, 600 °C	Unmodified NiCrBSi
	NiCrBSi-10wt% CuS			
	NiCrBSi-10wt% Bi ₂ S ₃			
4	Ni-40 wt.% W (-2 wt.% hBN)	HEBM, SPS	Unidirectional circular ball-on-disc Counterbody: Ø10 mm Al ₂ O ₃ ball Contact pressure: 1.16 GPa Load: 15 N Speed of 0.1 ms ⁻¹ Distance 1000 m Temp.: 800 °C	Ni-40 wt.% W
	Ni-40 wt.% W (-2 wt.% hBN)	SHS, SPS		Ni-40 wt.% W

3 Results and discussion

3.1 System 1, Ti-TiB₂ SPS-ed composite

3.1.1. Design and thermodynamic phase analysis

The design of system 1 addresses *objective 1*. The choice of TiB₂ was made from the general idea that ceramic addition enhances the mechanical property (hardness, creep resistance, constrained grain growth, etc.) of the produced material. Besides, the TiB/TiB₂ is very well compatible with titanium in the terms of close density value (4.5 g/cm³ for Ti and 4.56 g/cm³ for TiB), and coefficient of thermal expansion value ($8.2 \times 10^{-6} \text{ }^\circ\text{C}^{-1}$ for Ti and $6.2 \times 10^{-6} \text{ }^\circ\text{C}^{-1}$ for TiB). This might result in good interfacial bonding through enhanced densification during sintering. The choice of a high concentration of TiB₂ addition in the titanium matrix was selected due to the needed high mechanical stability of composite during 900 °C of tribological testing (carried at high loads).

Existing phase studies on Ti-B system (Ma, 2004) demonstrate that the formation of a thermodynamic and chemically stable TiB (titanium monoboride) phase in the sintering of Ti-TiB₂ precursors, assisted by TiB negative Gibbs free energies (-160 kJ/mol). Besides, the diffusion coefficient of boron in TiB₂ to the titanium matrix and the growth rate of TiB is very high, which causes the formation of TiB, rather than TiB₂. Due to whisker like morphology of TiB, it is sometimes pronounced as TiB_w in current system.

3.1.2. Microstructure

After SPS consolidation of precursor 1, the composites' surface was prepared (grinding, polishing) and characterized using SEM and XRD techniques. Figure 8 shows the surface SEM image, XRD patterns, and fractured SEM image of the Ti-TiB₂ composite surface.

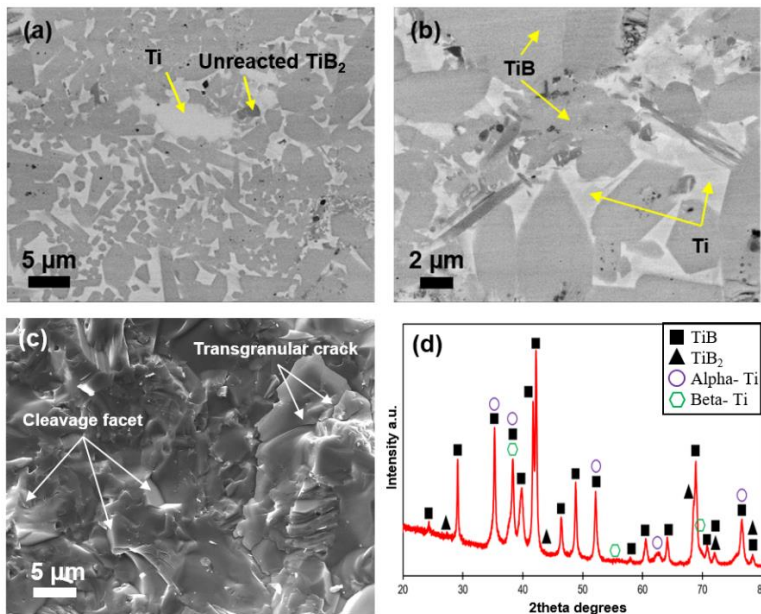


Figure 8: (a, b) surface SEM image, (c) fractured SEM image, and (d) XRD pattern of the Ti-TiB₂ composite surface (adapted from Publication I).

SEM images of composite surface exhibit a well-sintered bulk without the significant extent of pores or cracks (Figure 8a, b). The fractured SEM points to the brittle mode of fracturing (Figure 8c). However, a crack deflection mechanism of fracture was noticed in the way of lengths of the cracks generated during indentation fracture toughness (IFT) measurement using a Palmqvist approach. Table 3.1 details the density, hardness, and IFT value of the Ti-TiB₂ composite as reported in literature along with fabricated in the current study.

The revelation of TiB phase along with TiB₂ phase in XRD analysis points to incomplete conversion of TiB₂ into a thermodynamically stable TiB phase (Figure 8d). This could be due to the occurrence of some large TiB₂ particles in the initial precursor mixture (preventing the TiB₂ phases to completely react with the Ti matrix) or an insufficient time (due to a short holding time of 5 min in the SPS process) for a complete reaction between Ti and TiB₂ ($\text{Ti} + \text{TiB}_2 \rightarrow 2\text{TiB}$) (Publication IX; (Sabahi Namini, 2019)). Besides, the Gibbs free energy value for the aforementioned equation is continuously negative ($\Delta G = -154 \text{ kJ/mol}$) from the RT to the sintering temperature of 1500 °C supporting a spontaneous transformation of TiB₂ to TiB (or TiB_w, Titanium mono-boride whiskers). The existence of dual titanium boride (TiB₂ + TiB) in the composite microstructure is recognized to augment its mechanical and tribological properties. For more details, please refer Publication I and IX.

Table 3.1. Fabrication method, density, hardness, and fracture toughness of TiB-Ti composites (adapted from Publication IX).

Material	Process	Relative Density (%)	Hardness	IFT (MPa m ^{-1/2})
CpTi [136]	SPS	97.92 ±0.03	291 ±10 (HV30)	-
TiB-60wt% Ti [137]	Mixing + SPS	99.6%	-	9.35
TiB _w -50wt% Ti (current work)	Mixing + SPS	99.4%	1448.08 ±67.4 (HV10)	10.52
TiB- 33 vol% Ti [138]	Ball Milling + Reaction hot pressing	-	1351 (HV50)	-
TiB-30wt.%Ti [139]	SHS + PHIP	98.45	87.8 HRA	6.15
TiB-20wt.%Ti [139]	SHS + PHIP	97.57	86.7 HRA	5.23
TiB-12wt.%Ti (Publication IX)	SHS + SPS	99.7	1550 ±26 (HV30)	8.16

Considering above all, the production of a dense Ti-TiB₂ composite with a significantly high content of ceramic phase (50 wt.%) featuring a high hardness and good IFT using a quick, energy-efficient SPS approach (from commercially available powders) is demonstrated. In an additional study by Kumar et al. (Publication IX), the SHS-SPS fabrication of Ti-88 wt.% TiB dense composite (from combustion synthesized Ti-B powders) with an even higher ceramic concentration (88 wt.%) achieved an excellent hardness value (~1550 HV30) and a good IFT (8.16 MPa·m^{1/2}). The SHS-produced composite demonstrated a complete conversion of stable and hard TiB phase (1800 HV).

3.1.3. High temperature tribological studies

Unidirectional dry sliding wear of SPSed 50wt.% Ti-50wt.% TiB₂ specimens (25 × 5 mm²) carried out in ball-on-disc configuration using an Al₂O₃ ball as a counterbody was performed from RT to 900 °C (as shown in Figure 7). The parameters of the sliding tests are shown in Table 2.3. The 10 000 s of test takes into consideration the phenomena of running-in (to reach a steady-state regime) and the start-stop durations (after every 500 s), replicating the condition in real field bending or forming operations caused by part loading-offloading or any other process interruption and likely time delay, for example, due to human factors, etc. Moreover, an additional step of recalibrating of device through interruptions was made to increase the test precision during testing.

Figure 9 shows the wear rate and CoF curve for pure Ti (reference) and the Ti-TiB₂ composite sliding at different temperatures. A significant drop in wear rate and CoF value was noticed for the composites with an increase in temperature, especially at 700–900 °C sliding. However, reference pure Ti demonstrated increased wear and fluctuation in CoF evolution at HT of 700 °C accompanied by an extreme vibration of the test setup caused by its high ductility and increased thermal softening (at HT). For more details, please refer Publication I.

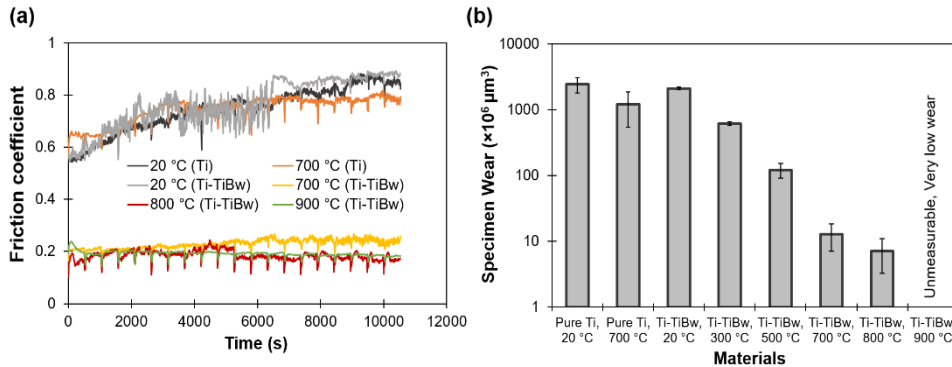


Figure 9: (a) CoF curves; and (b) wear rate for pure Ti and the Ti-TiB₂ composite after testing at various temperatures (adapted from Publication I).

Reference Ti and composite sliding against a harder Al₂O₃ ball counterbody (point contact can give rise to increased stress level) underwent significant wear at RT. Evident marks of ploughing and cutting exist at this stage. Besides, the occurrence of a hard third body (ceramic particles in the case of composite) might have escalated the wear and unsteady CoF evolution at RT sliding. Abrasion and adhesion were the main responsible mechanisms of wear for composites at RT sliding. Whereas, severe ploughing, cutting (abrasion), and plastic deformation were the major mechanisms of wear in the case of reference pure Ti. Figure 10 shows the SEM images of wear track after testing at different temperatures.

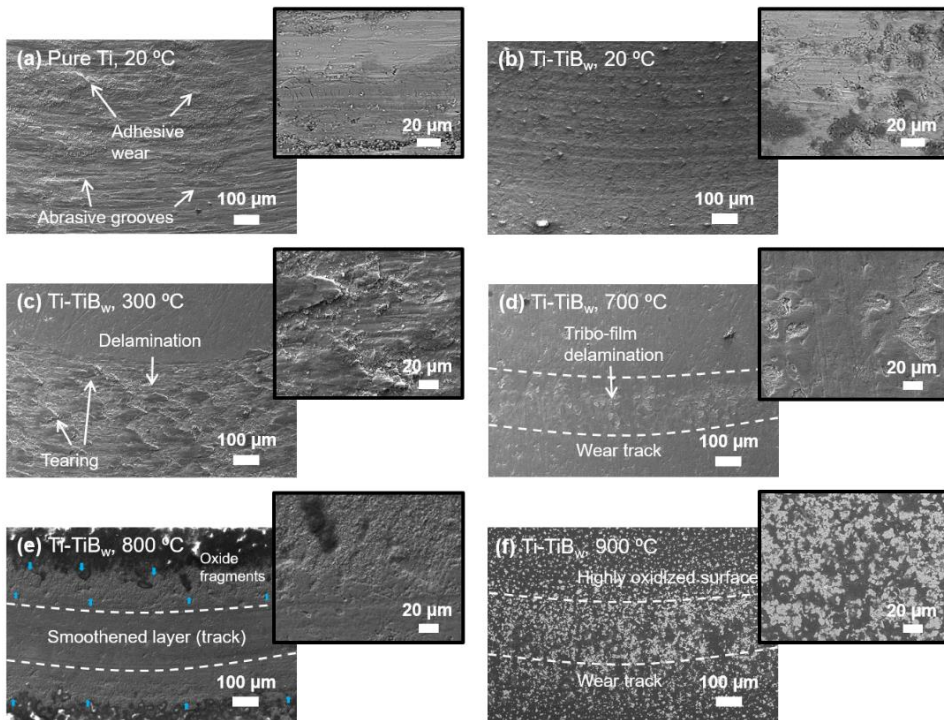


Figure 10: SEM images of materials surface after sliding at various temperatures; (a) Pure Ti, 20 °C; (b) Ti-TiB₂, 20 °C; (c) Ti-TiB₂, 300 °C; (d) Ti-TiB₂, 700 °C; (e) Ti-TiB₂, 800 °C; and (f) Ti-TiB₂, 900 °C (**adapted from Publication I**).

With an increase in temperature, the composite bared a formation of titania-rich (TiO₂) tribo-oxide layer (for XRD, refer to Publication I). The thickness of which increased with an increase in test temperature, being maximum at 900 °C i.e. 39 μm (Figure 11). However, the compactness and homogeneity of the developed layer were seen to be paramount at 700 and 800 °C, upon which (900 °C) the tribo-oxide layer features a detachment and fairly porous structure (possible due to thermal stress). Besides, the highest load bearing capacity (26 N, contact pressure = 1.4 GPa) along with low CoF value (<0.2) was demonstrated for tribo-oxide layer developed during 800 °C testing. For more details on load bearing capacity of developed tribo-oxide layer, please refer to Publication I.

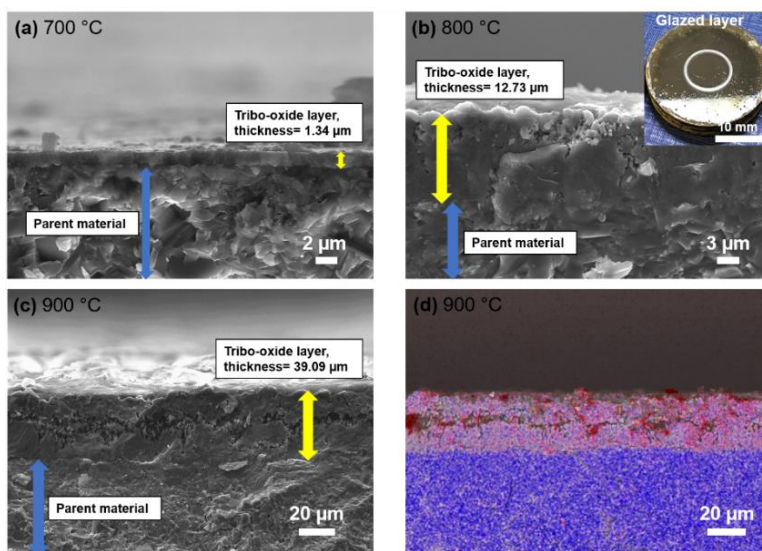


Figure 11: Cross-sectional SEM images of composites exhibiting the developed tribo-oxide layer after test at (a) 700 °C; (b) 800 °C; (c) 900 °C; and (d) EDS elemental mapping showing oxygen-red, blue-titanium. The formation of boric acid -rich glazed layer on the surface of composite after sliding at 800 is shown (**adapted from Publication I**).

At temperature of 300 and 500 °C, the composite wear track shows delamination of the tribo-oxide layer (oxidative wear, Figure 10c). However, a major decrease in delamination intensity was seen at and beyond 700 °C composite sliding. At 800 and 900 °C, the wear track surface (composite) features smoothing and signs of micropolishing (Figure 10e, f). Upon XRD analysis of the wear track, it was revealed that the developed tribo-oxide layer at this stage was simultaneously (along with TiO₂) rich in lubricious boric acid i.e. B(OH)₃. The occurrence of B(OH)₃ on the wear track of composites at 700–900 °C sliding was held responsible for a significantly reduced (and steady) friction (~0.17) and self-lubricating nature of the composite. A brief chemistry and tribo-influence of B(OH)₃ is detailed in Publication I.

In the case of pure Ti, the developed tribo-oxide layer (at HT) featured thin, poor cohesiveness, and was non-adherent to the substrate; thus, was easily removed during successive sliding passes. A low value of Pilling-Bedworth ratio (a measure of how protective is developed oxide-layer) in the case of pure Ti and its developed oxide is reported (Bertrand, 1984). For more details, please refer to Publication I.

For the counterbody Al₂O₃ (1450 HV10) which is of comparable hardness to the composite specimens (1324 ±18 HV30), a high wear (mainly adhesive) was measured when sliding at RT and 300 °C (please refer to publication I). However, a decrease was noted thereafter, especially at 800 and 900 °C due to the presence of a lubricious boric acid compound at tribo-contact and its transfer effects from the self-lubricating composite to the counterbody. Further, an EDS analysis confirmed high amount of material transfer (titanium) from the composite to counterbody at RT sliding; whereas at HT of 800 and 900 °C no titanium transfer was found on the ball surface (Figure 12). Nevertheless, a high amount of boric acid transfer at this stage is believed to occur, pointing to the fact that the generated self-lubricating glazed surface acted as the main sliding surface and thus, preventing the sliding bodies wear. For more details, please refer to Publication I.

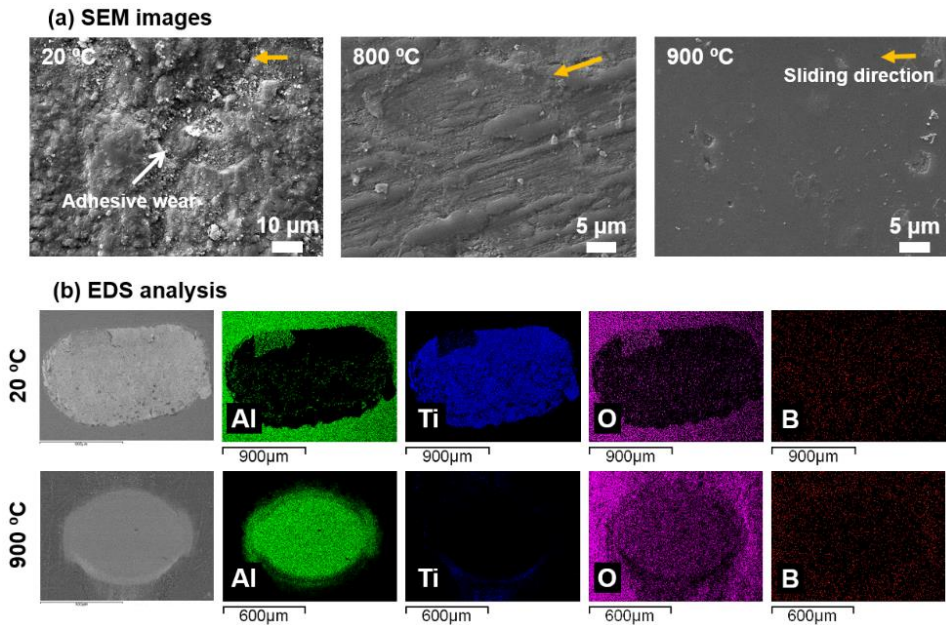


Figure 12: (a) SEM images of Al_2O_3 counterbody ball surface after test at 20, 800, and 900 °C; and (b) EDS analysis of wear scars after test at 20 °C and 900 °C (adapted from Publication I).

3.2 System 2, Ni-Bi/ Ti-TiB₂ laser modified composite

3.2.1. Design and thermodynamic phase analysis

As mentioned earlier, apart from studying bismuth (Bi) as an HT solid lubricant, the current study also claims to solve the problem of bismuth inhomogeneous distribution in the composite/coating (through simultaneous incorporation of Ni and Bi mixture). The design of system 2 takes over to *objectives 2 and 3*.

Phase equilibrium diagrams have been studied for the Ti-B-Ni-Bi quaternary system using the CALPHAD method to evaluate the realization of various phases. The choice of composition of the quaternary mixture of 0.676Ti-0.097B-0.092Bi-0.135Ni was considered from the approximations based on the compositions of the substrate (Ti-10wt%TiB₂) and dopant (Ni-70wt%Bi). Thermodynamic study shows the probable formation of TiB, NiTi, and TiBiNi solid solution phases in the majority. The existence of bismuth compounds along with hard phases of NiTi, and TiB in the composite microstructure can assist in determining the alleged lubrication behavior of bismuth at besides, maintaining the mechanical stability of the material. For more details, please refer to Publication II.

3.2.2. Laser surface melting and microstructure

Premixed Ni-Bi powder precursor by 30/70 wt.% ratio was laser deposited (laser surface melting) over Ti-10wt.% TiB₂ SPSed composite. The laser melting process resulted in the development of a 1–1.5 mm thick self-lubricating functional surface comprising phases from the Ti-B-Ni-Bi system (predicted by Thermocalc phase analysis software). XRD analysis conducted on the surface reveals the major existence of Ti₂Ni (~36 wt%) and a ternary stable phase of Ti₄NiBi₂ (~26 wt%) along with Ni₂B, and TiB_x. The calculated percentage of dilution (Eq.1, where D is the dilution ratio, A1 is the cross-sectional area

of the melted region in the substrate, and A2 is the cross-sectional area of the clad above the substrate) of <40% revealed a good adherence between the developed surface and substrate.

$$D = \frac{A1}{A1+A2} \quad (\text{Eq. 1})$$

SEM analysis of the self-lubricating surface demonstrates an interesting microstructure of uniformly spread areas featuring a hard B-rich phase (TiB_x - confirmed by XRD, dark area, Figure 13a, b, Table 3.2) encapsulated inside a lubricious Bi-rich phase ($\text{Bi} \sim 23 \text{ wt\%}$, bright orbicular-shaped area, Figure 13b, Table 3.2). The fact that B (an HT lubricant, $\geq 700 \text{ }^\circ\text{C}$) and Bi (a medium temperature lubricant, $\leq 600 \text{ }^\circ\text{C}$) exist together in the composite, points to a likelihood of an enlarged lubrication range of the composite (Publication I, II). A two times higher hardness ($\sim 620 \text{ HV1}$) of the functional surface (Ni-Bi samples) in comparison to the underlying substrate was measured (Figure 13d).

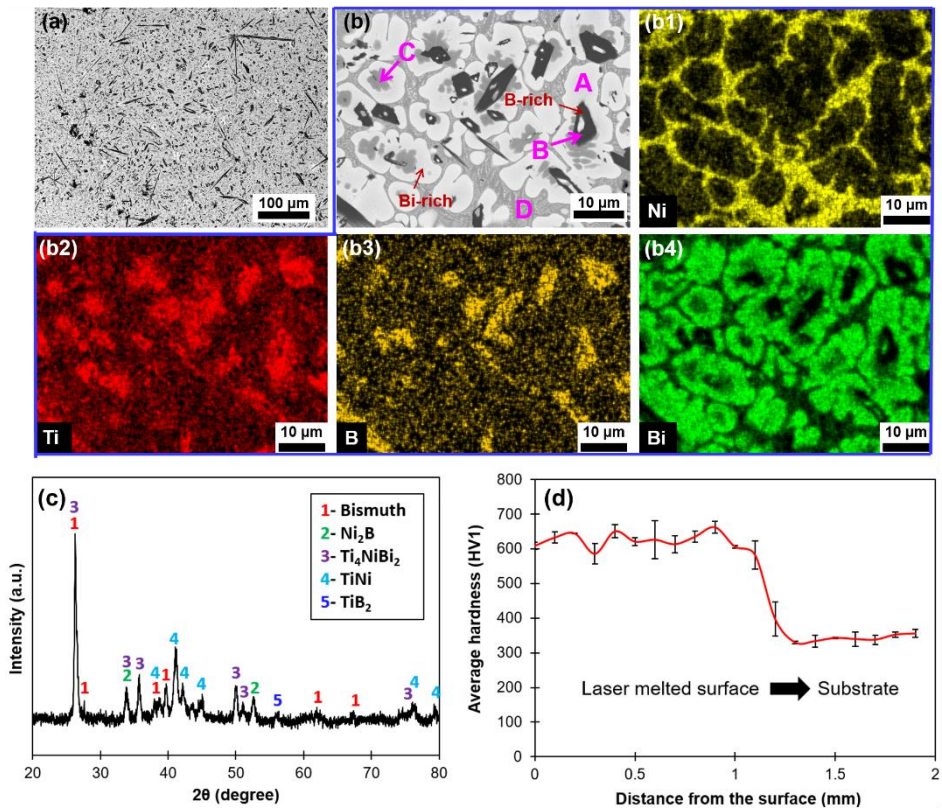


Figure 13: (a, b) as melted-surface SEM image; (b1, b2, b3, b4) EDS mapping signifying TiB phase encapsulation inside Bi-rich phase as detected in SEM and an EDS mapping thereof including titanium, boron, nickel and bismuth; (c) XRD pattern; and (d) Room temperature microhardness (HV1) values of Ni-Bi sample from surface to substrate (adapted from Publication II).

Table 3.2. Chemical composition in wt% as evaluated by EDS for the spots labelled in Figure 13b (adapted from Publication II).

Spot	Chemical composition (wt%)				
	Ti	B	Ni	Bi	O
A	71.9	-	4.5	23.5	0.1
B	92.2	7.8	-	-	-
C	87.5	-	0.6	11.7	0.3
D	64.4	-	33.5	2.1	-

An important point to note is that when melting sole Bi (without Ni) over the same composite, then a completely different microstructure featuring a cracked, and porous melted-surface with a high dilution, and non-uniform Bi distribution was noticed (Figure 14a, c). This hints at the fact that nickel in the Ni-Bi mixture aids in a thick developed surface featuring homogeneous bismuth distribution across the Ti-TiB₂ substrate (Figure 14b).

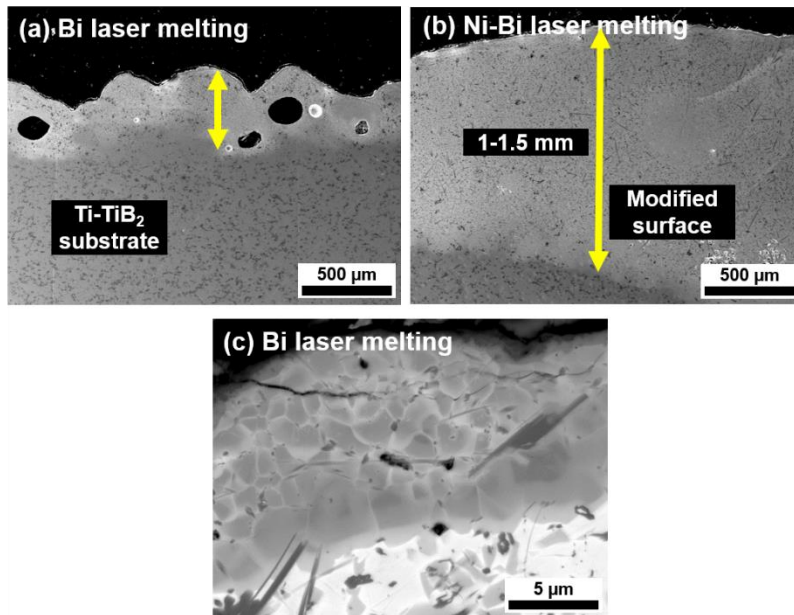


Figure 14: SEM images showing as-melted surface-substrate (Ti-TiB₂) interface after (a, c) Bi laser melting; (b) Ni-Bi laser melting (Unpublished data).

3.2.3. High temperature tribological studies

The produced specimens (25 mm × 4 mm) were put to reciprocating dry sliding wear in pin-on-flat configuration against a flat Ti alloy pin counterbody (in house manufactured from needle rollers, with the resulting edges being manually ground with grit 600 sandpaper to reduce the inception of edge effect and indentation during testing) at temperatures of room, 400 and 600 °C. The reciprocating flat-to-flat contact was expected to lead to a tribological behavior closer to forming processes in terms of contact

pressure (reported to lie close to 30 MPa). The maximum values for the lab-scale simulation of hot stamping/forming were stated to be lesser than 30 MPa in the published literature (Cora, 2012; Ghiotti, 2011; Naderi M, 2007), aligned with the current study. Details about the testing parameters are disclosed in Table 2.3. Further, the friction curves and wear rates were analyzed. The results are reported in comparison to unmodified Ti-TiB₂ composite (herein, Ref.).

Figure 15 shows the CoF curves, and wear rate of the tested specimens. Figure 16 demonstrates the 3D wear scar profiles of tested materials. A two-fold decrease in CoF value at RT and 400 °C sliding for Ni-Bi specimens (~0.5) in comparison to unmodified composite (~1.2) was noted. Besides, at this stage, the obtained friction curves for Ni-Bi specimens demonstrated a steady and stable evolution. The stable sliding of Ni-Bi at RT and 400 °C was supported by their revealed wear mechanisms (mainly adhesive delamination) (Figure 17a) which indicated a tribolayer formation, majorly pronounced (homogeneous) at 400 °C. Upon XRD, it was confirmed that the wear track (tribolayer) at this stage richly encompassed lubricious phases of bismuth, pointing to a conclusion that bismuth spread on the tribo-surface during operation resulting in easy sliding and lowering friction. A point to note is that the low CoF value of Ni-Bi at RT is partially at the expense of its wear rate (high), which hints at a conclusion that the presence of Bi (Bi-rich phase) might assist in lowering friction but not in depressing wear. For more details, please refer Publication II.

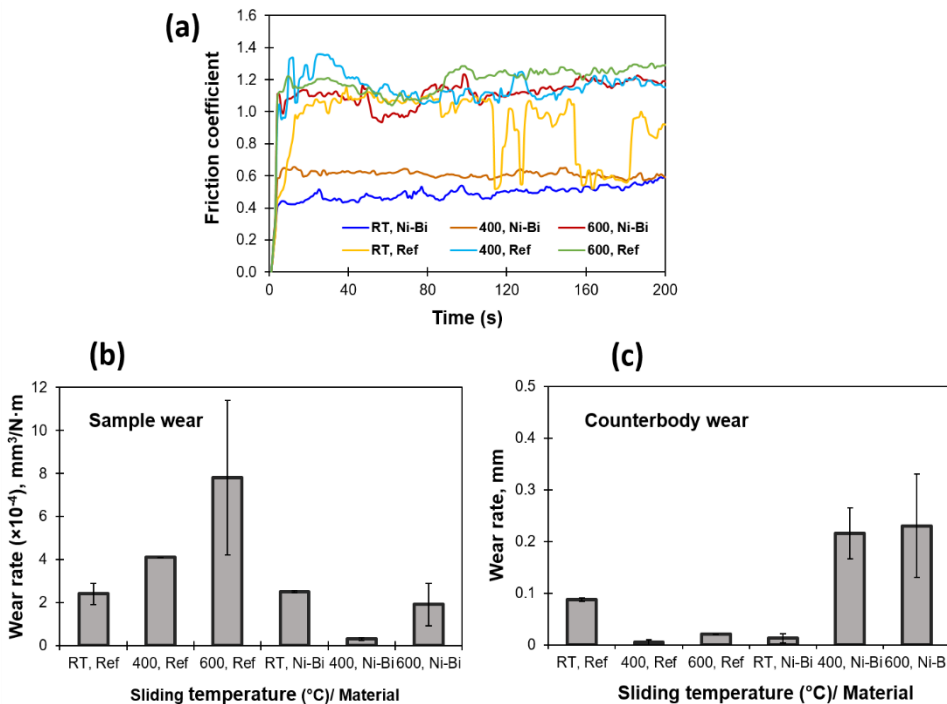


Figure 15: Reciprocating sliding results of materials tested at different temperatures, reference unmodified composites labelled as 'Ref' and Ni-Bi modified as 'Ni-Bi' (a) CoF curves; (b) specimens wear rates; (c) counterbody wear rate; and (d) 3D wear profiles of Ni-Bi specimens after testing at 400 °C (adapted from Publication II).

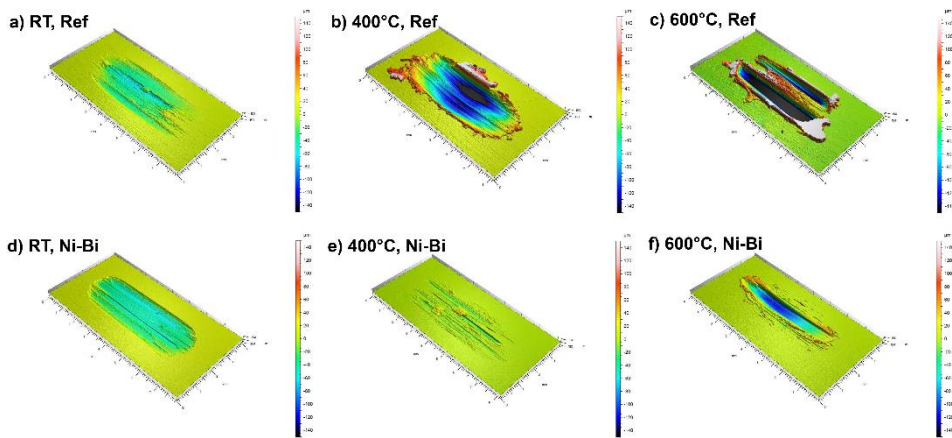


Figure 16: 3D wear profiles of Ref and Ni-Bi samples after test at RT, 400 and 600 °C (**adapted from Publication II**).

XRD analysis of Ni-Bi samples after 400 and 600 °C sliding indicates the presence of TiO_2 , Bi_2O_3 , and $\text{Bi}_4\text{Ti}_3\text{O}_{12}$ on the wear track (tribo-oxide layer). The occurrence of oxides in an adherent, compact, and homogeneous tribolayer (Publication II) developed over Ni-Bi specimens; is believed to enhance their wear resistance along with imparting low friction (offered by the Bi-rich phase, Bi_2O_3). Figure 17a (600 °C, Ni-Bi; spot A, Table 3.3) shows the entrapment of Bi-rich compounds in the formed tribolayer after 600 °C. Nevertheless, at 600 °C, Ni-Bi specimens (along with reference) show a rise in CoF value to ~ 1.0 ; which was supposed to occur due to the high wear of the counterbody pin (Publication II). Besides, a fair amount of counterbody material was detected on the wear track (tribolayer) of Ni-Bi specimen after sliding at 400 and 600 °C (Figure 17a, spot B, Table 3.3; and Figure 17b), which further supports the high wear of counterbody (resulting in material transfer) at this stage as shown in Figure 15c. Nevertheless, micropolishing and compaction of the tribo-oxide layer was the key mechanism of wear at 400 and 600 °C for the self-lubricating Ni-Bi samples. For more details, please refer to Publication II.

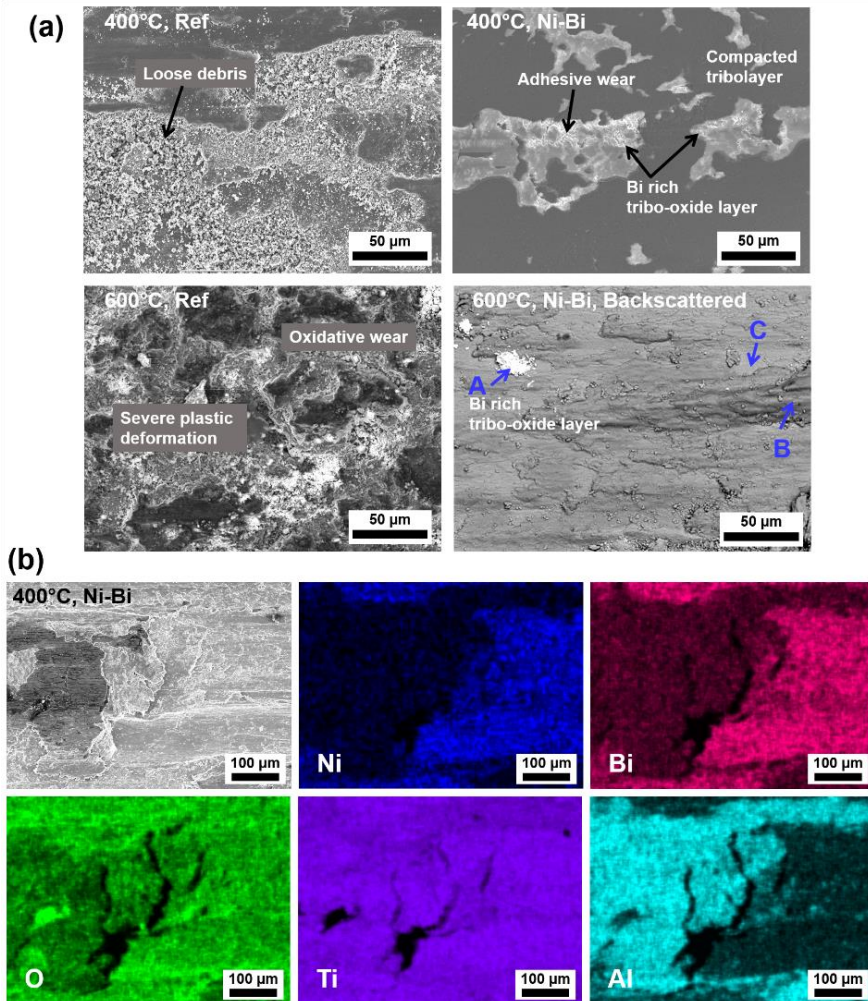


Figure 17: (a) SE and BE images of wear track for Ref and Ni-Bi samples after test at 400 and 600 °C sliding; and (b) EDS mapping of 400 °C wear track of Ni-Bi sample. Ti (moderately) and Al presence are contributed from the counterbody material. Bi spreads all over the plough mark resulting in lubrication during the test (*adapted from Publication II*).

Table 3.3. Chemical composition in wt% as evaluated by EDS for the spots labelled in Figure 17a at 600 °C, Ni-Bi (*adapted from Publication II*).

Spot	Chemical composition (wt%)						
	Ti	B	Ni	Bi	O	Al	V
A	12.8	0.9	39.2	40.9	6.0	0.2	-
B	79.0	0.5	0.3	0.2	7.6	9.5	2.9
C	83.8	4.4	0.4	0.8	10.3	0.3	-

As for the reference unmodified specimen, microcutting and delamination was common mechanism of wear at RT and 400 °C. Besides, no formation of tribo-layer or debris compaction was observed (unlike Ni-Bi). With an increase in sliding temperature to 600 °C, reference composite underwent severe oxidation and plastic deformation resulting in an unstable friction curve and a high wear. For more details, please refer Publication II.

It is to be noted that the current study reports an improved tribological performance of the designed material against a Ti-pin; which makes the research very important since, Ti-mating pairs are reported to perform worse during tribology, especially at HT. It is possible that if the current materials are tested against a better option (such as ceramic balls or such) the tribo-improvements might be enhanced.

3.3 System 3, NiCrBSi/Metal sulfide laser claddings

3.3.1. Design and thermodynamic phase analysis

The design of system 3 takes over to *objective 4*. Thermodynamic phase prediction in the NiCrBSi-metal sulfide laser cladding under thermal treatment was performed using Thermocalc software (utilizing TCFE9 database). The calculations were performed in the 3.64wt.%Cr-1.82wt.%Fe-87.8wt.%Ni-2.27wt.%Si-0.9wt.%B-2.64wt.%S-0.92wt.%Al (for NiCrBSi+10wt% Ni₃S₂) and 3.64wt.%Cr-1.82wt.%Fe-81.21wt.%Ni-2.27wt.%Si-0.9wt.%B-3.14wt.%S-6.1wt.%Cu-0.92wt.%A (for NiCrBSi+10wt% CuS) elementary systems. Due to the unavailability of sulfur and bismuth simultaneously in databases, the calculations for NiCrBSi+10wt% Bi₂S₃ laser cladding were not performed. In a 200–1600 °C interval, the calculations for both the systems with Ni₃S₂ and CuS showed the presence of Ni-based solid solution (with a minor amount with Si, Fe, and Al), Ni₃B, and Cr_xS_y as the major phases. Besides, the presence of Cu₂S at around 800 °C in the CuS added system was revealed. The positive occurrence of the high-temperature lubricant Cr_xS_y phase is predictable in all the systems under study.

3.3.2. Laser cladding and microstructure

The composite coatings were fabricated on a stainless steel substrate with preplaced mixed powders of NiCrBSi+10 wt% Ni₃S₂, CuS, or Bi₂S₃ (herein 10 Ni₃S₂; 10 CuS; and 10 Bi₂S₃ respectively) by laser cladding. The coatings demonstrate a compact, dense, and pore/crack-free microstructure. Figure 18 shows the cross-sectional optical microscope image of the as-deposited laser claddings. Upon a closer look at the optical and SEM images of the coatings, an interesting feature of dark areas spread uniformly across the sulfide-added claddings microstructure was noticed (Figure 19a, b, c, d). These dark areas or regions were inexistent for reference unmodified Ni-alloy cladding. EDS analysis (Figure 19d, Table 3.4) confirmed the darker areas to be rich in chromium (~50 wt.%) and sulfur (~39 wt.%) elements, along with a minor presence of manganese (possibly dissolved from the substrate steel). While, the coating matrix was majorly composed of nickel, iron, and chromium elements. Further, in the case of coating with 10 wt% Bi₂S₃, the dark areas encapsulated a bright area considerably rich in bismuth (~85 wt.%).

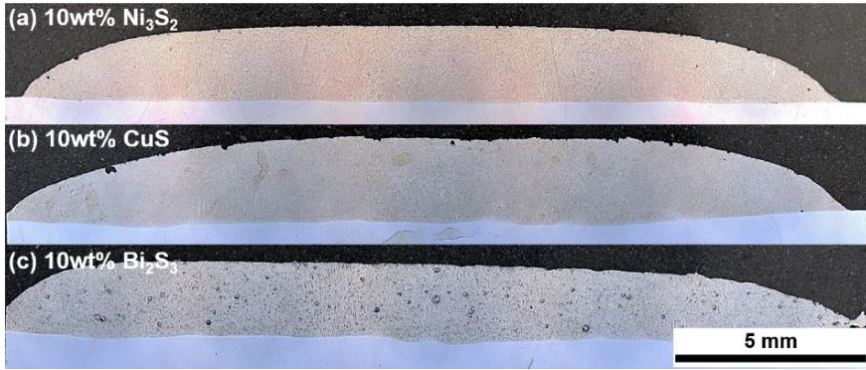


Figure 18: Cross-sectional optical microscope of as-deposited laser claddings with (a) 10wt% Ni_3S_2 ; (b) 10wt% CuS ; and (c) 10wt% Bi_2S_3 (Claddings produced at AC2T research GmbH).

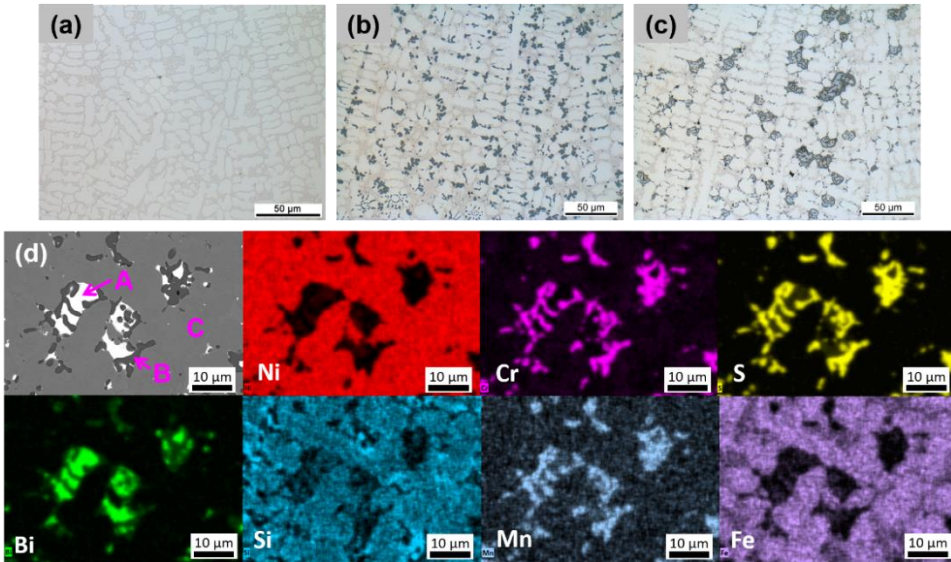


Figure 19: Optical image of as-deposited laser claddings (a) unmodified NiCrBSi ; (b) with Ni_3S_2 ; (c) with Bi_2S_3 ; (d) EDS analysis of cladding with Bi_2S_3 (Unpublished data).

Table 3.4. Chemical composition in wt% as evaluated by EDS for the spots labelled in Figure 19d.

Spot	Chemical composition (wt.%)						
	Ni	Cr	Si	Fe	Mn	Bi	S
A	10.2	0.5	0.1	0.6	-	87.9	0.7
B	1.8	54.0	-	0.1	3.0	1.6	39.5
C	78.3	4.2	2.3	15.2	-	-	-

Upon XRD analysis (Figure 20a), all the sulfide-added claddings demonstrate peaks belonging to Ni-based solution, Ni_3Fe , Cr_xS_y , NiS , and Ni_2B . The presence of a high concentration of lubricious Cr_xS_y (~16 wt.%) and NiS (~6 wt.%) compound in the sulfide-claddings aligns with the thermodynamic phase prediction by Thermocalc

software. Besides, previous studies have reported the formation of chromium sulfide compounds through thermal degradation of TMDs (in this case, laser cladding process) (Torres, 2022). It is assumed that copper or bismuth dissolved in the coating microstructure uniformly during the process of cladding.

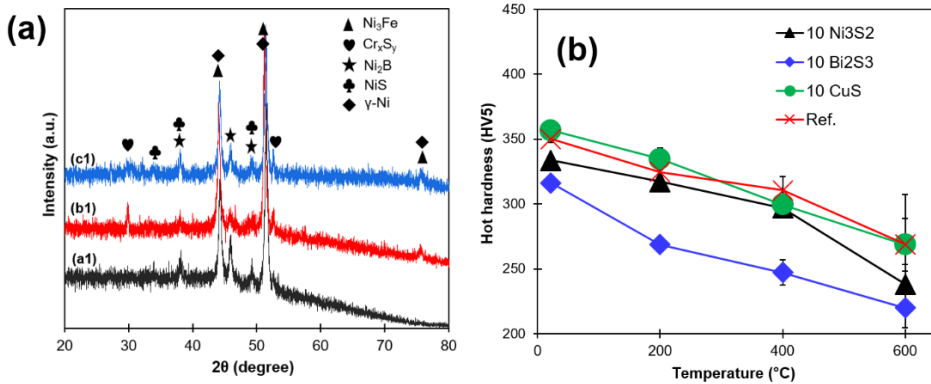


Figure 20: (a) XRD patterns of as-deposited laser claddings with Ni_3S_2 -a1, CuS -b1, Bi_2S_3 -c1; and (b) hot hardness of as-deposited laser claddings (Unpublished data).

Figure 20b plots the HT microhardness values (HV5) of the laser claddings. It is clear that the hardness of unmodified as well as sulfide-modified claddings decreased with the increase in temperature. However, unlike different steel grades where a sudden hardness fall was reported (Torres, 2016), the current claddings demonstrate a linear hardness decrease. The least hardness was seen for cladding with Bi_2S_3 with a 20 % decrease at all the measured temperatures. Besides, poor repeatability of results was recorded for all the laser claddings at 600 $^{\circ}C$ possibly due to increased ductility.

3.3.3. High temperature tribological studies

Upon fabrication of laser claddings of Ni alloy ($NiCrBSi$) with and without metal sulfides, the specimens were prepared for tribological testing (20 mm \times 20 mm \times 7 mm) and put under a reciprocating dry sliding test in a ball-on-plate configuration. AISI 52100 martensitic bearing steel balls (dia. of 10 mm and hardness of 873 ± 19 HV10) were selected as counterbody to imitate the environments of metal forming processes. The parameters of the test (Table 2.3) were selected as per the reported values in metal processing processes. Expected maximum contact pressures during the process was calculated to be 1.7 GPa at room temperature, supposing a Hertzian contact and no wear of the ball counterbody, by considering the thick coating as a bulk material.

Figure 21 shows the CoF curves for the unmodified Ni alloy (Ref.) and sulfide-modified claddings. A significant diminution in friction values of sulfide-claddings (by two times) in comparison to unmodified Ni-alloy is noticed at RT testing. The average CoF noted for 10 Ni_3S_2 , 10 CuS , and 10 Bi_2S_3 was noted close to ~ 0.55 , 0.58 , and 0.47 respectively whereas, for the unmodified Ni-alloy cladding the CoF value rose to ~ 1.2 . Besides, it is clear from Figure 22a that at RT sliding the unmodified Ni-alloy demonstrates a fluctuating CoF curve, unlike sulfide-claddings which demonstrated substantial stability in CoF curve. To add, where all the sulfide claddings demonstrated CoF steadiness after 50 s of running in, 10 Bi_2S_3 display no or very small running in coupled with the lowest friction among all laser claddings (i.e. ~ 0.45).

With an increase in testing temperature to 400 °C, all the claddings show a decrease in CoF value. However, similar to RT sliding all the sulfide-claddings reported a two-fold reduction in CoF in contrast to the reference Ni-alloy, of which 10 Bi₂S₃ again revealed the lowermost CoF i.e. ~0.43. At this stage, a steadily maintained CoF value until 200 s of testing was noticed, upon which a slow rise to ~0.55 was perceived for all the sulfide-claddings. In general, all the sulfide-claddings show a similar behavior at RT and 400 °C of sliding.

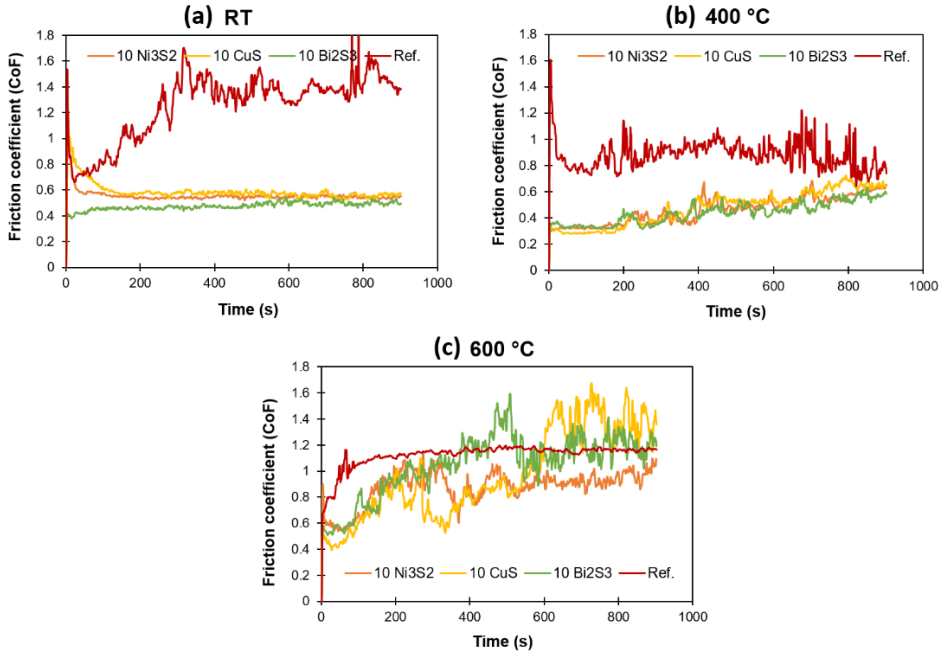


Figure 21: CoF curves for Ref. and sulfide-modified laser claddings underwent reciprocating sliding test against an AISI 52100 bearing balls at (a) RT; (b) 400 °C; and (c) 600 °C (**Unpublished data**).

At 600 °C, all the sulfide-claddings demonstrate a very unsteady friction (coupled with a long running in) with a continuous rise. At this stage, unmodified Ni-alloy showed the stablest but quite high CoF (~1.1). Among all the claddings, 10 Ni₃S₂ demonstrated the lowest CoF of ~0.87 (averaged).

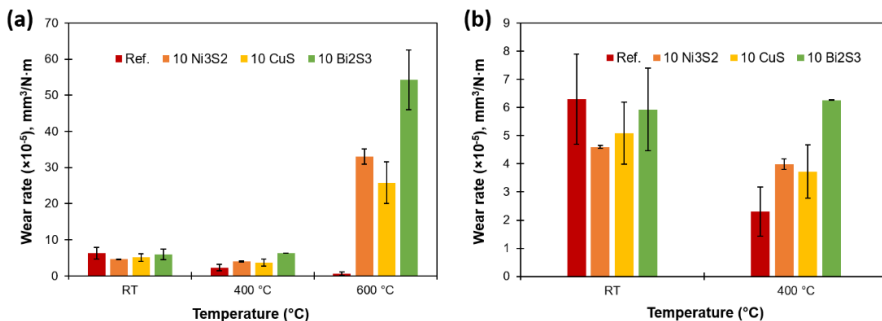


Figure 22: Wear rate for all the laser claddings (a) for RT, 400, and 600 °C; and (b) a closer look for RT and 400 °C (**Unpublished data**).

In regards to wear rate measurements (Figure 22), 10 Ni₃S₂ demonstrated the lowest wear rate at RT among all the claddings. However, with the rise in temperature to 400 and 600 °C, all the sulfide claddings demonstrate a higher wear in comparison to unmodified Ni-alloy. But, the enhancement in the wear rate of unmodified cladding at 400 °C was coupled with its high and unstable CoF (Figure 21b). Between the sulfide claddings, 10 Bi₂S₃ exhibited the highest wear rate at all the test temperatures. This supports the idea discussed in the section 4.3.2, that the presence of bismuth in the modified material aids in lubrication but fails to improve its wear resistance.

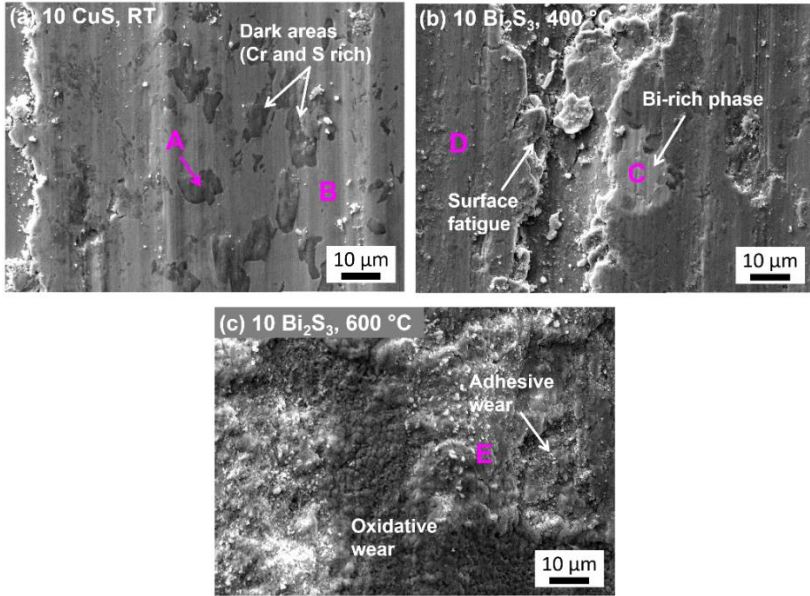


Figure 23: Wear track SEM images after the test at different temperatures. The respective laser cladding and temperature of the test are labelled (**Unpublished data**).

Figure 23 demonstrates the wear scar SEM images. Abrasive and adhesive mode of wear dominated at all the temperatures of sliding. However, at 600 °C, oxidative wear dominated. At RT and 400 °C, sulfide claddings demonstrate a significant spread of dark areas which were EDS-analysed to be rich in Cr and S- rich elements (Figure 23a, spot A, Table 3.5), and later XRD confirmed the presence of lubricious Cr_xS_y on the wear track (Figure 24). The existence of large amount of Cr_xS_y phases (of different stoichiometry) on the wear track confirms the self-lubrication mechanisms of cladding. Besides, evident formation of a tribolayer from wear debris compaction is believed to occur (Figure 23a, spot B; Figure 23d, spot D; Table 3.5). It is believed that at these stages, the relocated debris were compacted and later contributed to tribolayer (self-healing). However, the fact that tribolayer mainly consisted of materials (including lubricious Cr_xS_y phases) from cladding, demonstrated lubricity and offered reduced friction (Figure 23a, spot B; Figure 23d, spot D; Table 3.5). No counterbody material transfer was detected in the generated tribolayer at RT and 400 °C sliding. In the case of 10 Bi₂S₃, apart from Cr_xS_y phases, the existence of other solid-lubricants such as NiBi, Bi-rich phase is also detected after 400 °C sliding (XRD, Figure 24). Figure 25 shows the backscattered images of 400 °C wear track of self-lubricating sulfide claddings with their spot EDS analysis detailed in Table 3.5. Figure 25b shows a prevalent spread of the Bi-rich phase on the 10 Bi₂S₃ wear

track (Figure 25b, bright area, spot G, Table 3.5). Apart from abrasion, at RT and 400 °C testing, wear debris compaction/embedment resulting in tribolayer generation was the main mechanism of wear.

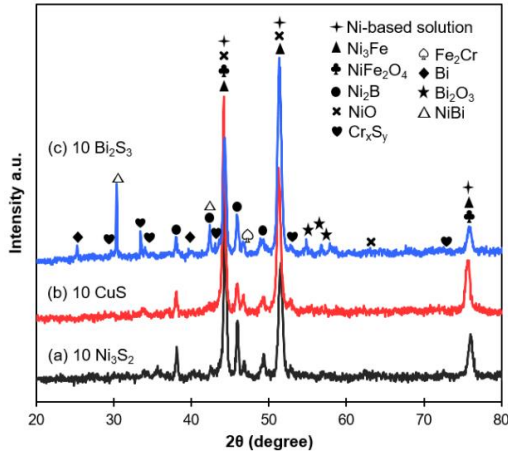


Figure 24: XRD patterns of the wear track after test at 400 °C for (a) 10 Ni₃S₂; (b) 10 CuS; and (c) 10 Bi₂S₃ (Unpublished data).

At 600 °C, the claddings demonstrate severe oxidation with limited (only for 10 Ni₃S₂) or no wear debris compaction/tribolayer formation. Moreover, patches of material removal point to the incidence of adhesive wear. At this stage, XRD detected a very low concentration of Cr_xS_y phases on the wear track (<2%), due to its possible oxidation. Besides, the oxides generated in this period show no cohesion featuring pores, and loose adherence to the surface (easily removed, high wear). Increased intensity of plastic deformation was noticed for the 10 CuS cladding wear track with significant bends/waviness (Figure 25c), which might have contributed in fluctuating CoF curve.

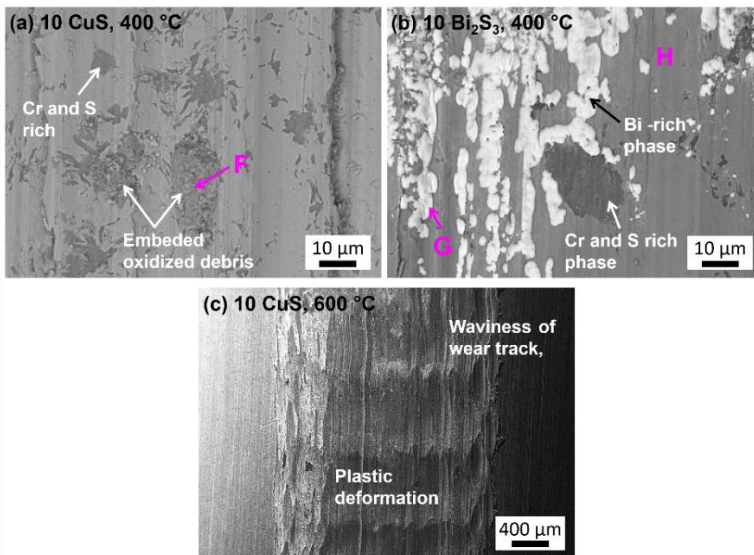


Figure 25: Backscattered image of wear track from (a) 10 CuS, 400 °C; (b) 10 Bi₂S₃, 400 °C; and (c) 10 CuS, 600 °C (Unpublished data).

Table 3.5. Chemical composition in wt% as evaluated by EDS for the spots labelled in Figure 23 and 25.

Spot	Chemical composition (wt%)							
	Ni	Cr	Si	S	Fe	Cu	Bi	O
A	40.96	38.33	4.01	11.19	2.40	3.11	-	-
B	79.50	1.75	0.31	2.62	9.29	6.33	-	0.2
C	17.45	0.04	-	-	0.39	-	82.12	-
D	75.90	4.93	2.49	1.51	12.40	-	2.77	-
E	41.17	1.94	1.79	0.34	5.31	-	27.34	22.11
F	51.87	5.42	1.62	1.94	6.01	4.38	-	28.76
G	37.20	0.83	0.39	-	2.63	-	56.89	2.06
H	84.0	2.82	2.33	0.24	7.59	-	0.9	2.12

In respects to reference Ni-alloy cladding, abrasion, and microscratching were the main wear modes at RT and 400 °C. At 600 °C, the transfer of oxidized wear debris from the counterbody was evident. For more details, please refer to ref. [63].

For the counterbody AISI 52100 steel balls sliding at RT and 400 °C, some degree of material transfer from the cladding surface was noticed. Tribopatches of Cr and S-rich elements along with Bi-rich (only for 10 Bi₂S₃) were identified on the counterbody surface. These tribopatches were believed to impart lubrication resulting in a friction reduction and wear of tribo-bodies. However, at 600 °C, significant oxidation of counterbody ball occurred. The uncompacted hard oxides resulted in third body generation, which might be linked to the instability of CoF curve of sulfide-claddings (Figure 21c). Figure 26 shows the SEM images of wear scars of counterbody ball.

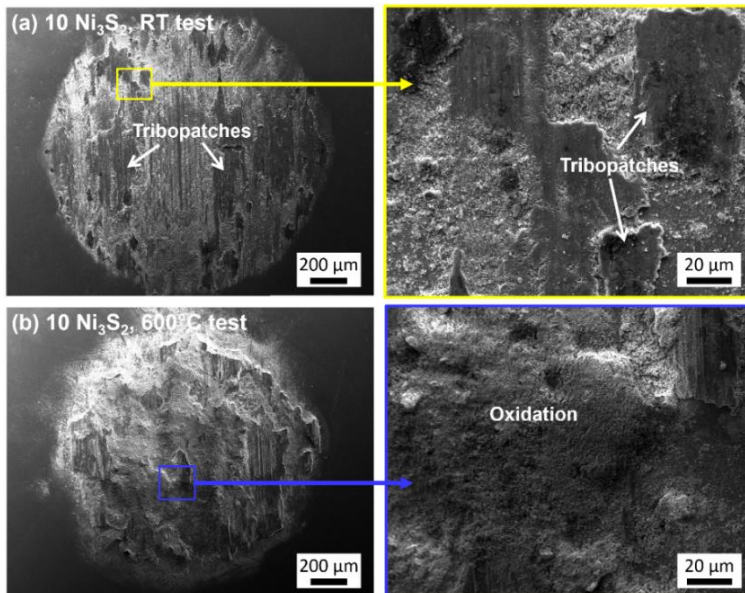


Figure 26: SEM images of wear scars on the counterbody AISI 52100 steel balls sliding against 10 Ni₃S₂ at (a) RT; and (b) 600 °C (**Unpublished data**).

3.3.4. Supplementary information (NiCrBSi/Ag and MoS₂ laser cladding)

In a study concerning the development of Ni- alloy self-lubricating claddings consisting of Ag/MoS₂ as solid lubricants it was seen that the addition of MoS₂ along with Ag contributed in a Ag encapsulation phenomena and its homogeneous distribution throughout the coating microstructure (Figure 27b, b1, b2). However, the addition of sole Ag resulted in the development of Ag-rich layer which was seen floating on the surface of the coating signifying agglomeration and inhomogeneous distribution of Ag in the developed coating (Figure 27a). Please see Figure 27 for more clarity.

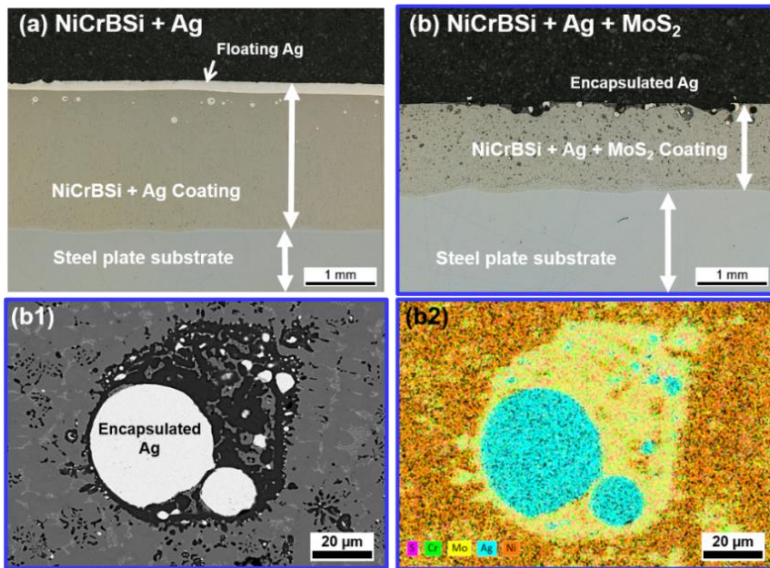


Figure 27: Cross-sectional SEM image of as-deposited coating on steel plate of (a) NiCrBSi + Ag showing thin layer of Ag floating (spread) on the coating surface; and (b) NiCrBSi + Ag + MoS₂ showing Ag-encapsulation aiding to its homogenous distribution in the coating microstructure (Unpublished data).

3.4 System 4, Ni-40 wt.% W (-hBN) SPS-ed composite

3.4.1. Design and thermodynamic phase analysis

For SHSed produced precursor 4, the thermodynamic phase calculation was made for the initial powders system i.e. 4NiO-WO₃-3.2Mg-3.2C (-2wt%hBN). The combustion synthesis was executed according to thermodynamic calculations bearing in mind the temperature of 4Ni-W alloy formation ($T_{ad} = 1100-1500$ °C) in the multi-element system (Figure 28a, b). The choice of T_{ad} was made to prohibit nickel melting during the SHS process. Nevertheless, the combustion temperature was around 150–200 °C higher than the adiabatic temperature (T_{ad}) due to the exothermic formation of the Ni-W intermetallic phases/solid solutions, in divergence to thermodynamic contemplation of merely the formation of individual metals. The introduction of hBN (2 wt%) reduced the combustion parameters by 200 °C and displayed the role of an inert diluent. The process was carried out at a pressure of 0.4 MPa to attain the joint reduction of oxides and to evade the evaporation of magnesium and tungsten oxides. For more details, please refer to Publication III.

Figure 28d demonstrates the SEM image of milled SHS-derived Ni-W-hBN powder. The SHS-derived powder demonstrate snowflake morphology of composite-particles. Generally, such types of SHS-derived composite powders (pre-sintered agglomerates of nanosize entities) exhibit an improved sinterability owing to high heating and cooling rates existing in exothermic combustion reactions. XRD analysis of SHS derived powders (Figure 28e) validates the desired chemical composition.

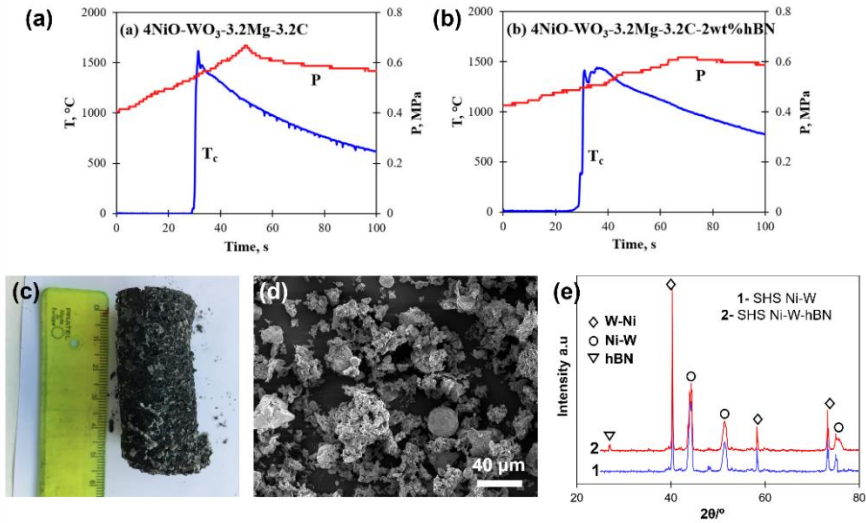


Figure 28: Combustion reaction thermograms of (a) 4NiO-WO₃-3.2Mg-3.2C; (b) 4NiO-WO₃-3.2Mg-3.2C-2wt%hBN mixtures; (c) SHS product; (d) SEM image of milled SHS-derived Ni-W-hBN; and (e) XRD patterns of SHS-derived powders (*adapted from Publication III*).

3.4.2. Sintering and microstructure

HEBM (Precursor 3) and SHSed (Precursor 4) powders were consolidated by means of SPS technique. Figure 29 shows the SEM image of sintered composite bulks. An impressive density and hardness were achieved in the sintered bulks, especially for those produced by SHS (Table. 4.6, hardness more than 4 times in comparison to pure Ni bulk ~110 HV). A comparison of density and hardness of produced composite with recent literature is available in Publication III.

Table 3.6. Relative density and hardness of Ni-40 wt.% W (-hBN) composites (*adapted from Publication III*).

Material	Process	Relative Density (%)	Hardness (HV10)
Pure Ni bulk	SPS	99.5	110
Ni-40 wt.% W (current work)	SHS + SPS	98.6	460 ±31
Ni-40 wt.% W-hBN (current work)	SHS + SPS	95.8	437 ±12
Ni-40 wt.% W (current work)	HEBM + SPS	98.9	284 ±10
Ni-40 wt.% W-hBN (current work)	HEBM + SPS	97.4	271 ±10

As per SEM images, it is clear that both processes (of precursors) result in a different microstructure. A much uniform distribution of phases is seen in SHS-processed composite in comparison to their HEBM counterparts. However, the existence of pores of different sizes is evident in hBN-containing composites. Their formation is linked to the reduced sinterability owing to hBN incorporation in the composites and further, hBN agglomeration may result in increasing the size of the pores. XRD of the composites produces via. both techniques demonstrated the peaks of intermetallic NiW along with carbides phases such as, WC, W_6Ni_6C and W_4Ni_2C . The formation of carbides is linked to the carbon diffusion from the graphite punch, die, or sheet used during SPS process.

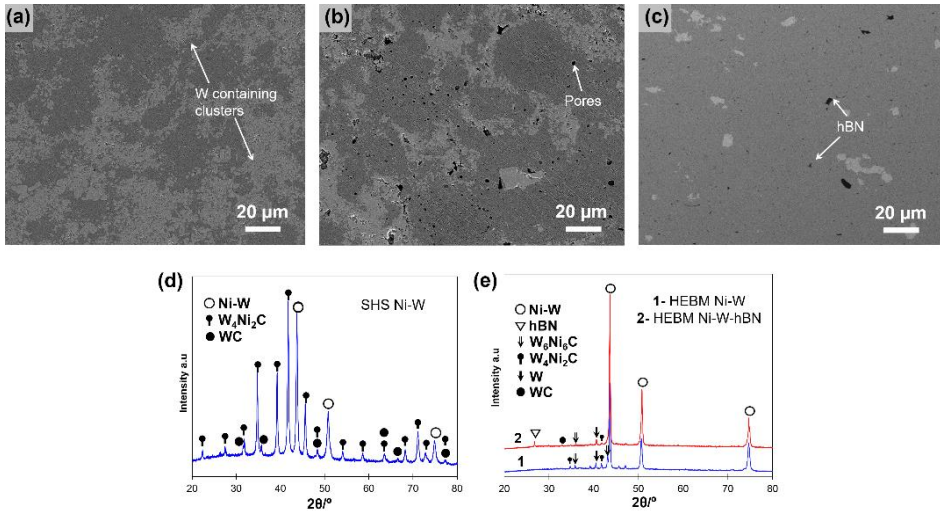


Figure 29: SEM images of SPS-derived composites (a) SHS-derived Ni-W; (b) SHS-derived Ni-W-hBN; (c) HEBM Ni-W-hBN; and XRD results of (d) SHS SPS-derived bulk; (e) HEBM SPS-derived bulks (**adapted from Publication III**).

SEM image for composites processed via. SHS and HEBM routes both, demonstrate the distribution of bright areas across the greyish Ni-rich (>65 wt.%) Ni-W solid solution. Upon EDS, the bright areas were confirmed to be rich in W-element (~84 wt.%). Since the existence of tungsten (W) was projected to be in different compounds including carbides, it was difficult to distinguish the tungsten in the matrix and its carbides. An interesting point to note is that the distribution of W-rich clusters/areas was found to be more homogeneously distributed in Ni-W alloy phase processed via SHS in comparison to HEBM-route. This can be linked to the reason behind the high hardness of composites produced via. SHS route in comparison to their counterparts from HEBM (Table 3.6).

3.4.3. High temperature tribological studies

Spark plasma sintered bulks of Ni-40 wt.% W (-2 wt.% hBN) produced via. HEBM and SHS route were put under unidirectional circular sliding ball-on-disc configuration against an Al_2O_3 ball (\varnothing 10 mm, hardness HV10 \approx 1450 and roughness $R_a = 0.02 \mu m$) as a counterbody at 800 °C (setup of test as shown in Figure 7). Details about the testing parameters are disclosed in Table 2.3, system 4. The results are reported in comparison with composites without hBN incorporation, produced via. respective routes.

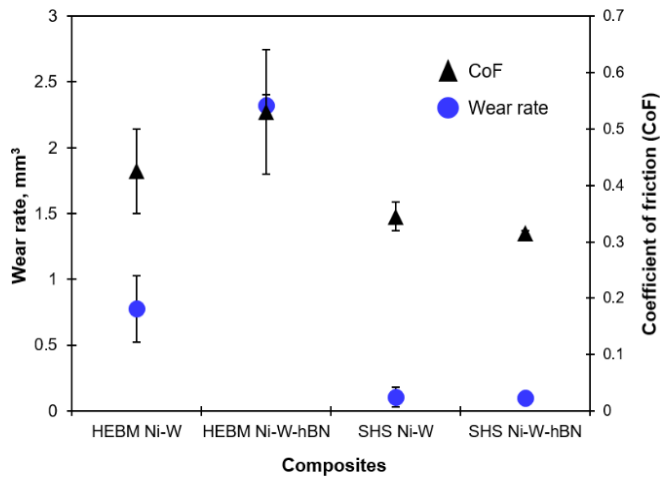


Figure 30: Average wear rate and CoF values of the composites after sliding at 800 °C.

A reduction in friction, as well as the wear rate of SHS-processed composites, is clearly seen in comparison to their HEBM counterparts (Figure 30). However, a significant drop in wear (~20 times) and friction value (~1.5 times) was seen for hBN-added composites processed via SHS route. Upon SEM study of the wear tracks (Figure 31), a wider track (~500 μm) was noticed for HEBM-processed composites in comparison to the ones processed via SHS-route (~300 μm). Besides, HEBM-processed composites demonstrated wider abrasive grooves. Abrasion led-wear debris on the HEBM samples may have led to intensified third body effect and higher material removal rate. Whereas, cyclic relocation and compaction of the wear debris (self-healing) resulted in protective tribolayer formation in the case of SHS-processed composites (Fig. 31c, d).

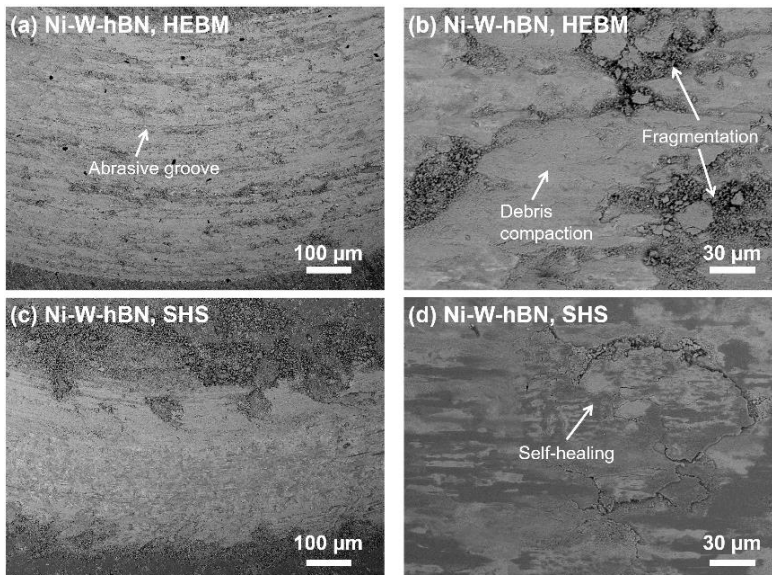


Figure 31: Wear track SEM images of the composites after test at 800 °C (a, b) HEBM Ni-W-hBN; and (c, d) SHS-derived Ni-W-hBN (**adapted from Publication III**).

4 Conclusions

Based on the outcomes of this work, the following main conclusions can be drawn:

- 1- For the first time, the dense (~99%), hard (~1300–1550 HV30), and thermodynamically stable Ti-TiB₂ composites with a high content of ceramic phase (50 and 88 wt.%) were produced using the energy-efficient approach of SPS and SHS. The composites show significant improvement in friction and wear at HT, especially in the range 700–900 °C (CoF: <0.18) owing to the in-situ formation of lubricious boric acid and a hard tribo-oxide layer. The generated tribo-oxide layer featured the highest load-bearing capability (maximum contact pressure = 1.4 GPa) at 800 °C without any significant damage. Abrasion and adhesion are the main mechanisms of wear at RT sliding, oxidative delamination wear at elevated temperature (up to 500 °C), and micropolishing of oxide surface at 700–900 °C.
- 2- A promising technique to evenly spread Ag or Bi throughout the composite/coating microstructure was found with combinational use of secondary reinforcement of MoS₂ or Ni respectively. Both the combinations i.e. Ag+MoS₂ or Ni+Bi resulted in the uniform distribution of soft metal though a unique 'encapsulation' phenomenon.
- 3- For the first time, bismuth as a 'green' HT solid lubricant (up to 600 °C) was developed. A promising method to disperse Bi in combination with Ni throughout the coating was proposed resulting in the development of a hard Bi-Ni-Ti-TiB_x functional surface with a homogeneously spread of Bi-rich phase encapsulating the hard TiB phase. A significant improvement in wear resistance against a Ti-alloy pin counterbody was noticed for the self-lubricating Ni-Bi specimens at the temperatures of 400 and 600 °C (13 and 4 times, respectively) in comparison to unmodified Ti-TiB₂. The developed materials exhibited a steady and stable friction evolution with a two-fold decrease in CoF value. The incorporation of bismuth into Ti-TiB₂ composite hints at the possibility of broadening the composite's lubrication range below 700 °C.
- 4- The successful laser cladding of wear-resistant NiCrBSi alloy in combination with metal sulfide of nickel (Ni₃S₂), copper (CuS), or bismuth (Bi₂S₃) was performed. The millimeter thick, compact, and pore-free coatings featured the formation of chromium sulfide by the thermal degradation of MS during laser cladding. The uniformly spread chromium sulfides have been revealed to be effective solid lubricants reducing friction up to 600 °C. In the case of Bi₂S₃ cladding, a unique microstructure signifying the homogeneous spread of Bi compounds encapsulated by chromium sulfide was revealed. Sulfide-added self-lubricating claddings resulted in 60 and 40% reduction in friction values of Ni-alloy at RT and 400 °C, respectively, Bi₂S₃ being the lowest ~0.45. The improved tribo-performance of sulfide claddings was owed to the existence of lubricious phases, and a prevailing debris relocation and embedment mechanism at the wear track. At 600 °C, due to an intensified oxidation of the tribo-bodies, the sulfide claddings show unstable friction and high wear rate. A high possibility of Ni₃S₂ as an HT solid lubricant was seen for manufacturing components that require powder feeding/high flowability.

- 5- Successful SPS of Ni-W (-hBN) composites from powder precursors obtained by (a) HEBM, and (b) SHS was carried out. Twice hard composites were obtained by SHS route in comparison to their high energy ball milling (HEBM) counterparts. Besides, lower CoF and wear rate values were perceived for the SHS-processed composites due to the phenomena of 'micro-polishing' and cyclic 'self-healing' of the surface during sliding.

hBN addition in the composites was evaluated to be detrimental. Not only it resulted in a compromised mechanical property (defects arising from poor sinterability), but also showed an ineffectiveness in its 'alleged' lubrication behavior.

5 Future work

The current works adds to the broader understanding of the chosen novel high-temperature solid-lubricating materials in terms of design, microstructure, tribology, and their tribo-improvement mechanisms. In order to broaden the understanding, the following further studies are proposed:

- 1- It is useful to explore the possibilities of depositing bismuth as thin coatings (PVD, CVD).
- 2- Laser deposition of metal sulfides using a powder feeder, as planned is expected.
- 3- Thermal and fatigue behavior of solid-lubricating materials need attention apart from their good tribological behavior.
- 4- The potential of 3D printing (or additive manufacturing) of solid lubricating materials is not reported yet, and might be an important area of work. Besides, the multi-layer deposition could be really beneficial in terms of gradient or synergetic lubrication.
- 5- One very important point could be studying HT solid lubricants which are not critical raw materials (CRM, as defined by EU).
- 6- Most studies on solid lubricating materials are based on sliding tests which are unable to comment on the dynamic mode of operation. A major lacking factor is atomistic- and nano-level analysis of such materials which might uncover the phenomena behind physical and chemical properties of surfaces, and/or sub-surfaces.
- 7- Modeling or numerical simulation of such materials at HT will definitely open doors to predictions in terms of the influence of inclusions, their morphology, chemistry and evolution of buried sliding surfaces, forecasting new inclusions, their reactions with the host matrix, the influence of the environment (cryogenics, vacuum), etc.
- 8- Studies regarding solid lubricant's surface energy could be useful to understand their adhesion mechanisms and whether they effect tribological process.

References

- Akhtar, S. S. (2021). A critical review on self-lubricating ceramic-composite cutting tools. *Ceramics International*, 47(15), 20745–20767.
- Antonov, M. (2012). Effect of temperature and load on three-body abrasion of cermets and steel. *Tribology International*, 46(1), 261–268.
- Aydinyan, S. (2021). SHS-Derived Powders by Reactions' Coupling as Primary Products for Subsequent Consolidation. *Materials*, 14(17), 5117.
- Aydinyan, S. (2022). The Influence of Thermal Dilution on the Microstructure Evolution of Some Combustion-Synthesized Refractory Ceramic Composites. *Crystals*, 12(1), 59.
- Ayyagari, A. V. (2020). Towards developing robust solid lubricant operable in multifarious environments. *Scientific Reports*, 10(1), 1–12.
- Balachander, N. (2013). Nanowire-filled polymer composites with ultrahigh thermal conductivity. *Applied Physics Letters*, 102(9), 093117.
- Benchakar, M. (2020). One MAX phase, different MXenes: A guideline to understand the crucial role of etching conditions on Ti₃C₂T_x surface chemistry. *Applied Surface Science*, 530, 147209.
- Bertrand, G. (1984). Morphology of oxide scales formed on titanium. *Oxidation of Metals*, 21(1), 1–19.
- Bowden, F. P. (2001). *The Friction and Lubrication of Solids*. Oxford University Press.
- Boyde, S. (2002). Green lubricants. Environmental benefits and impacts of lubrication. *Green Chemistry*, 4(4), 293–307.
- Chen, J. (2020). Tribological properties of h-BN matrix solid-lubricating composites under elevated temperatures. *Tribology International*, 148, 106333.
- Cora, Ö. N. (2012). Die wear in stamping of advanced high strength steels – Investigations on the effects of substrate material and hard-coatings. *Tribology International*, 52, 50–60.
- Cura, M. E. (2021). Mechanical and tribological properties of WO_{2.9} and ZrO₂ + WO_{2.9} composites studied by nanoindentation and reciprocating wear tests. *Wear*, 478–479, 203920.
- Deng, L. (2018). Experimental Evaluation of Galling Under Press Hardening Conditions. *Tribology Letters*, 66(3), 1–11.
- Donnet, C. (2004). Historical developments and new trends in tribological and solid lubricant coatings. *Surface and Coatings Technology*, 180–181, 76–84.
- Du, L. (2011). Preparation and wear performance of NiCr/Cr₃C₂–NiCr/hBN plasma sprayed composite coating. *Surface and Coatings Technology*, 205(12), 3722–3728.
- Efeoglu, I. (2008). Tribological characteristics of MoS₂–Nb solid lubricant film in different tribo-test conditions. *Surface and Coatings Technology*, 203(5–7), 766–770.
- Emmerlich, J. (2008). Micro and macroscale tribological behavior of epitaxial Ti₃SiC₂ thin films. *Wear*, 264(11–12), 914–919.
- Erkin Cura, M. (2013). Microstructure and tribological properties of pulsed electric current sintered alumina–zirconia nanocomposites with different solid lubricants. *Ceramics International*, 39(2), 2093–2105.
- Gassner, G. (2006). Magnéli phase formation of PVD Mo–N and W–N coatings. *Surface and Coatings Technology*, 201(6), 3335–3341.
- German, R. M. (2009). Review: Liquid phase sintering. *Journal of Materials Science*, 44(1), 1–39.

- Ghiotti, A. (2011). Tribological characteristics of high strength steel sheets under hot stamping conditions. *Journal of Materials Processing Technology*, 211(11), 1694–1700.
- Gonzalez-Rodriguez, P. (2016). Tribochemistry of Bismuth and Bismuth Salts for Solid Lubrication. *ACS Applied Materials and Interfaces*, 8(11), 7601–7606.
- Grützmaker, P. G. (2022). Solid lubricity of WS₂ and Bi₂S₃ coatings deposited by plasma spraying and air spraying. *Surface and Coatings Technology*, 446, 128772.
- Gupta, S. (2011). On the tribology of the MAX phases and their composites during dry sliding: A review. *Wear*, 271(9–10), 1878–1894.
- Hemmati, I. (2012). Dilution effects in laser cladding of Ni–Cr–B–Si–C hardfacing alloys. *Materials Letters*, 84, 69–72.
- Holmberg, K. (2017). Global energy consumption due to friction and wear in the mining industry. *Tribology International*, 115, 116–139.
- Kong, L. (2014). Friction and wear behavior of self-lubricating ZrO₂(Y₂O₃)–CaF₂–Mo–graphite composite from 20 °C to 1000 °C. *Ceramics International*, 40(7), 10787–10792.
- Kumar, R. (2020). Assessment of 3D printed steels and composites intended for wear applications in abrasive, dry or slurry erosive conditions. *International Journal of Refractory Metals and Hard Materials*, 86, 105126.
- Kumar, R. (2021). Hot Sliding Wear of 88 wt.% TiB–Ti Composite from SHS Produced Powders. *Materials*, 14(5), 1242.
- Kumar, R. (2020). Performance of polyimide and PTFE based composites under sliding, erosive and high stress abrasive conditions. *Tribology International*, 147, 106282.
- Kurzawa, A. (2020). Friction Mechanism Features of the Nickel-Based Composite Antifriction Materials at High Temperatures. *Coatings*, 10(5), 454.
- Lalas, C. (2006). An analytical model of the laser clad geometry. *The International Journal of Advanced Manufacturing Technology*, 32(1), 34–41.
- Li, S. (2003). Oxidation behavior of Ti₃SiC₂ at high temperature in air. *Materials Science and Engineering: A*, 341(1–2), 112–120.
- Lin, Z. J. (2007). High-temperature oxidation and hot corrosion of Cr₂AlC. *Acta Materialia*, 55(18), 6182–6191.
- Lince, J. R. (2020). Effective Application of Solid Lubricants in Spacecraft Mechanisms. *Lubricants*, 8(7), 74.
- Liu, C. (2022a). Tailoring Cu nano Bi self-lubricating alloy material by shift-speed ball milling flake powder metallurgy. *Journal of Alloys and Compounds*, 903, 163747.
- Liu, C. (2022b). Nano Bi Chemical Modification and Tribological Properties of Bi/SiO₂ Composite as Lubricating Oil Additives. *Tribology Letters*, 70(3), 1–15.
- Lou, M. (2021). Temperature-induced wear transition in ceramic-metal composites. *Acta Materialia*, 205, 116545.
- Ma, X. (2004). Thermodynamic assessment of the Ti–B system. *Journal of Alloys and Compounds*, 370(1–2), 149–158.
- Mamedov, V. (2013). Spark plasma sintering as advanced PM sintering method. *Powder Metallurgy*, 45(4), 322–328.
- Marian, M. (2020). Effective usage of 2D MXene nanosheets as solid lubricant – Influence of contact pressure and relative humidity. *Applied Surface Science*, 531, 147311.
- Mohammadi, A. V. (2021). The world of two-dimensional carbides and nitrides (MXenes). *Science*, 372(6547).

- Mozgovoy, S. (2018). Tribological Behavior of Tool Steel under Press Hardening Conditions Using Simulative Tests. *Journal of Tribology*, 140(1).
- Munagala, V. N. V. (2021). The role of metal powder properties on the tribology of cold sprayed Ti6Al4V-TiC metal matrix composites. *Surface and Coatings Technology*, 411, 126974.
- Naderi M. (2007). *Hot stamping of ultra high strength steels*. RWTH Aachen University, Dissertation / PhD Thesis.
- Pauschitz, A. (2008). Mechanisms of sliding wear of metals and alloys at elevated temperatures. *Tribology International*, 41(7), 584–602.
- Podgornik, B. (2015). Tribological behaviour and lubrication performance of hexagonal boron nitride (h-BN) as a replacement for graphite in aluminium forming. *Tribology International*, 81, 267–275.
- Prasad, Y. V. R. K. (2015). *Hot Working Guide: A Compendium of Processing Maps, Second Edition - Google Books*. ASM International.
- Prieto, G. (2022). Tribological properties of bismuth sulfide (Bi₂S₃) particles as grease additive for aluminum forming operations. *Wear*, 506–507, 204442.
- Radovic, M. (2002). Effect of temperature, strain rate and grain size on the mechanical response of Ti₃SiC₂ in tension. *Acta Materialia*, 50(6), 1297–1306.
- Rohr, O. (2002). Bismuth – the new ecologically green metal for modern lubricating engineering. *Industrial Lubrication and Tribology*, 54(4), 153–164.
- Rynio, C. (2014). The evolution of tribolayers during high temperature sliding wear. *Wear*, 315(1–2), 1–10.
- Sabahi Namini, A. (2019). Effect of TiB₂ addition on the elevated temperature tribological behavior of spark plasma sintered Ti matrix composite. *Composites Part B: Engineering*, 172, 271–280.
- Sergejev, F. (2006). Comparative study on indentation fracture toughness measurements of cemented carbides. *Proc. Estonian Acad. Sci. Eng*, 12, 388–398.
- Sliney, H. E. (1982). Solid lubricant materials for high temperatures—a review. *Tribology International*, 15(5), 303–315.
- Sliney, H. E. (2008). Fluoride Solid Lubricants for Extreme Temperatures and Corrosive Environments. <http://Dx.Doi.Org/10.1080/05698196508972103>, 8(4), 307–322.
- Souchet, A. (2005). Tribological duality of Ti₃SiC₂. *Tribology Letters*, 18(3), 341–352.
- Sun, H. (2022). Tribological characteristic of atmospheric plasma sprayed NiAl coatings with addition of nanostructured MoO₃/Bi₂O₃ binary oxides as high temperature lubricant. *Journal of Materials Research and Technology*, 17, 1662–1671.
- Sun, H. (2021). Effect of adding soft Bi₂O₃ on structural modification and tribological regulation of Ni-5 wt% Al composite coating in wide temperatures range. *Surface and Coatings Technology*, 405, 126517.
- Torres, H. (2022). Tribological performance of iron- and nickel-base self-lubricating claddings containing metal sulfides at high temperature. *Friction* 2022, 1–17.
- Torres, H. (2022). Compatibility of graphite, hBN and graphene with self-lubricating coatings and tool steel for high temperature aluminium forming. *Wear*, 490–491, 204187.
- Torres, H. (2017). Tribological behaviour of self-lubricating materials at high temperatures. *International Materials Reviews*, 63(5), 309–340.
- Torres, H. (2018). Microstructural design of self-lubricating laser claddings for use in high temperature sliding applications. *Surface and Coatings Technology*, 337, 24–34.

- Torres, H. (2016). High temperature hardness of steels and iron-based alloys. *Materials Science and Engineering: A*, 671, 170–181.
- Torres, H. (2018). Self-lubricating laser claddings for reducing friction and wear from room temperature to 600 °C. *Wear*, 408–409, 22–33.
- Toyserkani, E. (2004). *Laser Cladding*.
- Vilar, R. (1999). Laser cladding. *Journal of Laser Applications*, 11(2), 64.
- Wadsley, A. D. (2015). 12: Modern Structural Inorganic Chemistry (1958). *The Liversidge Research Lectures: The Royal Society of NSW Series 1931–2000*, 12. <https://openjournals.library.sydney.edu.au/LIV/article/view/9133>
- Wang, H. H. (2020). Repair of SiC coating on carbon/carbon composites by laser cladding technique. *Ceramics International*, 46(11), 19537–19544.
- Wyatt, B. C. (2021). 2D MXenes: Tunable Mechanical and Tribological Properties. *Advanced Materials*, 33(17), 2007973.
- Yang, N. (2011). Bismuth: environmental pollution and health effects. *Encyclopedia of Environmental Health*, 414.
- Zhang, S. (2008). Friction and wear behavior of laser cladding Ni/hBN self-lubricating composite coating. *Materials Science and Engineering: A*, 491(1–2), 47–54.
- Zhen, T. (2005). Compressive creep of fine and coarse-grained T3SiC2 in air in the 1100–1300 °C temperature range. *Acta Materialia*, 53(19), 4963–4973.
- Zhu, X. (2019). High-Temperature Friction and Wear Properties of NiCr/hBN Self-Lubricating Composites. *Metals*, 9(3), 356.

Acknowledgements

And finally it's a wrap (*inhales deeply*) ... learning of vast things while holding onto the small ones is what this journey has been all about. More than dozens of remarkable people have joined hands to make this Ph.D. work meaningful.

I am sincerely indebted to my supervisor Dr. Maksim Antonov, Head of Tribology and Material Testing Laboratory for showing me the world of tribology, and beyond tribology. His constant encouragement has always supported me in smoothly riding the uphill of my Ph.D. journey. Special thanks to my co-supervisor Prof. Irina Hussainova for involving and guiding me in projects which brought to the development of this thesis. She not only assisted me to come up with the thesis title but, also morally supported me and gave me the liberty to go on through the demanding times of thesis writing.

I am extremely thankful to many of my colleagues at AC2T research GmbH and especially to Dr. Markus Varga who made my visit to the center possible on very quick notice. His tremendous support in smoothly flowing the research works is highly appreciated. I express my deepest gratitude to my advisor Dr. Manel Rodriguez Ripoll whose immense guidance added to my understanding of several aspects of solid lubricants and further contributed to the building of this thesis. Additional special thanks to Dr. Hector Torres for helping with powder precursors and counterbody preparation, Kurt Pichelbauer for his guidance and fruitful discussions regarding laser cladding, Dr. Christian Tomastik for always being a savior and exceedingly helpful regarding SEM uses and materials' microstructural discussions, sometimes on a very quick request. Markus Premauer, Arpad Török, Norbert Nagy for helping with EBSD, hot hardness measurements and sample preparations. I would also like to thank Dr. Ewald Badisch and Dr. Andreas Pauschitz for their constructive feedback during my presentations and for creating an amazingly warm atmosphere at the center. Very personal thanks to my splendid officemate and a great friend and of course an Everest-return, Dr. Guido Boidi who for some reason appreciated me for every small thing I did at the center; I hope someday we trek the Himalayas as planned.

Special thanks to Dr. Piotr Klimczyk from Łukasiewicz Research Network- KIT, Poland for a very warm tie-up we held during the project "DURACER" and "DuplexCER" which surely has been a time of great learning and few outstanding research outcomes.

The highs and lows of my Ph.D. would have been an insurmountable challenge if not for my lovely labmates and later my dearest Tatevik and Mansoureh. While Tatev managed to escape to Canada, she always filled her absence without asking and offered her never-ending support to me. Special thanks to Nikhil paaji, Ramin, Yaroslav, Abrar paaji, Javad, Le, Jallouli, and Sibel for their warmest support and for either knowingly or unknowingly adding to my doctoral process. Appreciation for a few amazing super colleagues Roman, Sofiya, and Rocio who found time for me in their busy schedules to review, and assist in the research papers that made this thesis possible. If only I had a team like this, a second Ph.D. would indeed be a laidback exciting journey.

Sincere thanks to all the people from the Department of Mechanical and Industrial Engineering, and TalTech as a whole who put their effort into my smooth study and transition to a Ph.D.

Among a few notable mentions who inspired me in many ways, Dr. CP Paul is a must mention, who showed me the world of research and Additive Manufacturing; in fact, working at the Department of Atomic Energy, India was truly an incredible bend in my life and the main motivation for my Ph.D. studies. My best colleagues at PSIT Kanpur,

LK Mishra and DP Singh, whose abundant sources of energy and positivity constantly reminded me to live life to the fullest given the circumstances.

I would like to profoundly thank a few amazing people I met out of my work, who contributed to some lifelong cherished memories during this period. Among them, Maarja, Der, Olesya, Marko, Manu bhaiya, and Susmita di deserve a special place.

Thank you is a small word but love to my one in million very old friends, who are nothing less than a family and have always been there to cheer me up, travel the world, and try new adventures. Renu, Pushp, and Anurag deserve to be on this list. Thank you for making me a better man.

And finally, I finish with my home, India, where the prime source of energy comes from, my family. I truly have an amazing family, distinctive in some ways, nevertheless, their support has been unconditional all these years. They gave up on several things to make me what I am, including their wish for us to be together all these years I stayed abroad. Watching them grow old from afar has demanded a major strength in me. Rakhi, my younger sister completed her studies and got her first job as a Doctor of Surgery during my days of Ph.D., and since then she has been scheduling a month-long vacation around Europe. I hope after all this Ph.D. work; we can get back to planning that.

The current research work was funded by the Estonian Ministry of Education and Research, and by the Estonian Science Foundation under project nos. PRG643, PSG220, and M-ERA.Net projects (“DURACER” 18012, “DuplexCER” and “HOTselflub” MOBERA18 N.20097582-CA). Besides, received partial funding from ASTRA “TUT Institutional Development Programme for 2016–2022” Graduate School of Functional Materials and Technologies (2014-2020.4.01.16-0032). Financial support from Education and Youth Board (Harno), Estonia under Dora Plus mobility is highly acknowledged for attending scientific conferences, and other research visits.

A part of this work was funded by the “Austrian COMET-Programme” (Project InTribology, no. 872176) under the scope of K2 InTribology and was developed in collaboration with the “Excellence Centre of Tribology” (AC2T research GmbH).

RAHUL KUMAR
06 October 2022
TALLINN

Abstract

Development of solid lubricated composites for high-temperature tribological applications

The efficiency, performance, and reliability of mechanical systems at elevated temperatures are often compromised due to the temperature-dependent friction and wear characteristics of contacting solid surfaces. Wear-led degradation of materials at this stage might result in catastrophic failure and a huge economic loss. As one of the many factors that influence wear, temperatures affect wear behavior largely by altering materials' mechanical strength, adhesion property, oxidation kinetics, etc. The major mechanisms of wear playing a role in this period are highly dependent to the changes in microstructure.

The conventional approach to minimizing friction and wear through the use of liquid-based lubricants is limited by temperatures, as they rapidly decompose, volatilize, or mitigate at temperatures beyond 300 °C resulting in compromised lubrication. Besides, their harmful effect on the environment and human health (carcinogens) raises a serious concern. To add, liquid-based lubricants are often problematic when cleanliness (e.g. optical or electrically conductive surfaces), or a complex installment configuration is involved (e.g. space, gravity-dependent).

Solid-based lubricants have shown promising growth in this regard. Their ability to offer lubricity at a wide range of temperatures (up to 1000 °C), accompanied by good thermal and chemical stability, excellent dimensional steadiness necessary to achieve finishing with high precision during metal-processing, etc. have escalated their demand in the field of tribology.

Current research is focused on the design and production of novel solid lubricated composites (and coatings) accompanied by their microstructural, mechanical, and high-temperature tribological analysis. The production of self-lubricating materials is carried out using spark plasma sintering (SPS), self-propagating high-temperature synthesis (SHS), laser metal deposition, or laser cladding (surface coatings). Phase and microstructural prediction/analysis are accomplished using advanced characterization techniques (Thermocalc software, SEM-EDS, XRD, Raman spectroscopy, etc.). Sliding wear studies are made from room temperature up to 900 °C.

For the first time, a Ti-TiB₂ self-lubricating composite with a significantly high concentration of ceramic phase (50 and 88 wt.%) was produced using an energy-efficient sintering technique of SPS from (a) mechanical mixed powders, and (b) SHS-ed powder. The composites obtained a significant hardness (~1300–1550 HV30) with a close to defect-free microstructure. A major reduction in friction and wear values were noted at 700–900 °C. The tribo-improvement of the composites was owed to the development of a hard, substrate-adherent, glazed (lubricious) tribo-oxide layer rich in rutile-TiO₂ and boric acid. The reliable tribo-oxide layer developed at 800 °C showed an excellent load-bearing capability (up to 26 N, contact pressure = 1.4 GPa). To add, SHS was recognized as a promising method for the production of composite powder precursors with a high content of ceramic phase (i.e. TiB content of 88 wt.%).

The potential of 'environmentally friendly' bismuth (Bi) as a high-temperature (up to 600 °C) solid lubricant was revealed for the first time. A novel method to homogeneously spread soft metals (such as Bi and Ag) in coating/surface microstructure through their combinational use with the other elements (or compounds) was demonstrated.

The developed hard, compact, and substrate-adherent self-lubricating coating/surface resulted in friction and wear improvement. At HT, a Bi-encapsulated lubricious tribolayer aided in friction reduction. Laser surface deposition of Ni-Bi powders on Ti-TiB₂ composite was shown to be effective in widening the lubrication range of composite below 700 °C.

Due to the limitation of solid-lubricants MoS₂ and WS₂ to be used in powder feeding systems and deposition-based consolidation thereof (large-scale production); metal sulfides (MS) of nickel (Ni₃S₂), copper (CuS), and bismuth (Bi₂S₃) were mechanically and tribologically (as HT-600 °C solid-lubricant) explored as a replacement. The millimeter-thick developed laser-clad coatings of wear-resistant NiCrBSi+10 wt.% MS demonstrated a compact, defect-free, and substrate-adherent nature. The sulfide addition to the Ni-alloy resulted in the formation of chromium sulfide compound by the thermal degradation of MS during laser cladding. Besides, a reduction in friction values by 60 and 40 % of Ni-alloy at RT and 400 °C respectively was noted, Bi₂S₃ being the best (~0.4). The improvement in the tribological behavior of sulfide claddings was owed to the existence of lubricious phases in their microstructure, and a prevalent 'self-healing' mechanism (cyclic wear debris compaction and embedment).

An effort was made to produce an hBN-based self-lubricating composite using SPS of powders obtained from (a) high-energy ball milling, and (b) SHS. In both cases, the addition of hBN led to no significant improvement in friction or wear. Moreover, hBN addition led to poor sinterability of bulks featuring porosity, hBN agglomeration, and a drop in hardness (in comparison to their HEBM counterparts). On the other hand, SHS was recognized as a competent method to produce composite-powders and sintered bulks thereof, resulting in improved hardness and tribo-behavior.

Keywords: *Solid lubricant; Self-lubrication; Titanium; Bismuth; Chromium sulfide; Composite; Laser cladding; High temperature; Tribology*

Lühikokkuvõte

Tahkmäärdega komposiitide väljatöötamine kõrgtemperatuurseteks triborakendusteks

Mehaaniliste süsteemide tõhusus, jõudlus ja töökindlus kõrgetel temperatuuridel on sageli ohustatud kontaktis olevate tahkete pindade temperatuurist sõltuvate hõõrde- ja kulumisomadustega. Materjalide kulumisest tingitud lagunemine võib selles etapis põhjustada katastroofilisi tõrkeid ja tohutut majanduslikku kahju. Ühena paljudest kulumist mõjutavatest teguritest mõjutavad temperatuurid kulumiskäitumist suuresti, muutes materjalide mehaanilist tugevust, nakkeomadusi, oksüdatsioonikineetikat jne. Peamised sel perioodil rolli mängivad kulumismehhanismid sõltuvad suuresti muutustest mikrostruktuuris.

Tavapärane lähenemine hõõrdumise ja kulumise vähendamiseks vedelaid määrdeaineid kasutades on piiratud temperatuuridega, kuna need lagunevad kiirelt, lenduvad või nende omadused vähenevad temperatuuridel üle 300 °C, mille tulemuseks on halvenenud määrimine. Lisaks tekitab tõsist muret nende kahjulik mõju keskkonnale ja inimeste tervisele (kantserogeenid). Lisaks, on vedelmäärdeid sageli problemaatilised, kui tegemist on puhtusenõuetega (nt optilised või elektrit juhtivad pinnad) või keeruka paigalduskonfiguratsiooniga (nt maailmaruum, raskusjõumõju).

Tahked määrdeained on selles osas näidanud paljulubavat potentsiaali. Nende võime pakkuda määrdevõimet laias temperatuurivahemikus (kuni 1000 °C), millega kaasneb hea termiline ja keemiline stabiilsus, suurepärase mõõtmete püsivus, mis on vajalik metalli töötlemisel suure täpsusega lõppoperatsioonidel jne, on suurendanud nende nõudlust triboloogia valdkonnas.

Käesolev uuring on keskendunud uudsete tahkmäärdega komposiitide (ja pinnete) väljatöötamisele ja tootmisele koos nende mikrostruktuurse, mehaanilise ja kõrgtemperatuurse triboloogilise analüüsiga. Isemäärduvate materjalide tootmisel kasutatakse säde-plasma paagutamist (SPS), iselevikõrgtemperatuursünteesi (SHS), metalli lasersulatust või laserpealesulatust (pinnakatted). Faasi- ja mikrostruktuurianalüüs viiakse läbi kaasaegsete karakteriseerimismeetodite (Thermocalc tarkvara, SEM-EDS, XRD, Raman spektroskoopia jne) abil. Hõõrdkulumise uuringuid tehti temperatuurivahemikus toatemperatuurist kuni 900 °C.

Esmakordselt toodeti Ti-TiB₂ isemäärevat komposiiti märkimisväärselt kõrge keraamilise faasi sisaldusega (50 ja 88 massiprotsenti), kasutades SPS-i energiatõhusat paagutusmeetodit (a) mehaaniliselt segatud ja (b) SHS meetodiga saadud pulbrist. Komposiidid omandasid märkimisväärse kõvaduse (~1300-1550 HV30) ja peaaegu defektideta mikrostruktuuri. 700–900 °C juures täheldati hõõrdumise ja kulumise olulist vähenemist. Komposiitide tribo-iseparandusvõime tulenes kõva, aluspinnaga hästi nakkuva, glasuuritud (määritava toimega) tribooksiidikihi, mis oli rikas rutiil (TiO₂) ja boorhappe poolest, moodustumisest. 800 °C juures moodustunud töökindel tribooksiidikiht näitas suurepärase kandevõimet (kuni 26 N, kontaktsurve = 1,4 GPa). Lisaks tunnistati SHS paljulubavaks meetodiks kõrge keraamilise faasi sisaldusega (st TiB 88 massiprotsenti) komposiitpulbrist lähtematerjali tootmisel.

“Keskkonnasõbraliku” vismuti (Bi) potentsiaal kõrge temperatuuril (kuni 600 °C) töötava tahke määrdeainena selgitati esmakordselt. Näidati uutset meetodit pehmete metallide (nagu Bi ja Ag) homogeenseks jagunemiseks katte/pinna mikrostruktuuris nende kombineeritud kasutamise abil teiste elementidega (või ühenditega).

Väljatootatud kõva, kompaktna ja aluspinnaga nakkuv isemääriv kate/pind tagas hõõrdumis ja kulumisomaduste paranemise. Kõrgtemperatuuridel aitas hõõrdumist vähendada Bi sisaldusega pulbri abil valmistatud määrdekiht. Näidati, et Ni-Bi pulbrite lasersadestamine Ti-TiB₂ komposiidile oli tõhus komposiidi määrimisvahemiku laiendamisel temperatuuridel kuni 700 °C.

Nikli (Ni₃S₂), vase (CuS) ja vismuti (Bi₂S₃) metallsulfiide (MS) uuriti mehaaniliselt ja triboloogiliselt (tahke määrdeainena 600 °C juures), MoS₂ ja WS₂ pulbrite kasutuspiirangute (ummistumine) tõttu suurtootmise etteandestesüsteemides. Kulumiskindlast NiCrBSi+10 massiprotsenti metallsulfiidist valmistatud, millimeetri paksused, laseriga kaetud pinnad näitasid kompaktna, defektideta ja aluspinnaga nakkuvat olemust. Sulfiidi lisamine Ni-sulamile põhjustas kroomsulfiidühendi moodustumist metallsulfiidi termilisel lagunemisel laserpindamise protsessis. Lisaks täheldati Ni-sulami hõõrdenäitajate vähenemist vastavalt 60 ja 40% võrra toatemperatuuril ja 400 °C juures, kusjuures tähelepanuväärsemat vähenemist täheldati Bi₂S₃ puhul (~0,4). Sulfiidpinnete triboloogilise käitumise paranemine oli tingitud määrdefaaside olemasolust nende mikrostruktuuris ja prevaleerivast "iseparanemise" mehhanismist (tsükliline kulumisjäätmete tihendumine ja pindasurumine).

Tehti uuring hBN-põhise isemäärduva komposiitmaterjali tootmiseks, kasutades (a) kõrgenergeetilist kuuljahvatamise ja (b) SHS-meetodiga saadud pulbrite säde-plasma paagutamist. Mõlemal juhul ei toonud hBN lisamine kaasa märkimisväärset hõõrdumise ega kulumise paranemist. Veelgi enam, hBN-i lisamine põhjustas poorsust, hBN-i aglomeratsiooni ja kõvaduse langust (võrreldes kõrgenergeetilise jahvatamisega saadud materjalidega) ning halb paakuvust. Teiselt poolt tunnistati, et iselevikõrgtemperatuursüntees (SHS) on sobiv meetod komposiitpulbrite ja nendest paagutatud materjalide, mida iseloomustab parem kõvadus ja triboomadused, valmistamiseks.

Märksõnad: Tahke määrdeaine; Isemäärimine; titaan; vismut; kroomsulfiid; komposiit; Laserpealesulatus; Kõrgtemperatuur; Tribologia

List of publications not included in the thesis

- V **Kumar, R.**, Torres, H., Aydinyan, S., Antonov, M., Varga, M., Hussainova, I., Rodriguez Ripoll, M. (2022). Friction and wear behavior of Ni-based self-lubricating laser claddings containing sulfides of nickel (Ni₃S₂), copper (CuS), or bismuth (Bi₂S₃) at temperatures up to 600 °C. To be communicated.
- VI **Kumar, R.**, Antonov, M., Hussainova, I., Varga, M., Rodriguez Ripoll, M. (2023). Improved microstructure and tribology of Ag/MoS₂ containing self-lubricating laser cladding up to 800 °C owing to a unique encapsulation phenomenon. *Wear*, Selected for publishing from Nordtrib 2022 conference.
- VII **Kumar, R.**, Antonov, M., Klimczyk, P., Mikli, V., & Gomon, D. (2022). Effect of cBN content and additives on sliding and surface fatigue wear of spark plasma sintered Al₂O₃-cBN composites. *Wear*, 494, 204250.
- VIII Hussain, A., Podgursky, V., Goliandin, D., Antonov, M., **Kumar, R.**, Kamboj, N., ... & Krasnou, I. (2022). Tribological and circular economy aspects of polypropylene/cotton fibre hybrid composite. *Proceedings of the Estonian Academy of Sciences*, 71(2).
- IX **Kumar, R.**, Liu, L., Antonov, M., Ivanov, R., & Hussainova, I. (2021). Hot Sliding Wear of 88 wt.% TiB–Ti Composite from SHS Produced Powders. *Materials*, 14(5), 1242.
- X **Kumar, R.**, Antonov, M. (2021). Self-lubricating materials for extreme temperature tribo-applications. *Materials Today: Proceedings*, 44, 4583–4589.
- XI Liu, L., Ivanov, R., **Kumar, R.**, Minasyan, T., Antonov, M., & Hussainova, I. (2021). Functionally Gradient Ti6Al4V-TiB Composite Produced by Spark Plasma Sintering. In *IOP Conference Series: Materials Science and Engineering* (Vol. 1140, No. 1, p. 012004). IOP Publishing.
- XII Antonov, M., Zahavi, A., **Kumar, R.**, Tamre, M., & Klimczyk, P. (2021). Performance of Al₂O₃-CBN materials and perspective of using hyperspectral imaging during cutting tests. *Proceedings of the Estonian Academy of Sciences*, 70 (4), 524–532.
- XIII **Kumar, R.**, Antonov, M., Holovenko, Y., & Surzenkov, A. (2020). Erosive wear resistance of nature-inspired flexible materials. *Tribology Letters*, 68(2), 1–8.
- XIV **Kumar, R.**, Malaval, B., Antonov, M., & Zhao, G. (2020). Performance of polyimide and PTFE based composites under sliding, erosive and high stress abrasive conditions. *Tribology International*, 147, 106282.
- XV **Kumar, R.**, Antonov, M., Beste, U., & Goljandin, D. (2020). Assessment of 3D printed steels and composites intended for wear applications in abrasive, dry or slurry erosive conditions. *International Journal of Refractory Metals and Hard Materials*, 86, 105126.

Appendix

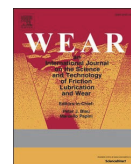
Publication I

Kumar, R., Antonov, M., Liu, L., & Hussainova, I. (2021). Sliding wear performance of in-situ spark plasma sintered Ti-TiB_w composite at temperatures up to 900 °C. *Wear*, 476, 203663.



Contents lists available at ScienceDirect

Wear

journal homepage: <http://www.elsevier.com/locate/wear>

Sliding wear performance of in-situ spark plasma sintered Ti-TiB_w composite at temperatures up to 900 °C

Rahul Kumar^a, Maksim Antonov^a, Le Liu^a, Irina Hussainova^{a,b,*}

^a Department of Mechanical & Industrial Engineering, Tallinn University of Technology, Tallinn, 19086, Estonia

^b ITMO University, Kronverkskiy 49, St, Petersburg, 197101, Russian Federation

ARTICLE INFO

Keywords:

Sliding wear
High-temperature
Ti-TiB_w composite
SPS

ABSTRACT

Although Ti-based composites find wide industrial applications, their tribological behaviour, especially at elevated and high temperatures, is not conclusively evaluated. In this work, a sliding wear performance of metal – ceramic composite of 50 wt%Ti–50 wt%TiB_w, which were in-situ produced by spark plasma sintering, was studied. Microstructural examination and X-ray diffraction analysis identified presence of two phases, Ti and TiB, and confirmed the formation of stable TiB whiskers-like grains (TiB_w) during reaction synthesis of Ti and TiB₂. Ball-on-plate dry sliding wear tests were performed against a 10 mm alumina ball under 5 N normal load with the sliding speed and distance of 0.1 ms⁻¹ and 1000 m, respectively. The tests were performed at RT and elevated temperatures of 300 °C, 500 °C, 700 °C, 800 °C and 900 °C. The worn surfaces were studied using scanning electron microscopy and 3D profilometry to understand the responsible wear mechanisms. Results have demonstrated significantly reduced wear rates of Ti-TiB_w composite as compared to reference pure Ti across all temperatures. The formation and the protective role of tribo-oxide layers on the surface of Ti-TiB_w composite during elevated temperature sliding is reported.

1. Introduction

Over the past few decades, titanium (Ti) based materials have matured at a large pace in various sectors including aviation, biomedical, chemical and structural industries due to their excellent combination of high strength, modulus and fracture toughness, biocompatibility and corrosion resistance [1]. Nevertheless, their poor wear resistance and relatively low hardness due to a low *c/a* ratio in a HCP unit cell limits their applicability in tribology related applications [2,3], especially at elevated and high temperatures (HT). Change in wear mechanism from mild to severe one, which is conditioned by the development of tribo-films, is a process of high probability during operation at the HT [4,5]. For many materials, including steels, the oxide-layers serve as protective layers against wear [6,7]. The tribo-layers developed on the surface of titanium alloys are reported to be thin, brittle, loosened and weakly adhered to a parent surface resulting in spallation during sliding [5,8,9]. Large difference in hardness between pure Ti substrate and developed surface oxides is reported to be a reason for non-adherent nature of tribo-layer [1]. Another possible reason owing to oxide delamination during room temperature (RT) sliding is a low value of Pilling-Bedworth ratio (PBR) [10], and therefore, a large lattice

mismatch between the layers. At temperatures beyond ~700 °C, a higher PBR value in Ti alloys results in scaling and oxides delamination [10,11]. However, the protective behavior of tribo-layer developed under sliding of Ti–6Al–4V and Ti–6.5Al–3.5Mo–1.5Zr–0.3Si alloys was reported in Refs. [5,8,12,13]; whereas, the formation of brittle titanium and vanadium oxides (such as TiO, TiO₂ and V₃O₄) over Ti–6Al–4V was demonstrated in Refs. [2,14]. Moreover, properties and performance of the tribo-layer are found to be highly dependent on temperature, sliding velocity and load applied [8,9,12]. Therefore, the role of surface tribo-layer during HT applications remains unclear and inconclusive for Ti-based composites.

The large number of works has been carried out to improve the wear performance of Ti-based composites exploiting a laser surface processing, coatings deposition, and reinforcements incorporation [15–20]. Most of these approaches does not result in a substantial enhancement of overall strength and hardness of materials [2,15,19]. Reinforcement with ceramic particles, such as TiN, TiC, TiB₂, TiB, B₄C, SiC and Al₂O₃, has demonstrated a great benefit in regards of improvement in mechanical as well as physical properties [1,2,17,18,21]. Titanium monoboride (TiB) is of the most widely used additive due to its excellent thermodynamic and chemical stability with Ti matrix, comparable

* Corresponding author. Department of Mechanical & Industrial Engineering, Tallinn University of Technology, Tallinn, 19086, Estonia.
E-mail address: irina.hussainova@taltech.ee (I. Hussainova).

<https://doi.org/10.1016/j.wear.2021.203663>

Received 3 September 2020; Received in revised form 3 January 2021; Accepted 6 January 2021

Available online 14 February 2021

0043-1648/© 2021 Elsevier B.V. All rights reserved.

densities of Ti and TiB, as well as a good interfacial bonding. Composites of Ti-TiB_w usually exhibit a high strength [1,3,21], low PBR and an overall biocompatibility.

Commonly, the reinforcements in metal matrix composites (MMCs) are prepared ex-situ and then added to the matrix. The other way is in-situ processing using exothermic reactions in solid-state processes or crystallization during solidification. More chemically and thermodynamically stable and homogeneous MMCs with a fine microstructure are demonstrated by the in-situ processed composites. The Gibbs free energy for the reaction between Ti and TiB₂ (i.e. Ti + TiB₂ → TiB) is of a negative value ($\Delta G \sim -154$ kJ/mol) [21,22], indicating thermodynamically instability of TiB₂ and Ti and, consequently, tendency to form TiB. Growth of needle-shaped TiB particles (whiskers-like) with a high aspect ratio (due to one dimensional growth along [010]) and well-developed interfacial bonds (due to no byproduct/intermediate phase) enhances stiffness, strength, and creep resistance of the composite [22]. In-situ formation of titanium boride whiskers (TiB_w) in titanium matrix demonstrates some benefits, such as constrained grain growth, increase in ultimate tensile strength and hardness as compared to the monolithic titanium [1,23,24]. In contrast, TiB₂ particles do not generate such a needle-like structure due to their two dimensional growth along $[1\bar{1}00]$ directions [22,23].

Several methods to fabricate titanium based bulk composites (TMCs) have come into picture in recent years including selective laser sintering [15,22], hot isostatic pressing [17,23], vacuum sintering [25], spark plasma sintering (SPS) or field-assisted sintering technique (FAST) [1, 24], etc. Very limited information is available on the microstructures and mechanical properties of the Ti-TiB_w composites fabricated by the SPS method. Unlike the conventional powder metallurgy (PM) techniques, no external heat supply is required for SPS; instead, a pulsed direct current is passed through the starting powders confined in an electrically conducting pressurized graphite die. The applied uniaxial pressure on the sample contributes to a high densification level of the products. SPS enables mixtures to be sintered at a lower temperature, as compared to the conventional PM sintering, within a relatively shorter time, which positively contribute to the dense fine-grained materials [26].

The 50 wt%Ti-50 wt%TiB_w ceramic-metal composite is an attractive candidate for a wide variety of applications not only at room temperature but also at elevated and high temperatures especially under conditions, where a good wear resistance is required. Although RT tribological performance of Ti-TiB composites have recently been extensively studied, very limited information is available on tribo-behavior of the composites at elevated temperatures. Consequently, the present paper aims at filling the existing gap and reporting on the tribological performance of the spark plasma sintered Ti-TiB_w composites identifying the role of the tribo-layer and wear associated mechanisms of materials damage. The transition from mild to severe wear is examined and variations in wear behavior at different temperatures are evaluated.

2. Experimental

2.1. Material processing

The powder mixture of Ti and TiB₂ was prepared by 2 h of mechanical rotation mixing of Ti (*Alfa Aesar*, Germany, particle size 0–50 μm) and TiB₂ (>99.5% *Alfa Aesar*, Germany, 0–44 μm) powders. The 50 wt%Ti-50 wt%TiB_w composites were fabricated by SPS (*FCT Systeme GmbH*, Germany) at temperature of 1500 °C in vacuum. The pressure of 35 MPa was applied under continuous application of electric current for a dwell time of 3 min.

The powder mixtures were loaded into a graphite mold of 25.4 mm in diameter and heated up to sintering temperature with a heating rate of 100 °C/min. The Ti-TiB_w composites are densified by means of solid

state sintering, which is a common pathway for production of high temperature ceramics and composites.

2.2. Microstructural characterization

After SPS, the sintered cylinders of 5 mm thickness and 25 mm diameter were polished to 1 μm finish using a Phoenix 4000 (*Buehler*) system and cleaned with acetone and ethylene alcohol.

Microstructural examination of the specimens was performed on mechanically polished and fractured surfaces using a scanning electron microscope (SEM, *Hitachi TM1000*) and a high-resolution scanning electron microscope (HR-SEM *Zeiss Merlin*) equipped with an energy dispersive spectrometer (EDS).

Phase identification was conducted by X-ray diffractometer (XRD, *Siemens Bruker D5005* X-ray analyzer with a Philips X'Pert PRO diffractometer, PANalytical, Netherlands) using Cu K α radiation (30 mA, 40 kV, $\lambda = 0.1542$ nm) in a $\theta - 2\theta^\circ$ scan with a step size of 0.02° and a count time of 0.4 s). Relative content of phases was estimated by Rietveld refinement method, which was performed by quantitative analysis of the crystalline phases detected by the corresponding XRD patterns.

2.3. Mechanical properties

The bulk density of composites was measured using Archimedes principle with a distilled water as the immersing medium using *Mettler Toledo ME204* balance with 0.1 mg accuracy. The density reported is the mean of 3 measurements.

The bulk Vickers hardness (HV30) was measured using *Indentec 5030* SKV unit with an indentation load of 30 kg for 10 s. The reported values are the mean of at least 5 indentations.

The indentation fracture toughness (IFT) was calculated from the length of radial cracks emanating from the corners of the indents following Palmqvist approach [27]. The load of 50 kgf for 10 s on the indenter resulted in quite well developed crack systems, which mitigate any surface effects of the indentation. Five equally spaced indents were recorded for each sample and values were averaged. The surface cracks initiated by the indenter were measured using optical microscopy (*Zeiss Discovery V20*) equipped with *AxioVision* software.

The surface roughness (R_a) was measured with the help of the *Mahr* perthometer, PGK 120, in contact mode.

2.4. Wear tests

A universal materials test device (UMT-2) supplied by CETR (*Bruker*) was employed for materials testing under dry circular sliding ball-on-plate configuration. Al₂O₃ Ø10 mm ball (*Redhill Precision, Czech Republic*) of HV10 \approx 1450 and $R_a = 0.02$ μm was used as a counterbody with an applied load of 5 N (0.51 kgf), sliding speed of 0.1 ms⁻¹ and distance of 1000 m (duration of sliding - 10000 s) with a radius of wear track of 4.5 mm. Tests were conducted at room and elevated temperatures of 300 °C, 500 °C, 700 °C and 800 °C. As the materials may be of interest for applications at a higher than titanium phase transformation temperatures of about 883 °C, the tests were also conducted at 900 °C. The heating rate was settled to 6 °C/min. Coefficient of friction (CoF) was recorded during sliding. CpTi was used as a reference material. After the tests, the surface of the wear tracks was examined under SEM and evaluated by means of the 3D profilometer. The profiles of worn surfaces were assessed with the help of *Bruker Contour GT-K0* + 3D profilometer to determine the depth, shape and volume of material removed (net missing volume).

The performed tests take into consideration the phenomena of running-in as well as the start-stop durations during the test imitating the situation in real field bending or forming operations due to required part loading-offloading or any other process interruption and possible time delay, for example, due to human factors, etc. The running-in is

described as an initial surface and subsurface conditioning process occurring at the interface of sliding bodies during sliding test [28]. The current work is represented by a non-conformal tribo-test; the test duration is long enough to reach a steady state wear regime [28,29]. Besides, the additional step of recalibrating of device during interruptions was made to increase the test precision during testing. Therefore, the tests consist of 20 periodic restarting during a single test to assess friction evolution during each period (start, running and stop). The other parameters, such as load and frequency, were unchanged during all periods.

The fractured cross-sections were studied to evaluate the nature of the developed tribo-oxide layers. An essential step to understand the strength of the tribo-oxide layer formed at elevated temperatures, the effect of varying load at temperatures of 700, 800 and 900 °C was explored. These tests were carried out for a short time (1 min) for each load until the sufficient (more than 20%) increase in CoF or unacceptable vibration was observed. The results are reported in terms of 'load bearing capability' of the material, which includes its ability to bear a high load in addition to impart a stable and low CoF. The complex of studied properties is an important criterion for design of a tool material for forming and forging applications.

3. Results and discussion

3.1. Microstructural analysis

Fig. 1a demonstrates a uniform distribution of whiskers-like TiB grains throughout the titanium matrix and absence of spurious phases or reaction products. The XRD patterns of the composite (Fig. 1b) identifies just a few peaks of TiB₂ confirming the presence of in-situ formed TiB phase together with semi-reacted TiB₂ particles in titanium matrix containing both α (alpha) and β (beta) phases of titanium. The parent HCP alpha microstructure dissolves into the BCC structured beta phase as temperature increases beyond ≈ 883 °C (allotropic transformation in Ti), leading to a decrease in alpha phase content with an increase temperature [30]. However, due to presence of some impurities of alpha

stabilizers (such as, Al, O, C) in the starting powder of CpTi, the α phase transformation is incomplete.

3.2. Mechanical properties

The density, hardness and indentation fracture toughness values of the spark plasma sintered Ti-TiB_w composites are reported in Table 1.

SEM inspections of the fractured specimen (Fig. 1c) reveal the relatively fine TiB particles, incorporation of which increases the extent of nucleation sites providing new interfaces between Ti and TiB for grain growth inhibition during the sintering process [24].

3.3. Tribological performance

3.3.1. Wear and CoF analysis

The effect of temperature on wear rates and CoF is summarized in Figs. 2 and 3, respectively. Figs. 4 and 5 show the SEM and 3D profilometry images of the worn surface. The XRD patterns of the composites tested at 700, 800 and 900 °C are given in Fig. 6.

It was found that the wear performance of the materials tested is significantly improved with the increase in temperatures; being particularly pronounced at temperatures of 700 °C and higher. To be accurate, the wear measurements at high temperatures is greatly influenced by the oxide layer formation. At 900 °C, due to considerable oxidation of the surface, differentiation between the wear track and the pristine surface was rather difficult due to a comparable roughness.

A significant drop in CoF is indicated for composites tested at

Table 1
Density, hardness and fracture toughness of SPSeD samples.

Material	Density, g·cm ⁻³	Relative Density	Hardness, HV30	Indentation Fracture Toughness, MPa·m ^{1/2}
Ti	4.443	98.6%	287 ± 33	–
Ti-TiB _w	4.487	99.4%	1324 ± 18	10.52

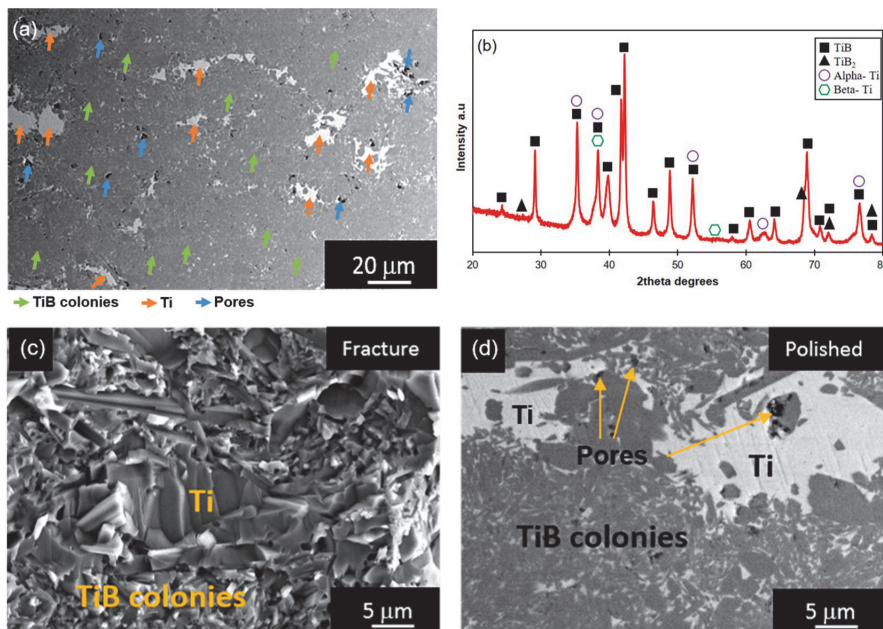


Fig. 1. Composite surface (a) SEM image; (b) XRD pattern; (c) SEM image of fractured surface; and (d) SEM image of polished surface.

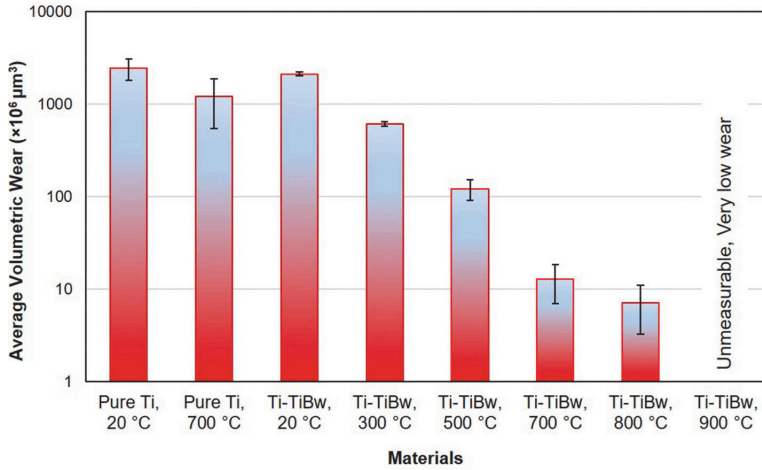


Fig. 2. The effect of temperature on wear rate of materials (logarithmic scale).

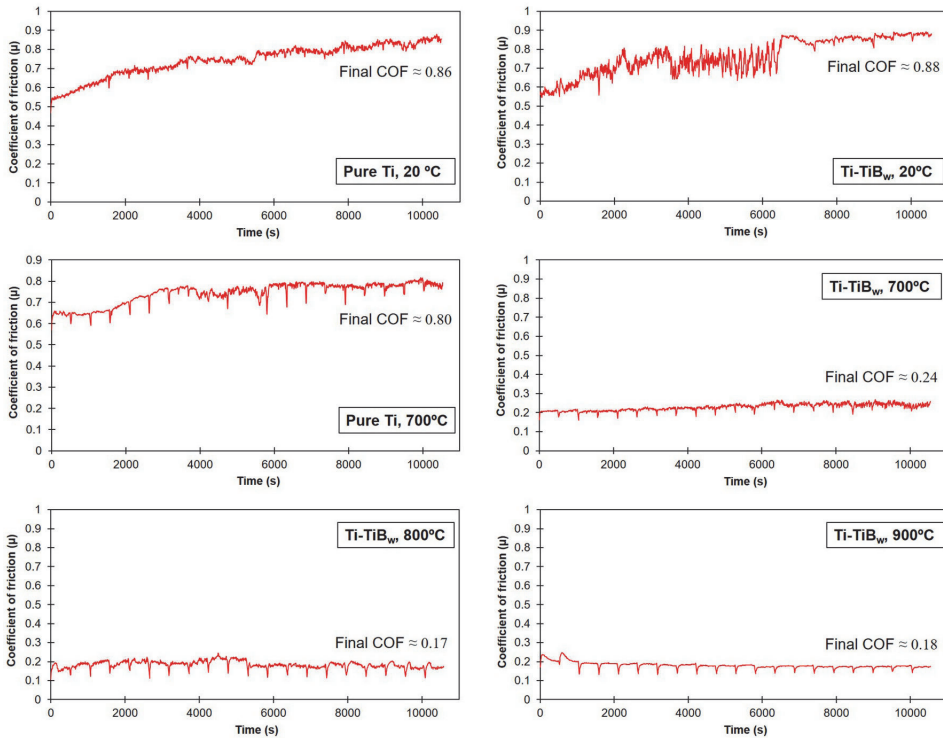


Fig. 3. Coefficient of friction of pure Ti and Ti-TiB_w composite at several test temperatures.

elevated temperatures. For the most of the cases, CoF stabilization was recorded during approximately 10 m of test run. However, at temperatures of 800 and 900 °C, the stabilization took a longer time of up to ≈50 m. High CoF in the case of pure Ti is conditioned by its lower hardness and instability of the tribo-layer [10,11,31]. Moreover, the wear debris or third bodies [32,33] accumulated during the tests might promote wear and fluctuation in CoF. Generated third bodies result in the high

localized stresses (stress concentration) and facilitate the removal of soft binder phase. However, at elevated temperatures, retained debris might be compacted and contribute to tribo-layer formation which is believed to reduce CoF. CoF fluctuation was also seen under RT composite sliding. At 300 and 500 °C, the SEM images (Fig. 4c) demonstrate a corrugation-like surface, which may be regarded as responsible for unstable CoF. The lowest friction was detected for composite tested at 800

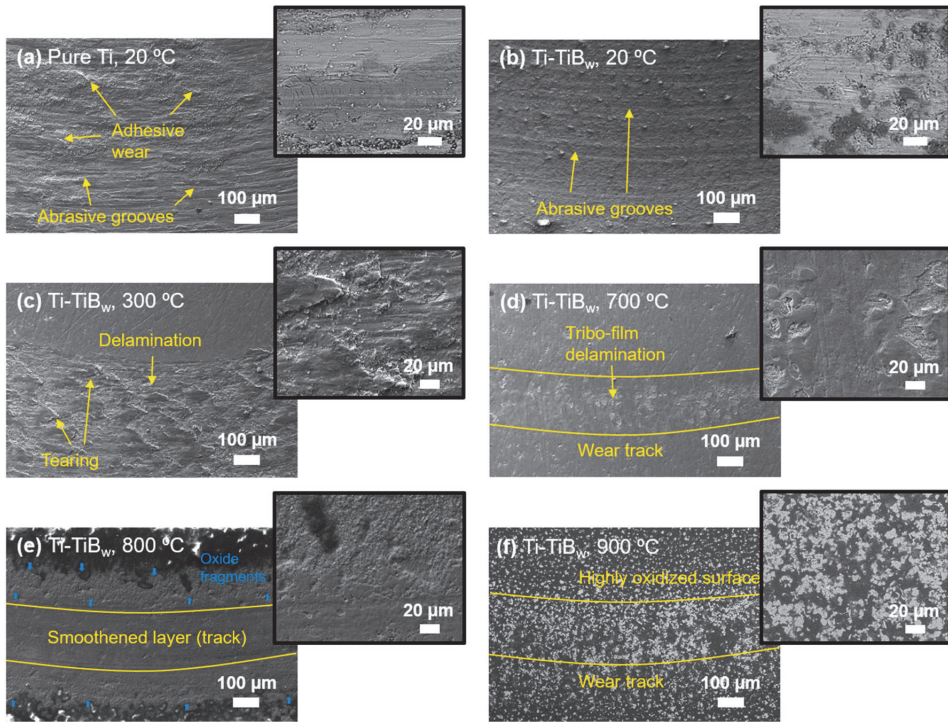


Fig. 4. SEM images of materials surface after sliding at various temperatures; (a) Pure Ti, 20 °C; (b) Ti-TiB_w, 20 °C; (c) Ti-TiB_w, 300 °C; (d) Ti-TiB_w, 700 °C; (e) Ti-TiB_w, 800 °C; and (f) Ti-TiB_w, 900 °C.

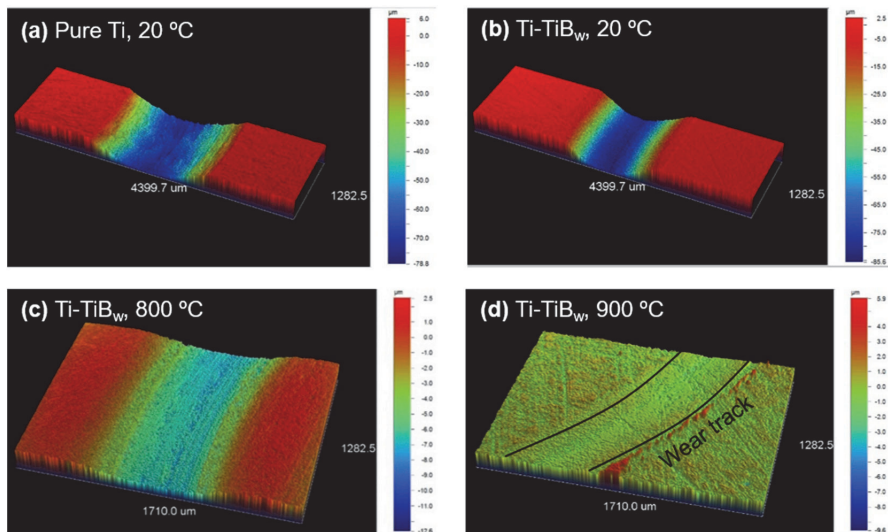


Fig. 5. 3D wear profiles of; (a) Pure Ti, 20 °C; (b) Ti-TiB_w, 20 °C; (c) Ti-TiB_w, 800 °C; and (d) Ti-TiB_w, 900 °C.

and 900 °C (i.e. CoF≈0.18).

Fig. 4 demonstrates the different wear mechanisms of sliding wear of pure Ti and the composites. Wear of pure Ti is associated with severe ploughing, plastic deformation and cutting resulting in significant

material removal. This increase in wear of pure Ti is amplified due to the characteristic of thermal softening (accompanied by conversion of frictional work into heat) during sliding. Abrasive wear and patches of adhesive wear mark were found on the surface of Ti specimens due to

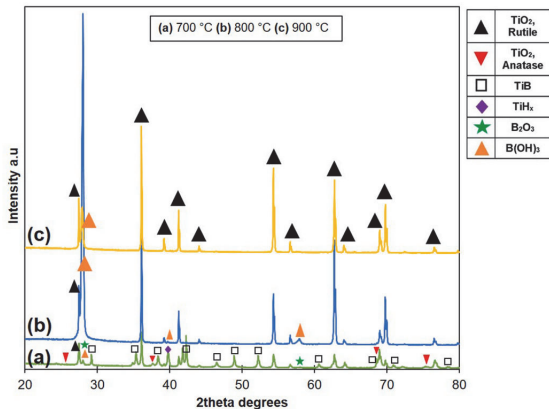


Fig. 6. XRD patterns of composite surface after test at (a) 700 °C; (b) 800 °C; and (c) 900 °C.

sliding against a much harder Al₂O₃ counterbody [31]. In addition, the wear of Ti as well as of RT tested composite is intensified by the phenomena of third body. Extreme vibration of test setup during testing of pure Ti was observed at 700 °C due to ‘stick-slip’ adhesive behaviour of Ti.

Normally, it is reported that a longer duration of wear test results in a high strain level at the surface, which is in contact with the counter disc, leading to the formation of surface and sub-surface cracks or fatigue-driven delamination [34]. SEM images demonstrate limited amount of delamination or local material removal along the ploughing grooves in Ti as well as the composite. The main wear mechanisms related to

Ti-TiB_w composite sliding at RT is similar to that of pure Ti except the fact that the intensity of occurring is significantly lower and is further suppressing with an increase in testing temperature. Adhesion and abrasion were dominant wear at RT composite sliding.

The XRD pattern, Fig. 6, displays the peaks of titania (TiO₂) on the surface of composite. Composite tested at 700 °C generated some peaks of TiB, which was suppressed when materials were tested at 800 and 900 °C due to intensive oxide layer development. Tribo-oxide layer delamination was evident at the lower temperatures of 300 and 500 °C tests. However, a significant diminution in tribo-layer delamination was detected at 700 °C and was almost not evident during sliding at 800 and 900 °C. The main wear mechanism at temperatures between 300–700 °C was oxidative in nature. A decrease in tribo-layer delamination from the surface during test at 700 °C and above is conditioned by the low CoF between tribo-pairs sliding and, therefore, relatively low shear stresses on the surface area. The stability and thickness of tribo-oxide layer increased with the increase in temperature of the test, which was also confirmed with cross sectional SEM imaging, Fig. 7. The principal mechanism involved into process of composite wear at 800 and 900 °C was a micro-polishing by the counterbody alumina.

The XRD patterns of the specimens tested at 700 and 800 °C, Fig. 6, reveal peaks of the compounds containing hydrogen (titanium hydride, boron oxide) owing to the precipitation of water vapour near ≈ 600–800 °C. Water vapour release at this temperature range is reasoned by the presence of chlorine impurities, TiH_x or formation of hydrated oxides [35–37].

Anatase is often the first titanium dioxide phase to form in many processes (mainly at low temperatures) due to its lower surface energy; however, anatase tends to convert into rutile phase at elevated temperatures. The XRD patterns in Fig. 6 demonstrate a significant decrease in the peaks intensity of anatase at 800 °C and disappearance of these peaks at 900 °C. The precipitated water vapour preferably reacts with the existing metastable, less dense anatase to form the most stable,

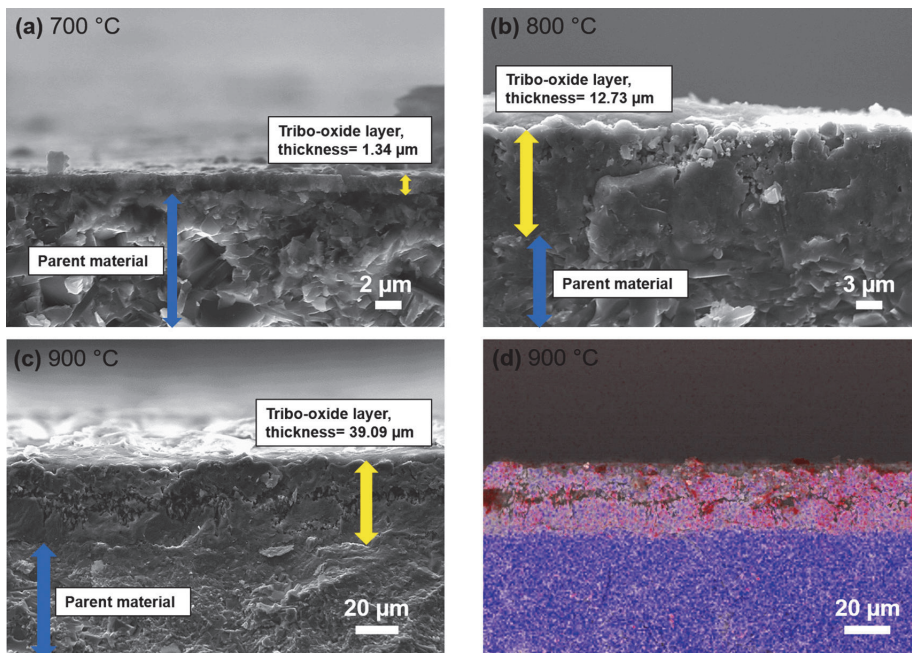


Fig. 7. SEM images of wear track cross-section of the composites tested at (a) 700 °C; (b) 800 °C; and (c) 900 °C with indication of the thickness of oxide layer formed; (d) EDS mapping of cross-section of the composite tested at 900 °C (red – oxygen; blue – titanium). (For interpretation of the references to colour in this figure legend, the reader is referred to the Web version of this article.)

dense, hard, and well-adherent rutile at elevated temperatures [38]. In addition, a decrease in the peak of hydrogen related compounds together with the increase in peaks of rutile TiO_2 was seen in XRD.

Fig. 7 demonstrates the cross-sectional examination of the composites tested at 700, 800 and 900 °C. During examination of the surface inside and outside of the wear track, it was found that the thickness of tribo-oxide layer was kept almost unchanging with no detectable alterations on the original surface. Therefore, the formation of protective tribo-layer on the surface of the composites at 700 °C and above can be stated. The thickness of oxide layer and its adherence with the parent material readily increased with the increase in test temperature from 700 to 900 °C. This situation states the role of temperature on oxidation rate by activating diffusing species. It should be noted that the accelerated oxidation rate due to increasing temperature can put the oxide layer in a more stressed condition as a result of thermal effects [39], which results in their gradual detaching from the surface as fragments. This could be the reason behind a fairly porous (or not as homogeneous as surfaces of materials tested at 700 and 800 °C) oxide layer over the composites tested at 900 °C, Fig. 7c.

The XRD patterns at Fig. 6 demonstrate the presence of lubricious boric acid, B(OH)_3 , on the composite surfaces characterized by a glazed/glassy layer (Fig. 8) at 700–900 °C. Moreover, the presence of boron oxide (B_2O_3) at 700 °C confirmed the formation of B(OH)_3 films from a spontaneous chemical reaction between water molecules and B_2O_3 coatings in a humid environment (Eqs. (1) and (2)). At 800 °C, TiB peaks get suppressed by extensive formation of TiO_2 phase, mainly rutile. The instant B_2O_3 phase was barely detected. Since TiO_2 formation is faster than B_2O_3 formation, it is possible that B_2O_3 are scarcely detected by XRD. A new peak for B(OH)_3 is detectable at 800 °C, Fig. 6b, confirming the reaction described by Eq. (2). At 900 °C, apart from strong rutile TiO_2 phase, the formed B(OH)_3 peak is still recognizable, Fig. 6c. The lubricious property of formed boric acid films is believed to contribute in lowering of CoF during tribo-pair sliding [40,41]. The formation of such self-lubricating and lubricious layer of boric acid on TiB_2 containing composites closer to ~1000 °C was also reported in Refs. [40–42]. However, a decline in its concentration at temperatures beyond 1000 °C, due to evaporation as gaseous phase is reported in Refs. [41,42]. According to the results of the current research it is possible to expect that initiation of the evaporation of in-situ formed B(OH)_3 took place already at 900 °C that resulted in its deficiency and intensification of titanium oxidation. This is confirmed by a decrease in the B(OH)_3 peak intensity at 900 °C, Fig. 6c. The highest peak intensity of boric acid and resulting glaziness was observed at 800 °C (Fig. 8b). As the temperature decreased after the test, the glazed film gradually faded away as shown in Fig. 8c. Fig. 8d shows the accumulation of liquid droplets (supposedly, boric acid) around the counterbody ball after composite sliding at 800 °C. The formation of glassy glazed layer in various metals and alloys at HT sliding and termed it to be wear protective is reported in Ref. [43]. Moreover, since the average surface roughness measured for pure Ti as well as composite specimens tested from RT to 800 °C was in the same range i.e. $R_a \sim 0.15 \pm 0.05 \mu\text{m}$, it is believed that there is no significant surface smoothing due to glazed layer formation.

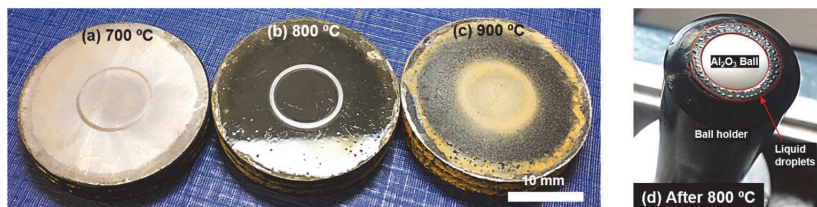


Fig. 8. Composite surfaces; (a) minimal glazed layer, 700 °C; (b) maximum glazed layer, 800 °C; (c) faded glazed layer after cooling, 900 °C; and (d) Liquid droplets staying around ball after test at 800 °C.



3.3.2. Effect of load on coefficient of friction

The effect of applied load on coefficient of friction is illustrated in Fig. 9, wherein the CoF is plotted as a function of varying loads at test temperatures of 700, 800 and 900 °C. Dense, thick and stable (adherent) tribo-layer during the test at 800 °C resulted in the lowest and stable (at wider range of loads) CoF as compared to CoF detected at temperatures of 700 or 900 °C. Comparatively thin tribo-oxide layer developed at 700 °C resulted in unstable CoF (and increased vibration during sliding) as the load approached 14 N. The protective layer in Ti based materials usually benefit the best until 800 °C and under approaching 900–1000 °C, it tends to spall off and gradually lose its protective nature. Composite sliding under 900 °C exhibits a very fluctuating and unstable CoF with increasing loads. This was also confirmed by a high surface roughness value obtained for composite after the test at 900 °C, i.e. $R_a \sim 1.80 \pm 0.2$. An important point to note is that there was no oxide-layer breaking (or increase in CoF) during 800 °C test even at 26 N. However, during the test at 900 °C, a sudden jump in CoF at 17 N was found, which could be due to the oxide-layer breaking. Nevertheless, there could be other reasons for CoF jump, such as third body or debris particles present on the sliding track. Hereby, it can be established that the protective nature of tribo-oxide layer formed at 700 and 800 °C is the most stable and reliable, whereas the one formed at 800 °C has the highest load bearing capacity.

3.3.3. Counterbody ball wear

The ball wear (Fig. 10a) was measured using 3D profilometer and studied under SEM and analysed by EDS. No ball wear was seen for pure Ti at RT as well as 700 °C. High to average wear of alumina balls sliding against composite counterpart at RT, 300 and 500 °C was detected. Formation of patches of material removal clearly indicated the adhesion between the composite and alumina balls. At temperatures below 500 °C, the EDS mapping (RT sliding, Fig. 10c) demonstrated a significant amount of Ti transfer from the composite specimen to the alumina counterbody signifying that a severe adhesion took place between them [44,45]. However, wear is reduced with the increase in test temperature. The main mechanism responsible for wear of the ball at RT–500 °C was mainly adhesive wear (Fig. 10b).

The EDS analysis (Fig. 10c for 900 °C) shows that a worn area on the ball surface after the tests at 700, 800 and 900 °C consists of nearly zero Ti transfer from the composite surface. This is due to the well adhered tribo-layer on the tribo-surfaces mating, which is difficult to wear out. Moreover, Ti transfer was also prevented by the formation of lubricious boric acid covering the composite surface, and acting as the main sliding surface. Besides, boron transfer was evident on the balls surface (Fig. 10c). A visually smoothed/polished surface was evident on the balls at 800 and 900 °C. It is understood that transferred boron on the balls surface transformed to boric acid at 800 and 900 °C, thus

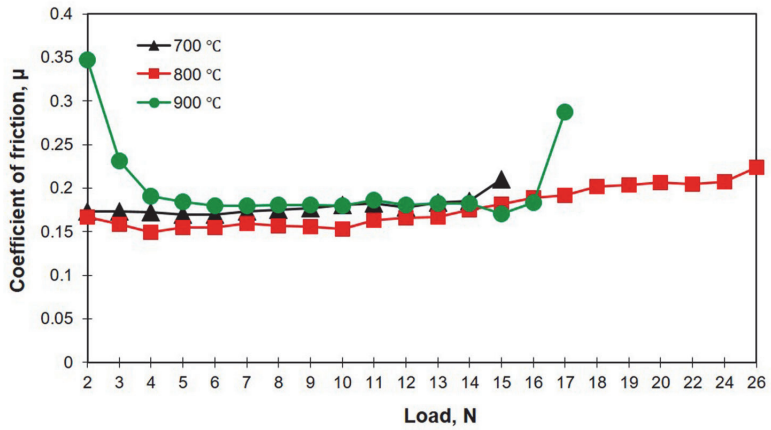
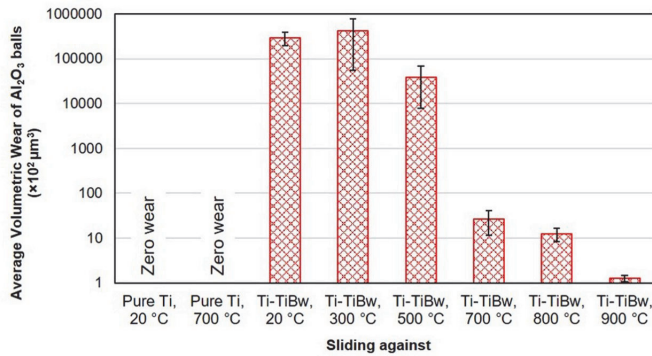
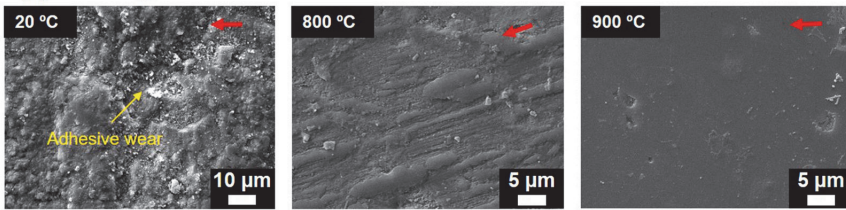


Fig. 9. Effect of increasing load and sliding temperature on CoF.

(a) Ball wear



(b) SEM images



(c) EDS analysis

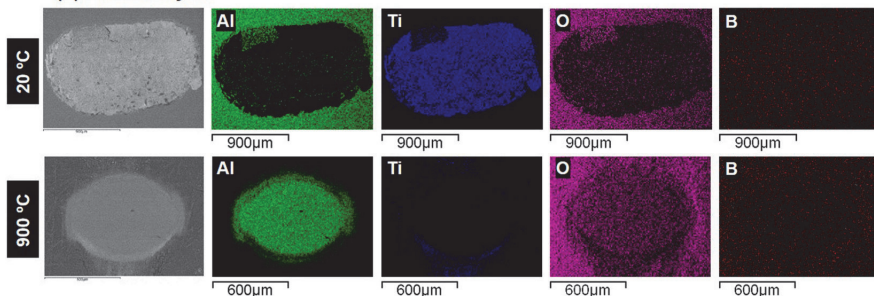


Fig. 10. (a) Ball wear; (b) SEM images of ball worn surface at 20 °C, 800 °C and 900 °C; and (c) EDS analysis of ball scars at 20 °C and 900 °C.

significantly reducing friction and wear. The main wear mechanism of alumina balls at 800 and 900 °C was mainly attributed to micro-polishing.

4. Conclusions

In the current work, a fully dense 50 wt%Ti-50 wt%TiB_w composite was in-situ produced with the help of SPS; and their tribological behavior under dry sliding conditions at temperatures up to 900 °C was evaluated. The effect of increasing temperature was demonstrated by a significant reduction in composite wear rate and lowering CoF due to development of protective tribo-layers. The formation of lubricious boric acid on the composite surface contributed into self-lubricating properties of the tribo-couple at temperatures of 700–900 °C. The highest load bearing capacity (up to 26 N) in combination with a lower CoF (<0.2) of the generated tribo-oxide layer was demonstrated at 800 °C. The wear mechanism of composite changed from adhesive and abrasive (at room temperature) to oxidative with an increase in test temperature. At temperatures of 800 and 900 °C, the micropolishing was considered as a prevailing wear mechanism.

Declaration of competing interest

The authors declare that they have no known competing financial interests or personal relationships that could have appeared to influence the work reported in this paper.

Acknowledgements

This work was supported by the Estonian Research Council grants PRG643 (I. Hussainova) and M-ERA.Net project “HOTselflub” MOBERA18.N.20097582-CA. The authors would like to thank Dr. Mart Viljus and Mr. Rainer Traksmaa for their help with SEM and XRD analysis.

References

- [1] A.S. Namini, S.A.A. Dilawary, A. Motallebzadeh, M.S. Asl, Effect of TiB₂ addition on the elevated temperature tribological behavior of spark plasma sintered Ti matrix composite, *Compos. B Eng.* 172 (2019) 271–280.
- [2] Y. Qin, L. Geng, D. Ni, Dry sliding wear behavior of extruded titanium matrix composite reinforced by in situ TiB whisker and TiC particle, *J. Mater. Sci.* 46 (14) (2011) 4980–4985.
- [3] A. Bloyce, P.H. Morton, T. Bell, Surface engineering of titanium and titanium alloys, *ASM Handbook* 5 (1994) 2232–2233.
- [4] M. Antonov, I. Hussainova, J. Kübarsapp, R. Traksmaa, Oxidation-abrasion of TiC-based cermets in SiC medium, *Wear* 273 (1) (2011) 23–31.
- [5] Y.S. Mao, L. Wang, K.M. Chen, S.Q. Wang, X.H. Cui, Tribo-layer and its role in dry sliding wear of Ti-6Al-4V alloy, *Wear* 297 (1–2) (2013) 1032–1039.
- [6] M. Antonov, R. Veinthal, E. Huttunen-Saarivirta, I. Hussainova, A. Vallikivi, M. Lelys, J. Priss, Effect of oxidation on erosive wear behaviour of boiler steels, *Tribol. Int.* 68 (2013) 35–44.
- [7] D.-L. Yung, A. Zikin, I. Hussainova, H. Danninger, E. Badish, A. Gavrilovic, Tribological performances of ZrC-Ni and TiC-Ni cermet reinforced PTA hardfacings at elevated temperatures, *Surf. Coating. Technol.* 309 (2017) 497–505.
- [8] X.X. Li, Y. Zhou, X.L. Ji, Y.X. Li, S.Q. Wang, Effects of sliding velocity on tribo-oxides and wear behavior of Ti-6Al-4V alloy, *Tribol. Int.* 91 (2015) 228–234.
- [9] Q.Y. Zhang, Y. Zhou, X.X. Li, L. Wang, X.H. Cui, S.Q. Wang, Accelerated formation of tribo-oxide layer and its effect on sliding wear of a titanium alloy, *Tribol. Lett.* 63 (1) (2016) 2.
- [10] G.K.J.M. Bertrand, K. Jarraya, J.M. Chaix, Morphology of oxide scales formed on titanium, *Oxid. Metals* 21 (1–2) (1984) 1–19.
- [11] M. Antonov, I. Hussainova, R. Veinthal, J. Pirso, Effect of temperature and loading rate on three-body abrasion of cermets and steel, *Tribol. Int.* 46 (2012) 261–268.
- [12] Q.Y. Zhang, Y. Zhou, L. Wang, X.H. Cui, S.Q. Wang, Investigation on tribo-layers and their function of a titanium alloy during dry sliding, *Tribol. Int.* 94 (2016) 541–549.
- [13] N. Dalili, A. Edrissy, K. Farokhzadeh, J. Li, J. Lo, A.R. Riahi, Improving the wear resistance of Ti-6Al-4V/TiC composites through thermal oxidation (TO), *Wear* 269 (7–8) (2010) 590–601.
- [14] Y. Qin, W. Lu, J. Qin, D. Zhang, Oxidation behavior of in situ synthesized TiB/Ti composite in air environment, *Mater. Trans.* 45 (12) (2004) 3241–3246.
- [15] M. Antonov, I. Hussainova, Experimental setup for testing and mapping of high temperature abrasion and oxidation synergy, *Wear* 267 (2009) 1798–1803.
- [16] E. Atar, E.S. Kayali, H. Cimenoglu, Characteristics and wear performance of borided Ti6Al4V alloy, *Surf. Coating. Technol.* 202 (19) (2008) 4583–4590.
- [17] Y. Pu, B. Guo, J. Zhou, S. Zhang, H. Zhou, J. Chen, Microstructure and tribological properties of in situ synthesized TiC, TiN, and SiC reinforced Ti3Al intermetallic matrix composite coatings on pure Ti by laser cladding, *Appl. Surf. Sci.* 255 (5) (2008) 2697–2703.
- [18] S. Zhang, W.T. Wu, M.C. Wang, H.C. Man, In-situ synthesis and wear performance of TiC particle reinforced composite coating on alloy Ti6Al4V, *Surf. Coating. Technol.* 138 (1) (2001) 95–100.
- [19] R. Kumar, M. Antonov, Self-lubricating materials for extreme temperature tribo-applications, *Mater. Today: Proc.* (2020), <https://doi.org/10.1016/j.matpr.2020.10.824>.
- [20] Y. Holovenko, M. Antonov, L. Kollo, I. Hussainova, Friction studies of metal surfaces with various 3D printed patterns tested in dry sliding conditions, Part J: *J. Eng. Tribol.* 232 (1) (2018) 43–53.
- [21] K. Morsi, V.V. Patel, S. Naraghi, J.E. Garay, Processing of titanium-titanium boride dual matrix composites, *J. Mater. Process. Technol.* 196 (1–3) (2008) 236–242.
- [22] L. Liu, T. Minasyan, R. Ivanov, S. Aydinian, I. Hussainova, Selective laser melting of TiB₂-Ti composite with high content of ceramic phase, *Ceram. Int.* 46 (13) (2020) 21128–21135.
- [23] H. Singh, M. Hayat, H. Zhang, R. Das, P. Cao, Effect of TiB₂ content on microstructure and properties of in situ Ti-TiB composites, *Int. J. Miner., Metall. Mater.* 26 (7) (2019) 915–924.
- [24] A.S. Namini, M. Azadbeh, M.S. Asl, Effect of TiB₂ content on the characteristics of spark plasma sintered Ti-TiBw composites, *Adv. Powder Technol.* 28 (6) (2017) 1564–1572.
- [25] M.S. Kumar, P. Chandrasekar, P. Chandramohan, M. Mohanraj, Characterisation of titanium-titanium boride composites processed by powder metallurgy techniques, *Mater. Char.* 73 (2012) 43–51.
- [26] I. Hussainova, M. Antonov, N. Voltshihin, J. Kübarsapp, Wear behavior of Co-free hardmetals doped with zirconia and produced by conventional PM and SPS routines, *Wear* 312 (1–2) (2014) 83–90.
- [27] F. Sergejev, M. Antonov, Comparative study on indentation fracture toughness measurements of cemented carbides, *Proc. Estonian Acad. Sci. Eng.* 12 (4) (2006) 388–398.
- [28] J. Baronins, M. Antonov, S. Bereznev, T. Raadik, I. Hussainova, Raman spectroscopy for reliability assessment of multilayered AlCrN coating in tribo-corrosive conditions, *Coatings* 8 (7) (2018) 229.
- [29] P.J. Blau, Running-in: art or engineering? *J. Mater. Eng.* 13 (1) (1991) 47–53.
- [30] M. Villa, J.W. Brooks, R.P. Turner, H. Wang, F. Boitout, R.M. Ward, Microstructural modeling of the α - β phase in Ti-6Al-4V: a diffusion-based approach, *Metall. Mater. Trans. B* 50 (6) (2019) 2898–2911.
- [31] D.S.R. Krishna, Y.L. Brama, Y. Sun, Thick rutile layer on titanium for tribological applications, *Tribol. Int.* 40 (2) (2007) 329–334.
- [32] Q. Yang, T. Senda, N. Kotani, A. Hirose, Sliding wear behavior and tribofilm formation of ceramics at high temperatures, *Surf. Coating. Technol.* 184 (2–3) (2004) 270–277.
- [33] R. Kumar, M. Antonov, U. Beste, D. Goljandin, Assessment of 3D printed steels and composites intended for wear applications in abrasive, dry or slurry erosive conditions, *Int. J. Refract. Metals Hard Mater.* 86 (2020) 105126.
- [34] N.P. Suh, The delamination theory of wear, *Wear* 25 (1) (1973) 111–124.
- [35] M. Yan, H.P. Tang, M. Qian, Scavenging of oxygen and chlorine from powder metallurgy (PM) titanium and titanium alloys, in: *Titanium Powder Metallurgy*, Butterworth-Heinemann, 2015, pp. 253–276.
- [36] S. Malinow, W. Sha, Z. Guo, C.C. Tang, A.E. Long, Synchrotron X-ray diffraction study of the phase transformations in titanium alloys, *Mater. Char.* 48 (4) (2002) 279–295.
- [37] W. Feng, Q. Wang, Q. Kong, X. Zhu, J. Wu, C. Sun, Influence of high-temperature water vapor on titanium film surface, *Oxid. Metals* 86 (3–4) (2016) 179–192.
- [38] D.A. Hanaor, C.C. Sorrell, Review of the anatase to rutile phase transformation, *J. Mater. Sci.* 46 (4) (2011) 855–874.
- [39] C. Coddet, A.M. Craze, G. Beranger, Measurements of the adhesion of thermal oxide films: application to the oxidation of titanium, *J. Mater. Sci.* 22 (8) (1987) 2969–2974.
- [40] Y.H. Koh, S.Y. Lee, H.E. Kim, Oxidation behavior of titanium boride at elevated temperatures, *J. Am. Ceram. Soc.* 84 (1) (2001) 239–241.
- [41] A. Erdemir, G.R. Fenske, R.A. Erck, A study of the formation and self-lubrication mechanisms of boric acid films on boron oxide coatings, *Surf. Coating. Technol.* 43 (1990) 588–596.
- [42] C. Higdon, B. Cook, J. Harringa, A. Russell, J. Goldsmith, J. Qu, P. Blau, Friction and wear mechanisms in AlMgB₁₄-TiB₂ nanocoatings, *Wear* 271 (9–10) (2011) 2111–2115.
- [43] A. Pauschitz, M. Roy, F. Franek, Mechanisms of sliding wear of metals and alloys at elevated temperatures, *Tribol. Int.* 41 (7) (2008) 584–602.
- [44] M. Antonov, H. Afshari, J. Baronins, A. Adoberg, T. Raadik, I. Hussainova, The effect of temperature and sliding speed on friction and wear of Si₃N₄, Al₂O₃, and ZrO₂ balls tested against AlCrN PVD coating, *Tribol. Int.* 118 (2018) 500–514.
- [45] Der-Liang Yung, Maksim Antonov, Renno Veinthal, Irina Hussainova, Wear behaviour of doped WC-Ni based hardmetals tested by four methods, *Wear* 352–353 (2016) 171–179.

Publication II

Kumar, R., Torres, H., Aydinyan, S., Antonov, M., Varga, M., Rodriguez Ripoll, M., Hussainova, I. (2022). Microstructural and high temperature tribological behaviour of self-lubricating Ti-TiB_x composite doped with Ni-Bi. *Surface and Coatings Technology*, 128827.



Contents lists available at ScienceDirect

Surface & Coatings Technology

journal homepage: www.elsevier.com/locate/surfcoat

Microstructure and high temperature tribological behaviour of self-lubricating Ti-TiB_x composite doped with Ni—Bi

R. Kumar^{a,b,*}, H. Torres^a, S. Aydinyan^b, M. Antonov^b, M. Varga^a, M. Rodriguez Ripoll^{a,**}, I. Hussainova^b

^a AC2T research GmbH, Viktor-Kaplan-Straße 2/C, Wiener Neustadt 2700, Austria

^b Tallinn University of Technology, Department of Mechanical and Industrial Engineering, Ehitajate Tee 5, 19086 Tallinn, Estonia

ARTICLE INFO

Keywords:

Sliding wear
Surface deposition
Titanium
High temperature
Self-lubrication
Bismuth
TiB₂

ABSTRACT

It is a well-established fact, that the tribological performance of titanium and its alloys at high temperatures is poor, especially for self-mated titanium-titanium pairs. Previous work has shown a significant improvement in mechanical and high temperature tribological behaviour (700–900 °C) for pure Ti sintered with TiB₂ ceramic, occasioned by the in-situ formed boric acid lubricant. The current work explores the possibility to extend the lubrication temperature range (below 700 °C) of Ti-TiB₂ composites through the incorporation of a nickel-bismuth mixture (Ni—Bi) as a solid lubricant using laser melting. To this end, phase equilibrium diagrams have been calculated for the Ti-B-Ni—Bi quaternary system using the CALPHAD method to evaluate the possibility of the formation of different phases due to dilution between the substrate and deposit, as well as their possible interactions. The self-lubricating Ni—Bi samples feature a formation of Bi-Ni-Ti-TiB_x functional surface. The functional surface demonstrates a compact and unique microstructure of a hard B-rich phase encapsulated inside a lubricous Bi-rich phase. A two-fold increase in hardness of the surface in comparison to the underlying substrate was noted for Ni—Bi laser-melted samples. Further, the Ni—Bi samples were studied under a reciprocating sliding configuration against a Ti-alloy flat-pin counterbody at temperatures including RT, 400 and 600 °C. The resulting wear scars were analysed utilizing SEM, XRD and 3D profilometry to understand the prevalent wear mechanisms. A significant decrease in coefficient of friction and wear rate was observed for the Ni—Bi laser-melted samples sliding at 400 °C and 600 °C due to the formation of a self-lubricating tribo-oxide layer rich in Bi-compounds. The results are reported in comparison to the unmodified reference Ti-TiB₂ composite.

1. Introduction

Over decades, titanium and its alloys have rapidly gained importance as their demand in applied engineering (aero-engines, structural parts of rockets, turbojet engines, turbines, etc.) has grown exponentially due to its good mechanical properties, corrosion resistance, lightweight and relatively low cost [1]. However, a drawback of the widespread implementation of titanium alloys is their poor tribological performance under high temperatures, which may result in galling, seizing, ploughing and adhesion. To solve these issues, many different techniques have been used through the years: surface-engineering such as coatings, laser processing or metallurgical techniques such as the reinforcement of alloys with hard ceramic phases. [2–6]. In [1,7], a considerable

improvement in friction and wear performance of Ti-TiB₂ composite was reported for the temperature range from 700 to 900 °C. A similar friction reduction has been reported also in [8,9] for ceramic phase reinforced pure Ti or Ti6Al4V alloy at HT sliding [8,9].

Minimizing the friction and wear at HT through the use of solid lubricants or additives has become an essential approach to cut back on the harmful effects of conventional liquid-based lubricants causing respiratory illness due to vaporization as well a harmful decomposition effect on an environment [10]. The benefits of a cleaner atmosphere, the capability to work at temperatures above 300 °C and strict enforcement of new standards have made solid lubricants and self-lubricating materials a more efficient alternative to conventional lubricants.

One of the possible solid lubricants is bismuth (Bi), studies on which

* Correspondence to: R. Kumar, Tallinn University of Technology, Department of Mechanical and Industrial Engineering, Ehitajate Tee 5, 19086 Tallinn, Estonia

** Corresponding author.

E-mail addresses: rahul.kumar@taltech.ee (R. Kumar), ripoll@ac2t.at (M. Rodriguez Ripoll).

<https://doi.org/10.1016/j.surfcoat.2022.128827>

Received 27 July 2022; Received in revised form 22 August 2022; Accepted 24 August 2022

Available online 28 August 2022

0257-8972/© 2022 Elsevier B.V. All rights reserved.

are rare. Nevertheless, Bi demonstrates easy shearing upon an externally applied load due to its intrinsic ductility and a close-packed layered structure [11,12]. Its low toxicity has brought it to the research mainstream. Due to its low hardness (2–2.5 Mohs) and melting point ($\sim 270^\circ\text{C}$), Bi is believed to disperse easily under asperity contacts during relative motion between tribo-bodies as frictional flash temperatures are usually enough for Bi melting [11]. Furthermore, the easy dispersion of Bi during tribo-service can generate a lubricious tribo-layer, which, in turn, can prevent direct contact between tribo-bodies and minimise friction [13]. There are several studies available on Bi as a solid lubricant [12–15]; still, a detailed investigation of its performance at HT, wear mechanisms and frictional behaviour is scarce. Sun et al. [12] studied the role of Bi_2O_3 on a Ni-5 wt% Al composite coating and reported a decrease in coefficient of friction (CoF) from 0.55 to 0.13 under sliding at 800°C . Conversely, Rodriguez et al. [13] described the smearing of Bi rich tribo-layer resulting in a low CoF below 200°C . However, upon a temperature rise above its melting point, the CoF increased due to the formation of bismuth oxide, which is contradictory to the results given in [12]. On the other hand, bismuth, similar to its soft metal counterparts (Ag, Cu), is reported to agglomerate and segregate throughout a matrix [11,15–17] resulting in an inconsistent self-lubrication along with a compromise in mechanical properties of the material [15]. In this work, a novel method of using Bi added and modified by Ni (nickel) to develop a self-lubricating composite surface of Ti/TiB₂ bulk is proposed for the first time. Nickel is a widely used material owing to its excellent behaviour in applications demanding protection against severe wear conditions. Besides, Ni-based alloys are believed to demonstrate a strong bonding to many substrate materials even under HT environments [16].

Various methods including powder metallurgy, PVD, CVD, microwave sintering etc. are available to fabricate Ni-based self-lubricating coatings/composites [11,16,17]. Generally, Ni-based alloys are deposited using a thermally spraying technique, which usually possesses a low to moderate adhesion to the substrate and has porosity [18]. Conversely, the laser deposition (melting) method is highly undervalued despite its effectiveness and high added value. Laser deposition (melting) refers to the heating of powder particles (either preplaced or fed) on the surface of a substrate material using a high-power laser source to their melting point followed by rapid solidification of the melted zone. The idea behind the process is to incorporate the surface-fed powders into the substrate material to enhance the surface or core microstructure of the substrate material. The generated surface is believed to impart superior properties (wear or corrosion resistance etc.) to the base substrate. The main features of laser melting involve (1) surface microstructure refinement; (2) homogenization of composition; and (3) dissolution of precipitates [18]. Moreover, imparting a fast deposition rate, minimum distortion, controlled dilution, dense coating, strong adhesion to the substrate, and a minor heat affected zone (HAZ) are the characteristic features of surface modification by laser [1,16].

The idea behind the current research was to assess the capability of Bi incorporated into Ti-TiB₂ composite to serve as a lubricant at temperatures below 700°C targeting a friction reduction at elevated temperatures (applications involving HT-forming, forging, stamping, turbines etc.). To overcome the limitations associated with Bi dispersion over the surface, the Ni-Bi mixture was used as a combinational powder precursor for laser treatment. Recent work has exploited the addition of Ni-Bi by laser melting for improving the frictional performance of Ti6Al4V alloy below 600°C [19]. However, a significant improvement of the wear performance requires the use of composite materials incorporating wear-resistant ceramic phases. In the current work, Ni-Bi laser melting/deposition was performed on Ti-10wt%TiB₂ spark plasma sintered (SPS) bulks. The fundamental characteristics of laser melted self-lubricating surfaces were studied for phase and microstructure evolution. Dry reciprocating sliding tests were carried out on the Ni-Bi laser melted samples at room temperature (RT), 400°C and 600°C . The wear rates and coefficients of friction were recorded and analysed. The

wear scars were studied to reveal the underlying wear mechanisms. Particular attention was paid to the effect of Bi addition on the self-lubricating behaviour of the composite. The results are reported using unmodified Ti-10wt%TiB₂ bulks as the reference material.

2. Experimental

2.1. Material preparation

In the present study, the incorporation of self-lubricating Ni-Bi pre-milled powders (Ni- *Oerlikon Metco, Germany* (CAS no. 7440-02-0), 99.3 % purity, 45–75 μm and Bi- *Sigma Aldrich, Germany* (CAS no. 7440-69-9), 99 % purity, 100 mesh) was carried on through laser surface deposition (melting) using a direct diode laser system with a wavelength of 975 nm. Deposition parameters were optimized to achieve a minimum dilution and good adhesion to the substrate. The Ni-70wt%Bi powder was mechanically mixed using ethanol as the binder and spread over the substrate surface. As Ni affects the homogeneous distribution of Bi, the optimized Ni-Bi ratio of 30:70 wt% was selected through a series of tests to ensure optimal bismuth homogenization in the composite. Subsequently, a heating stage was executed in an oven at 100°C for 1 h, to evaporate the ethanol binder. The last stage of laser deposition (melting) was performed using a rectangular-shaped laser beam of $6 \times 13 \text{ mm}^2$ area under a shielding argon atmosphere to prevent any oxidation of the subsequent coatings using a beam speed of $6 \text{ mm}\cdot\text{s}^{-1}$ and laser power of 3500 W. The thickness of the as-melted surface was measured to lie between 1 and 1.5 mm. The dilution percentage observed was $<40\%$. The LD surface microstructure revealed a good quality, without porosity and other surface defects as seen in optical microscopy. Consequently, the samples were ground to ensure parallelism and polished to achieve a Ra of $0.2 \pm 0.04 \mu\text{m}$ for tribo-testing.

Disks of Ti-10wt%TiB₂ composite were chosen as the substrate material for laser deposition, prepared through spark plasma sintering (*FCT Systeme GmbH, Germany*) at a pressure of 50 MPa, a temperature of 1050°C , a dwell time of 5 min, and a heating rate of $100^\circ\text{C}/\text{min}$ under vacuum conditions. Before sintering, the powder mixture of Ti and TiB₂ was prepared by mechanical rotation mixing of Ti (*Alfa Aesar, Germany*, particle size 0– $<50 \mu\text{m}$) and TiB₂ ($>99.5\%$ *Alfa Aesar, Germany*, 0– $<44 \mu\text{m}$) powders for 2 h (Fig. 1a). Fig. 1 shows the SEM images of the precursor powders and the surface of the sintered composites. In-situ formation of thermodynamically stable TiB phase together with untransformed TiB₂ is evident from both SEM images (Fig. 1b) and XRD pattern (Fig. 1c) of the composite. A detailed discussion of the reaction mechanisms in the Ti-TiB₂ system is presented in the co-authors' work [1]. The fabricated discs were further grounded to Ra $1 \pm 0.02 \mu\text{m}$ before laser deposition.

2.2. High temperature sliding wear tests

The sliding wear behaviour of the reference and Ni-Bi samples were studied using an Optimol SRV tribometer (*Optimol Instruments Prüftechnik GmbH, Germany*) under a reciprocating pin-on-flat configuration as described in [20]. The tests were performed at a normal load of 100 N and sliding frequency of 13 Hz and a stroke length of 4 mm. The counterbody material was chosen to be an in-house manufactured flat Ti alloy (Ti6Al4V) pin of 2 mm diameter as the flat contacts can assist in a wear debris entrapment (here, solid lubricants) [21]. The pins were manually grounded with sandpaper to prevent any edge effect during sliding. Later, the pin counterbody was loaded against a fixed flat sample (Fig. 2) using a spring deflection mechanism and, subsequently, oscillated through an electromagnetic drive.

Reciprocating frequency and stroke length were attuned to give an average sliding speed of $0.1 \text{ m}\cdot\text{s}^{-1}$. The normal load was set to 100 N, as to attain a contact pressure of 30 MPa. The test duration was 200 s. The tests were carried out at room temperature (RT), 400°C and 600°C . The disc samples with a diameter of 25 mm and thickness of 5 mm were

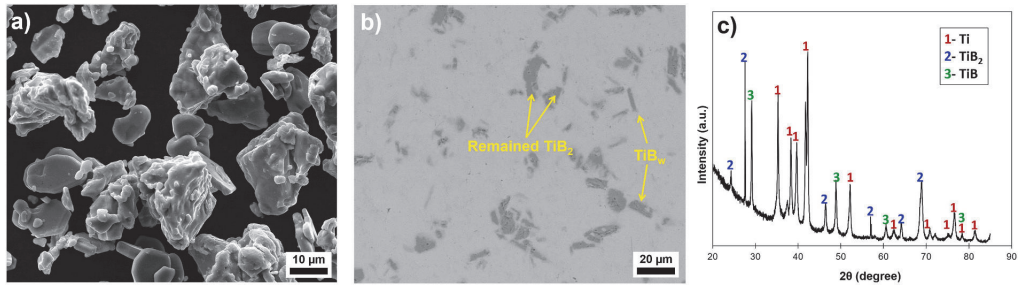


Fig. 1. SEM image of Ti-10wt%TiB₂ (a) powder mixture; (b) sintered specimen surface; and (c) XRD pattern of the sintered bulk.

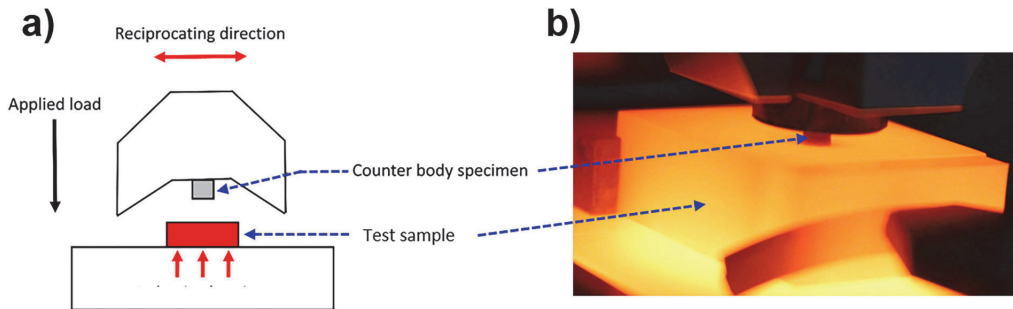


Fig. 2. (a) Schematic of a high temperature reciprocating sliding test; and (b) real-time testing environment.

heated up to the test temperature and measured using a surface thermocouple before the test for its conformity. The evolution of the coefficient of friction (CoF) during the test was continuously recorded. For each temperature, at least two repetitions of each test were performed and the results were averaged. The wear rate, K , is calculated using Archard's equation (Eq. (1)), dividing the measured wear volume V_w by the normal load N and the total reciprocating distance d . The test parameters of HT sliding are listed in Table 1.

$$K = \frac{V_w}{N \cdot d} \quad (1)$$

2.3. Characterization

The samples were examined under a Zygo New View 7300 3D optical profiler (*Lambda Photometrics*, UK). Additionally, the microstructure and chemical composition of the LM surface before and after the wear tests were analysed using a high-resolution SEM (JSM-IT300 scanning electron microscope, *Jeol BV*, Netherlands) including energy dispersive x-ray spectroscopy (EDS).

Phase analysis of the samples was performed using an X-ray diffractometer (XRD, *Siemens Bruker D5005* X-ray analyzer with a

Philips X'Pert PRO diffractometer (Panalytical, Netherlands) with radiation of 30 mA, 40 kV, $\lambda = 0.1542$ nm, a step size of 0.02° and a count time of 0.4 s. Relative phase content was assessed using a Rietveld refinement method. Mapping of the elements was performed in an area of $16.5 \times 11.5 \mu\text{m}^2$ with a step size of 40 nm under a 20 kV acceleration voltage. Patterns were acquired for a 200×200 pixel surface area and an acquisition time of 30 ms.

Hardness measurements of the samples were performed with the help of a microhardness (HV1) tester using a standard Vickers hardness machine (*Future-Tech FV-700*). At least three indents were made at three different spots and the values were averaged. The diagonals of the indent marks were measured through optical microscopy.

3D wear topography measurements for the samples were performed using a Leica Map (*Leica Microsystems*). Counterbody pin wear (length of the pin lost) was measured manually using a Vernier calliper.

3. Results and discussion

3.1. Phase equilibria in the Ti-B-Ni—Bi system

Thermodynamic modelling of the Ti-B-Ni—Bi system was performed using ThermoCalc software (TCAL6 database) to evaluate the formation of interfacial phases between the substrate and the self-lubricating surface, their possible interaction during the laser deposition process, as well as to estimate thermodynamic conditions of phase formation (Fig. 3). The composition of the quaternary mixture of 0.676Ti-0.097B-0.092Bi-0.135Ni was assessed as the estimations were based on the compositions of the substrate (Ti-10wt%TiB₂) and coating (Ni-70wt% Bi).

According to the binary Ni—Bi diagram [22], above the Bi melting point (above 544 K), the Rhombo-A7 (liquid bismuth) phase exists. Peritectic reactions $L + \text{fcc}(\text{Ni}) \rightarrow \text{BiNi}$ at 927 K and $L + \text{BiNi} \rightarrow \text{Bi}_3\text{Ni}$ at 744 K occur. Hence, the NiBi phase is stable up to about 927 K and the

Table 1
Parameters of sliding wear tests.

Test parameter	Value
Configuration	Reciprocating pin-on-flat
Temperature (°C)	RT, 400, 600
Load (N)	100
Contact pressure	30 MPa
Sliding frequency (Hz)	13
Stroke length (mm)	4
Duration (s)	200
Sliding speed ($\text{m}\cdot\text{s}^{-1}$)	0.1

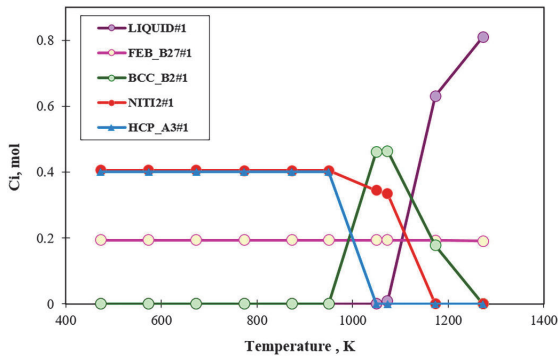


Fig. 3. Thermodynamic modelling of the 0.676Ti-0.097B-0.092Bi-0.135Ni system, $P = 1$ atm, TCAL6 database.

NiBi₃ phase is stable up to about 744 K. Considering the Ni₃₀-Bi₇₀ composition under consideration (3:2 M ratio), the possible product is expected to be in the form of fcc(Ni) and NiBi mixture under the given cladding conditions. However, due to the low diffusion coefficients of constituents, the NiBi₃ phase is more favourable to be formed in the reaction between Ni and Bi regardless of the ratio in the binary system [23].

In the quaternary system, the equilibrium phases were assessed in the temperature range from 573 to 1273 K. In particular, from 573 to 1073 K, 0.19 mol FEB_B27#1 ((Ti)1(B)1 in the database) phase corresponding to TiB is present along with 0.4 mol of HCP_A3#1 phase, which is TiBi solid solution with (BiNiTi)₁(BVA)_{0.5} constitution. Another major phase is NiTi₂ (0.41 mol) (NiTi₂#1 in the ThermoCalc database). Increasing the temperature by 400 K does not result in a change in the composition of the product. At 1073 K, a liquid phase of 0.008 mol is

formed with (B, Bi, Ni, Ti)₁ constitution, corresponding to a TiBi-rich phase (0.54:0.4) with a minor amount of dissolved Ni (of 0.06 mol fraction). Ternary Ti-Bi-Ni phase, denoted as BCC_B2#1 solid solution of 3 sublattices (with (Bi,Ni,Ti,VA)_{0.5}(Bi,Ni,Ti,VA)_{0.5}(B,VA)₃ constitution and Ti_{0.76}Bi_{0.19}Ni_{0.05} composition) is formed at 1050 K and above. The amount of FEB_B27#1 phase corresponding to TiB is not altered, but the NiTi₂ amount decreases down to 0.334 mol at the expense of the formation of the ternary phase. At 1273 K, the ternary phase of Ti:Bi:Ni = 0.72:0.17:0.11 compositional ratio exists only in the liquid state along with the titanium monoboride phase.

3.2. Microstructure

Figs. 4 and 5 show the representative SEM images of the as-melted (deposited) surface and the elemental mapping thereof, respectively. The functional surface reveals a poreless and crack-free microstructure comprising three areas of different intensity - namely bright, grey and dark regions. Table 2 lists the elemental composition (as obtained by EDS) of the spots labelled as A, B and C in Fig. 4c. The uniform distribution of a Bi-rich phase is evident across the surface region. However, the largest Bi content (~23 wt%) is found to be in a bright orbicular-shaped area (point A, Fig. 4c) together with Ti (~71 wt%) and Ni (~4 wt%). A similar phase formation of BCC_B2#1 solid solution of 3 sub-lattices with (Bi,Ni,Ti,VA)_{0.5}(Bi,Ni,Ti,VA)_{0.5}(B,VA)₃ constitution and Ti_{0.76}Bi_{0.19}Ni_{0.05} composition was observed in the thermodynamic calculation at around 1073 K. In addition, the favourable kinetic conditions may result in the formation of a ternary phase, that is, a quantitative predominance of titanium at the interface of the substrate and melted surface, the availability of multiple bismuth-titanium diffusion pairs, the feasibility of the penetration of fusible bismuth into titanium. However, the fast diffusion of titanium along the fissures or so-called grain-boundary diffusion has also been reported in [24]. The orbicular-shaped Bi-rich region features a diameter in the range of 5–15 μm. An interesting feature of encapsulated Ti and/or B phase in the

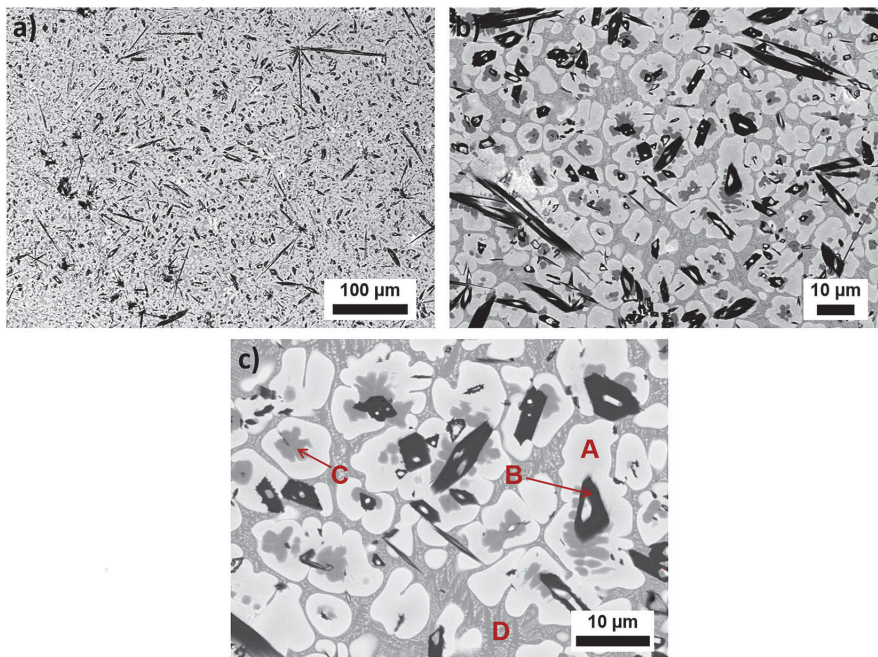


Fig. 4. SEM microstructure of as-melted surface at different magnifications.

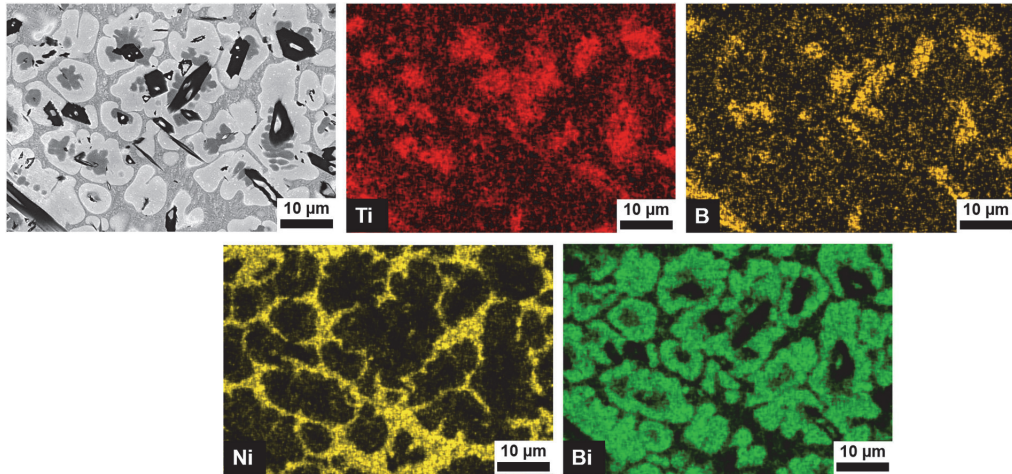


Fig. 5. Details of the surface microstructure signifying TiB phase encapsulation inside Bi phase as detected in SEM and an EDS mapping thereof including titanium, boron, nickel and bismuth.

Table 2

Chemical composition in wt% as evaluated by EDS for the spots labelled in Fig. 4c for the as-melted surface microstructure.

Spot	Chemical composition (wt%)				
	Ti	B	Ni	Bi	O
A	71.9		4.5	23.5	0.1
B	92.2	7.8			
C	87.5		0.6	11.7	0.3
D	64.4		33.5	2.1	

orbicular-shaped Bi-rich region is evidenced. The existence of encapsulated Ti in the surface region is found in two major phases, i.e. with B (~8 wt%, dark region, point B, Fig. 4c) and the other without B but with a large concentration of Bi (~11 wt%, grey region, point C, Fig. 4c). As per thermocalc calculations, the existence of TiBi solid solution may coexist with Ti₂Ni (in equal amounts) up to 1073 K. However, upon that the formation of (B,Bi,Ni,Ti) phase in a liquid state remained evident. The presence of Ti (~64 wt%) together with Ni (~33 wt%) and some amount of Bi is also perceived in the matrix surrounding the orbicular-shaped regions (Fig. 4c, point D, Fig. 4c). The existence of the Ti₂Ni phase (titanium-rich alloy) is justified by thermocalc calculations. It should be noted that the self-lubricating surface demonstrates a beneficial form of a whisker-like TiB phase (darker region, confirmed by EDS, XRD). Transformation of unreacted TiB₂ (from the substrate after SPS, Fig. 1b) to a thermodynamically stable TiB upon a longer heat input (during laser cladding) is stated in ref. [1]. Therefore, the microstructural features can be summarized as follows: (1) Ti is relatively uniformly distributed throughout the melted-surface region; (2) the grains of TiB/TiB₂ exhibit a so-called core-shell structure wherein TiB core is encapsulated by Bi rich phase; and (3) Ni is majorly concentrated around the orbicular shaped Bi-rich region. In contrast to other evidence [15,25], where the non-uniform distribution of soft metals such as Ag or Bi has been stated, the current study reveals a homogeneously distributed Bi mainly around titanium and/or titanium borides, which points to a positive choice of Ti-TiB₂ as a substrate material. A high affinity between Ti and Bi to form compounds at 600–700 °C is also confirmed in thermocalc phase study [26]. Moreover, the presence of both the compounds i.e. B and Bi might aid in better lubricity of the Ni–Bi incorporated composite. For instance, the Bi compounds could act as a lubricant at temperatures below 600 °C [12,13] and B (upon formation

of glazed boric acid tribolayer, H₃BO₂) could aid in friction reduction above 600 °C [1].

3.3. Surface-substrate interface

Fig. 6 displays the low and high magnified images of the melted region featuring the surface-substrate interface section. A gradual and compact evolution of phases in the interface is clearly shown. The intermixing of different phases at the interface hereby points to improved adhesion. Table 3 (a, b) displays the elemental composition of various spots on the melted region. A concentration gradient of Ni and Bi (bright region) can be measured from the interface to the surface i.e. Point B to A. Moreover, their absence on spots C and D points to a minimum dilution of the Ni–Bi during laser deposition. The presence of Ti and B elements across the melted surface confirms the idea of titanium diffusion and TiB dissolution in the melt zone during the laser deposition process. In addition, due to its high hardness (1800 HV), TiB is believed to enhance the mechanical properties of the material [7]. Even though the laser deposition was carried out in an inert atmosphere, the presence of oxygen in some amount (<4 %) is detectable as the unsealed argon chamber used during the deposition process can allow oxygen contamination from the surrounding air atmosphere.

3.4. X-ray diffraction analysis

The XRD spectra of the as-melted surface (Fig. 7) allow for the identification of intermetallics compound phases such as Ti₂Ni (~36 wt %) and a ternary stable phase of Ti₄NiBi₂ (~26 wt%), which is in an agreement with the calculations considering to the presence of major ternary Ti-Bi-Ni phase. Besides, the thermodynamically foreseen NiTi₂ phase existed with TiNi. The absence of the NiBi phase can be explained by difficulties in nucleation and diffusion of Ni and Bi elements in each other from one hand, and multiphase binary products availability and more feasible interdiffusion process of titanium and liquid bismuth from another. The development of these phases is justified by their phase diagram (Fig. 3). Besides, the presence of Ti₄NiBi₂ is linked to a strong interaction between Ti and Bi leading to a strong bonding [27]. The characteristic XRD peaks of the rhombohedral free Bi phase of the negligible amount are observed. The presence of orthorhombic Ni₂B was found to be scarce i.e. ~1.2 wt%. The possibility of the formation of nickel borides under the Ar atmosphere at a high temperature (through

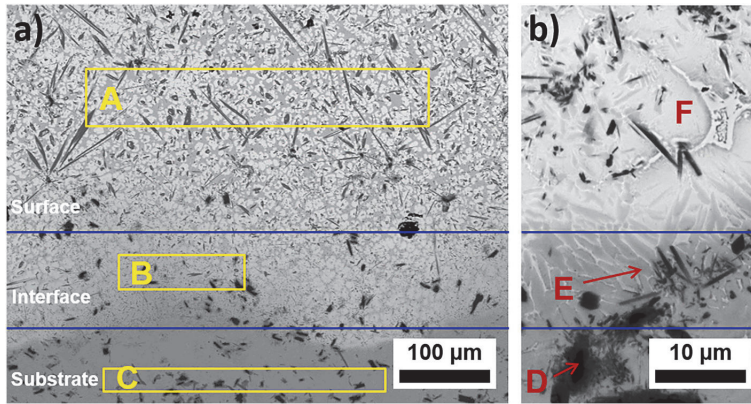


Fig. 6. Cross-section SEM microstructure (at different magnifications) showing the surface-interface-substrate region in the composite. Region A and F- surface (laser melted); region B and E- interface; region C and D- substrate (unmelted zone).

Table 3
Chemical composition in wt% as evaluated by EDS for the spots labelled in Fig. 6.

Spot	Chemical composition (wt%)				
	Ti	B	Ni	Bi	O
A	76.5	0.8	11.9	9.9	0.9
B	83.7	0.9	9.2	5.5	0.7
C	97.4	1.7			0.9
D	85.5	13.8			0.7
E	96.6		0.4	2.2	0.8
F	86.7	0.6	5.8	6.4	0.5

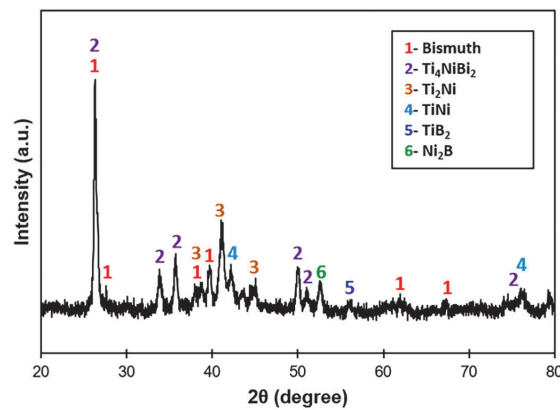


Fig. 7. XRD spectra of as-melted Ni-Bi surface on Ti-TiB₂ composite.

annealing, plasma spraying etc.) aligns with the previously reported result [28]. Surprisingly, no peaks of pure Ni are found, advocating the fact that all Ni is consumed during phase transformation. Furthermore, the coating features the peaks of TiB and TiB₂ due to titanium and boron dissolution from the substrate during the laser deposition process. The occurrence of dual titanium boride (TiB₂ + TiB) in the composite microstructure is proven to enhance its mechanical and tribological properties [29].

3.5. Microhardness

Fig. 8 shows the microhardness (HV1) plot taken from a cross-section ranging from the surface to the substrate of Ni-Bi samples. The measured microhardness of the melted surface of ~620 HV1 is almost twice the hardness of the substrate material (around ~348 HV1). This upsurge in the hardness of the surface can be attributed to the intrinsic hardness of each constituent phase and densification within it. The positive effect of Ti₂Ni and TiNi phases on the resulting mechanical, corrosion as well as tribological properties is studied in [30-32]. It is reported that the hardness of FCC Ti₂Ni intermetallic solid solution is ~700 HV_{0.025} [30,32]. The concentration of Ti₂Ni intermetallic alloy in the surface region is around 36 wt%, which may be a reason for an enhancement in hardness. Furthermore, the indents produced during the microhardness tests displayed a sharp edge and generated no cracks, signifying the desired interfacial compatibility between the various phases in the laser-melted zone.

3.6. High temperature sliding performance

Fig. 9 presents the measured friction curves for the Ni-Bi laser-melted samples (Ni-Bi) and the reference unmodified samples (Ref) sliding against flat Ti-alloy pins at RT, 400 and 600 °C.

For sliding at RT and 400 °C, the Ni-Bi samples show a substantial

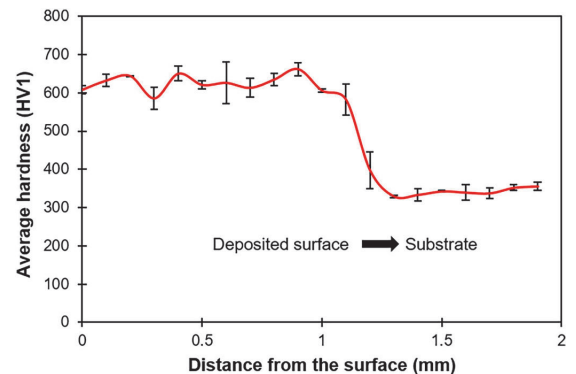


Fig. 8. Room temperature microhardness (HV1) values of Ni-Bi sample from surface to substrate.

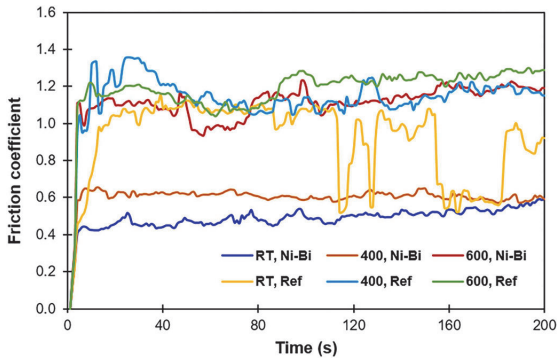


Fig. 9. CoF of studied samples for reciprocating tests against a flat counterbody pin. Reference unmodified samples are labelled as 'Ref' and Ni—Bi laser-melted samples are labelled as 'Ni—Bi'. The temperature of the test is mentioned.

reduction in friction at RT (~ 0.5) and 400 °C (~ 0.6) compared to the unmodified reference. (~ 1.2). At RT sliding, the Ni—Bi not only demonstrates a considerably reduced CoF but also a stable and relatively smooth friction curve (Fig. 9); while, an unstable CoF along with a vibration of test setup was noticed during sliding of the reference specimen at RT. The unstable CoF of the reference specimen can be associated with an extensive 'stick-slip' adhesive phenomena or an unsteady tribolayer formation due to a high concentration of ductile pure Ti in it [1]. A significant increase in CoF at 600 °C sliding is noticed for both Ni—Bi and the reference samples (above 1.0). However, the CoF of the Ni—Bi is more stable than the unmodified reference. A point to note is that both the materials demonstrate similar patterns of CoF evolution at 600 °C. Besides, their initial running-in time for friction stabilization (reaching the steady state) is similar i.e. around 100 s. This may hint at the ineffectiveness of the Ni—Bi lubrication at 600 °C.

Fig. 10 demonstrates the HT volumetric wear rate of the materials tested and the counterbody pin used. Fig. 11 exhibits the 3D wear profiles of specimens after the test. It can be seen that the wear rate of the Ni—Bi samples significantly decreased at 400 °C (~ 13 times) and 600 °C (~ 4 times) in comparison to the corresponding sliding temperatures of unmodified reference. However, at RT sliding, the Ni—Bi demonstrates comparable wear with the reference specimen. Another point is that the reference exhibits twofold higher wear with a consecutive increase in the test temperature, whereas the Ni—Bi demonstrates a major reduction in wear rate at HT sliding in comparison to its RT

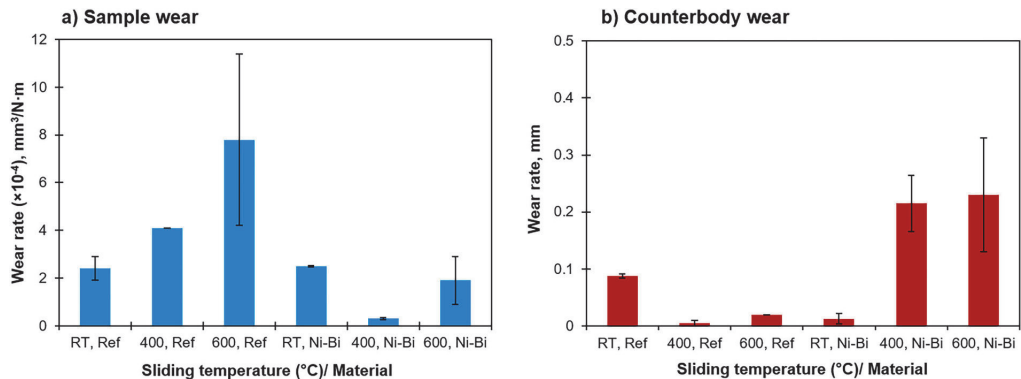


Fig. 10. Wear rate after reciprocating sliding tests against flat counterbody pins for all test temperatures; a) sample wear; and b) counterbody pin wear. Reference unmodified samples are termed as 'Ref' and Ni—Bi laser-melted samples as 'Ni—Bi'.

value, particularly at 400 °C (>8 times decrease compared to its RT wear). A key point to note is that the diminution in wear rate of the Ni—Bi sample at 600 °C is coupled with a high CoF (~ 1.0), which may be linked to severe wear of the counterbody pin.

The maximum depths of the wear scars correlated well with wear rates, as seen in Fig. 11. In general, at all testing temperatures, the reference unmodified specimen demonstrates a higher wear depth than the Ni—Bi specimen. The scar depths observed after RT, 400 and 600 °C test for the reference specimen were as high as 70, 200 and 250 μm , respectively; whereas the self-lubricating Ni—Bi, it exhibits a much shallower depth of 50, 22 and 120 μm , respectively.

Fig. 12 demonstrates the SEM images of the worn surfaces illustrating the main wear mechanisms of the unmodified reference and Ni—Bi laser-melted samples.

At RT sliding, the Ni—Bi specimens showed signs of adhesive wear and microploughing. Patches of detached material (darker region) on the surface of the Ni—Bi are visible (Fig. 12). Upon EDS analysis it was found that the surfaces after detachment were enriched with Ti and Ni. Later, the worn surface XRD confirmed the existence of the Ti_2Ni phase (also present at 400 and 600 °C Ni—Bi sliding, a Ti-rich NiTi alloy, Fig. 13). Meanwhile, the surface around the detached patches (detached patches are seen at a lower height than vicinity surface), were found to be rich in Bi concentration leading to an inference that bismuth spreads during the test (accompanied by a surface temperature rise due to frictional heating), which in turn offered stable low friction and protected the surface. Whereas, for the unmodified reference sliding at RT, microcutting and surface cracks-led delamination was the dominant mechanism of wear leading to a fluctuating friction curve. The formation of surface cracks can be attributed to the fatigue wear of the reference composite surface or the residual stresses generated during the deposition process. However, in the case of Ni—Bi samples, it is possible that such surface cracks (if exist) could entrap the soft Bi particles forming a smooth tribolayer, besides acting as lubricant storage [33]. It can be seen that a significantly low friction coefficient of the Ni—Bi sample at RT is at the expense of wear rate; hence, can be settled that the presence of Bi might not lead to a low wear rate of the coating but offers lubrication.

At 400 and 600 °C sliding, the Ni—Bi specimen exhibited a significant decrease in delamination as compared to RT sliding (Fig. 12). A homogeneously spread tribo-oxide layer existed at this stage. EDS and XRD confirmed the presence of TiO_2 and Bi_2O_3 on the surface of Ni—Bi (tribo-oxide layer; Fig. 13). A fresh phase of $\text{Bi}_4\text{Ti}_3\text{O}_{12}$ (JCPDS file no. 47-0398) was identified after this test temperature, which is attributed to the solid state reaction between TiO_2 and Bi_2O_3 at high temperature [31]. Moreover, in comparison with the as-melted Ni—Bi sample, the wear scars on the Ni—Bi reveal no XRD peaks related to Ni_2B and

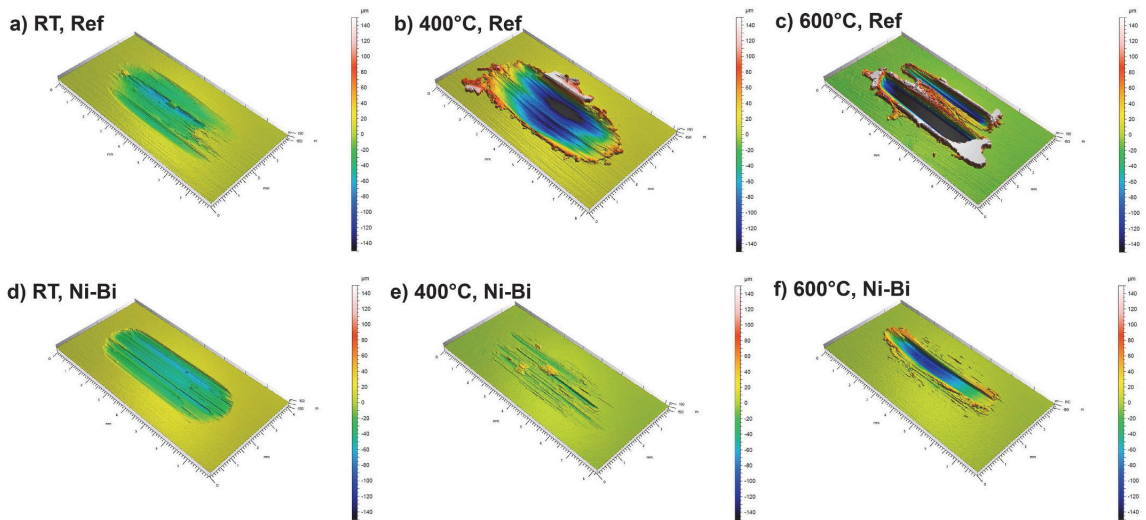


Fig. 11. 3D wear profiles of (a) reference, RT; (b) reference, 400 °C; and (c) reference, 600 °C; (d) Ni—Bi, RT; (e) Ni—Bi, 400 °C; and (f) Ni—Bi, 600 °C. Reference unmodified samples are termed as ‘Ref’ and Ni—Bi laser-melted samples as ‘Ni—Bi’.

Ti₄NiBi₂. The tribo-oxide layer featured entrapped Bi areas (Fig. 14 and Table 4). These Bi areas served as lubricants packets, which spread on the tribo-surface during HT sliding due to its easy melting (~270 °C). The lubricating nature of Bi₂O₃ during HT sliding is reported in [34,35]. The tribo-oxide layer formed at 600 °C exhibited a rough surface in comparison to 400 °C. Signs of wear debris relocation (after their removal) on the Ni—Bi sample surface are highly evident. In addition, the tribo-oxide layer features a high concentration of Al and V on the surface pointing to a material transfer from the counterbody. An EDS examination confirmed the counterbody material on the sliding Ni—Bi surface and vice-versa (Fig. 15). A high counterbody wear against the Ni—Bi sliding at 600 °C is also measured after the test (Fig. 10b). It is likely that the counterbody (Ti6Al4V alloy) suffers wear loss at high temperature sliding against a formed hard tribo-oxide layer (rutile-TiO₂). Additionally, the fact that Ni—Bi surface constantly (due to high wear of counterbody pin) added up a transfer of counterbody material during the test might have generated a ‘material pile-up’ situation resulting in an unstable and a higher CoF at 600 °C sliding (Fig. 9). Fatigue driven minor cracks of the tribo-oxide layer were evident on the Ni—Bi surface after 400 and 600 °C sliding. The main responsible wear mechanism at 400 and 600 °C Ni—Bi sliding is micropolishing and compaction of the tribo-oxide layer. Conversely, the reference unmodified samples at 400 and 600 °C sliding demonstrated severe wear characterized by plastic deformation, shearing, material transfer and oxidation of the surface. Besides, there were no signs of debris compaction occurring (Fig. 12 c, e). Here, the loose debris (mainly TiO₂) stayed on the tribo-surface during the test (a virtue of flat on flat configuration) and perhaps resulted in a third body abrasion during sliding giving a high CoF and wear value [36]. At this stage, the main mechanism of wear is severe plastic deformation and oxidative wear. An interesting point is that in the case of Ni—Bi samples, the presence of lubricating debris (Bi-rich phases or Bi₂O₃) on the test surface would have served in a positive way of minimizing friction.

To understand correctly the nature of counterbody wear, the pins were analysed through SEM and EDS. Fig. 16 shows counterbody wear scars after testing at 400 and 600 °C against the unmodified reference and the laser-melted Ni—Bi samples. It can be seen that sliding against Ni—Bi at 400 °C produced an even surface resulting in a very stable friction coefficient. However, against unmodified reference at the same

sliding temperature, the counterbody underwent substantial delamination along with visible patches of adhesive wear resulting in an unstable friction curve. It must be noted here that the chosen Ti alloy (counterbody material) is susceptible to softening at high temperatures [37]. This mechanism resulted in a high softening and plastic deformation of the counterbody during sliding at 600 °C. Severe marks of adhesion and material detachment were noticed at this stage (Fig. 16c). Such severity of plastic deformation resulted in a ‘material flow’ and an uneven surface resulting in an unstable CoF curve. Gross plastic deformation, ploughing and smearing characterized the counterbody wear scars at 600 °C. Moreover, in the case of the hard laser melted surface, the counterbody (lower hardness) underwent high wear, as shown also in Fig. 10b. This suggests that the wear resistance of Ni—Bi at 600 °C is high (as shown in Fig. 10b) and the unstable friction coefficient is due to high wear and resultant bumpy surface of the sliding counterbody pin.

4. Conclusions

In the current work, a self-lubricating nickel-bismuth powder mixture (Ni—Bi) was successfully incorporated into spark plasma sintered Ti-10wt%TiB₂ composite using laser melting. The produced laser-melted bulks were examined for thermodynamic modelling, microstructure, hardness and high temperature sliding performance, and the following conclusions have been made:

- Thermodynamic modelling demonstrates the likelihood of the formation of titanium monoboride, Ti₂Ni and TiBiNi solid solution phases in the quaternary Ti-B-Ni—Bi system, which is further supported by the phase analysis of the surface, interface, and substrate areas.
- The fabricated Ni—Bi bulks demonstrated the formation of a 1–1.5 mm thick Bi-Ni-Ti-TiB_x functional surface. The surface features a compact, poreless and crack-free microstructure with the major phases of Ti₂Ni, Ni₂B, and Ti₄NiBi₂. The laser melting process leads to the formation of core-shell structures in which the ceramic core (TiB_x) is surrounded by the Bi-rich solid solution shell.
- The functional surface exhibits a two-fold increase in hardness (HV1 ~ 620 HV) as compared to the underlying substrate owing to

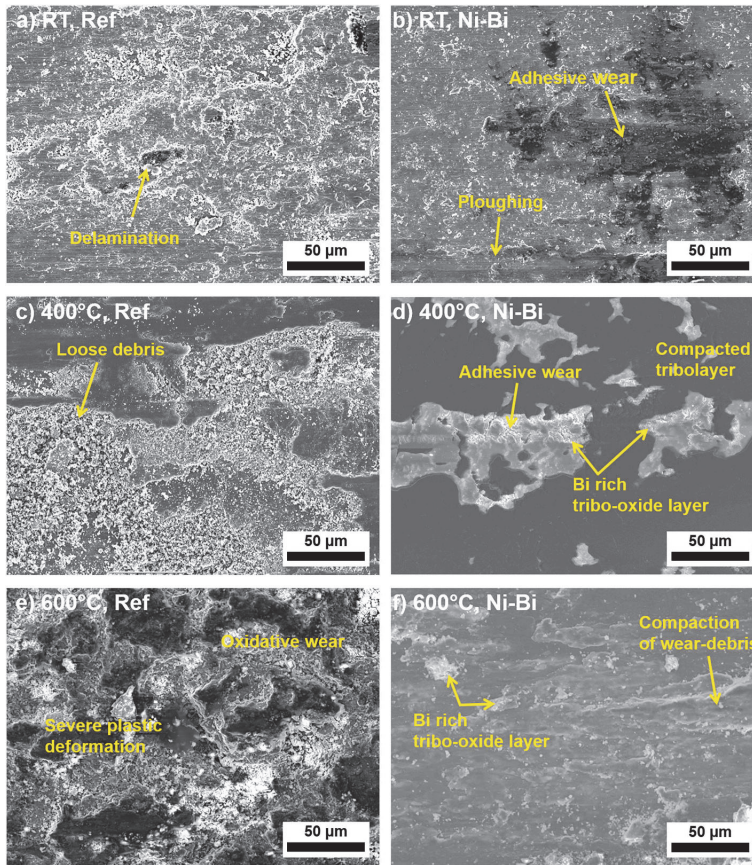


Fig. 12. Wear scar SEM images of unmodified reference and Ni–Bi melted samples demonstrating their respective wear mechanisms for all test temperatures. The temperature of the tests is labelled. Reference unmodified samples are termed as ‘Ref’ and Ni–Bi laser-melted samples as ‘Ni–Bi’.

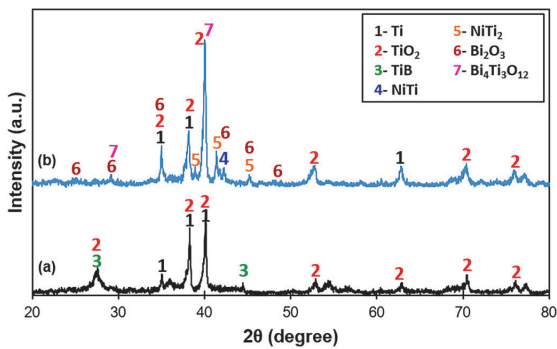


Fig. 13. XRD phase analysis of wear scars after test at 400 °C for (a) reference and; (b) Ni–Bi sample.

the intrinsic hardness of constituents phases and strong bonding between them.

- A significant reduction in the wear rate of the Ni–Bi samples under the reciprocating sliding test against the Ti-alloy flat-pin counterbody is noticed at high temperatures of 400 and 600 °C. Meanwhile,

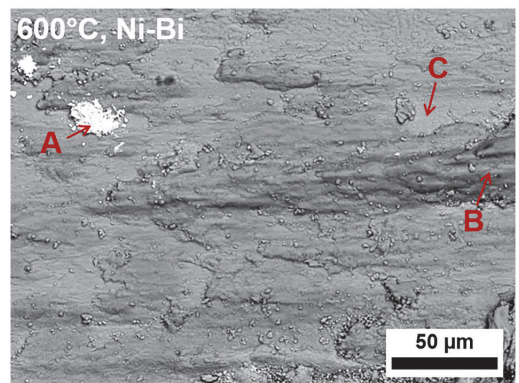


Fig. 14. Back scattered image of Ni–Bi sample surface after test at 600 °C showing entrapment of Bi (spot A) in the generated tribo-oxide layer. The spots labelled as A, B and C are analysed for chemical composition and illustrated in Table 4.

Table 4
Chemical composition in wt% as evaluated by EDS for the spots labelled in Fig. 14.

Spot	Chemical composition (wt%)						
	Ti	B	Ni	Bi	O	Al	V
A	12.8	0.9	39.2	40.9	6.0	0.2	
B	79.0	0.5	0.3	0.2	7.6	9.5	2.9
C	83.8	4.4	0.4	0.8	10.3	0.3	

a higher CoF value at 600 °C sliding is coupled with severe counterbody wear. At RT and 400 °C, the Ni–Bi samples demonstrate a stable and a twofold lower CoF of ~0.5–0.6 as compared to the reference composite (~1.2).

- The low CoF value of the laser-melted Ni–Bi samples is linked to a homogeneously spread bismuth at RT sliding (melting during frictional heating and providing smooth sliding); while at high temperatures, an adherent tribo-oxide layer rich in TiO₂ and Bi₂O₃ is responsible for a significantly reduced wear as well as CoF. The tribo-oxide layer features entrapped Bi-rich regions. The lubrication behaviour of bismuth at room and high temperature is confirmed.
- The polishing and compaction of the tribo-oxide layer is the main mechanism of wear at 400 and 600 °C for the self-lubricating Ni–Bi samples; while the main mechanism of wear is the severe plastic deformation and oxidation for the unmodified composite.

CRediT authorship contribution statement

R. Kumar: Conceptualization, Methodology, Formal analysis, Investigation, Data curation, Writing – original draft, Visualization, Writing – review & editing. **H. Torres:** Methodology, Investigation, Data curation, Writing – review & editing. **S. Aydinyan:** Methodology, Software, Investigation, Writing – review & editing. **M. Antonov:** Validation, Methodology, Resources, Visualization. **M. Varga:** Resources, Project administration, Funding acquisition, Visualization. **M. Rodriguez Ripoll:** Conceptualization, Methodology, Validation, Resources, Project administration, Funding acquisition, Supervision, Investigation, Visualization, Writing – review & editing. **I. Hussainova:** Validation, Resources, Project administration, Funding acquisition, Supervision, Visualization, Writing – review & editing.

Declaration of competing interest

We have NO affiliations with or involvement in any organization or entity with any financial interest (such as honoraria; educational grants; participation in speakers' bureaus; membership, employment, consultancies, stock ownership, or other equity interest; and expert testimony or patent-licensing arrangements), or non-financial interest (such as personal or professional relationships, affiliations, knowledge or beliefs) in the subject matter or materials discussed in this manuscript.

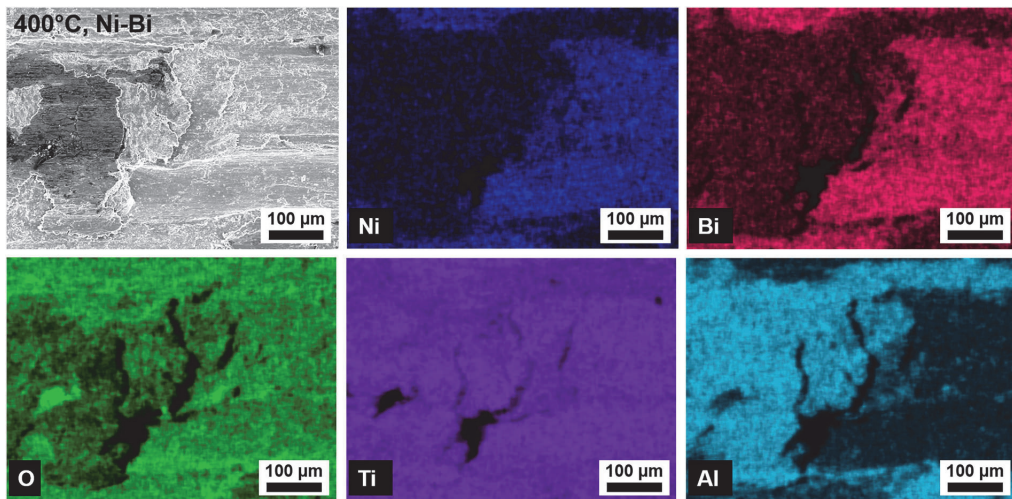


Fig. 15. EDS analysis of an area of Ni–Bi sample surface after test at 400 °C showing the presence of different elements. Ti (partially) and Al presence are contributed from the counterbody material. Bi spreads all over the plough mark resulting in lubrication during the test.

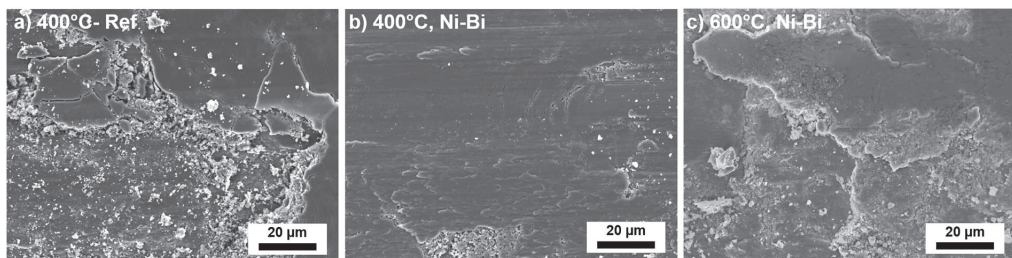


Fig. 16. SEM images of counterbody pin surface sliding at/against (a) 400 °C - Ref; (b) 400 °C - Ni–Bi; and (c) 600 °C - Ni–Bi. Unmodified reference samples are labelled as 'Ref' and laser-melted Ni–Bi as 'Ni–Bi'.

Data availability

Data will be made available on request.

Acknowledgements

This work was supported by the Estonian Research Council grants (PRG643, PSG220) and M-ERA.Net project “HOTselflub” MOBERA18 N.20097582-CA. A significant part of this work was funded by the “Austrian COMET-Programme” (Project InTribology1, no. 872176) under the scope of K2 InTribology and was developed in collaboration with the “Excellence Centre of Tribology” (AC2T research GmbH).

References

- [1] R. Kumar, M. Antonov, L. Liu, I. Hussainova, Sliding wear performance of in-situ spark plasma sintered Ti-TiBw composite at temperatures up to 900° C, *Wear* 476 (2021), 203663, <https://doi.org/10.1016/j.wear.2021.203663>.
- [2] R. Kumar, I. Hussainova, R. Rahmani, M. Antonov, Solid lubrication at high-temperatures—a review, *Materials* 15 (2022) 1695, <https://doi.org/10.3390/ma15051695>.
- [3] Y. Pu, B. Guo, J. Zhou, S. Zhang, H. Zhou, J. Chen, Microstructure and tribological properties of in situ synthesized TiC, TiN, and SiC reinforced Ti3Al intermetallic matrix composite coatings on pure ti by laser cladding, *Appl. Surf. Sci.* 255 (5) (2008) 2697–2703, <https://doi.org/10.1016/j.apsusc.2008.07.180>.
- [4] S. Zhang, W.T. Wu, M.C. Wang, H.C. Man, In-situ synthesis and wear performance of TiC particle reinforced composite coating on alloy Ti6Al4V, *Surf. Coat. Technol.* 138 (1) (2001) 95–100, [https://doi.org/10.1016/S0257-8972\(00\)01133-6](https://doi.org/10.1016/S0257-8972(00)01133-6).
- [5] J. Li, X. Luo, G.J. Li, Effect of Y2O3 on the sliding wear resistance of TiB/TiC-reinforced composite coatings fabricated by laser cladding, *Wear* 310 (1–2) (2014) 72–82, <https://doi.org/10.1016/j.wear.2013.12.019>.
- [6] D. Dey, K.S. Bal, A.K. Singh, A.R. Choudhury, Hardness and wear behaviour of multiple component coating on ti-6Al-4V substrate by laser application, *Optik* 202 (2020), 163555, <https://doi.org/10.1016/j.ijleo.2019.163555>.
- [7] R. Kumar, L. Liu, M. Antonov, R. Ivanov, I. Hussainova, Hot sliding Wear of 88 wt. % TiB–Ti composite from SHS produced powders, *Materials* 14 (5) (2021) 1242, <https://doi.org/10.3390/ma14051242>.
- [8] Y.L. Qin, L. Geng, D.R. Ni, Dry sliding wear behavior of titanium matrix composites hybrid-reinforced by in situ TiBw and TiCp, *J. Compos. Mater.* 46 (21) (2012) 2637–2645, <https://doi.org/10.1177/0021998311417645>.
- [9] V. Ocelik, D. Matthews, J.T.M. De Hosson, Sliding wear resistance of metal matrix composite layers prepared by high power laser, *Surf. Coat. Technol.* 197 (2–3) (2005) 303–315, <https://doi.org/10.1016/j.surfcoat.2004.09.003>.
- [10] H. Torres, M. Rodríguez Ripoll, B. Prakash, Tribological behaviour of self-lubricating materials at high temperatures, *Int. Mater. Rev.* 63 (5) (2018) 309–340, <https://doi.org/10.1080/09506608.2017.1410944>.
- [11] R. Mirabal-Rojas, O. Depablos-Rivera, C.L. Gómez, A. Fonseca-García, J.C. Medina, C.C. Barrera-Ortega, S.E. Rodil, Reduction of the coefficient of friction of niobium nitride coatings by the addition of bismuth, *Vacuum* 125 (2016) 146–153, <https://doi.org/10.1016/j.vacuum.2015.12.016>.
- [12] H. Sun, G. Yi, S. Wan, P. Shi, J. Yang, S.T. Pham, T.D. Ta, Effect of adding soft Bi2O3 on structural modification and tribological regulation of Ni-5 wt% Al composite coating in wide temperatures range, *Surf. Coat. Technol.* 405 (2021), 126517, <https://doi.org/10.1016/j.surfcoat.2020.126517>.
- [13] P. Gonzalez-Rodriguez, K.J. van den Nieuwenhuijzen, W. Lette, D.J. Schipper, J. E. Ten Elshof, Tribochemistry of bismuth and bismuth salts for solid lubrication, *ACS Appl. Mater. Interfaces* 8 (11) (2016) 7601–7606, <https://doi.org/10.1021/acsami.6b02541>].
- [14] V. Oksanen, A. Lehtovaara, M. Kallio, Load capacity of lubricated bismuth bronze bimetal bearing under elliptical sliding motion, *Wear* 388–389 (2017) 72–80, <https://doi.org/10.1016/j.wear.2017.05.001>.
- [15] C. Liu, Y. Yin, C. Li, M. Xu, R. Li, Q. Chen, Nano bi chemical modification and tribological properties of Bi/SiO2 composite as lubricating oil additives, *Tribol. Lett.* 70 (3) (2022) 1–15, <https://doi.org/10.1007/s11249-022-01610-6>.
- [16] H. Torres, S. Slawik, C. Gachot, B. Prakash, M.R. Ripoll, Microstructural design of self-lubricating laser claddings for use in high temperature sliding applications, *Surf. Coat. Technol.* 337 (2018) 24–34, <https://doi.org/10.1016/j.surfcoat.2017.12.060>.
- [17] C. Liu, Y. Yin, C. Li, M. Xu, R. Li, Q. Chen, Tailoring cu nano bi self-lubricating alloy material by shift-speed ball milling flake powder metallurgy, *J. Alloys Compd.* 903 (2022), 163747, <https://doi.org/10.1016/j.jallcom.2022.163747>.
- [18] J. Dutta Majumdar, I. Manna, Laser material processing, *Int. Mater. Rev.* 56 (5–6) (2011) 341–388, <https://doi.org/10.1179/1743280411Y.0000000003>.
- [19] Torres, H., Pichelbauer, K., Schachinger, T., Gachot, C., & Rodríguez Ripoll, M. A Ni–Bi self-lubricating Ti6Al4V alloy for high temperature sliding contacts. “To be communicated”.
- [20] H. Torres, T. Vuchkov, M.R. Ripoll, B. Prakash, Tribological behaviour of MoS2-based self-lubricating laser cladding for use in high temperature applications, *Tribol. Int.* 126 (2018) 153–165, <https://doi.org/10.1016/j.triboint.2018.05.015>.
- [21] R. Kumar, M. Antonov, P. Klimczyk, V. Mikli, D. Gomon, Effect of cBN content and additives on sliding and surface fatigue wear of spark plasma sintered Al2O3-cBN composites, *Wear* 494 (2022), 204250, <https://doi.org/10.1016/j.wear.2022.204250>.
- [22] W.A.N.G. Jiang, F.G. Meng, L.B. Liu, Z.P. Jin, Thermodynamic optimization of Bi-Ni binary system, *Trans. Nonferrous Metals Soc. China* 21 (1) (2011) 139–145, [https://doi.org/10.1016/S1003-6326\(11\)60690-0](https://doi.org/10.1016/S1003-6326(11)60690-0).
- [23] M.S. Lee, C. Chen, C.R. Kao, Formation and absence of intermetallic compounds during solid-state reactions in the Ni–Bi system, *Chem. Mater.* 11 (2) (1999) 292–297, <https://doi.org/10.1021/cm980521>.
- [24] G.P. Vassilev, Contribution to the Ti-Bi phase diagram, *Cryst. Res. Technol.* 41 (4) (2006) 349–357, <https://doi.org/10.1002/crat.200510586>.
- [25] H. Torres, T. Vuchkov, S. Slawik, C. Gachot, B. Prakash, M.R. Ripoll, Self-lubricating laser claddings for reducing friction and wear from room temperature to 600° C, *Wear* 408 (2018) 22–33, <https://doi.org/10.1016/j.wear.2018.05.001>.
- [26] S. Maruyama, Y. Kado, T. Uda, Phase diagram investigations of the bi-ti system, *J. Phase Equilib. Diffus.* 34 (4) (2013) 289–296, <https://doi.org/10.1007/s11669-013-0243-0>.
- [27] R. Rytz, R. Hoffmann, Chemical bonding in the ternary transition metal bismuthides Ti4 T Bi2 with T= Cr, Mn, Fe, Co, and Ni, *Inorg. Chem.* 38 (7) (1999) 1609–1617, <https://doi.org/10.1021/ic981075v>.
- [28] V. Vitry, A.F. Kanta, F. Delaunoi, Mechanical and wear characterization of electroless nickel-boron coatings, *Surf. Coat. Technol.* 206 (7) (2011) 1879–1885, <https://doi.org/10.1016/j.surfcoat.2011.08.008>.
- [29] Y. Song Zhu, Y. Fei Liu, X. Nong Wei, D. Sun, W. Zhuang Lu, T.J. Ko, Tribological characteristics of the dual titanium boride layers (TiB2+ TiB) on titanium alloy, *Ceram. International* 47 (10) (2021) 13957–13969, <https://doi.org/10.1016/j.ceramint.2021.01.265>.
- [30] Z. Wang, Z. He, Y. Wang, X. Liu, B. Tang, Microstructure and tribological behaviors of Ti6Al4V alloy treated by plasma ni alloying, *Appl. Surf. Sci.* 257 (23) (2011) 10267–10272, <https://doi.org/10.1016/j.apsusc.2011.07.040>.
- [31] F. Gao, H.M. Wang, Dry sliding wear property of a laser melting/deposited Ti2Ni/TiNi intermetallic alloy, *Intermetallics* 16 (2) (2008) 202–208, <https://doi.org/10.1016/j.intermet.2007.09.008>.
- [32] M.M. Verdian, K. Raeissi, M. Salehi, S. Sabooni, Characterization and corrosion behavior of NiTi–Ti2Ni–Ni3Ti multiphase intermetallics produced by vacuum sintering, *Vacuum* 86 (1) (2011) 91–95, <https://doi.org/10.1016/j.vacuum.2011.04.022>.
- [33] Y. Holovenko, M. Antonov, L. Kollo, I. Hussainova, Friction studies of metal surfaces with various 3D printed patterns tested in dry sliding conditions, *Proc. Inst. Mech. Eng. B J. Eng. Tribol.* 232 (1) (2018) 43–53, <https://doi.org/10.1177/1350650117738920>.
- [34] X. Wang, X. Feng, C. Lu, G. Yi, J. Jia, H. Li, Mechanical and tribological properties of plasma sprayed NiAl composite coatings with addition of nanostructured TiO2/Bi2O3, *Surf. Coat. Technol.* 349 (2018) 157–165, <https://doi.org/10.1016/j.surfcoat.2018.05.055>.
- [35] S.S. Jaffar, I.A. Baqer, W.A. Soud, Effect of Bi2O3 nanoparticles addition to lubricating oil on the dynamic behavior of rotor-bearing systems, *J. Vibra. Eng. Technol.* 1–13 (2022), <https://doi.org/10.1007/s42417-022-00495-y>.
- [36] R. Kumar, S. Aydinyan, R. Ivanov, L. Liu, M. Antonov, I. Hussainova, High-temperature Wear performance of hBN-added ni-w composites produced from combustion-synthesized powders, *Materials* 15 (3) (2022) 1252, <https://doi.org/10.3390/ma15031252>.
- [37] H. Mohseni, P. Nandwana, A. Tsoi, R. Banerjee, T.W. Scharf, In situ nitrided titanium alloys: microstructural evolution during solidification and wear, *Acta Mater.* 83 (2015) 61–74, <https://doi.org/10.1016/j.actamat.2014.09.026>.

Publication III

Kumar, R., Aydinyan, S., Ivanov, R., Liu, L., Antonov, M., & Hussainova, I. (2022). High-Temperature Wear Performance of hBN-Added Ni-W Composites Produced from Combustion-Synthesized Powders. *Materials*, 15(3), 1252.

Article

High-Temperature Wear Performance of hBN-Added Ni-W Composites Produced from Combustion-Synthesized Powders

Rahul Kumar ¹, Sofiya Aydinyan ^{1,2}, Roman Ivanov ¹, Le Liu ¹, Maksim Antonov ¹ and Irina Hussainova ^{1,*}

¹ Department of Mechanical & Industrial Engineering, Tallinn University of Technology, 19086 Tallinn, Estonia; rahul.kumar@taltech.ee (R.K.); sofiya.aydinyan@taltech.ee (S.A.); roman.ivanov@taltech.ee (R.I.); le.liu@taltech.ee (L.L.); maksim.antonov@taltech.ee (M.A.)

² A.B. Nalbandyan Institute of Chemical Physics NAS RA, P. Sevak 5/2, Yerevan 0014, Armenia

* Correspondence: irina.hussainova@taltech.ee

Abstract: This work reports on the spark plasma sintering (SPS) of self-propagating high-temperature-synthesis (SHS)-derived Ni-W and Ni-W-2wt%hBN (4:1 molar ratio of metals) powders. The synthesis was carried out from a mixture of NiO and WO₃ using Mg + C combined reducers through a thermo-kinetic coupling approach. Experiments performed in the thermodynamically optimal area demonstrated the high sensitivity of combustion parameters and product phase composition to the amount of reducers and hBN powder. The powder precursors with and without the addition of hBN were consolidated using SPS at a temperature and pressure of 1300 °C and 50 MPa, respectively, followed by a thorough phase and microstructural characterization of the obtained specimens. SHS-derived powders comprised the nano-sized agglomerates and were characterized by a high sinterability. The specimens of >95% density were subjected to ball-on-plate dry sliding wear tests at a sliding speed of 0.1 ms⁻¹ and a distance of 1000 m utilizing an alumina ball of 10 mm in diameter under a 15 N normal load. The tests were performed at a temperature of 800 °C. A significant improvement in wear behavior was demonstrated for SHS-processed composites in comparison with their counterparts produced via conventional high-energy ball milling technique owing to the phenomena of ‘micro-polishing’, cyclic ‘self-healing’ and fatigue. However, the decisive effect of hBN addition in imparting lubrication during an HT wear test was not confirmed.

Keywords: self-propagating high-temperature synthesis; spark plasma sintering; sliding wear; high temperature; friction; Ni-W; hBN



check for updates

Citation: Kumar, R.; Aydinyan, S.; Ivanov, R.; Liu, L.; Antonov, M.; Hussainova, I. High-Temperature Wear Performance of hBN-Added Ni-W Composites Produced from Combustion-Synthesized Powders. *Materials* **2022**, *15*, 1252. <https://doi.org/10.3390/ma15031252>

Academic Editors: Salvatore Grasso and Kyosuke Yoshimi

Received: 30 December 2021

Accepted: 5 February 2022

Published: 8 February 2022

Publisher’s Note: MDPI stays neutral with regard to jurisdictional claims in published maps and institutional affiliations.



Copyright: © 2022 by the authors. Licensee MDPI, Basel, Switzerland. This article is an open access article distributed under the terms and conditions of the Creative Commons Attribution (CC BY) license (<https://creativecommons.org/licenses/by/4.0/>).

1. Introduction

Mechanical, chemical or electro-chemical wear is a major concern in industries such as mining, material processing, electrical, chemical and surface engineering. The material damage by wear in such areas is sometimes a simultaneous approach of more than one wear mode (e.g., mechanical, corrosion or oxidation). Furthermore, in applications involving high temperatures (HTs), such as hot forming or forging, the wear mechanisms can be dramatically changed, resulting in a catastrophic failure and significant downtime. The incorporation of refractory metals, such as W, Mo, Ni and Cu in the transition metals, to enhance mechanical, tribological and corrosion properties, in conjunction with the preservation of thermal and electrical properties, is gaining popularity. In this respect, nickel-tungsten (Ni-W) alloys have shown fair potential for enhanced surface protection in electronics and mechanical industries; as high-temperature substrates for superconductors, barriers or capping layers in micro-electromechanical circuits; as catalysts for hydrogen evolution processes, etc., in comparison with elemental Ni [1]. Moreover, owing to its environmentally friendly nature, Ni-W alloys (composite or coating) can replace electroplated hard chromium or cadmium coatings in the areas of wear and corrosion protection, which are considered environmentally hazardous in the EU directives [2]. In recent years, the

main fabrication techniques used for Ni-W alloys involve electrodeposition and mechanical alloying [3]. Alternative methods include the joint reduction of Ni and W oxides under heating in H₂ or CO [4,5]. Nevertheless, due to large differences in their melting points ($T_{m(Ni)} = 1455$ °C, $T_{m(W)} = 3422$ °C), lattice structures and possibilities of various phase (intermetallics, solid solutions) formation, it is difficult to tailor the phase composition and achieve homogeneity in the alloy. Furthermore, electrochemical deposition of Ni-W results in a high amount of developed residual stress, which produces crack development [6,7]. Ni-W compositions with a moderate tungsten content (40 wt% vs. conventionally examined 15 wt% of W) are more complicated to deal with in terms of both synthesis and processing. To address this major challenge, there is a need to develop novel techniques aimed at the preparation of Ni-W composite powder that ensures a homogeneous distribution of phase and microstructure, along with improved mechanical and tribological characteristics.

Combustion synthesis (CS) fundamentally contributes to the field of green process intensification and has already demonstrated the ability to develop an extensive range of powders, near net shape products from ceramics, intermetallic, composites and multifunctional materials [8]. The intrinsic ‘green’ characteristics of CS or SHS are mainly related to the energy consumption arising exceptionally from the harnessing of heat produced during the reaction between reactants, the extremely reduced reaction time and sustainability. CS or self-propagating high-temperature synthesis (SHS) is an easy and inexpensive technique with tunable thermal settings for the fabrication of Ni-W (1:1 molar or 24:76 mass ratio) composite powder from a NiO-WO₃-Mg-C powder mixture [9]. In previous studies, SHS was shown to deliver powders of Mo-Cu and W-Cu in the nano-to-submicron size range using a similar pathway [10–12]. It was earlier reported [13] that the incorporation of W into Ni matrix results in grain refinement at micro and nano levels promoted properties such as hardness and wear; however, a higher amount of W induced a decrease in oxidation stability of the sintered materials.

Hexagonal boron nitride (hBN) is a laminar solid with an easily sheared layered structure that is reported to offer a friction-reducing property [14]. Moreover, due to its high oxidation resistance (~1000 °C), good thermal conductivity and chemical inertness, it is often utilized in HT wear applications. A Ni-hBN electrodeposited coating to efficiently improve hardness, wear and corrosion resistance is reported in [15]. However, the incorporation of hBN in a Ni-W system to acquire better mechanical performance was conveyed by very few studies [16,17]. Moreover, studies on Ni-W-hBN systems fabricated via combustion synthesis technique are absent to the best of our knowledge. The current work reports the fabrication of Ni-W and Ni-W-hBN systems with moderate tungsten content (40 wt%) through a more efficient method of SHS. Phase and structure evolution in Ni-W and Ni-W-hBN systems, along with homogeneous distribution of phases (metals, intermetallics, solid solutions), are essential issues regarding the synthesis and sintering to overcome phase segregation, under-sintered areas and cracking. The adiabatic combustion temperature and equilibrium phase composition of the products were first evaluated using thermodynamic modeling for the 4NiO-WO₃-Mg-C mixture and combustion peculiarities were disclosed. The possibility of one-stage preparation of 4Ni-W and 4Ni-W-hBN composite powders (hereinafter Ni-W and Ni-W-hBN) from oxide precursors by using the effective energy-efficient way (by using the thermo-kinetic coupling approach) at moderate temperature conditions was explored. The SHS-derived Ni-W and Ni-W-hBN composite powders were further put through densification via spark plasma sintering (SPS). The SPS-derived specimens were assessed for their response to HT in an 800 °C tribological environment. The results are discussed in reference to the SPS-consolidated bulks from high-energy ball-milled (HEBM) Ni-W and Ni-W-hBN composites.

2. Experimental

2.1. Combustion Synthesis

The following precursors were used for the combustion experiments (via SHS): tungsten (VI) oxide (>99.8%, 10–20 µm, Alfa Aesar, Haverhill, MA, USA), nickel oxide (>99%,

<44 μm , Alfa Aesar), magnesium powder (>99%, 150 μm , Alfa Aesar), graphite KS6 and hexagonal boron nitride powder (>99%, 20 μm). The initial powders were homogeneously mixed using a pestle in a ceramic mortar for 20 min, and 23.4 mm in diameter cylinder-shaped green bodies of 1.7–1.8 g/cm^3 density and 40–45 mm height were prepared. The prepared cold compacts were then placed in a constant pressure reactor CPR-3L (Sapphire Co., Abovyan, Armenia). The chamber was closed, evacuated, purged with nitrogen (>99.98%) and filled to the intended pressure up to 0.4 MPa. Short heating (3 s) of the tungsten spiral attached to the top surface of the sample initiated the combustion wave propagation in the mixture under study. Combustion temperature and wave propagation velocity were registered via W/Re5-W/Re20 thermocouples that were 100 μm in diameter. The maximum combustion temperature (T_c) was taken from the temperature profile. The $U_c = L/t$ formula was used for the calculation of the combustion velocity, where the distance between two thermocouples is indicated by L and the time interval between signals from thermocouples is indicated by t. The standard error for the T_c measurement was ± 20 °C and $\pm 5\%$ for U_c . The reacted sample was then crushed to a powder, sieved through a sieve with a mesh size of 100 microns and exposed to acid leaching by a 10% HCl solution at 40 °C for 20 min to remove the magnesia by-product. The combustion product after leaching comprised <20 μm particles of bimodal morphology: agglomerates of glued nanoparticles and pre-sintered crystals in both mixtures with and without hBN.

2.2. High-Energy Ball Milling (HEBM)

Mechanical milling of Ni and W powder mixture was implemented in a high-energy ball mill (Emax, Retch GmbH, Haan, Germany) in 125 mL jars. Metal powders (60 wt% of nickel and 40 wt% of tungsten) were first dry mixed in a ceramic mortar. Wet milling in the presence of ethanol (75 vol% of the jar) was performed using 3 mm zirconia balls as a milling media with a powder-to-ball mass ratio of 1:1. The milling conditions were set as follows: 1000 rpm for 12 h using intervals of 15 min and a pause for 5 min. After milling, the mixture was sieved to detach the balls and dried at 50 °C to remove the ethanol.

2.3. Spark Plasma Sintering (SPS)

The combustion synthesized powders were consolidated via the spark plasma sintering technique (KCE-FCT HP D 10-GB, FCT Systeme GmbH, Frankenblick, Germany) with simultaneous application of 50 MPa pressure, up to 1300 °C (1050, 1150, 1200, 1300 °C) temperature and a high-density current within a vacuum for dwell times of 5, 10, 20 and 30 min. The SHS powder was poured into a graphite die of 20 mm inner diameter. Graphite sheets were placed between the punch and the powder. The hBN spray was utilized to hinder the graphite interaction with the tungsten. The heating rate was set to 100 °C/min. The thickness of the produced specimens was 3 mm.

2.4. Mechanical, Phase and Microstructural Characterization

The Archimedes method was used to measure the bulk density of the prepared SPS-derived composites (Mettler Toledo ME204, Greifensee, Switzerland), where distilled water was needed as an immersion medium. The theoretical density of the mixture was calculated using the rule of mixture (the densities of nickel and tungsten were taken as 8.90 $\text{g}\cdot\text{cm}^{-3}$ and 19.25 $\text{g}\cdot\text{cm}^{-3}$, respectively). According to the rule of mixture, the densities of the Ni-W and Ni-W-2wt%hBN composites were calculated as being 11.65 $\text{g}\cdot\text{cm}^{-3}$ and 10.69 $\text{g}\cdot\text{cm}^{-3}$, respectively.

Phase analysis was accomplished via X-ray diffraction (XRD) using a Philips X'Pert PRO diffractometer (40 mA, 40 kV, $\text{CuK}\alpha$ radiation, $\lambda = 0.1542$ nm, step size of 0.02°, PANalytical, Malvern Panalytical B.V., Almelo, The Netherlands) for both crashed powders (after SHS) and SPS specimens. The HighScore Plus software database was used to determine the XRD peaks (ICCD cross-referenced). The relative amounts of different phases in the composites were estimated through the Rietveld refinement method

A field-emission scanning electron microscope (FE-SEM, Zeiss Evo MA15, Oberkochen, Germany) equipped with an EDS detector was utilized. Samples were subjected to a hot conductive (resin) mounting, polishing and coating (not required for tribological testing) using a thin layer of Pt to provide sufficient conductivity. The fabricated specimens were polished (Phoenix 4000, Buehler) down to a 0.5 μm finish using water as a medium with 8-inch diamond grinding discs (DGD Terra, Buehler, Esslingen, Germany). The polishing was performed with a speed of 200 rev/min for 4 min for each grinding disc. The polished specimens were cleaned using acetone and ethanol for their further study.

The Vickers hardness tester (Indentec 5030 SKV, Stourbridge, West Midlands, UK) was applied to estimate the hardness of the bulk samples against the indentation load of 10 kg applied for 10 s. The average of at least 5 indentations is reported.

2.5. High-Temperature Wear Tests

HT-800 °C wear tests were performed on a universal tribo-test device (CETR/Bruker, Billerica, MA, USA) in a dry unidirectional-sliding ball-on-plate arrangement (Figure 1) [18]. The counterbody was an Al_2O_3 ceramic ball (Redhill Precision, Prague, Czech Republic) with $\text{Ø}10$ mm, hardness HV10 \approx 1450 and roughness Ra = 0.02 μm . The sample surface was cleaned with acetone and dried before the tests. The speed and distance of the sliding were set to 0.1 $\text{m}\cdot\text{s}^{-1}$ and 1000 m, respectively, with an applied load of 15 N. The duration of the test was 165 min. The choice of the load was made upon optimization to generate measurable wear. A heating rate of 6 °C/min was decided to avoid unwanted thermal shock for the materials and equipment under the test. The coefficient of friction (CoF) was recorded during sliding. The generated wear tracks were inspected through SEM and XRD, and were calculated using a 3D optical profilometer (Bruker Contour GT-K0+, USA) to determine the volume of the wear scar. The results reported are an average of at least five tests. The tests were conducted in ambient air.

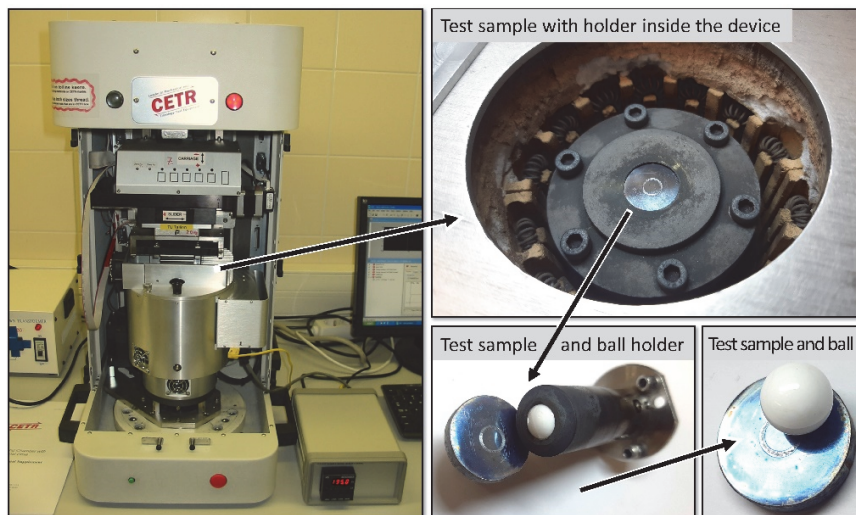


Figure 1. A universal tribo-test device (UMT-2) employed for the HT dry unidirectional sliding.

3. Results and Discussion

3.1. Thermodynamic Modeling and Combustion Synthesis

Thermodynamic considerations implemented for the $4\text{NiO}\cdot\text{WO}_3\cdot\text{yMg}\cdot\text{xC}$ system allowed for modeling the optimal parameters for the combined and entire reduction of the corresponding metals' oxides using the 'ISMAN-THERMO' software package. The system was designed to obtain Ni-W alloys with a molar composition ratio of Ni:W = 4:1.

The thermodynamic design enabled evaluating the combustion temperature (T_{ad}) in adiabatic conditions and the equilibrium phase composition of combustion products in the multielement system [8]. As a result, a diagram of phases with corresponding adiabatic temperatures (in °C) was created depending on the reducers' (Mg, C) contents (in moles) (Figure 2). Various compositional areas were identified according to the composition of the initial mixture, namely, the amounts of Mg and C. According to the diagram, a wide compositional range corresponded to the formation of the target product (magnesium from 2.7 to 4.8 moles and carbon from 2 to 4 moles) (marked in Figure 2) at a T_{ad} of 1000–2200 °C. Compared with the Ni-W 1:1 mixture (where magnesium ranged from 1.7 to 2.2 mol and carbon from 1.6 to 2.3 mol), a thermodynamically wider area of the 4Ni-W desired product was expected. It is to be noted that the thermodynamic calculations were performed excluding the possibility of the formation of tungsten carbides (WC, W_2C) by considering the kinetic inhibition of carbide formation processes at moderate temperatures over a short duration. Furthermore, a necessity of minimum temperature, i.e., 1700 °C, to form tungsten carbides upon a short interaction duration of less than a few seconds (compared to the characteristic duration of combustion wave propagation) was also reported in [19,20]. However, during a slow combustion process (0.1–0.2 mm/s), the formation of some amount of tungsten carbides is mostly inevitable.

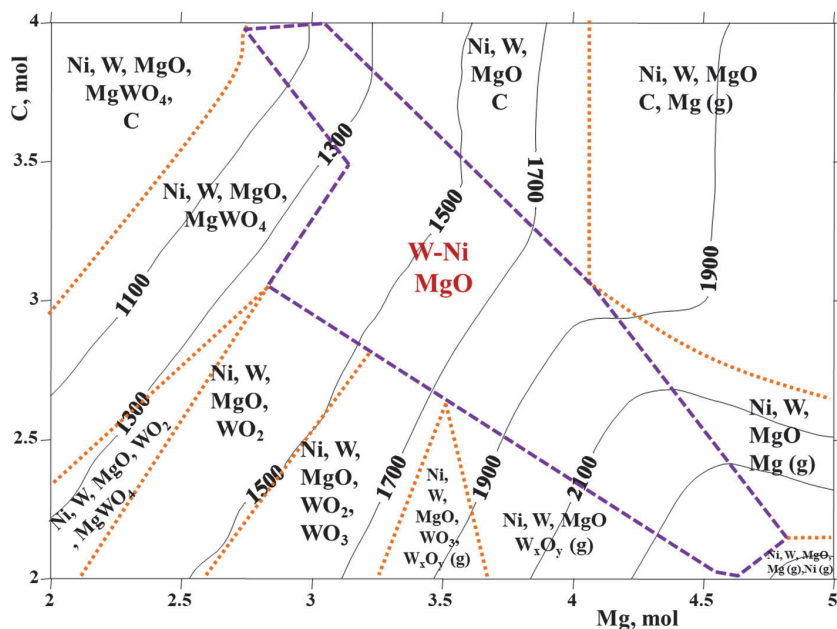


Figure 2. Thermodynamic modeling of the $4NiO-WO_3-yMg-xC$ system ($P_{N_2} = 0.4$ MPa).

According to the thermodynamic calculations, within the entire range of the reducers' quantity, the main gaseous products were CO and CO_2 . Their ratios depended on the combustion temperature and shifted to CO formation at a higher amount of Mg (>3.2 mol), a lower amount of carbon (<3 mol) and a higher temperature. Moreover, at high temperatures, magnesium (Mg), WO_2 and $(WO_3)_n$ were also evident.

To achieve the combined and accomplished reduction of oxides, as well as to avoid the evaporation of magnesium and various tungsten oxides, a pressure of 0.4 MPa was found to be optimal. To avoid nickel melting, the experiments were performed only in the lower temperature range (1100–1500 °C) of the optimal range (marked as violet borders on the diagram) for different contents of magnesium and carbon. During the synthesis, an increase in combustion temperature was observed with a decrease in carbon amount

and increasing Mg amount, conditioned by the decrease in the portion of low caloric carbothermic reactions ($\text{Ni} + \text{C}$ and/or $\text{WO}_3 + \text{C}$) and an increase in the high caloric mixture ($\text{WO}_3 + \text{Mg}$). Combustion velocity, heating and cooling rates were also increased. Combustion thermograms with the pressure change during the combustion reaction of the optimal mixtures are presented in Figure 3. The addition of hBN (2 wt% according to the mass of the final Ni-W product) decreased the combustion parameters by 200 °C and played the role of an inert diluent.

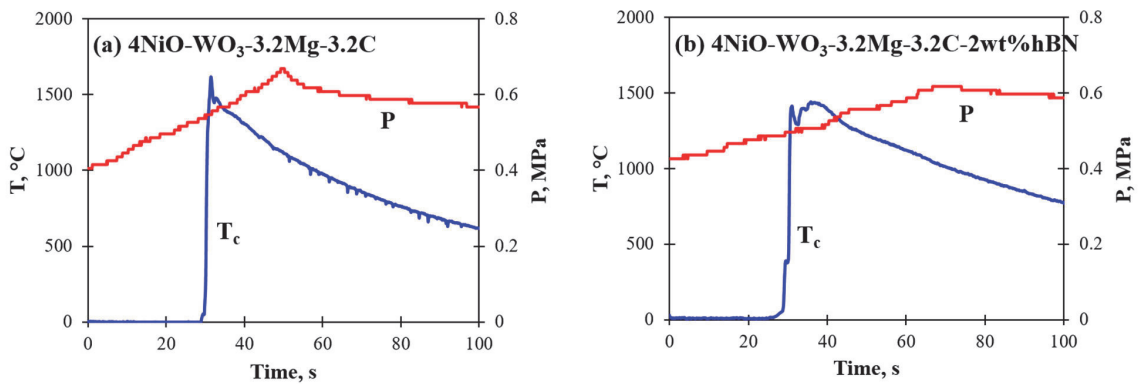


Figure 3. Combustion reaction thermograms of (a) 4NiO-WO₃-3.2Mg-3.2C and (b) 4NiO-WO₃-3.2Mg-3.2C-2wt%hBN mixtures.

The combustion parameters of the reactive mixtures (Figure 3a,b) are presented below in Table 1, mainly denoting the changes in T_c and U_c , which were sensitive to the changes in the reducers' amount and hBN powder. In addition, mass and pressure changes were observed due to CO/CO₂ formation. The combustion temperature was about 150–200 °C higher than the adiabatic temperature conditioned by the exothermic formation of the Ni-W intermetallic phases/solid solutions, in contrast to thermodynamic consideration of only the formation of individual metals.

Table 1. Optimized combustion parameters of the mixtures (a) 4NiO-WO₃-3.2Mg-3.2C and (b) 4NiO-WO₃-3.2Mg-3.2C-2wt%hBN ($P = 0.4$ MPa).

No.	T_c (T_{ad}), °C	U_c , mm/s	$U_{heating}$, °C/s	$U_{cooling}$, °C/s	Δm_{exp} , %	Δm_{theor} , %	CO/CO ₂	ΔP , atm
a	1610 ± 20 (1450)	0.76 ± 0.04	870 ± 90	14 ± 2	23.7 ± 2.1	15.4	2.6/0.6	2.2 ± 0.1
b	1420 ± 20 (1280)	0.63 ± 0.03	700 ± 70	6 ± 1	19.7 ± 1.8	15.3	3.2/0.3	2.1 ± 0.1

XRD analysis of the combustion products revealed the presence of trace amounts of tungsten carbides and partially reduced WO₂ oxide, together with Ni-W, W-Ni and MgO phases in the 4NiO-WO₃-3.2Mg-3.2C and 4NiO-WO₃-3.2Mg-3.2C-2wt%hBN mixtures. A BCC-structured W-rich W_{0.968}Ni_{0.032} intermetallic phase with Im-3m space group symmetry was detected at $2t = 40.28, 58.28, 73.2$ and 87.04 (pure tungsten $2t = 39.966$, $d = 2.254$ (hkl 210)). Broad lines of Ni-rich two phases with Ni₉W_{0.4} and Ni_{0.954}W_{0.046} phase compositions with FCC structures of Fm-3m space group symmetry were located at $2t = 44.24, 51.32, 75.04$ and 91.68 (for pure nickel $2t = 43.97$ (hkl 211), $d = 2.0576$). Further, a MgO periclase phase was successfully removed with a hot leaching procedure. The Scherrer equation (d (nm) = $k\lambda/\beta\cos\theta$) was used for the assessment of the average crystallite size of the W-rich and Ni-rich phases. The W-rich phase had an average crystallite size of 84.62 nm, and the nickel-rich phase had an average crystallite size of 22–42 nm (as two different Ni₉W_{0.4} and Ni_{0.954}W_{0.046} phases were merged into one peak).

Figure 4 shows the SEM and XRD of SHS- and high-energy ball milling (HEBM)-derived powders. The XRD patterns of the SHS-derived Ni-W powder (Figure 4e) showed broader peaks of Ni-W and W-Ni (compared with the elemental Ni and W, Figure 4f), confirming the partial dissolution (the formation of solid solution) of W in Ni and vice versa during the combustion synthesis. Apart from the phase dissolution, the SHS technique formed composite particles or agglomerates of Ni and W of bimodal morphology (Supplementary Figure S1).

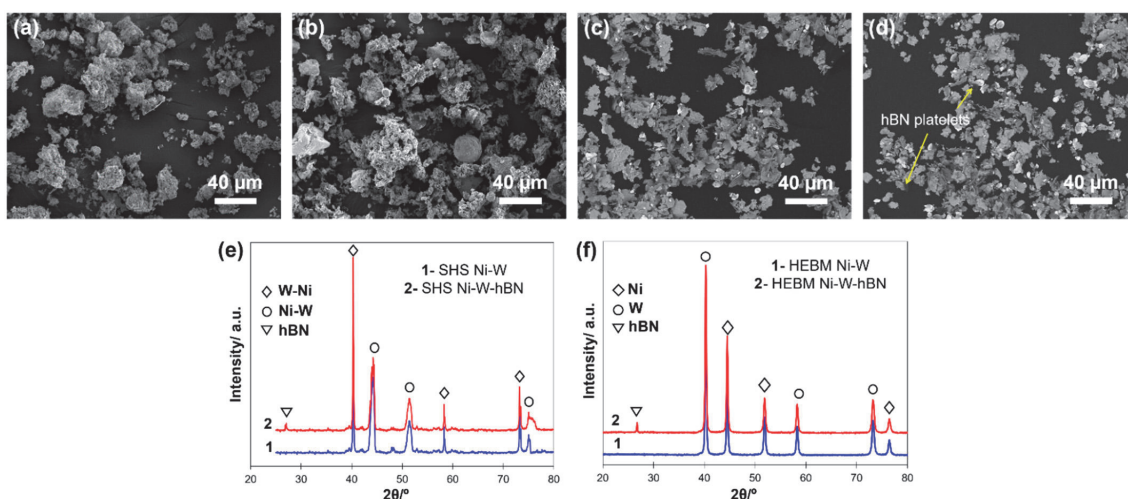


Figure 4. SEM images of powders mixtures of (a) SHS-derived Ni-W, (b) SHS-derived Ni-W-hBN, (c) HEBM Ni-W and (d) HEBM Ni-W-hBN, and XRD results of (e) SHS-derived powders and (f) HEBM powders.

Snowflake particles of up to 100 nm average size and spheroidal particulates of up to 300 nm in size and with well-defined grain boundaries were observed. Usually, such kinds of SHS-derived powders (pre-sintered agglomerates of nanosize entities) demonstrate an enhanced sintering ability due to high heating and cooling rates present in exothermic combustion reactions and a significant defect concentration that largely contributes to the mass transfer phenomena during the sintering.

3.2. Spark Plasma Sintering and Microstructural Analysis

SHS-derived and commercial powders were subsequently subjected to SPS at various temperatures (1050, 1150, 1200 and 1300 °C) at a pressure of 50 MPa with a dwell time of 5–30 min to bring out an optimal sintering condition with a maximum product density. It was found that the composites sintered at 1300 °C exhibited a relative density of >95%. SHS-processed composites sintered at 1300 °C and 50 MPa with a dwell time of 5 min and HEBM-processed composites sintered at 1100 °C and 50 MPa with a dwell time of 30 min achieved an improved relative density, as well as hardness. The influence of the processing technique and hBN inclusion on the density and hardness of the Ni-W (-hBN) sintered bulks (optimized at 1300 °C and 50 MPa—current work) is outlined in Table 2, along with values taken from the recently published literature reporting on Ni-W sintering. The SHS-processed composites in the current work show a significant rise in hardness and density owing to the developed phases and microstructure (discussed later).

Table 2. Comparison of fabrication technique, relative density and hardness of Ni-W composites.

Composite	Fabrication Technique	Relative Density (%)	Hardness (HV)
Ni-30 wt.% W [21]	Mechanical alloying (MA) + pressureless sintering	97.8	367 ± 21 *
Ni-30 wt.% W [22]	MA + SPS	96.7	430 ± 10 *
Ni-30 wt.% W-hBN [22]	MA + SPS	95.3	410 ± 12 *
Ni-40 wt.% W [23]	MA + pressureless sintering	91.1	425 ± 05 *
Ni-35 wt.% W [24]	Blending + SPS	-	321 ± 26 *
Ni-50 wt.% W [24]	Blending + SPS	-	414 ± 34 *
Ni-40 wt.% W (current work)	SHS + SPS	98.6	460 ± 31
Ni-40 wt.% W-hBN (current work)	SHS + SPS	95.8	437 ± 12
Ni-40 wt.% W (current work)	HEBM + SPS	98.9	284 ± 10
Ni-40 wt.% W-hBN (current work)	HEBM + SPS	97.4	271 ± 10

* relates to microhardness, load 100–200 g. Current work involved a load of 10 kg.

Figure 5 shows the SEM and XRD results of the sintered composites produced from SHS, as well as commercial powders. Based on the XRD analysis (Figure 5f,g) of the composites, it can be stated that, apart from primary intermetallic NiW, the contained phases in the bulks were carbides, such as WC, W_6Ni_6C and W_4Ni_2C . The presence of carbides in the composites was due to the fact that graphite was used as a die, punch and covering sheet during the SPS, which might have resulted in carbon diffusion to the composites. In order to gain insight into this phenomenon, the cross-sections of composites were also analyzed using XRD, and unexpectedly, the presence of W_6Ni_6C , W_4Ni_2C and sometimes W_2C phases were still evident. The formation of W_6Ni_6C and W_4Ni_2C at the cross-section (subsurface) was supported by the fact that it required the least amount of carbon (<0.8%) in comparison with WC or W_2C , which was mostly seen at the surface. A similar result of carbon uptake throughout the volume of the sintered Ni-W compacts was reported by [20,25]. It was conveyed that nickel, unlike tungsten, does not form stable carbides; nevertheless, it provides a channel for carbon diffusion inside the compacts. This demonstrates the fact that the diffusion of carbon was deep (at least 1.5 mm) into the sintered compacts. SPS samples prepared from SHS powder comprised comparatively more intense peaks of W-C and W-Ni-C phases than that of HEBM ones (as well as sintered bulks reported in the literature [21–25]). This was conditioned by the enhanced reactivity of the SHS powder and inherently high defect concentration. Even with the presence of a negligible amount of carbon, the tungsten solid solution dissolved it, forming WC while simultaneously precipitating nickel and W-Ni-C without nickel precipitation. Limited peaks of residual W existed in the XRD results of the HEBM-processed composites, conveying its inability to be sintered using the lower sintering temperature. From the SEM images (Figure 5a,b) of the SHS SPS-derived samples' surfaces, a homogeneous distribution of different phases was obvious with the presence of random pores. With the addition of hBN powder, the phase distribution did not present changes, but the number of pores increased (Figure 5b).

As per the SEM images with a higher magnification (Figure 5c–e), the two techniques demonstrated different microstructures. The bright whitish patches (columns in the magnified image) are believed to be the clusters of tungsten distributed in the Ni-rich matrix. Since it was difficult to differentiate between the W in the matrix and its carbides during the EDS analysis, the bright whitish clusters were anticipated to be enriched by tungsten,

as well as its carbides. The grey matrix was a Ni-rich Ni-W solid solution. A homogeneous distribution of W clusters was evident in the Ni-W alloy phase processed via SHS.

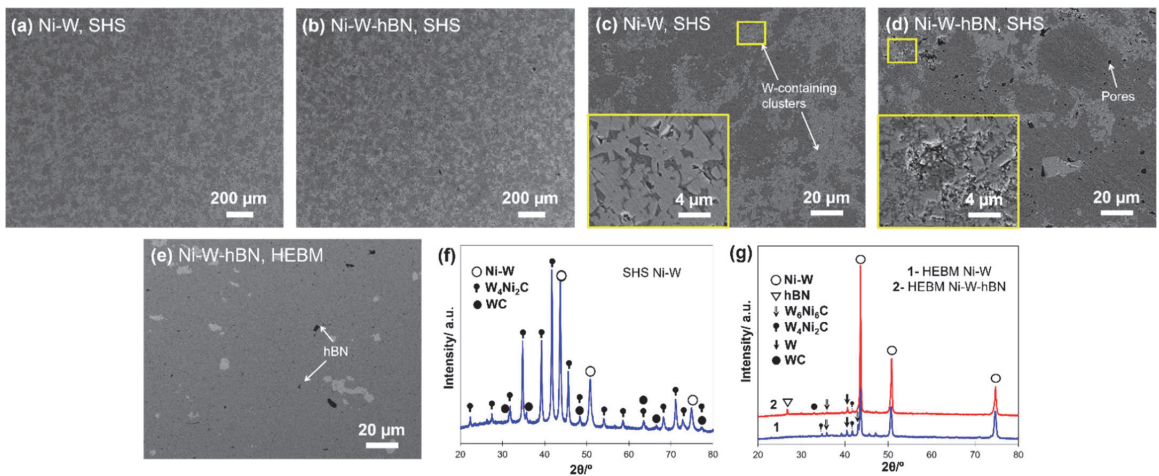


Figure 5. SEM images of SPS-derived composites (a,c) SHS-derived Ni-W, (b,d) SHS-derived Ni-W-hBN and (e) HEBM Ni-W-hBN and XRD results of (f) SHS SPS-derived bulk and (g) HEBM SPS-derived bulks.

An increase in the surface pores (Figure 5d,e) upon hBN addition was clearly visible in the respective composites, regardless of the fabrication method. A higher-magnification image showed the detachment of grains due to the reduced sinterability owing to hBN incorporation. It is possible that the hBN agglomerated, further growing the size of pores and decreasing the adhesion between grains, resulting in their detachment and easy falling out during the polishing stage.

All composites revealed a higher hardness in comparison to the pure Ni bulk (~110 HV). The improved hardness of the composites (more than 4 and 2 times for SHS and HEBM powder-processed bulk, respectively) is explained by a solid solution strengthening and the effective densification during sintering. The obtained values for SHS processed composites were consistent with the reported results of Ni-W systems (about 4.3 GPa) [21–24]. A larger margin in the hardness results between two processing techniques could be explained by the phenomena of solid solution strengthening. The formation of a considerable amount of ductile Ni-rich solution in HEBM-processed composites of Ni-W (~85.5%) was responsible for the relatively low hardness of the material. The in situ formation of carbides during the SPS allowed not only for successful sintering but also for enhanced performance. An increase in the hardness of sintered Ni-W bulks due to the presence of W-based carbides (mainly WC) was also reported in [21,22]. A slightly reduced hardness of hBN-containing composites in comparison to their counterparts was mainly due to the residual porosity of the sintered bulks (Figure 5d,e).

3.3. High-Temperature Wear Tests

Figure 6 shows the CoF and wear rate of Ni-W and Ni-W-hBN composite produced from HEBM and SHSed powders. A decrease in friction and wear rate (up to 20 times for the wear of the hBN-containing composite) was noted for the SHS-processed composites in comparison to their HEBM-processed counterparts. However, since (1) the reduction in friction and wear rate was noted for both (with and without hBN) composites and (2) their respective values remained in a comparable range, it is hard to comment on the positive influence of hBN. Moreover, the hBN inclusion led to a considerable rise in the wear rate and CoF for the HEBM-processed samples. Similar behavior of composites containing

hBN was reported in [26–28]. Nevertheless, the friction coefficient values of SHS-processed composites were seen to be up to 40% lower than that of the HEBM-processed samples, signifying a positive effect of the SHS technique on Ni-W composite preparation.

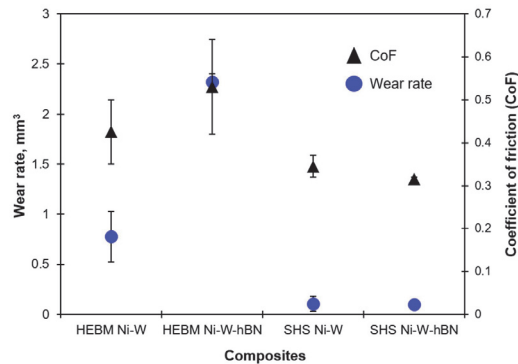


Figure 6. Wear rate and CoF of SPS-derived composites. The method of powder preparation is mentioned.

From the micrographs of the wear tracks, as shown in Figure 7, the high severity of the abrasive grooves and surface delamination is clearly evident on the surface of HEBM-processed Ni-W-hBN specimen (Figure 7a). Figure 7b displays a compacted layer of adhered wear debris, indicating the prevalence of adhesive wear. Such adhered debris can greatly increase wear resistance via the formation of an effective tribolayer or healing the defected areas [29,30]. However, during successive sliding passes, the tribolayer underwent fragmentation, resulting in a loss of the tribolayer protection. A similar wear behavior was demonstrated by the HEBM-processed Ni-W composite. Therefore, it was realized that abrasion and adhesion were the main wear mechanisms for the HEBM-processed composites. In contrast, the SHS-processed composites showed a considerably reduced severity of wear and demonstrated a more compact adhered tribolayer on the surface.

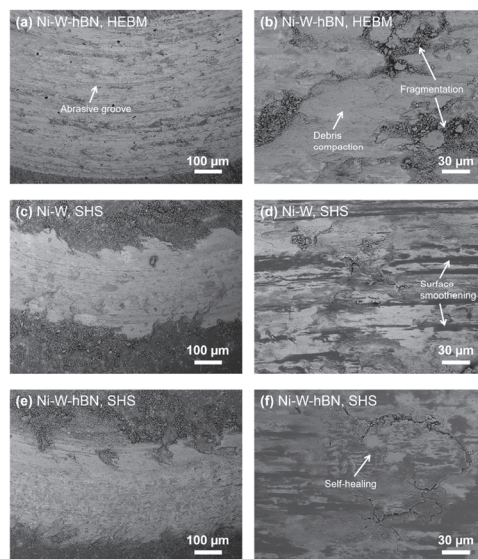


Figure 7. SEM images with two magnifications of worn surfaces of SPS-derived composites (a,b) HEBM Ni-W-hBN, (c,d) SHS-derived Ni-W and (e,f) SHS-derived Ni-W-hBN.

Compaction and smoothening (or micro-polishing) of the surface during consecutive sliding passes were dominant for SHS-processed composites. It is possible that some debris that was generated during the test were relocated into the voids and grooves, resulting in a ‘debris-entrapment’ and compaction phenomena during sliding that can be termed as ‘self-healing’ [14,31]. During a relatively long wear test of 165 min, the fatigue-induced delamination of debris may occur [18]. The SEM images of SHS-processed composites (Figure 7d,f) demonstrated traces of surface fatigue cracks showing material removal from the surface. Here, the cyclic delamination and repair of the tribolayer, along with mild abrasions, were considered as the main wear mechanisms.

The XRD patterns of the wear tracks for all composites, presented in Figure 8, displayed the sharp peaks of Ni-W oxides, along with an insignificant amount of the broad peaks of NiO, WO₃ and WC. Since the oxides were formed during the HT wear test, as their presence was not detected after the SPS, it can be concluded that the compaction of generated oxides or oxide debris took part in the tribolayer formation.

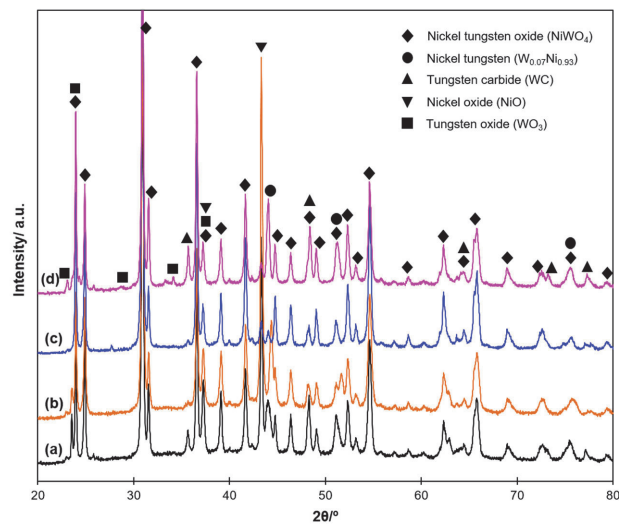


Figure 8. XRD analysis of the wear track of the SPS-derived composites (a) HEBM Ni-W, (b) HEBM Ni-W-hBN, (c) SHS-derived Ni-W and (d) SHSed Ni-W-hBN.

4. Conclusions

A thermodynamic model of a $4\text{NiO}-\text{WO}_3-y\text{Mg}-x\text{C}$ system was used to estimate the optimal criteria for obtaining Ni-W alloys with a molar composition ratio of Ni:W = 4:1. Experiments conducted according to the model indicated the influence of the reducer’s amount and hBN addition on the combustion parameters and product phase composition. XRD analysis of combustion products revealed the presence of BCC-structured W-rich and FCC-structured Ni-rich phase compositions. The combustion synthesized (via SHS) powders demonstrated a ‘snow-flake structure’, encompassing pre-sintered agglomerates of nano-sized entities.

SHS and HEBM powders of Ni-W and Ni-W-hBN were successfully consolidated with full density using SPS. The SHS-derived ‘snow-flake structured’ powders demonstrated a high sinterability (5 min vs. 30 min for HEBM powders), commendable hardness and a superior high-temperature tribological performance (800 °C). In comparison to their counterparts, SHS-processed composites displayed a lower CoF and wear rate owing to the phenomena of ‘micro-polishing’ and cyclic ‘self-healing’ of the surface during sliding. However, the role of hBN in imparting lubrication during the HT wear test was not confirmed.

Supplementary Materials: The following are available online at <https://www.mdpi.com/article/10.3390/ma15031252/s1>, Figure S1: XRD patterns (a); and SEM image (b) of combustion product of mixtures 4NiO-WO₃-3.2Mg-3.2C-2wt%h-BN before acid leaching.

Author Contributions: Conceptualization, I.H.; Data curation, R.K. and L.L.; Formal analysis, M.A.; Investigation, R.K., S.A., R.I. and L.L.; Methodology, S.A. and M.A.; Project administration, I.H.; Resources, M.A. and I.H.; Supervision, I.H.; Validation, I.H.; Visualization, R.I.; Writing—original draft, R.K. and S.A.; Writing—review & editing, I.H. All authors have read and agreed to the published version of the manuscript.

Funding: This work was supported by the Estonian Research Council grants PRG643 (I. Hussainova), PSG220 (S. Aydinian) and M-ERA.Net project “HOTselflub” MOBERA18 N.20097582-CA.

Institutional Review Board Statement: Not applicable.

Informed Consent Statement: Not applicable.

Data Availability Statement: Data available on request.

Conflicts of Interest: The authors declare no conflict of interest.

References

1. Cardinal, M.F.; Castro, P.A.; Baxi, J.; Liang, H.; Williams, F.J. Characterization and frictional behavior of nanostructured Ni–W–MoS₂ composite coatings. *Surf. Coat. Technol.* **2009**, *204*, 85–90. [[CrossRef](#)]
2. Brooman, E. Corrosion performance of environmentally acceptable alternatives to cadmium and chromium coatings: Chromium—Part II. *Met. Finish.* **2000**, *98*, 39–45. [[CrossRef](#)]
3. Yamasaki, T. High-strength nanocrystalline Ni–W alloys produced by electrodeposition and their embrittlement behaviors during grain growth. *Scr. Mater.* **2001**, *44*, 1497–1502. [[CrossRef](#)]
4. Ahmed, H.M.; Seetharaman, S. Isothermal dynamic thermal diffusivity studies of the reduction of NiO and NiWO₄ precursors by hydrogen. *Int. J. Mater. Res.* **2011**, *102*, 1336–1344. [[CrossRef](#)]
5. Valendar, H.M.; Rezaie, H.; Samim, H.; Barati, M.; Razavizadeh, H. Reduction and carburization behavior of NiO–WO₃ mixtures by carbon monoxide. *Thermochim. Acta* **2014**, *590*, 210–218. [[CrossRef](#)]
6. Indyka, P.; Beltowska-Lehman, E.; Tarkowski, L.; Bigos, A.; Garcia-Lecina, E. Structure characterization of nanocrystalline Ni–W alloys obtained by electrodeposition. *J. Alloys Compd.* **2014**, *590*, 75–79. [[CrossRef](#)]
7. Królikowski, A.; Płowska, E.; Ostrowski, A.; Donten, M.; Stojek, Z. Effects of compositional and structural features on corrosion behavior of nickel–tungsten alloys. *J. Solid State Electrochem.* **2008**, *13*, 263–275. [[CrossRef](#)]
8. Kumar, R.; Liu, L.; Antonov, M.; Ivanov, R.; Hussainova, I. Hot Sliding Wear of 88 wt.% TiB–Ti Composite from SHS Produced Powders. *Materials* **2021**, *14*, 1242. [[CrossRef](#)]
9. Zakaryan, M.; Aydinian, S.; Kharatyan, S. Combustion Synthesis and Consolidation of Ni–W Nanocomposite Material. *Ceram. Mod. Technol.* **2019**, *1*, 67–74. [[CrossRef](#)]
10. Sun, X.M.; Song, Y.P.; Gao, D.S.; Li, J.-T.; Chen, Y.-X.; Guo, S.-B. Adiabatic temperature calculation and microstructure of W–Cu alloy fabricated by combustion synthesis infiltration technique under ultra-gravity field. *Trans. Mater. Heat Treat.* **2013**, *6*, 158–162. [[CrossRef](#)]
11. Kumar, R.; Antonov, M. Self-lubricating materials for extreme temperature tribo-applications. *Mater. Today Proc.* **2021**, *44*, 4583–4589. [[CrossRef](#)]
12. Aydinian, S.; Kharatyan, S.; Hussainova, I. SHS-Derived Powders by Reactions’ Coupling as Primary Products for Subsequent Consolidation. *Materials* **2021**, *14*, 5117. [[CrossRef](#)] [[PubMed](#)]
13. Sunwang, N.; Wangyao, P.; Boonyongmaneerat, Y. The effects of heat treatments on hardness and wear resistance in Ni–W alloy coatings. *Surf. Coat. Technol.* **2011**, *206*, 1096–1101. [[CrossRef](#)]
14. Kumar, R.; Antonov, M.; Klimczyk, P.; Mikli, V.; Gomon, D. Effect of cBN content and additives on sliding and surface fatigue wear of spark plasma sintered Al₂O₃-cBN composites. *Wear* **2022**, *494–495*, 204250. [[CrossRef](#)]
15. Pompei, E.; Magagnin, L.; Lecis, N.; Cavallotti, P. Electrodeposition of nickel–BN composite coatings. *Electrochim. Acta* **2009**, *54*, 2571–2574. [[CrossRef](#)]
16. Sangeetha, S.; Kalaignan, G.P. Tribological and electrochemical corrosion behavior of Ni–W/BN (hexagonal) nano-composite coatings. *Ceram. Int.* **2015**, *41*, 10415–10424. [[CrossRef](#)]
17. Ünal, E.; Karahan, İ.H. Production and characterization of electrodeposited Ni–B/hBN composite coatings. *Surf. Coat. Technol.* **2018**, *333*, 125–137. [[CrossRef](#)]
18. Kumar, R.; Antonov, M.; Liu, L.; Hussainova, I. Sliding wear performance of in-situ spark plasma sintered Ti–TiBw composite at temperatures up to 900 °C. *Wear* **2021**, *476*, 203663. [[CrossRef](#)]
19. Kharatyan, S.; Chatilyan, H.; Arakelyan, L. Kinetics of tungsten carbidization under non-isothermal conditions. *Mater. Res. Bull.* **2008**, *43*, 897–906. [[CrossRef](#)]

20. Bokhonov, B.B.; Ukhina, A.V.; Dudina, D.V.; Anisimov, A.G.; Mali, V.I.; Batraev, I.S. Carbon uptake during spark plasma sintering: Investigation through the analysis of the carbide “footprint” in a Ni–W alloy. *RSC Adv.* **2015**, *5*, 80228–80237. [[CrossRef](#)]
21. Genç, A.; Öveçoğlu, M.L. Characterization investigations during mechanical alloying and sintering of Ni–W solid solution alloys dispersed with WC and Y₂O₃ particles. *J. Alloys Compd.* **2010**, *508*, 162–171. [[CrossRef](#)]
22. Genç, A.; Kaya, P.; Ayas, E.; Öveçoğlu, M.L.; Turan, S. Microstructural evolution of mechanically alloyed and spark plasma sintered Ni–W alloy matrix composites. *J. Alloys Compd.* **2013**, *571*, 159–167. [[CrossRef](#)]
23. Genç, A.; Öveçoğlu, M.L.; Baydoğan, M.; Turan, S. Fabrication and characterization of Ni–W solid solution alloys via mechanical alloying and pressureless sintering. *Mater. Des.* **2012**, *42*, 495–504. [[CrossRef](#)]
24. Sadat, T.; Dirras, G.; Tingaud, D.; Ota, M.; Chauveau, T.; Faurie, D.; Vajpai, S.; Ameyama, K. Bulk Ni–W alloys with a composite-like microstructure processed by spark plasma sintering: Microstructure and mechanical properties. *Mater. Des.* **2016**, *89*, 1181–1190. [[CrossRef](#)]
25. Marvel, C.J.; Cantwell, P.R.; Harmer, M.P. The critical influence of carbon on the thermal stability of nanocrystalline Ni–W alloys. *Scr. Mater.* **2015**, *96*, 45–48. [[CrossRef](#)]
26. Torres, H.; Podgornik, B.; Jovičević-Klug, M.; Ripoll, M.R. Compatibility of graphite, hBN and graphene with self-lubricating coatings and tool steel for high temperature aluminium forming. *Wear* **2021**, *490–491*, 204187. [[CrossRef](#)]
27. Zhu, X.; Wei, X.; Huang, Y.; Wang, F.; Yan, P. High-Temperature Friction and Wear Properties of NiCr/hBN Self-Lubricating Composites. *Metals* **2019**, *9*, 356. [[CrossRef](#)]
28. Wang, Y.; Wan, Z.; Lu, L.; Zhang, Z.; Tang, Y. Friction and wear mechanisms of castor oil with addition of hexagonal boron nitride nanoparticles. *Tribol. Int.* **2018**, *124*, 10–22. [[CrossRef](#)]
29. Varga, M.; Rojacz, H.; Winkelmann, H.; Mayer, H.; Badisch, E. Wear reducing effects and temperature dependence of tribolayer formation in harsh environment. *Tribol. Int.* **2013**, *65*, 190–199. [[CrossRef](#)]
30. Antonov, M.; Hussainova, I. Cermets surface transformation under erosive and abrasive wear. *Tribol. Int.* **2010**, *43*, 1566–1575. [[CrossRef](#)]
31. Islam, S.; Bhat, G.S. Progress and challenges in self-healing composite materials. *Mater. Adv.* **2021**, *2*, 1896–1926. [[CrossRef](#)]

Publication IV

Kumar, R., Hussainova, I., Rahmani, R., & Antonov, M. (2022). Solid Lubrication at High-Temperatures—A Review. *Materials*, 15(5), 1695.

Review

Solid Lubrication at High-Temperatures—A Review

Rahul Kumar ^{1,2,*}, Irina Hussainova ^{1,*}, Ramin Rahmani ^{1,3} and Maksim Antonov ¹

¹ Department of Mechanical & Industrial Engineering, Tallinn University of Technology, Ehitajate tee 5, 19086 Tallinn, Estonia; ramin.rahmaniahranjani@taltech.ee (R.R.); maksim.antonov@taltech.ee (M.A.)

² AC2T Research GmbH, Viktor-Kaplan-Straße 2/C, 2700 Wiener Neustadt, Austria

³ Laboratory for Nonlinear Mechanics, Faculty of Mechanical Engineering, University of Ljubljana, Askerceva 6, SI-1000 Ljubljana, Slovenia

* Correspondence: rahul.kumar@taltech.ee (R.K.); irina.hussainova@taltech.ee (I.H.)

Abstract: Understanding the complex nature of wear behavior of materials at high-temperature is of fundamental importance for several engineering applications, including metal processing (cutting, forming, forging), internal combustion engines, etc. At high temperatures (up to 1000 °C), the material removal is majorly governed by the changes in surface reactivity and wear mechanisms. The use of lubricants to minimize friction, wear and flash temperature to prevent seizing is a common approach in engine tribology. However, the degradation of conventional liquid-based lubricants at temperatures beyond 300 °C, in addition to its harmful effects on human and environmental health, is deeply concerning. Solid lubricants are a group of compounds exploiting the benefit of wear diminishing mechanisms over a wide range of operating temperatures. The materials incorporated with solid lubricants are herein called ‘self-lubricating’ materials. Moreover, the possibility to omit the use of conventional liquid-based lubricants is perceived. The objective of the present paper is to review the current state-of-the-art in solid-lubricating materials operating under dry wear conditions. By opening with a brief summary of the understanding of solid lubrication at a high temperature, the article initially describes the recent developments in the field. The mechanisms of formation and the nature of tribo-films (or layers) during high-temperature wear are discussed in detail. The trends and ways of further development of the solid-lubricating materials and their future evolutions are identified.



check for updates

Citation: Kumar, R.; Hussainova, I.; Rahmani, R.; Antonov, M. Solid Lubrication at High-Temperatures—A Review. *Materials* **2022**, *15*, 1695. <https://doi.org/10.3390/ma15051695>

Academic Editor: Pawel Pawlus

Received: 27 January 2022

Accepted: 22 February 2022

Published: 24 February 2022

Publisher’s Note: MDPI stays neutral with regard to jurisdictional claims in published maps and institutional affiliations.



Copyright: © 2022 by the authors. Licensee MDPI, Basel, Switzerland. This article is an open access article distributed under the terms and conditions of the Creative Commons Attribution (CC BY) license (<https://creativecommons.org/licenses/by/4.0/>).

Keywords: self-lubrication; solid lubricants; wear; tribology; high temperature; friction; glaze layer; smart materials

1. Introduction

A significant increase in the number of operations performed at high temperatures (HT~upto 1000 °C) has led to an exponential growth of interest in the field of hot tribology (Figure 1a). Wear at HT is a serious concern in a wide variety of technological processes and working systems, including but not limited to material processing, bearings, automotive, metal cutting, hot forging, stamping, forming, etc. In particular, many components function beyond a normal temperature range, unfolding numerous tribological complications, pose a substantial uncertainty in material reliability and performance due to enhanced friction and wear. Changes at tribo-contacts of the interacting bodies and possible new phase formation are common attributes of the HT wear process [1]. The tribo-bodies are highly influenced by a complex transformation of physical, mechanical, and surface reactivity due to simultaneous synergy of oxidation, diffusion, and tribological stress [2]. However, some materials such as steel and its alloys are reported to benefit from the protective nature of the tribo-oxide layer generated over its surface at HT sliding [3]. Nonetheless, easy spallation of the generated tribo-oxide layer owing to its non-adherent nature, ineffective Pilling–Bedworth ratio, or lattice mismatch with a host surface is largely conveyed [4].

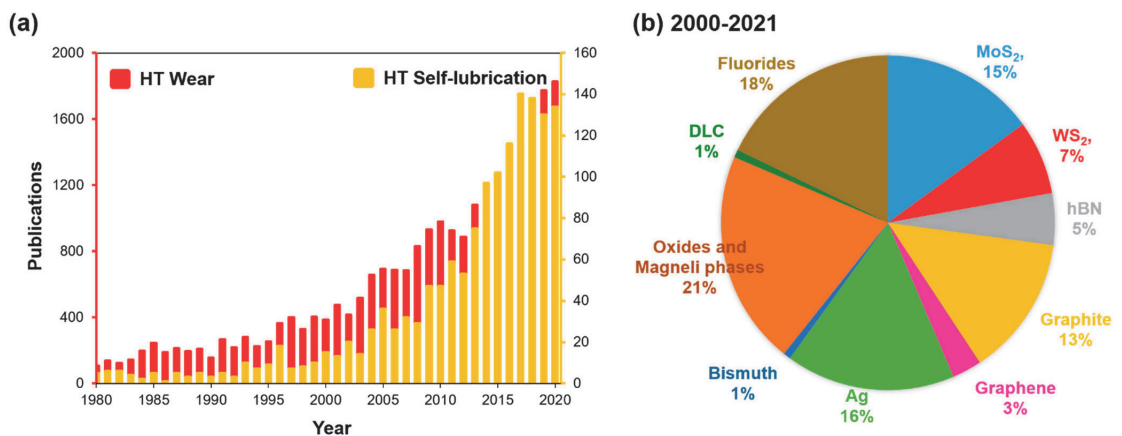


Figure 1. Number of published articles on (a) high-temperature wear and self-lubrication (1980–2020); and (b) high-temperature self-lubrication based on respective solid lubricants (percentage, 2000–2021), as recovered from Scopus database.

Minimizing the wear of tribo-bodies through the application of a conventional liquid lubricant is a common phenomenon. However, the oils and greases limitation are their decomposing at temperatures beyond 300 °C and their harmful effects on environmental and human health [3]. Volatilization, mitigation, and condensation of oil- and grease-based lubricating mediums at extreme conditions (temperature, pressure, altitude) such as in aircrafts, piston–cylinder arrangements, optical or thermal control surfaces, etc. are widely accepted. Considering these limitations of liquid lubricants, if applied in the scenario of extreme working conditions, the durability of the mechanical system as a whole may be limited. The use of solid-based lubricants (SL), such as MoS₂, WS₂, graphite, PTFE, Ag, hBN, etc., is a viable solution to minimize friction and wear over a wide range of temperatures from room up to ~1000 °C. Solid lubricants are usually incorporated into the materials (or at the interface of two mating surfaces) in a relative motion, which then is believed to in situ form a lubricious phase or compound due to tribo-chemical reactions at HT [3,4] and to provide a constant transfer of lubricant at the tribo-interface. It is reported that under precise conditions of temperature, humidity, and material composition, they tend to form a ‘glazed’ self-lubricating layer on the material surface under sliding wear [4,5], which offers a significant reduction in coefficient of friction (CoF) and wear. The main advantages of SL over the liquids are better lubricity, good thermal and chemical stability, improved dimensional stability to achieve finishing with high precision, etc.; however, limitations include its inability to carry away heat and provide damping effects during operation [6]. Few works on near-dry or minimum quantity lubrication (MQL) or minimum quantity cooling (MQC) utilizing cutting fluids or vegetable oils in combination with solid lubricants (such as PTFE, hBN, CaF₂, WS₂, boron oxide, etc.) during machining of difficult-to-cut materials (Ni superalloy) have come into the picture [6]. However, a lack of promising HT tribological studies in combination with a poor environmental outcome still exists and limits their widespread usage. Figure 1b shows the percentage of research works published concerning notable solid lubricants in HT tribology since 2000–2021.

In the framework of industrial applications, such as HT forming, forging, stamping, cutting, including areas of relative motion in engines, etc., the foremost importance for a solid-lubricating material is to minimize friction and wear, and also deliver chemical, corrosion, thermal, and mechanical stability. Irrespective of the chosen manufacturing process for material fabrication, low and steady friction in addition to low wear rates must be demonstrated at a wider range of temperatures since the work piece employed during operations can easily extend to or beyond ~1000 °C [7]. This demands the synergetic effect of several solid lubricants in order to achieve a low friction and wear at a large scale of

temperatures; as few SLs responsible for minimizing friction at low temperatures are also seen to chemically react and generate a lubricious glazed layer at HT and further enlarge the solid-lubrication range [8]. The key characteristics of an HT solid lubricant (self-lubricating material) are shown in Table 1. Figure 2 represents the classes of HT solid-lubricants based on their chemistry (structure) and their general mechanism of friction reduction, which will be discussed in detail in the subchapters.

Table 1. Key characteristics of high-temperature solid lubricants (self-lubricating material).

Characteristics of High-Temperature Solid-Lubricants	
1.	Demonstrate low shear strength.
2.	Adequately high cohesion strength of lubricious film formed at HT so as the film does not break upon high load and/or friction.
3.	Mechanical strength, thermal and chemical stability, oxidation and corrosion resistance.
4.	High thermal conductivity in order to dissipate heat.
5.	Controlled depletion during tribological operations.

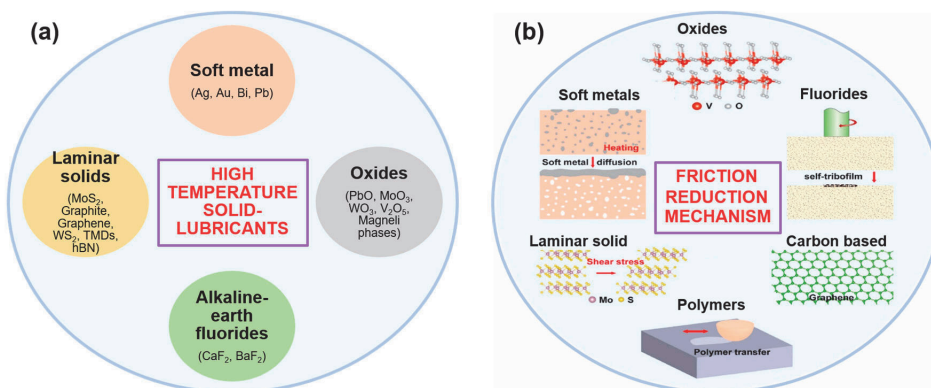


Figure 2. (a) Classification of HT solid-lubricants based on their chemical composition; and (b) a scheme showing the mechanism of their friction reduction.

This paper is an effort to review the notable SLs (and their based composites) used in tribological applications to impart reduced friction and wear at HT in dry sliding conditions. The mechanism behind their lubricity, chemistry and friction reduction is discussed in detail. A summarized graph showing the range of working temperature for various SLs and their demonstrated CoF during dry sliding is also presented. The idea of a futuristic ‘smart’ tribo-material is introduced.

2. Potential High-Temperature Solid-Lubricants

2.1. Soft Metals

Soft metals categories an array of materials with relatively low hardness (2.5–4 Mohs), such as gold, silver, lead, bismuth, indium, and platinum. The responsible mechanism of lubrication in soft metals is their greater ductility and low shearing strength [5]. The ease to plastically deform during sliding results in the formation of tribo-surfaces allowing a low coefficient of friction (CoF) and wear. Usually, the dynamic hardness for soft metals is higher as compared to static hardness; therefore, a larger force is required to cause the plastic deformation in a dynamic state [9]. However, an increased softness at HT may result in surface extrusion or failure and, thus, in inefficient lubrication [10]. In general, silver (Ag) and gold (Au) are of great interest in the field of solid lubrication due to a good thermal conductivity in combination with a low shear strength, especially in the areas of a high frictional heat development at the wear interface.

2.1.1. Silver (Ag)

Due to its high thermal conductivity (430 W/mK), non-toxicity, and relatively low cost, silver is the most commonly used noble metal as a solid lubricant. However, silver, upon a high inclusion (or coating thicker than 1 μm) in the matrix, can cause high friction and wear rate (in comparison to a virgin substrate). An increased plastic deformation, cutting, plowing, and material transfer to the counter body is commonly reported in such cases [11,12]. Commonly, it is considered that soft metals as reinforcements in matrix tend to be more durable and provide a long-lasting lubricity as compared to the coatings. Quick exhaustion of Ag and its limited lubricity at temperatures above 300 $^{\circ}\text{C}$, resulting in the coating lapse and increased porosity, is reported in [13]. Figure 3 demonstrates a scheme of lubrication via the diffusion mechanism in a soft metal-based SL.

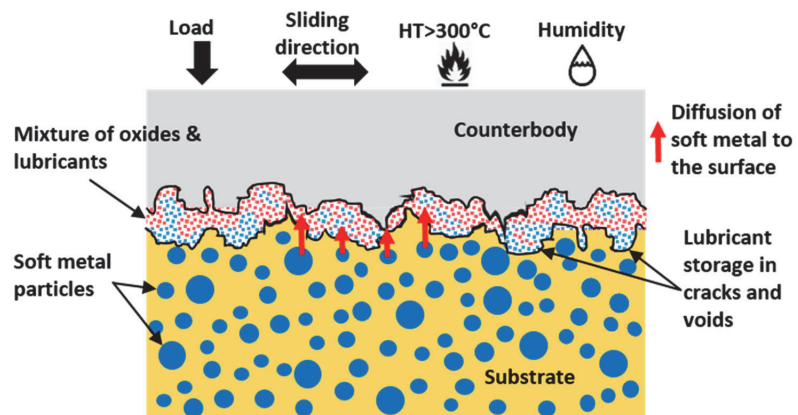


Figure 3. Diffusion mechanism of soft metal-based solid lubrication during HT tribological operations.

It is seen that a silver content of ~15 wt% or more in a host material is beneficial in a decrease in CoF and wear with an increase in temperature [14,15]. At temperature < 400 $^{\circ}\text{C}$, sufficient reduction in CoF and wear of Ag deposited on Al_2O_3 substrate is demonstrated [16,17]. However, upon an increase in temperature, the wear rate is accelerated due to expulsion and an increased softening of Ag layers [17]. A reduced and stable CoF at both 400 and 600 $^{\circ}\text{C}$ was reported in Ni-Ag composite [18]. In another study, a significant decrease in CoF and wear was noticed at 200 $^{\circ}\text{C}$ for Ni-Cr alloy-based coating with 10 wt% of each Mo and Ag [19]. However, at a temperature of 400 $^{\circ}\text{C}$, a high Ag expulsion from the coating results in increased wear. A significant decrease in friction and wear of TiAl alloys incorporated with Ag was demonstrated from room temperature up to 400 $^{\circ}\text{C}$ as compared to a neat alloy in [20]. A five-fold drop in the wear for the Ag-containing films was demonstrated at 600 $^{\circ}\text{C}$ owing to a lubricious tribo-film formation [21]. In most of the works, a 10–15 wt% Ag inclusion was found to be the optimum concentration for wear reduction. Figure 4 shows the CoF and relative wear rates for various Ag-based solid-lubricating materials on a wide range of sliding temperatures, as reported in recent publications [10,13–21]. The relative wear rate values are calculated after dividing the wear rate value at the reported temperature by room temperature (RT) value. An efficient lubrication range is shaded in Figure 4b.

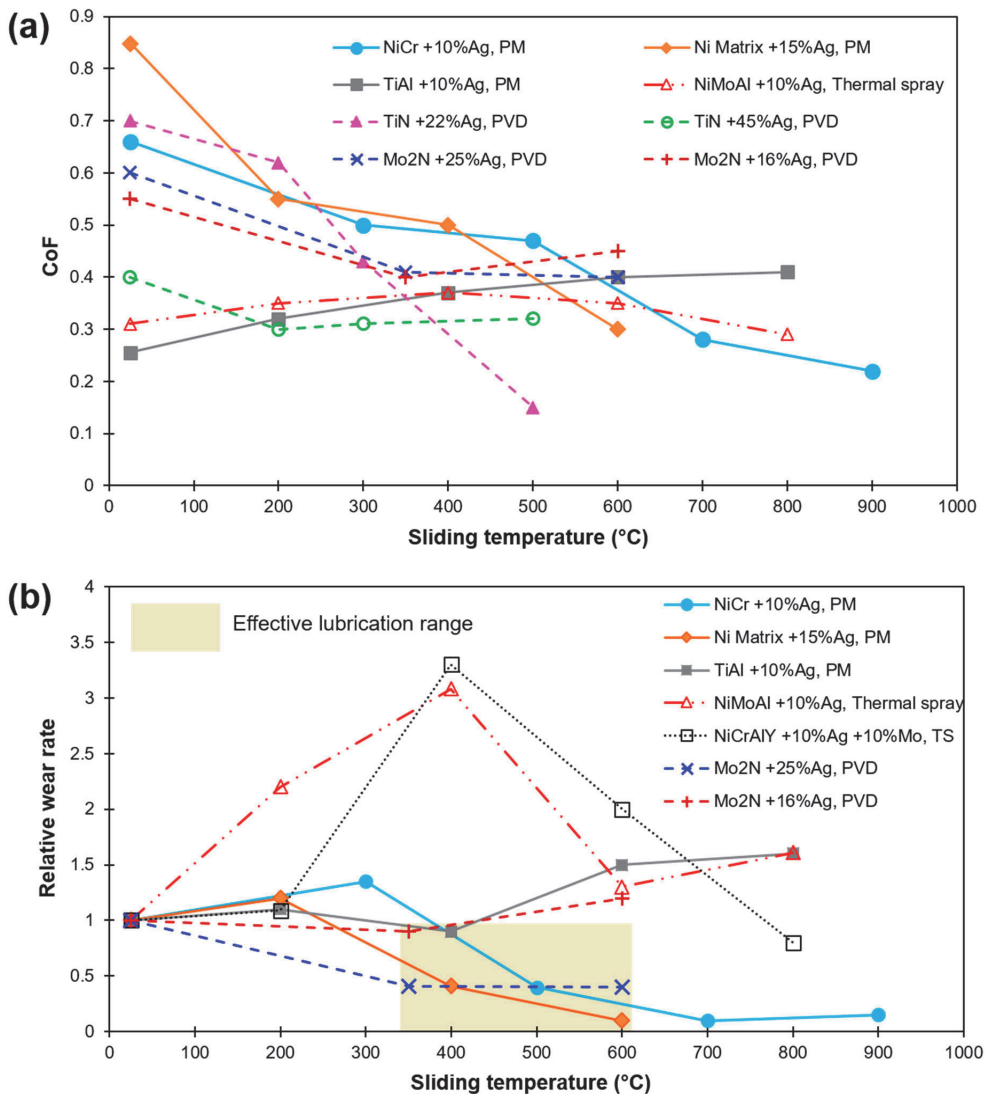


Figure 4. HT sliding results of Ag-based composites and coatings as found in recent literature (a) CoF; (b) Relative wear rate (in relation to their corresponding RT wear). Values are labeled as per Ag concentration, matrix material, and fabrication method [10,13–21].

A sizeable level of variance in the range of temperature of effective lubrication has been noted. In addition, a disparity in the range of friction and wear values is possible due to the design in the experiment, test methods, and external factors (operator, etc.) in play. Certainly, the microstructure and pre-existing defects (vacancy, lattice mismatch, voids, pores, etc.) can also greatly affect the diffusion of Ag into the surface, resulting in variation in lubricating capacity. However, pores or cracks may also improve the efficiency of lubrication due to the storage of lubricant in the existing defects [22], demonstrating a self-adaptive behavior due to squeezing out or the storing back of the lubricant so as to accommodate the lubricating film for better lubrication (Figure 3).

2.1.2. Bismuth (Bi)

Bismuth has been fairly little recognized and mostly confused with soft metals such as Pb and Ti, which share similar physical properties. In recent years, the combinational use of Bi with Pb/Graphite or Cu as a solid lubricant to improve wear property in the material has come into the picture [23,24]. The restricted use of Pb due to its toxicity has raised the interest in Bi as a 'green and ecologically clean' solid lubricant [25].

Bismuth has a low hardness (2–2.5 Mohs) and a low melting point (~270 °C), which results in its easy dispersal under asperity contacts, during which local flash temperatures are high enough for Bi melting [25]. Under tribo-conditions, smearing of generated Bi tribolayer protects the direct contact between tribo-bodies. The bismuth tin bronze with 10% Bi exhibited lower friction in comparison to 5% Bi but underwent shrinkage porosity, and bismuth precipitation on the grain boundaries of the matrix has been specified in [26]. Limited shrinkage porosity was shown by solid-lubricating Cu-Sn bearings produced by powder metallurgy [27]. Bismuth is susceptible to forming grain boundary phases that are unfavorable to the mechanical properties of Cu-Bi alloys. However, Sn is shown to be the best alloying element for preventing Bi precipitation on the grain boundaries [28]. The optimal Bi content for bimetal bronze bearings operating under the boundary lubrication condition is 3 wt% of Bi [29]. The mechanical performance of bismuth bronze alloys, $\text{CuSn}_{10}\text{Bi}_4$ and CuSn_6Bi_6 in the thrust bearing tests concluded that Bi is not as good dry-lubricant as the lead in the tested alloys due to its poor bearing performance having both low load capacity and a high coefficient of friction (CoF) [30]. Lead (Pb), in addition to Bi and/or graphite, as an inclusion to synergistically obtain the best tribo-property, is shown to have the best results.

2.1.3. Other Soft Metals (Au, Cu, In)

The use of electroplated Au-based coating as a solid lubricant in micromechanical and electronics industries is quite common. Gold high ductility and malleability results in easy distribution of frictional stresses during sliding wear conditions [31]. The use of Au in the yttria-stabilized zirconia (YSZ) matrix is shown to improve the sliding wear of YSZ ceramics [32]. Ball-on-disk tribotest results showed that in comparison to reference YSZ ceramic, YSZ/Au coatings demonstrated a significant decrease in CoF and generated less wear debris with limited smearing of Au from the surface. The decrease in CoF (up to 0.2) was owed to the microstructure adaptive changes at elevated temperatures in addition to the formation of lubricious Au transfer films. At least 20 wt% of Au inclusion was stated to cause a diminution of abrasive wear mechanism and impart gold-based lubricity. A considerable decrease in CoF in the range of 0.36–0.5 was recorded from RT–800 °C upon 30 wt.% of CaF_2 and Au inclusion in a $\text{ZrO}_2(\text{Y}_2\text{O}_3)$ matrix composites [33]. Plastic deformation and material flow were encountered for both CaF_2 and Au while sliding. Extrusion or transfer of Au from subsurface to the surface resulted in its dispersion and provided enough lubrication during low-temperature sliding. At temperatures of 400 °C or above, the sliding surface showed the existence of both CaF_2 and Au, pointing to a synergetic solid-lubrication phenomenon. The use of Au in conjunction with other solid lubricants to enlarge the lubrication temperature range has also been reported in [34,35]. However, due to Au's high cost, its use is limited in large-scale fields.

Copper (Cu) is another member of the soft metal group, which is widely accepted as a solid lubricant. Its high thermal conductivity (398 W/mK) helps to maintain a low temperature at the tribo-pair contact zone. A decrease in CoF in partially stabilized zirconia (PSZ) from 0.40 to 0.20, 0.17, and 0.14 upon copper powder, copper films, and CuO films inclusions/formations, respectively, is reported in [36]. The effect of Cu in brake friction materials has been studied in [37], and the existence of Cu particles within a definite concentration has been stated resulting in the stabilization of sliding by forming a granular layer of the mechanically mixed layer (MML), which are showing main contact sites of pad and disc and further, decreasing the average CoF and fluctuation peaks during sliding. The recrystallized Cu nanoparticles might act as lubricant in the tribolayer formed during sliding at 650 °C [37]. An addition of 40 vol.% graphite to the copper–tin composites showed a low coefficient of friction of 0.15 [38].

Indium (In) based solid lubricants are still scarcely reported. For example, in [39], PVD TiN coatings with indium demonstrated a superior performance up to 450 °C.

2.2. Laminar Solids

Lamellar solids, also entitled layered lattice compounds, have a planar or hexagonal layered structure, where the atoms within the planes or layers are strongly bonded to each other. However, the bonding between the individual layers or planes is characterized by weaker Vander Wall forces. The weak interlayer forces provide an isotropic shear ability with an easy shear along the basal planes [17]. Hence, this class of materials, when included in the matrix as an SL, offers notable anti-friction capability [3]. Layered sodium silicates such as δ -Na₂Si₂O₅, α -Na₂Si₂O₅, β -Na₂Si₂O₅, and kanemite represent another group of relatively inexpensive materials to reduce wear due to their layered structure similar to other transition-metal dichalcogenides [40]. The widely known materials of this category include graphene, graphite, hexagonal boron nitride (hBN), TMDs, and particularly MoS₂ and WS₂ (Figure 5).

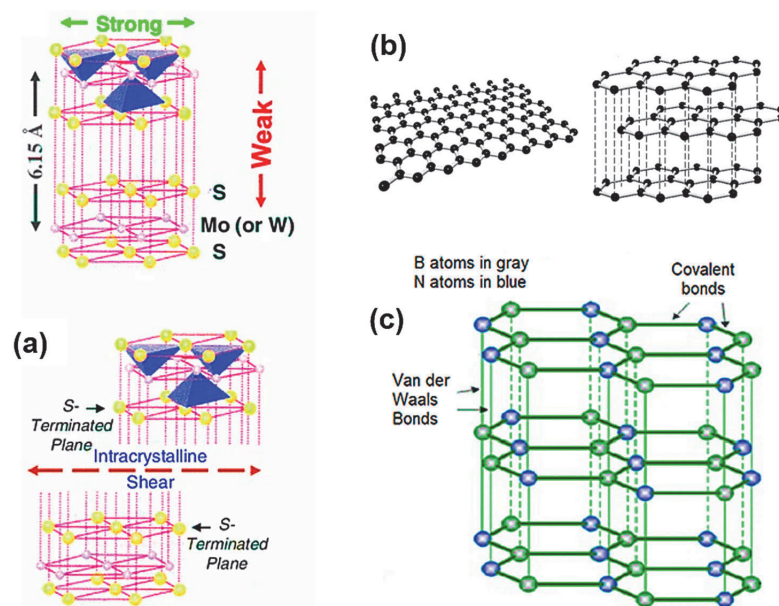


Figure 5. Crystal structures demonstrating the weak Vander walls forces present in the inter-lamellar layers/planers resulting in an easy slip between them (a) MoS₂ (or WS₂); (b) a single layer of graphene and graphite as a heap of multiple graphene layers; and (c) hexagonal boron nitride (h-BN) [17].

2.2.1. Molybdenum Disulfide (MoS₂)

Until recently, MoS₂ has been one of the most used solid lubricants worldwide [41]. This compound is found naturally in the earth's crust as a mineral Molybdenite. Upon refinement and treating, it is commercially accessible in the form of fine particles, suspensions, films, or inclusions in the composites. Considered as a laminar solid, the sulfur lamellae in the compound is bonded by weak van der Waals, which eases the shearing phenomena resulting in layer arrangements (or alignment) during sliding. Moreover, the strong covalent bonding among sulfur and molybdenum provides the lamellae a needed resistance to asperity penetration [41]. The laminar structure is shown in Figure 5a. The mean CoF of unmodified MoS₂ is about 0.08 at room temperature and up to 300 °C. In a vacuum, MoS₂ provides acceptable lubrication up to ~1000 °C depending on various factors such as sliding speed, load, and working conditions [42].

The effectiveness of MoS₂ considerably decreases due to oxidation [3,43]. Formation of molybdenum oxide (MoO₃) upon oxidation of MoS₂ results in an increase in friction and wear rate. Abrasive behavior of MoO₃ to several alloys was reported [41,44]. In contradictory, an improvement in tribological behavior upon MoO₃ additions to MoS₂ was seen in ref [45]. Oxidation of MoS₂ is a function of powder particle size and the accessibility to air [7], as well as the type and composition of inclusion [41]. However, protection from oxidation through the use of inclusions with MoS₂ is shown [46], resulting in the elimination of air from the particles.

NiAl based composites with 5 wt%Ti₃SiC₂-5 wt%MoS₂ demonstrated an outstanding tribo-behavior from RT to 800 °C with a continuous decrease in friction with rising temperature [47]. A noteworthy drop in both CoF and wear rates was noted at 400 °C. Apart from the formation of a self-lubricious layer, the generation of protective oxides of TiO₂ and SiO₂ is held to lower CoF and wear. In [48], ZrO₂/Y₂O₃ composites with an inclusion of 10 wt% MoS₂ and 10 wt% CaF₂ showed the lowest CoF and wear rate at 200 °C; at higher temperatures up to 1000 °C, oxidation of MoS₂ to a less lubricious MoO₃ occurs [49]. A decrease in CoF and wear was accounted for up to 300 °C for YSZ coating with Mo [50]. However, at temperatures beyond 300 °C, a coating failure occurred. In spite of this, MoS₂ inclusion diminished the CoF up to temperatures of 700 °C, but the initiation of oxides and non-lubricious effect of MoS₂ was accounted for. In another tribological study [51], Ni₃Si-based composite coatings with varying content of MoS₂ and BaF₂/CaF₂ showed that the MoS₂ decomposed into Mo₂S₃, resulting in increased friction and wear values (due to the non-lubricant property of Mo₂S₃). Further, the composite was seen to demonstrate poor tribological property at HT due to the low content of solid lubricant. However, upon a higher solid lubricant content (i.e., 15 wt.% MoS₂ and 10 wt.% BaF₂/CaF₂), an admirable self-lubricating property was seen as the temperature exceeds 400 °C due to the formation of a glazed layer. A low and stable CoF~0.15 of PVD films with MoS₂ was noted at 350 °C. However, a degradation of MoS₂ to MoO₃ was reported at around 370 °C [52,53]. Figure 6 demonstrates the effect of sliding temperature over CoF and relative wear rates for various MoS₂ based solid-lubricating materials reported in recent literature [47–53]. The relative wear rate values are calculated after dividing the wear rate value at the reported temperature by room temperature (RT) value.

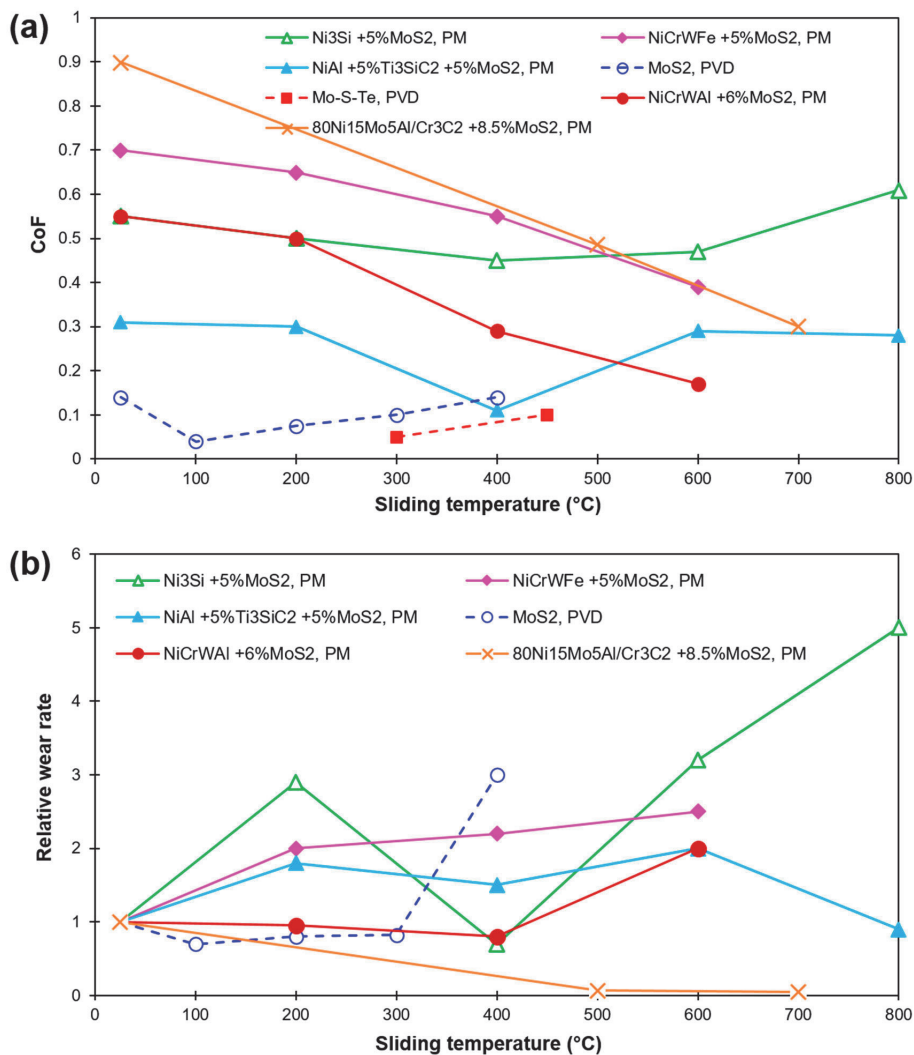


Figure 6. HT sliding results of MoS₂-based composites and coatings as found in recent literature (a) CoF; (b) Relative wear rate (in relation to their corresponding RT wear). Values are labeled as per MoS₂ concentration, matrix material, and fabrication method [47–53].

2.2.2. Graphite

Graphite is a layered solid and an allotrope of carbon with a hexagonal lattice arrangement (Figure 5b). The carbon atoms in the layers are strongly held by a covalent bond, while the individual layers held themselves by weak van der Waal cohesive forces, ensuing an easy shear. Its high thermal conductivity (470 W/mK) raises its demand for HT applications. Unlike MoS₂ and WS₂, the existence of water vapor and oxygen in the environment aids the interlamellar shearing of graphite crystals and demonstrates lubricity [3]. On the other hand, oxidation of graphite at elevated temperatures is the foremost hindrance to its use [54]. As per reported data, graphite undergoes oxidation to CO beyond 400 °C and even CO₂ at temperatures beyond 500 °C [55]. Due to this, graphite is majorly employed at medium-range temperatures. Nevertheless, its superior mechanism of lubrication has compelled researchers to look for a way to stabilize graphite at higher

temperatures [56]. Coating graphite with a ‘protective barrier’ of W, Re, Mo, Nb, Hf, Ti, Zr, their oxides, silicides, borides, carbides, nitrides, and the respective composites, which would rather hinder its contact with atmospheric oxygen and thus, improve oxidation resistance is seen [55–57]. Amongst which, SiC [56] and MoSi₂ [58] are the most efficient at HT oxidation. Admirable lubrication without adsorption of water vapors and oxidation of graphite fluoride (CF_x)_n was earlier reported in [59], whereas the formation of a lubricious glazed layer in the presence of humid air accounted for the decrease in CoF and the wear in Fe-Cu-Sn alloy with 3 wt% graphite content at 423 K [59].

A synergism of graphite and inter-metallic Al₂Cu was reported to improve friction and wear in comparison to the base alloy, Al-20Si-5Fe-2Ni [58]. Conversely, another synergetic effect of Ag, BaF₂/CaF₂ with graphite inclusion in Ni-alloy matrix was reported to increase the CoF of composites with graphite addition at HT up to 500 °C [60]. An excellent diminution in CoF and wear from RT to 600 °C in addition to an improvement in compressive strength and hardness of graphite incorporated composites was reported in [61]. A synergetic influence of three solid lubricants, i.e., graphite, Sb₂S₃, and MoS₂, in the brake friction material to improve friction stability and fade resistance in comparison to material without graphite was reported in [62]. A similar synergetic influence of Mo, CaF₂, and graphite was reported to provide improved lubrication due to graphite inclusion at a temperature range up to 400 °C due to the formation of CaF₂ and CaMoO₄ during a tribo-reaction of Mo and CaF₂. Severe brittle fracturing and delamination were seen at 400 and 600 °C. However, from 800 to 1000 °C, the worn surface was covered with the lubricating film [63]. An outstanding solid-lubricating behavior over a varied range of temperature up to 600 °C was shown in [64] due to the synergistic lubricating effect of graphite and MoS₂ on Nickel-based composites prepared using the PM route. The main mechanisms of wear at RT were adhesive and abrasive. However, at elevated temperatures, the mechanisms were suppressed significantly. Several other studies [65–67] discuss the synergetic effect of lubrication of graphite and other solid lubricants. However, a good explanation regarding the occurring synergetic wear mechanisms at HT is scarcely reported.

2.2.3. Graphene

Graphene is an allotrope of carbon with a two-dimensional honeycomb structure and is believed to offer outstanding friction-reducing properties. The mechanism of friction reduction during sliding is the same as graphite and MoS₂. However, unlike graphite, graphene shows lubrication in a dry environment. Due to its exceptional thermal (~4000 W/mK), electrical (~10² S/m), and mechanical properties, it is widely used as a lubricant in mechanical as well as electronics industries. Its use as in solid or colloidal liquid-based lubricant is also well-recognized [68,69]. High strength, easy shear ability, and chemical inertness have made it a perfect choice in the solid lubricant category. In addition, due to its super-thin dimension, it is widely used in micro and nano mechanical systems [70].

Outstanding tribological performance of graphene nanoplatelets (1.5 wt%) reinforced NiAl matrix due to the formation of a lubricious tribo-layer up to 400 °C reduced CoF and the wear significantly [71]. However, with the rise in sliding temperature up to 500 °C, the protective behavior of graphene nanoplatelets (GNPs) diminishes/dies out due to its oxidation, resulting in intensive adhesive wear and delamination. In another study [72], multilayer graphene reinforced TiAl matrix composite (MLG-TiAl) was reported to demonstrate excellent lubrication from 100 to 550 °C due to graphene’s excellent shear ability. Nonetheless, a loss in the lubrication above 600 °C due to its oxidation resulted in unstable friction and intensified wear. In most of the works regarding graphene as a solid lubricant, a transition period of an increase in friction and wear between 550 and 600 °C is noticed. A study on the wear-reducing behavior of graphene layers and its oxide demonstrated that the former delivered the best wear protection, reducing the wear by 3–4 orders of magnitude in comparison to bare steel sliding interfaces. At the same time, graphene oxide demonstrated a larger wear rate by 1–2 orders of magnitude in comparison to that of graphene layers [73]. Very limited research on graphene as a solid lubricant state,

its friction diminishing behavior is up to 500 °C, above which is termed to be severe for their composites due to its degradation.

2.2.4. Hexagonal Boron Nitride (hBN)

hBN is a laminar solid reported to demonstrate lubricity due to its easily sheared ‘graphite like’ layered structure [3]. hBN, due to its high thermal conductivity (~500 W/mK at RT), chemical and oxidation resistance is a potential candidate for HT tribological applications [74]. hBN, unlike graphite and MoS₂, is understood to be very well effective at HT applications (such as for metalworking processes where lubrication at high temperatures is often sought) and does not appreciably oxidize up to 1000 °C [74]. Nevertheless, non-wettability and poor sinterability of hBN accompanied with its poor adhesiveness to most of the metals and ceramics results in low strength and inferior quality composites or coatings hindering its wide-scale usage.

So far, the results on tribological studies of hBN as a solid lubricant give no clear idea of its usage. On the one hand, few studies report a positive influence of hBN in solid lubrication [3,10,74–76], while others state its negative or no effect on lubrication [77–80]. A decrease in CoF and wear rate with an increase in temperature up to 800 °C in Ni/hBN coating on stainless steel was perceived [75]. Conversely, a drop in friction and wear properties with an increase in sliding temperature in NiCr/hBN self-lubricating composite was reported in [80]. Wear reducing behavior of Ni60-10% hBN coating at 300 and 600 °C sliding was conveyed in ref. [79]. A similar content of hBN (10 wt.%) as inclusion was recommended in [80]. A reduction in HT CoF and wear rate was seen for Ni-based composite due to a synergism of Ag and hBN [81]. An extensive review points to 5–15 vol% of hBN as the optimal reinforcement in the composites to impart effective lubrication at a temperature range of 600–900 °C [81–83]. A larger hBN concentration resulted in significant deteriorating mechanical properties of materials. Figure 7 demonstrates the effect of sliding temperature on CoF and relative wear rates for various hBN based solid-lubricating materials available in recent literature [80–86]. The relative wear rate values are calculated after dividing the wear rate value at the reported temperature by room temperature (RT) value.

2.2.5. Tungsten Disulfide (WS₂)

WS₂ is an excellent solid lubricant due to its laminar structure, where tungsten (W) atoms occupy the center layer of the hexagon, while the sulfur (S) atoms reside on the top and bottom layers of each hexagon (Figure 5a). The mechanism behind its friction reduction is due to the easy sliding between the adjacent layers, which are held by weak van der Waal forces similar to the structure of MoS₂ [87]. Nevertheless, WS₂, unlike MoS₂, is conveyed to work at higher temperatures with their oxidation specified to be at 540 °C (for MoS₂-350 °C) [88].

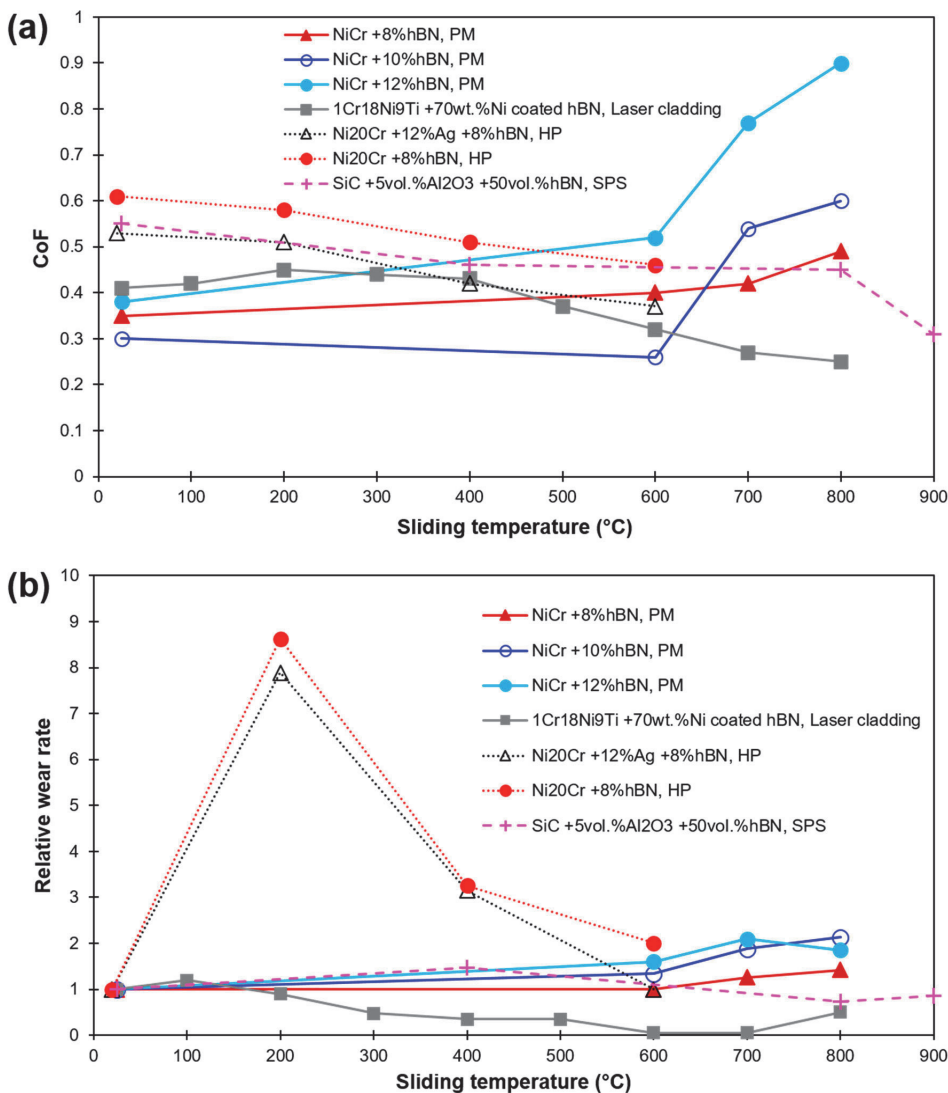


Figure 7. HT sliding results of hBN-based composites and coatings as found in recent literature (a) CoF; (b) Relative wear rate (in relation to their corresponding RT wear). Values are labeled as per hBN concentration, matrix material, and fabrication method [80–86].

A significant reduction in friction and wear rate for Cu/WS₂ composites due to the formation of the beneficial hard phase of W and lubricating phase of Cu₂S was reported in [89,90]. The inclusion of WS₂ in the Cu matrix demonstrated an improved mechanical and tribological property as compared to the composite with the same concentration of graphite due to the high strength of interfacial bonding between the Cu matrix and WS₂, resulting in a decreased plastic deformation (cracks formation) during sliding passes. Exceptional lubrication in the temperature range from 25 to 800 °C with WS₂ and ZnO addition to TiAl matrix was demonstrated due to the formation of WS₂ rich lubricating films (thickness ~500 nm) at temperatures below 600 °C and effective lubrication by ZnO beyond 600 °C [91]. A similar mechanism of wear was demonstrated in M50 steel+10%WS₂ after wear tests under different temperatures [87]. At RT to 400 °C, the composite exhibits a delaminated

worn surface. However, at high temperatures from 600 to 800 °C, the composite exhibits a mildly rough surface. In addition, at 600 and 800 °C, WS₂ is damaged by oxidation and loses its lubricious effect to form wear debris of oxide particles (consist of WO₃) which raises the friction coefficient [87]. In another study of 30%WS₂ laser clad on Cr18Ni9 austenitic stainless, a decline in CoF and wear rate of the coating was demonstrated at all the testing temperatures (RT, 300 and 600 °C) [92]. However, the coating underwent decomposition and oxidation, resulting in no lubrication effect at the 600 °C. Figure 8 exhibits the effect of sliding temperature on CoF and relative wear rate of several WS₂-based composites and coatings as reported in recent literature [10,87,88,90–92]. The wear rates are relative to the material’s corresponding room temperature values (material’s wear rate at a particular HT divided by their RT value).

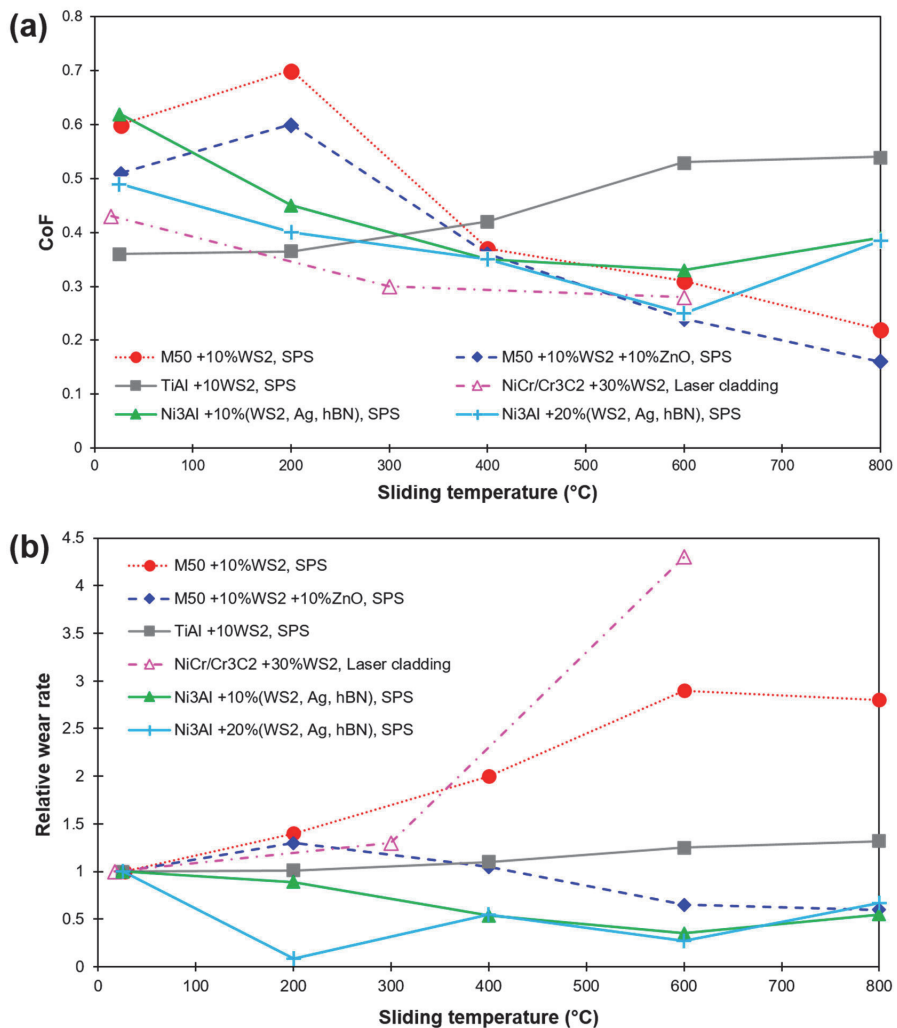


Figure 8. HT sliding results of WS₂-based composites and coatings as found in recent literature (a) CoF; (b) Relative wear rate (in relation to their corresponding RT wear). Values are labeled as per WS₂ concentration, matrix material, and fabrication method [10,87,88,90–92].

2.3. Alkaline-Earth Fluorides

Alkaline-earth fluorides such as LiF, CaF₂, and BaF₂ are well-known to provide solid lubrication at HT of 500–900 °C [3]. This is due to the reason that the material (CaF₂) exists at a slip plane (compacting Ca atomic plane), and at HT conditions, the atomic force in the phase decreases, resulting in an easy shearing. However, alkaline-earth fluorides demonstrate poor tribological behavior at low-to-moderate temperature ranges. The responsible mechanism of friction and wear reduction in fluorides of alkaline-earth metals are reported to be their ‘softening’ around 500 °C, termed as the ‘transition point’ from a brittle to plastic or ductile state [93]. At low-to-moderate temperatures, they tend to be brittle, resulting in amplified wear (mainly abrasion) due to the third body effect [94]. Though the introduction of both mixtures of CaF₂ and BaF₂ to decrease the lubrication temperature to 400 °C as a result of lowering the melting point of composites is also reported in ref. [95]. Incorporation of rare earth trifluorides such as LaF₃, NdF₃ to reduce friction and wear at HT are also conveyed in ref. [96].

An improved friction and wear property of the SPSed ZrO₂(Y₂O₃) matrix composites with an inclusion of 31 wt% BaF₂ and 19 wt% CaF₂ was demonstrated at temperatures beyond 400 °C [97]. The CoF of the composite stabilized around 0.4, while it escalated for the reference material up to 1 at 800 °C. At RT sliding, the composites demonstrate poor behavior with signs of significant plastic deformation and delamination. A considerable decrease in friction and wear of Al₂O₃-50 wt% CaF₂ composite at 400 °C was reported in [98], while a further decrease by two orders of magnitude at 650 °C, in comparison to the reference Al₂O₃ was noted. The formation of a Ca-rich lubricious layer on the surface of composites was held responsible for it. However, delamination of the formed lubricious tribolayer was seen at 800 °C, resulting in unstable friction. Similar to the previous works by ref. [96,97] the composites performed poorly at RT.

Cura et al. reported a synergetic effect of Ag and CaF₂, resulting in enlarging the lubrication range from 200 to 650 °C [99]. Additionally, widening of lubrication range through the use of CaF₂ and Au lubricants in the ZrO₂(Y₂O₃) matrix was studied in [33]. At 400 °C and beyond, the composites demonstrated the formation of a smooth CaF₂ lubricating layer, including Au lubricants. A similar effect of synergism was shown by others [100–102]. Figure 9 demonstrates the effect of sliding temperature on CoF and relative wear rate of several fluoride-based composites and coatings as reported in recent literature [10,33,97–99]. The wear rates are relative to the material’s corresponding room temperature values (material’s wear rate at a particular HT divided by their RT value).

In general, the mechanism of synergetic lubrication can be divided into three steps: (1) tribo-chemistry—at HT, the generation of lubricious compounds from the reaction between fluorides and matrix material occurs, resulting in low friction. (2) Transfer-layer—at moderate temperatures, the formation of tribo layer or transfer layer (rich in solid lubricants) protects the direct contact between tribo-bodies and thus minimizing friction and wear. (3) Glaze layer—at extreme HT, the formation of an oxide-rich glaze layer (with lubricating compounds) is seen. The glazed layer is reported to carry a wear-resistant and friction-reducing property [1,4]. A schematic of the synergetic effect at HT is presented in Figure 10.

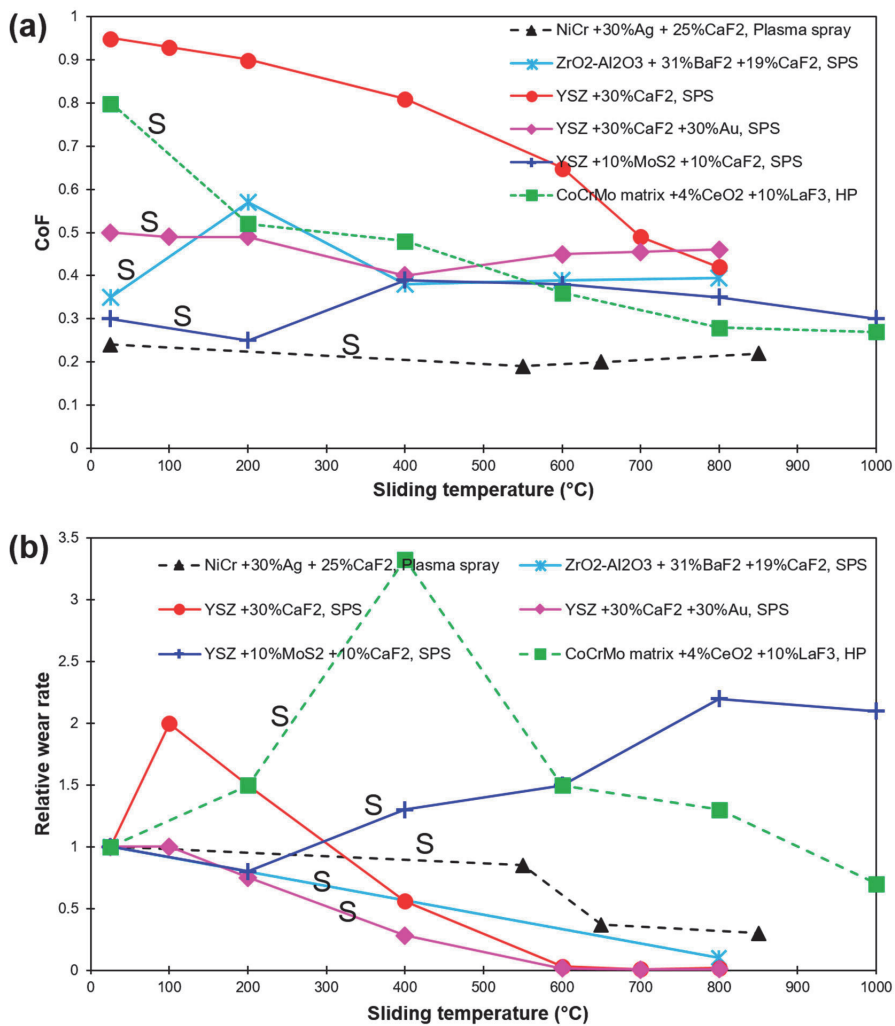


Figure 9. HT sliding results of Fluorides-based composites and coatings as found in recent literature (a) CoF; (b) Relative wear rate (in relation to their corresponding RT wear). Values are labeled as per Fluorides concentration, matrix material, and fabrication method [10,33,97–99]. Synergic effect of more than one solid lubricant is labeled with S.

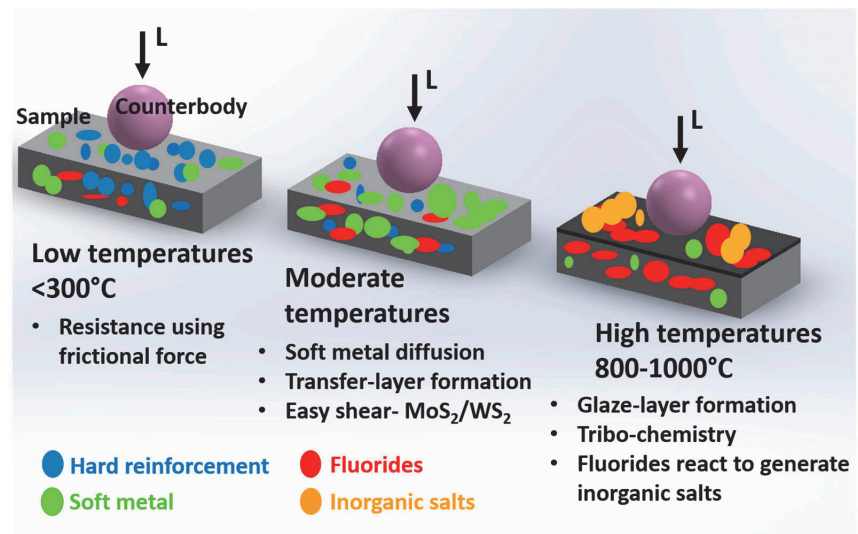


Figure 10. Schematic showing synergism of solid lubricants, i.e., soft metal/laminar solids and fluorides to broaden the range of lubricating temperature.

2.4. Lubricious Oxides and Magneli Phases

In order to expand the range of working temperature of materials to around ~ 1000 °C or more, often oxides of metals are sought [3]. Lubrication from oxides is a complicated subject. Several works have been performed in this regard to report the HT lubrication range of various metal oxides in regards to their stability, adhesion strength, and lubrication mechanism. However, in situ formation of oxides is regarded as the most efficient method due to their abrasive nature at lower temperatures [103]. Generally, under a certain condition of temperature and chemical composition, a transformation (due to changes in the crystal chemistry of oxides) from brittle-to-ductile proceeds, resulting in their easy plastic deformation. Additionally, the tribological response of such oxides also depends on their respective ionic potential [10].

The protective behavior of oxides due to their optimum thickness, adherence to the substrate, a large load-bearing capacity, and a balanced Pilling–Bedworth ratio (PBR) during dry-sliding is reported in [104]. The developed oxide layer (or tribo-layer) at this point is thick enough to prevent contact between tribo-bodies and thus, resist wear. However, spalling, delamination and plastic deformation of the generated oxide layer is usually reported at low to moderate temperatures. A significant decrease in wear at 800 and 900 °C sliding due to the formation of thick, well-adhered, and hard rutile TiO_2 phase on the surface of the Ti-TiB_w composite is demonstrated in ref [4] (Figure 11). Apart from the protective tribo-oxide layer, the formation of a glazed layer on the surface of composite, as well as counter body during 800 °C, sliding was also stated (Figure 11). The generated glassy-glazed layer at 700–900 °C on the surface of Ti-TiB_w carried a friction-reducing property (CoF~0.18). A similar formation of glassy layer phase of Cu_2O was reported to diminish friction and wear of Cu-TZP composite at 600 and 700 °C (CoF~0.35 and 0.4 respectively) [105]. A similar lubricious effect of CuO (CoF~0.2) was reported by a few others [106,107]. The self-lubrication from lead monoxide (PbO) due to its soft, ductile and efficient shearing ability at HT is well-known. Nevertheless, their toxicity to the environment and human health has significantly limited their usage, putting them out of the main study.

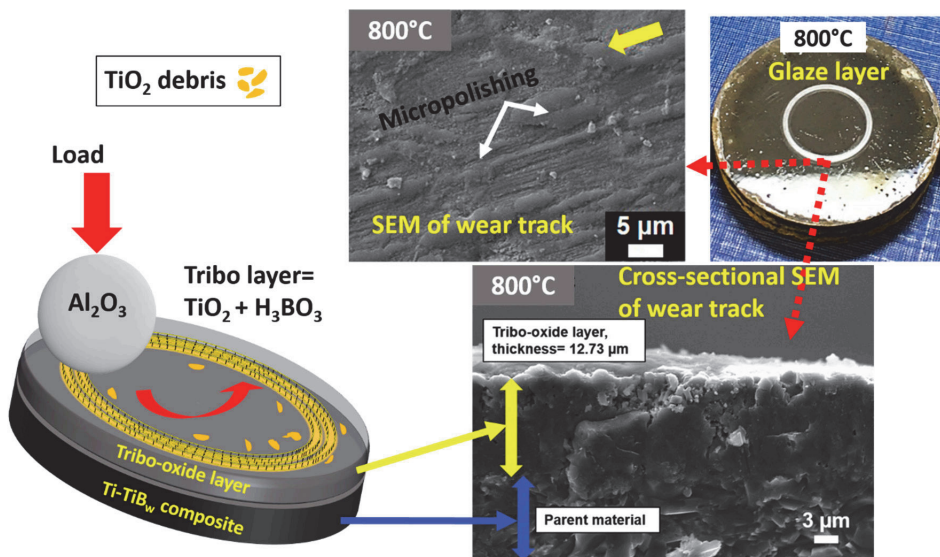


Figure 11. A collection of images from ref. [4] showing the mechanism of wear reduction at HT due to the formation of thick, homogeneous tribolayer. Tribolayer consisted of TiO_2 and boric acid.

For few oxides with a low melting point, the self-lubricity is demonstrated due to their quick melting; on the other hand, for others, the shear strength is relatively lower in specific crystal orientations owing to an absence plane of oxygen atoms; known as a crystallographic shear (CS) plane [108]. The latter has the tendency to impart low friction due to their lattice structure and are termed as Magnéli phase oxides. In addition, due to their high chemical stability, they are stated to show significantly low tribo-oxidation and adhesion to the counter body material. Figure 12 shows a relationship between de-cohesion energy (energy required to separate the cleaved layers) and elastic constant of certain oxides reported to demonstrate Magnéli phases [109]. A greater layer distance leads to lower de-cohesion energy and elastic shear constant, which is a degree of shear strength (Figure 12). As per calculation, V_2O_5 has the maximum layer distance and henceforth the lowest energy requisite to detach its layers, which specifies that its CS oxides will have superior lubricious nature than its peers.

The Magnéli phase formation due to the oxidation of W-N coating during HT sliding is reported to impart a significant decrease in CoF and wear of the coating beyond 200 °C [110]. In another study [111], the lubricious Magnéli phase of Mo_4O_{11} in Al_2O_3 -Mo composites demonstrated the lowest CoF of 0.27 at 400 °C sliding due to their shear in the lattice of MoO_3 . Few studies on the W-O system [112,113] report the transformation of Magnéli phase oxide of WO_3 to $\text{WO}_{2.9}$ during sintering, further resulting in a considerably diminished CoF (up to 0.10).

Titanium shows a higher inclination towards oxygen and actively reacts to form oxides (TiO_2) [114]. Few studies on titanium report Magnéli phases formation (transformation from TiO_2) of $\gamma\text{-Ti}_3\text{O}_5$, Ti_5O_9 , Ti_9O_{17} ($\text{Ti}_n\text{O}_{2n-1}$), and $\text{TiO}_{1.93-1.98}$ [115,116] during HT sliding; resulting in a noticeable reduction in the shear strength on the surface as well as in the bulk materials. A drop in shear strength from 21 MPa to 8 MPa upon a transformation in stoichiometry from $\sim\text{TiO}_2$ to $\text{TiO}_{1.93-1.98}$ was conveyed in ref. [116].

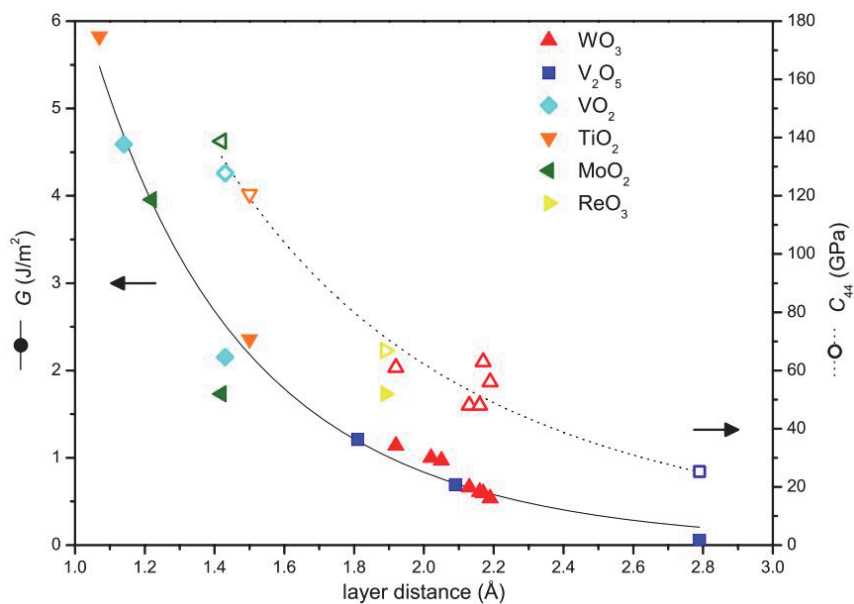


Figure 12. Contemplation of oxides forming Magnéli phase based on their de-cohesion energy (G) and elastic constant (C_{44}) as a function of the distance between the cleaved layers [109].

Vanadium oxides are stated to form similar Magnéli lubricious phases as that of titanium, analogous to the general formulations V_nO_{2n-1} and V_nO_{2n+1} , with V_2O_5 [117]. The de-cohesion energy of the layers of V_2O_5 is the lowest resulting in an easy crystallographic shearing (Figure 12) [109]. The formation of wear-reducing phases of V_2O_5 and TiO_2 on (V, Ti)N coating at 500–700 °C resulted in CoF to drift around 0.5 [118]. However, at 700 °C, a jump in CoF value to 0.6 was noted due to the coating damage and partial melting. Similar phenomena of coating melting close to 680 °C were stated in [119]. Particularly, Magnéli phases of vanadium show a steady decrease in CoF at temperatures between 400–700 °C due to liquid lubrication resulting in an easy-to-shear microstructure by V_2O_5 , VO_2 , and V_6O_{13} [120–122], accounting for the melting and smearing of such phases. However, a complete melting and vaporization of V_2O_5 around 700 °C results in a lubrication failure [118–123]. Figure 13 demonstrates the effect of sliding temperature on CoF and relative wear rate values of composites and coatings forming oxides (and Magnéli phases), as reported in recent literature [4,13,118,120,123–127]. The efficient lubrication range is shaded.

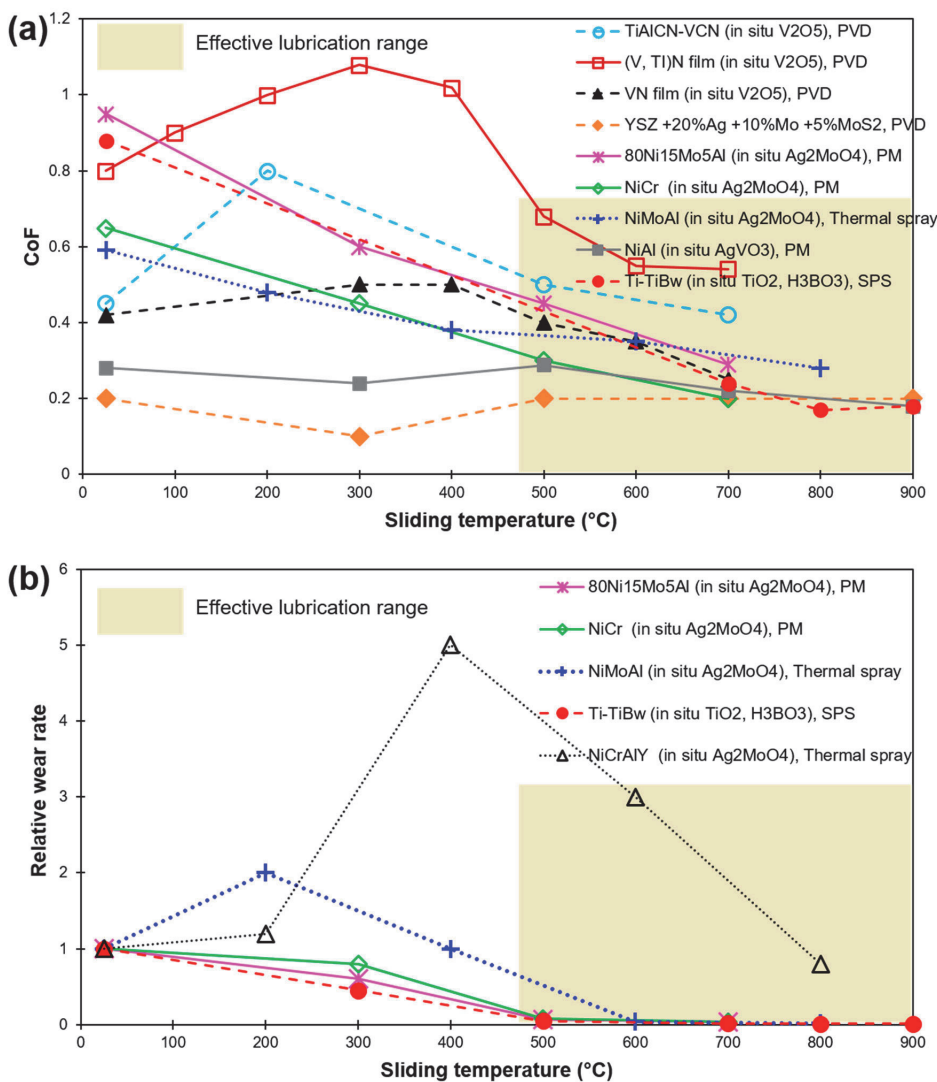


Figure 13. HT sliding results of oxide-based lubrication and coatings as found in recent literature (a) CoF; (b) Relative wear rate (in relation to their corresponding RT wear). Values are labelled as per oxide formation (in situ), matrix material, and fabrication method [4,13,118,120,123–127].

2.5. Challenges, Opportunities, and Concluding Remarks

Production of solid-lubricating materials via powder sintering is widely reported. Limitations such as grain growth, poor mechanical properties due to a long holding time during sintering, etc., have surfaced to a quicker sintering technique, i.e., spark plasma sintering (SPS). However, a more efficient, faster, and low-energy consuming technique known as microwave sintering (MS) is equally heightening [128]. The quick heating incurred during MS due to the energy transformation rather than energy transfer (as in SPS) results in volumetric heating, further giving rise to a much finer and uniform microstructure. Apart from powder metallurgy (sintering), PVD techniques to fabricate solid-lubricating coatings have been widely observed. On the other hand, laser claddings to produce thick solid-lubricating coatings have been greatly undervalued despite their

effectiveness. Deposition of a single layer using laser cladding technique is studied by several. However, very few exist on multilayer deposition due to limitations in mechanical property of sub-layer during re-melting [129].

The potential of additive manufacturing (3D printing) to fabricate bulks or coatings through layer-by-layer deposition is not yet reported. The possibility to generate complex geometries of solid-lubricating materials can be of high importance. Alternatively, the production of ‘smart’ solid-lubricating materials [3] demonstrating variations in their mechanical and chemical behavior upon an applied external stimuli using an approach of 4D printing is also foreseen [130].

Figures 14 and 15 demonstrate a graphical approximation of effective temperature range and their corresponding CoF for various groups of solid-lubricating materials (solid lubricants), respectively. In general, no single material exists that can cope with the complete tribological demands of working from room-to-extremely high temperatures (~1200 °C). However, the combination of various solid lubricants (such as soft metals, fluorides, etc.) to widen the lubrication temperature range (up to 1000 °C) is perceived (described in former sections). In order to accomplish the extreme temperature tribological needs, an HT solid-lubricating material should be designed as per the following considerations: (a) a CoF value below 0.2, (b) wear rate below 10^{-6} mm³/Nm, and to work on a wide-ranging temperature from cryogenics to HT. There is a need for a more detailed study to understand the synergism of solid lubricants to provide lubrication under the aforementioned considerations over a wide temperature range.

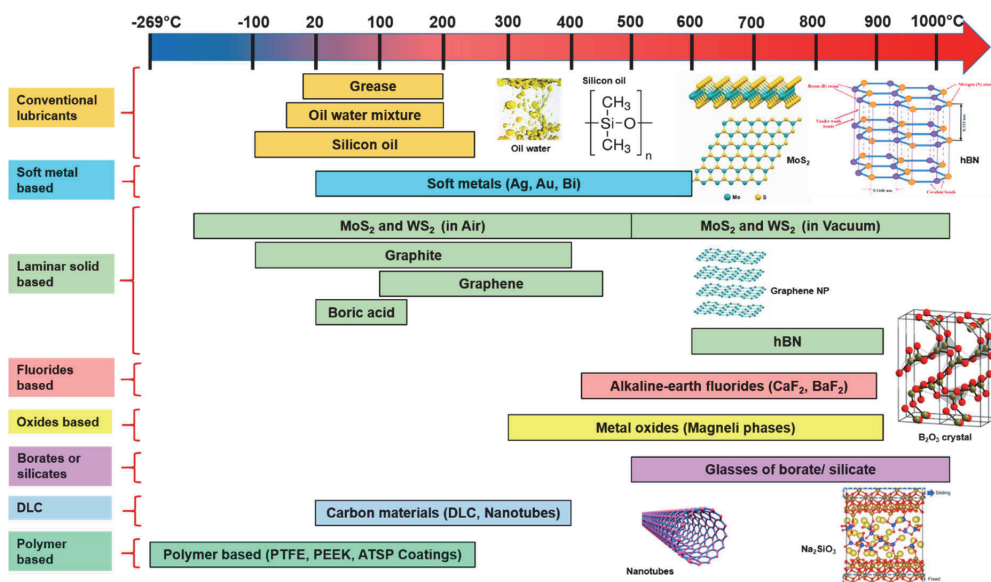


Figure 14. A graphical representation of effective temperature ranges for solid-lubricating materials (solid lubricants).

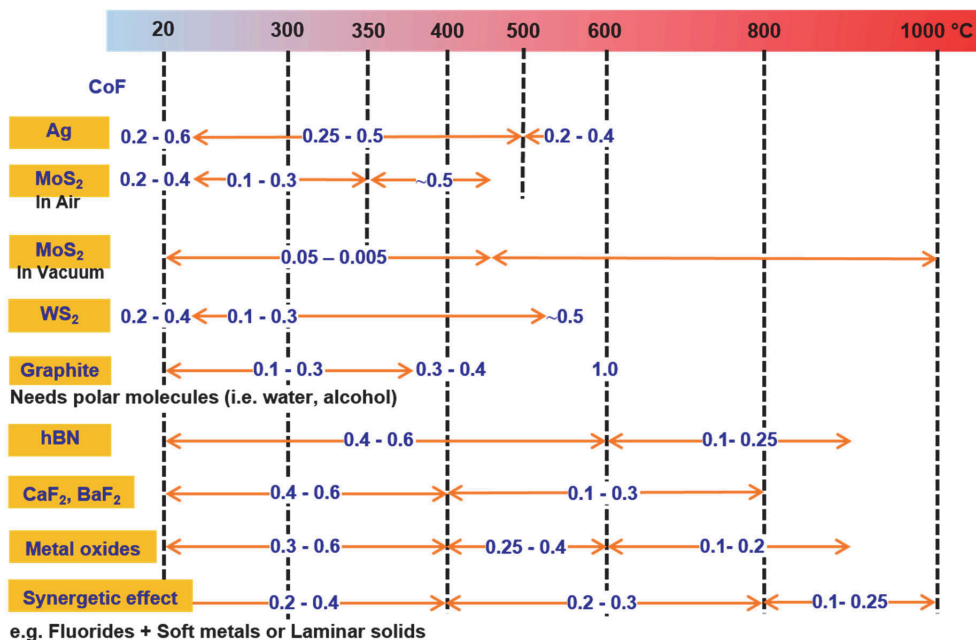


Figure 15. An approximate range of CoF under effective temperature ranges for widely used solid-lubricating materials (solid lubricants).

The promising study of new age ‘diamond like carbon’ (DLC) coatings to minimize friction (up to <0.01) and wear is reported in few studies [131,132]. Their ability to regulate surface chemistry and structure under sliding conditions has conferred it to be ‘adaptive’ in nature. In addition to this, the combination of DLC with other solid lubricants such as TMDs, soft metals, etc., is stated to increase the lubrication range [133,134]. A low CoF and long endurance (operation) in dry/humid environmental sliding conditions under humid air, vacuum, and dry nitrogen atmosphere was reported for DLC-based nanocomposite coatings of WC/DLC/WS₂ phases [133]. The CoF was 0.1 in humid air, 0.03 in a vacuum, and 0.007 in dry nitrogen. However, more research is needed for DLC-based coatings to understand the phenomena of surface adaptation and wear mechanism, especially during synergetic effects with other solid lubricants.

The current study brings into consideration the dependence of several factors during the self-lubrication of solid lubricants such as environment, operating conditions, the preciseness of testing methods, etc. Most of the work is based on a sliding test, which is incapable of a detailed comment on the behavior of solid lubricants in a dynamic mode of operations [135]. In addition, there exists a major lack of atomistic- and nano-level analysis of the evolving physical and chemical properties of surfaces and/or sub-surfaces, which is expected to broaden the understanding behind discussed mechanisms of operation. There still remains an unclarity in the details of feedstock/precursors composition and their methodical study, raising the concern for the correct experimental inputs. In this regard, the approach of simulation possibly will open the doors for better understanding about the effect of inclusions, their concentration and morphology, chemistry and evolution of buried sliding surface, predicting new inclusions, their reactions with the host matrix, the effect of the environment (cryogenics, vacuum), etc. on the lubrication behavior of solid-lubricating materials.

With an increasing demand for materials to perform at extreme temperature applications to reduce friction and wear in the present industrial revolution, there is a parallel approach to save the environment, energy, and incurred life cycle cost. This exponential

rise in material developments has not only propelled us towards environment-friendly foot-steps but also towards designing a ‘smart’ tribo-material, which can be perceived as more efficient and multifunctional in approach (Figure 16). In addition to being adaptive and re-structurable, the new generation of tribo-materials is expected to show properties such as bio-mimicking (inspired from nature such as human skin, snake skin, fish scales, etc. to minimize friction, erosion) [16] and the ability to self-diagnose (such as, in fiber-reinforced plastics, useful in fast damage diagnosis, etc.).

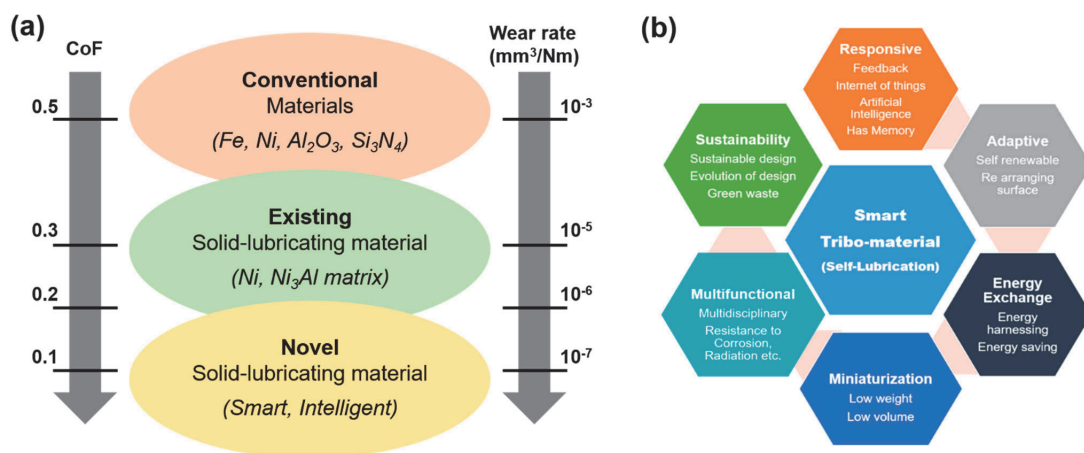


Figure 16. (a) Evolution of an HT solid-lubricating material in terms of CoF and wear rate; (b) features of a ‘smart’ solid-lubricating material [3].

Multidisciplinary studies in the designing of solid-lubricating materials are also foreseen. Cross-connection of tribology with other areas of physics, materials, mechanical engineering, and biomedical might help to strengthen the investigation in the design of a multifunctional and smart tribo-material. Clubbing with other areas such as information technology is believed to make advancements in ‘self-diagnosis’ and ‘repair’ through the use of artificial intelligence [3,136,137]. It is certain that under the canopy of a multidisciplinary approach, the tribology of HT solid/self-lubricating materials will take a leap from ‘self-adaptive’ to ‘smart’ to ‘intelligent’ lubricating material.

Author Contributions: Conceptualization, I.H. and M.A.; Data curation, R.K.; Formal analysis, R.K. and M.A.; Investigation, R.K., R.R. and M.A.; Methodology, I.H. and R.K.; Project administration, I.H.; Resources, I.H. and M.A.; Supervision, I.H.; Validation, I.H.; Visualization, R.K. and R.R.; Writing—original draft, R.K.; Writing—review & editing, R.K. and I.H. All authors have read and agreed to the published version of the manuscript.

Funding: This research work is supported by the Estonian Research Council grants PRG643 (I. Hussainova), M-ERA.Net project “HOTselflub” MOBERA18 N.20097582-CA and M-ERA.NET “Durracer” 18012.

Conflicts of Interest: The authors declare no conflict of interest.

References

- Shah, R.; Chen, R.; Woydt, M.; Baumann, C.; Jurs, J.; Iaccarino, P. High Temperature Tribology under Linear Oscillation Motion. *Lubricants* **2020**, *9*, 5. [CrossRef]
- Yu, H.; Zheng, Z.; Chen, H.; Qiao, D.; Feng, D.; Gong, Z.; Dong, G. An investigation of tribochemical reaction kinetics from the perspective of tribo-oxidation. *Tribol. Int.* **2021**, *165*, 107289. [CrossRef]
- Kumar, R.; Antonov, M. Self-lubricating materials for extreme temperature tribo-applications. *Mater. Today Proc.* **2020**, *44*, 4583–4589. [CrossRef]

4. Kumar, R.; Antonov, M.; Liu, L.; Hussainova, I. Sliding wear performance of in-situ spark plasma sintered Ti-TiBw composite at temperatures up to 900 °C. *Wear* **2021**, *476*, 203663. [[CrossRef](#)]
5. Zhu, S.; Cheng, J.; Qiao, Z.; Yang, J. High temperature solid-lubricating materials: A review. *Tribol. Int.* **2018**, *133*, 206–223. [[CrossRef](#)]
6. Marques, A.; Suarez, M.P.; Sales, W.F.; Machado, R. Turning of Inconel 718 with whisker-reinforced ceramic tools applying vegetable-based cutting fluid mixed with solid lubricants by MQL. *J. Mater. Process. Technol.* **2018**, *266*, 530–543. [[CrossRef](#)]
7. Antonov, M.; Klimczyk, P.; Kumar, R.; Tamre, M.; Zahavi, A. Performance of Al₂O₃-cBN materials and the perspective of using hyperspectral imaging during cutting tests. *Proc. Est. Acad. Sci.* **2021**, *70*, 524. [[CrossRef](#)]
8. Shi, X.; Zhai, W.; Xu, Z.; Wang, M.; Yao, J.; Song, S.; Wang, Y. Synergetic lubricating effect of MoS₂ and Ti₃SiC₂ on tribological properties of NiAl matrix self-lubricating composites over a wide temperature range. *Mater. Des.* **2014**, *55*, 93–103. [[CrossRef](#)]
9. Pelcastre, L.; Hardell, J.; Rolland, A.; Prakash, B. Influence of microstructural evolution of Al-Si coated UHSS on its tribological behaviour against tool steel at elevated temperatures. *J. Mater. Process. Technol.* **2016**, *228*, 117–124. [[CrossRef](#)]
10. Torres, H.; Ripoll, M.R.; Prakash, B. Tribological behaviour of self-lubricating materials at high temperatures. *Int. Mater. Rev.* **2017**, *63*, 309–340. [[CrossRef](#)]
11. Li, J.; Xiong, D.; Huang, Z.; Kong, J.; Dai, J. Effect of Ag and CeO₂ on friction and wear properties of Ni-base composite at high temperature. *Wear* **2009**, *267*, 576–584. [[CrossRef](#)]
12. Ye, F.; Lou, Z.; Wang, Y.; Liu, W. Wear mechanism of Ag as solid lubricant for wide range temperature application in micro-beam plasma cladded Ni60 coatings. *Tribol. Int.* **2021**, *167*, 107402. [[CrossRef](#)]
13. Aouadi, S.M.; Paudel, Y.; Simonson, W.J.; Ge, Q.; Kohli, P.; Muratore, C.; Voevodin, A.A. Tribological investigation of adaptive Mo₂N/MoS₂/Ag coatings with high sulfur content. *Surf. Coat. Technol.* **2009**, *203*, 1304–1309. [[CrossRef](#)]
14. Torres, H.; Slawik, S.; Gachot, C.; Prakash, B.; Ripoll, M.R. Microstructural design of self-lubricating laser claddings for use in high temperature sliding applications. *Surf. Coat. Technol.* **2018**, *337*, 24–34. [[CrossRef](#)]
15. Voevodin, A.; Muratore, C.; Aouadi, S. Hard coatings with high temperature adaptive lubrication and contact thermal management: Review. *Surf. Coat. Technol.* **2014**, *257*, 247–265. [[CrossRef](#)]
16. Kumar, R.; Antonov, M.; Holovenko, Y.; Surzhenkov, A. Erosive Wear Resistance of Nature-inspired Flexible Materials. *Tribol. Lett.* **2020**, *68*, 1–8. [[CrossRef](#)]
17. Akhtar, S.S. A critical review on self-lubricating ceramic-composite cutting tools. *Ceram. Int.* **2021**, *47*, 20745–20767. [[CrossRef](#)]
18. Duan, W.; Sun, Y.; Liu, C.; Liu, S.; Li, Y.; Ding, C.; Ran, G.; Yu, L. Study on the formation mechanism of the glaze film formed on Ni/Ag composites. *Tribol. Int.* **2016**, *95*, 324–332. [[CrossRef](#)]
19. Chen, J.; An, Y.; Yang, J.; Zhao, X.; Yan, F.; Zhou, H.; Chen, J. Tribological properties of adaptive NiCrAlY–Ag–Mo coatings prepared by atmospheric plasma spraying. *Surf. Coat. Technol.* **2013**, *235*, 521–528. [[CrossRef](#)]
20. Shi, X.; Xu, Z.; Wang, M.; Zhai, W.; Yao, J.; Song, S.; Din, A.Q.U.; Zhang, Q. Tribological behavior of TiAl matrix self-lubricating composites containing silver from 25 to 800 °C. *Wear* **2013**, *303*, 486–494. [[CrossRef](#)]
21. Aouadi, S.M.; Paudel, Y.; Luster, B.; Stadler, S.; Kohli, P.; Muratore, C.; Hager, C.; Voevodin, A.A. Adaptive Mo₂N/MoS₂/Ag tribological nanocomposite coatings for aerospace applications. *Tribol. Lett.* **2008**, *29*, 95–103. [[CrossRef](#)]
22. Li, X.; Chen, X.; Zhang, C.; Luo, J. Preparation of self-lubricating NiTi alloy and its self-adaptive behavior. *Tribol. Int.* **2018**, *130*, 43–51. [[CrossRef](#)]
23. Cheng, J.; Zhu, S.; Tan, H.; Yu, Y.; Yang, J.; Liu, W. Lead-bismuth liquid metal: Lubrication behaviors. *Wear* **2019**, *430–431*, 94–99. [[CrossRef](#)]
24. Rosales, I.; Gonzalez-Rodriguez, G.; Gama, J.L.; Guardian, R. Bismuth Effect on the Mechanical Properties of Antifriction Al-Sn Alloys. *Mater. Sci. Appl.* **2014**, *5*, 330–337. [[CrossRef](#)]
25. Oksanen, V.; Lehtovaara, A.; Kallio, M. Load capacity of lubricated bismuth bronze bimetal bearing under elliptical sliding motion. *Wear* **2017**, *388–389*, 72–80. [[CrossRef](#)]
26. Thomson, J.; Zavadil, R.; Sahoo, M.; Dadouche, A.; Dmochowski, W.; Conlon, M. Development of a Lead-Free Bearing Material for Aerospace Applications. *Int. J. Met.* **2010**, *4*, 19–30. [[CrossRef](#)]
27. Chen, K.; Wu, X.; Zhang, A.; Zhang, J.; Chen, X.; Zhu, Y.; Wang, Z. Development of wear resistant Cu-12Sn-1.5Ni alloy via minor addition of Fe during casting process. *Appl. Surf. Sci.* **2022**, *573*, 151623. [[CrossRef](#)]
28. Liu, C.; Yin, Y.; Li, C.; Xu, M.; Li, R.; Chen, Q. Tailoring Cu nano Bi self-lubricating alloy material by shift-speed ball milling flake powder metallurgy. *J. Alloy. Compd.* **2022**, *903*, 163747. [[CrossRef](#)]
29. Liu, C.; Yin, Y.; Li, C.; Xu, M.; Li, R.; Chen, Q. Properties of lead-free copper matrix composites prepared through in situ Ni-coated FeS surface modification and mechanical alloying. *J. Alloy. Compd.* **2021**, *881*, 160580. [[CrossRef](#)]
30. Kallio, M.; Vuorinen, P.; Fuentes, E.; Marañón, O.; Ruusila, V.; Nyyssönen, T.; Kuokkala, V.T.; Lehtovaara, A. Tribological Behavior of Bronze Alloys with Solid Lubricants. *Key Eng. Mater.* **2012**, *527*, 205–210. [[CrossRef](#)]
31. Heymans, G.; Muñoz, A.I.; Mischler, S. Tribological behaviour of galvanic gold coatings reinforced with silica nanoparticles. *Wear* **2020**, *462–463*, 203512. [[CrossRef](#)]
32. Voevodin, A.; Hu, J.; Fitz, T.; Zabinski, J. Tribological properties of adaptive nanocomposite coatings made of yttria stabilized zirconia and gold. *Surf. Coat. Technol.* **2001**, *146–147*, 351–356. [[CrossRef](#)]
33. Ouyang, J.H.; Sasaki, S.; Murakami, T.; Umeda, K. The synergistic effects of CaF₂ and Au lubricants on tribological properties of spark-plasma-sintered ZrO₂ (Y₂O₃) matrix composites. *Mater. Sci. Eng. A* **2004**, *386*, 234–243. [[CrossRef](#)]

34. Magnin, V.; Mischler, S. Tribological response of multilayered gold nickel coating deposited on fine turned surfaces. *Wear* **2019**, *426–427*, 1195–1202. [[CrossRef](#)]
35. Chen, Z.; Wagner, J.; Turq, V.; Hillairet, J.; Taberna, P.-L.; Laloo, R.; Duluard, S.; Bernard, J.-M.; Song, Y.; Yang, Q.; et al. Surfactant-assisted electrodeposition of Au–Co/WS₂ self-lubricating coating from WS₂ suspended cyanide electrolyte. *J. Alloy. Compd.* **2020**, *829*, 154585. [[CrossRef](#)]
36. Wang, Y.; Worzala, F.; Lefkow, A. Friction and wear properties of partially stabilized zirconia with solid lubricant. *Wear* **1993**, *167*, 23–31. [[CrossRef](#)]
37. Österle, W.; Prietzel, C.; Kloß, H.; Dmitriev, A. On the role of copper in brake friction materials. *Tribol. Int.* **2010**, *43*, 2317–2326. [[CrossRef](#)]
38. Kato, H.; Takama, M.; Iwai, Y.; Washida, K.; Sasaki, Y. Wear and mechanical properties of sintered copper–tin composites containing graphite or molybdenum disulfide. *Wear* **2003**, *255*, 573–578. [[CrossRef](#)]
39. Guleryuz, C.G.; Krzanowski, J.E.; Veldhuis, S.C.; Fox-Rabinovich, G.S. Machining performance of TiN coatings incorporating indium as a solid lubricant. *Surf. Coat. Technol.* **2009**, *203*, 3370–3376. [[CrossRef](#)]
40. Zhang, X.; Sun, W.; Ma, H.; Xu, H.; Dong, J. Investigation of the Tribological Properties of Two Different Layered Sodium Silicates Utilized as Solid Lubrication Additives in Lithium Grease. *Ind. Eng. Chem. Res.* **2013**, *53*, 182–188. [[CrossRef](#)]
41. Vazirisereshk, M.R.; Martini, A.; Strubbe, D.A.; Baykara, M.Z. Solid Lubrication with MoS₂: A Review. *Lubricants* **2019**, *7*, 57. [[CrossRef](#)]
42. Furlan, K.P.; de Mello, J.D.B.; Klein, A.N. Self-lubricating composites containing MoS₂: A review. *Tribol. Int.* **2018**, *120*, 280–298. [[CrossRef](#)]
43. Ripoll, M.R.; Tomala, A.M.; Pirker, L.; Remškar, M. In-Situ Formation of MoS₂ and WS₂ Tribofilms by the Synergy between Transition Metal Oxide Nanoparticles and Sulphur-Containing Oil Additives. *Tribol. Lett.* **2020**, *68*, 41. [[CrossRef](#)]
44. Gopinath, V.M.; Arulvel, S. A review on the steels, alloys/high entropy alloys, composites and coatings used in high temperature wear applications. *Mater. Today Proc.* **2020**, *43*, 817–823. [[CrossRef](#)]
45. Jing, W.; Du, S.; Chen, S.; Liu, E.; Du, H.; Cai, H. Tribological behavior of VN–MoS₂/Ag composites over a wide temperature range. *Tribol. Trans.* **2022**, *65*, 66–77. [[CrossRef](#)]
46. Afanasiev, P.; Lorentz, C. Oxidation of Nanodispersed MoS₂ in Ambient Air: The Products and the Mechanistic Steps. *J. Phys. Chem. C* **2019**, *123*, 7486–7494. [[CrossRef](#)]
47. Shi, X.; Zhai, W.; Wang, M.; Xu, Z.; Yao, J.; Song, S.; Wang, Y. Tribological behaviors of NiAl based self-lubricating composites containing different solid lubricants at elevated temperatures. *Wear* **2014**, *310*, 1–11. [[CrossRef](#)]
48. Kong, L.; Bi, Q.; Niu, M.; Zhu, S.; Yang, J.; Liu, W. ZrO₂ (Y₂O₃)–MoS₂–CaF₂ self-lubricating composite coupled with different ceramics from 20 °C to 1000 °C. *Tribol. Int.* **2013**, *64*, 53–62. [[CrossRef](#)]
49. Hardell, J.; Efeoglu, I.; Prakash, B. Tribological degradation of MoS₂–Ti sputtered coating when exposed to elevated temperatures. *Tribol.-Mater. Surf. Interfaces* **2010**, *4*, 121–129. [[CrossRef](#)]
50. Muratore, C.; Voevodin, A.; Hu, J.; Zabinski, J. Tribology of adaptive nanocomposite yttria-stabilized zirconia coatings containing silver and molybdenum from 25 to 700 °C. *Wear* **2006**, *261*, 797–805. [[CrossRef](#)]
51. Niu, M.; Bi, Q.; Zhu, S.; Yang, J.; Liu, W. Microstructure, phase transition and tribological performances of Ni₃Si-based self-lubricating composite coatings. *J. Alloy. Compd.* **2013**, *555*, 367–374. [[CrossRef](#)]
52. Serpini, E.; Rota, A.; Ballestrazzi, A.; Marchetto, D.; Gualtieri, E.; Valeri, S. The role of humidity and oxygen on MoS₂ thin films deposited by RF PVD magnetron sputtering. *Surf. Coat. Technol.* **2017**, *319*, 345–352. [[CrossRef](#)]
53. Hu, J.; Bultman, J.; Muratore, C.; Phillips, B.; Zabinski, J.; Voevodin, A. Tribological properties of pulsed laser deposited Mo–S–Te composite films at moderate high temperatures. *Surf. Coat. Technol.* **2009**, *203*, 2322–2327. [[CrossRef](#)]
54. Zhou, Y.; Dong, Y.; Yin, H.; Li, Z.; Yan, R.; Li, D.; Gu, Z.; Sun, X.; Shi, L.; Zhang, Z. Characterizing thermal-oxidation behaviors of nuclear graphite by combining O₂ supply and micro surface area of graphite. *Sci. Rep.* **2018**, *8*, 13400. [[CrossRef](#)] [[PubMed](#)]
55. Li, C.; Chen, X.; Shen, L.; Bao, N. Revisiting the Oxidation of Graphite: Reaction Mechanism, Chemical Stability, and Structure Self-Regulation. *ACS Omega* **2020**, *5*, 3397–3404. [[CrossRef](#)]
56. Kim, T.; Singh, D.; Singh, M. Enhancement of Oxidation Resistance of Graphite Foams by Polymer Derived-silicon Carbide Coating for Concentrated Solar Power Applications. *Energy Procedia* **2015**, *69*, 900–906. [[CrossRef](#)]
57. Huai, W.; Zhang, C.; Wen, S. Graphite-based solid lubricant for high-temperature lubrication. *Friction* **2020**, *9*, 1660–1672. [[CrossRef](#)]
58. Tan, H.; Wang, S.; Yu, Y.; Cheng, J.; Zhu, S.; Qiao, Z.; Yang, J. Friction and wear properties of Al-20Si-5Fe-2Ni-Graphite solid-lubricating composite at elevated temperatures. *Tribol. Int.* **2018**, *122*, 228–235. [[CrossRef](#)]
59. Mushtaq, S.; Wani, M.F. High-temperature friction and wear studies of Fe-Cu-Sn alloy with graphite as solid lubricant under dry sliding conditions. *Mater. Res. Express* **2018**, *5*, 026504. [[CrossRef](#)]
60. Zhen, J.; Zhu, S.; Cheng, J.; Li, M.; Lu, Y.; Qiao, Z.; Yang, J. Influence of graphite content on the dry sliding behavior of nickel alloy matrix solid lubricant composites. *Tribol. Int.* **2017**, *114*, 322–328. [[CrossRef](#)]
61. Lu, J.; Yang, S.; Wang, J.; Xue, Q. Mechanical and tribological properties of Ni-based alloy/CeF₃/graphite high temperature self-lubricating composites. *Wear* **2001**, *249*, 1070–1076. [[CrossRef](#)]
62. Cho, M.H.; Ju, J.; Kim, S.J.; Jang, H. Tribological properties of solid lubricants (graphite, Sb₂S₃, MoS₂) for automotive brake friction materials. *Wear* **2006**, *260*, 855–860. [[CrossRef](#)]

63. Kong, L.; Zhu, S.; Bi, Q.; Qiao, Z.; Yang, J.; Liu, W. Friction and wear behavior of self-lubricating ZrO₂ (Y₂O₃)–CaF₂–Mo–graphite composite from 20 °C to 1000 °C. *Ceram. Int.* **2014**, *40*, 10787–10792. [[CrossRef](#)]
64. Li, J.L.; Xiong, D.S. Tribological properties of nickel-based self-lubricating composite at elevated temperature and counterface material selection. *Wear* **2008**, *265*, 533–539. [[CrossRef](#)]
65. Bijwe, J.; Kumar, K.; Panda, J.N.; Parida, T.; Trivedi, P. Design and development of high performance tribo-composites based on synergism in two solid lubricants. *Compos. Part B Eng.* **2016**, *94*, 399–410. [[CrossRef](#)]
66. Sun, Q.; Wang, Z.; Yin, B.; Yang, J.; Liu, J.; Liu, Y.; Cheng, J.; Zhu, S.; Qiao, Z. The tribological properties and wear mechanism of copper coated graphite doped Sialon ceramic composites at wide range temperature from 25 to 800 °C. *Tribol. Int.* **2018**, *123*, 10–16. [[CrossRef](#)]
67. Wang, Y.; Gao, Y.; Li, Y.; Li, M.; Sun, L.; Zhai, W.; Li, K. Research on synergistic lubrication effect of silver modified Cu–Ni–graphite composite. *Wear* **2019**, *444–445*, 203140. [[CrossRef](#)]
68. Berman, D.; Erdemir, A.; Sumant, A.V. Graphene: A new emerging lubricant. *Mater. Today* **2014**, *17*, 31–42. [[CrossRef](#)]
69. Kumar, P.; Wani, M.F. Synthesis and tribological properties of graphene: A review. *J. Tribol.* **2017**, *13*, 36–71.
70. Essa, F.A.; Elsheikh, A.H.; Yu, J.; Elkady, O.A.; Saleh, B. Studies on the effect of applied load, sliding speed and temperature on the wear behavior of M50 steel reinforced with Al₂O₃ and/or graphene nanoparticles. *J. Mater. Res. Technol.* **2021**, *12*, 283–303. [[CrossRef](#)]
71. Xiao, Y.; Shi, X.; Zhai, W.; Yang, K.; Yao, J. Effect of Temperature on Tribological Properties and Wear Mechanisms of NiAl Matrix Self-Lubricating Composites Containing Graphene Nanoplatelets. *Tribol. Trans.* **2015**, *58*, 729–735. [[CrossRef](#)]
72. Xu, Z.; Zhang, Q.; Jing, P.; Zhai, W. High-Temperature Tribological Performance of TiAl Matrix Composites Reinforced by Multilayer Graphene. *Tribol. Lett.* **2015**, *58*, 1–9. [[CrossRef](#)]
73. Wei, M.; Wang, S.; Cui, X. Comparative research on wear characteristics of spheroidal graphite cast iron and carbon steel. *Wear* **2012**, *274–275*, 84–93. [[CrossRef](#)]
74. Podgornik, B.; Kosec, T.; Kocijan, A.; Donik, Č. Tribological behaviour and lubrication performance of hexagonal boron nitride (h-BN) as a replacement for graphite in aluminium forming. *Tribol. Int.* **2015**, *81*, 267–275. [[CrossRef](#)]
75. Zhang, S.; Zhou, J.; Guo, B.; Zhou, H.; Pu, Y.; Chen, J. Friction and wear behavior of laser cladding Ni/hBN self-lubricating composite coating. *Mater. Sci. Eng. A* **2008**, *491*, 47–54. [[CrossRef](#)]
76. Lu, X.-L.; Liu, X.-B.; Yu, P.-C.; Qiao, S.-J.; Zhai, Y.-J.; Wang, M.-D.; Chen, Y.; Xu, D. Synthesis and characterization of Ni60-hBN high temperature self-lubricating anti-wear composite coatings on Ti₆Al₄V alloy by laser cladding. *Opt. Laser Technol.* **2015**, *78*, 87–94. [[CrossRef](#)]
77. Kumar, R.; Aydinian, S.; Ivanov, R.; Liu, L.; Antonov, M.; Hussainova, I. High-Temperature Wear Performance of hBN-Added Ni-W Composites Produced from Combustion-Synthesized Powders. *Materials* **2022**, *15*, 1252. [[CrossRef](#)]
78. Torres, H.; Podgornik, B.; Jovičević-Klug, M.; Ripoll, M.R. Compatibility of graphite, hBN and graphene with self-lubricating coatings and tool steel for high temperature aluminium forming. *Wear* **2021**, *490–491*, 204187. [[CrossRef](#)]
79. Du, L.; Huang, C.; Zhang, W.; Li, T.; Liu, W. Preparation and wear performance of NiCr/Cr₃C₂–NiCr/hBN plasma sprayed composite coating. *Surf. Coat. Technol.* **2011**, *205*, 3722–3728. [[CrossRef](#)]
80. Zhu, X.; Wei, X.; Huang, Y.; Wang, F.; Yan, P. High-Temperature Friction and Wear Properties of NiCr/hBN Self-Lubricating Composites. *Metals* **2019**, *9*, 356. [[CrossRef](#)]
81. Tyagi, R.; Xiong, D.; Li, J.; Dai, J. Elevated temperature tribological behavior of Ni based composites containing nano-silver and hBN. *Wear* **2010**, *269*, 884–890. [[CrossRef](#)]
82. Zhang, Y.; Wang, W.; Hu, Z.; Liu, K.; Chang, J. Investigation of hBN powder lubricating characteristics of die steel H13–ceramic Si₃N₄ tribopair at 800 °C. *Proc. Inst. Mech. Eng. Part J. Eng. Tribol.* **2019**, *234*, 622–631. [[CrossRef](#)]
83. Chen, J.; Chen, J.; Wang, S.; Sun, Q.; Cheng, J.; Yu, Y.; Yang, J. Tribological properties of h-BN matrix solid-lubricating composites under elevated temperatures. *Tribol. Int.* **2020**, *148*, 106333. [[CrossRef](#)]
84. Yan, H.; Zhang, P.; Gao, Q.; Qin, Y.; Li, R. Laser cladding Ni-based alloy/nano-Ni encapsulated h-BN self-lubricating composite coatings. *Surf. Coat. Technol.* **2017**, *332*, 422–427. [[CrossRef](#)]
85. Zhang, W.; Yi, M.; Xiao, G.; Ma, J.; Wu, G.; Xu, C. Al₂O₃-coated h-BN composite powders and as-prepared Si₃N₄-based self-lubricating ceramic cutting tool material. *Int. J. Refract. Met. Hard Mater.* **2018**, *71*, 1–7. [[CrossRef](#)]
86. Chen, H.; Xu, C.; Xiao, G.; Chen, Z.; Ma, J.; Wu, G. Synthesis of (h-BN)/SiO₂ core-shell powder for improved self-lubricating ceramic composites. *Ceram. Int.* **2016**, *42*, 5504–5511. [[CrossRef](#)]
87. Essa, F.; Zhang, Q.; Huang, X. Investigation of the effects of mixtures of WS₂ and ZnO solid lubricants on the sliding friction and wear of M50 steel against silicon nitride at elevated temperatures. *Wear* **2017**, *374–375*, 128–141. [[CrossRef](#)]
88. Heshmat, H.; Hryniewicz, P.; Ii, J.F.W.; Willis, J.P.; Jahanmir, S.; DellaCorte, C. Low-friction wear-resistant coatings for high-temperature foil bearings. *Tribol. Int.* **2005**, *38*, 1059–1075. [[CrossRef](#)]
89. Wang, Q.; Chen, M.; Shan, Z.; Sui, C.; Zhang, L.; Zhu, S.; Wang, F. Comparative study of mechanical and wear behavior of Cu/WS₂ composites fabricated by spark plasma sintering and hot pressing. *J. Mater. Sci. Technol.* **2017**, *33*, 1416–1423. [[CrossRef](#)]
90. Shi, X.; Song, S.; Zhai, W.; Wang, M.; Xu, Z.; Yao, J.; Din, A.Q.U.; Zhang, Q. Tribological behavior of Ni3Al matrix self-lubricating composites containing WS₂, Ag and hBN tested from room temperature to 800 °C. *Mater. Des.* **2014**, *55*, 75–84. [[CrossRef](#)]
91. Xu, Z.; Zhang, Q.; Zhai, W. Tribological properties of TiAl matrix self-lubricating composites incorporated with tungsten disulfide and zinc oxide. *RSC Adv.* **2015**, *5*, 45044–45052. [[CrossRef](#)]

92. Yang, M.-S.; Liu, X.-B.; Fan, J.-W.; He, X.-M.; Shi, S.-H.; Fu, G.-Y.; Wang, M.-D.; Chen, S.-F. Microstructure and wear behaviors of laser clad NiCr/Cr₃C₂-WS₂ high temperature self-lubricating wear-resistant composite coating. *Appl. Surf. Sci.* **2012**, *258*, 3757–3762. [[CrossRef](#)]
93. Kim, S.-H.; Lee, S.W. Wear and friction behavior of self-lubricating alumina–zirconia–fluoride composites fabricated by the PECS technique. *Ceram. Int.* **2014**, *40*, 779–790. [[CrossRef](#)]
94. Kumar, R.; Antonov, M.; Beste, U.; Goljandin, D. Assessment of 3D printed steels and composites intended for wear applications in abrasive, dry or slurry erosive conditions. *Int. J. Refract. Met. Hard Mater.* **2019**, *86*, 105126. [[CrossRef](#)]
95. Kong, L.; Bi, Q.; Zhu, S.; Yang, J.; Liu, W. Tribological properties of ZrO₂ (Y₂O₃)–Mo–BaF₂/CaF₂ composites at high temperatures. *Tribol. Int.* **2012**, *45*, 43–49. [[CrossRef](#)]
96. Mazumder, S.; Metselaar, H.S.C.; Sukiman, N.L.; Zulkifli, N.W.M. An overview of fluoride-based solid lubricants in sliding contacts. *J. Eur. Ceram. Soc.* **2020**, *40*, 4974–4996. [[CrossRef](#)]
97. Ouyang, J.; Li, Y.; Wang, Y.; Zhou, Y.; Murakami, T.; Sasaki, S. Microstructure and tribological properties of ZrO₂(Y₂O₃) matrix composites doped with different solid lubricants from room temperature to 800 °C. *Wear* **2009**, *267*, 1353–1360. [[CrossRef](#)]
98. Jin, Y.; Kato, K.; Umehara, N. Tribological properties of self-lubricating CMC/Al₂O₃ pairs at high temperature in air. *Tribol. Lett.* **1998**, *4*, 243–250. [[CrossRef](#)]
99. Cura, M.E.; Kim, S.-H.; Muukkonen, T.; Varjus, S.; Vaajoki, A.; Söderberg, O.; Suhonen, T.; Kanerva, U.; Lee, S.W.; Hannula, S.-P. Microstructure and tribological properties of pulsed electric current sintered alumina–zirconia nanocomposites with different solid lubricants. *Ceram. Int.* **2012**, *39*, 2093–2105. [[CrossRef](#)]
100. Murakami, T.; Ouyang, J.H.; Sasaki, S.; Umeda, K.; Yoneyama, Y. High-temperature tribological properties of Al₂O₃, Ni–20 mass% Cr and NiAl spark-plasma-sintered composites containing BaF₂–CaF₂ phase. *Wear* **2005**, *259*, 626–633. [[CrossRef](#)]
101. Li, F.; Zhu, S.; Cheng, J.; Qiao, Z.; Yang, J. Tribological properties of Mo and CaF₂ added SiC matrix composites at elevated temperatures. *Tribol. Int.* **2017**, *111*, 46–51. [[CrossRef](#)]
102. Cheng, J.; Qiao, Z.; Yin, B.; Hao, J.; Yang, J.; Liu, W. High temperature tribological behaviors of (WAl)C–Co ceramic composites with the additions of fluoride solid lubricants. *Mater. Chem. Phys.* **2015**, *163*, 262–271. [[CrossRef](#)]
103. Kumar, R.; Liu, L.; Antonov, M.; Ivanov, R.; Hussainova, I. Hot Sliding Wear of 88 wt.% TiB–Ti Composite from SHS Produced Powders. *Materials* **2021**, *14*, 1242. [[CrossRef](#)] [[PubMed](#)]
104. Kumar, R.; Malaval, B.; Antonov, M.; Zhao, G. Performance of polyimide and PTFE based composites under sliding, erosive and high stress abrasive conditions. *Tribol. Int.* **2020**, *147*, 106282. [[CrossRef](#)]
105. Valefi, M.; de Rooij, M.; Schipper, D.J.; Winnubst, L. Effect of temperature on friction and wear behaviour of CuO–zirconia composites. *J. Eur. Ceram. Soc.* **2012**, *32*, 2235–2242. [[CrossRef](#)]
106. Zhu, S.; Bi, Q.; Niu, M.; Yang, J.; Liu, W. Tribological behavior of NiAl matrix composites with addition of oxides at high temperatures. *Wear* **2012**, *274–275*, 423–434. [[CrossRef](#)]
107. Zhu, S.; Cheng, J.; Qiao, Z.; Tian, Y.; Yang, J. High Temperature Lubricating Behavior of NiAl Matrix Composites with Addition of CuO. *J. Tribol.* **2016**, *138*, 031607. [[CrossRef](#)]
108. Berger, L.M.; Stahr, C.C.; Saaro, S.; Thiele, S.; Woydt, M.; Kelling, N. Dry sliding up to 7.5 m/s and 800 C of thermally sprayed coatings of the TiO₂–Cr₂O₃ system and (Ti,Mo)(C,N)–Ni(Co). *Wear* **2009**, *267*, 954–964. [[CrossRef](#)]
109. Cura, M.E. Ceramic Composites with Solid Lubricants Processed by Pulsed Electric Current Sintering. Ph.D. Thesis, Aalto University, Helsinki, Finland, 2021.
110. Gassner, G.; Mayrhofer, P.H.; Kutschej, K.; Mitterer, C.; Kathrein, M. Magnéli phase formation of PVD Mo–N and W–N coatings. *Surf. Coat. Technol.* **2006**, *201*, 3335–3341. [[CrossRef](#)]
111. Cura, M.; Liu, X.; Kanerva, U.; Varjus, S.; Kivioja, A.; Söderberg, O.; Hannula, S.-P. Friction behavior of alumina/molybdenum composites and formation of MoO_{3–x} phase at 400 °C. *Tribol. Int.* **2015**, *87*, 23–31. [[CrossRef](#)]
112. Cura, M.E.; Trebala, M.; Ge, Y.; Klimczyk, P.; Hannula, S.-P. Mechanical and tribological properties of WO_{2.9} and ZrO₂ + WO_{2.9} composites studied by nanoindentation and reciprocating wear tests. *Wear* **2021**, *478–479*, 203920. [[CrossRef](#)]
113. Polcar, T.; Parreira, N.; Cavaleiro, A. Tungsten oxide with different oxygen contents: Sliding properties. *Vacuum* **2007**, *81*, 1426–1429. [[CrossRef](#)]
114. Liu, L.; Ivanov, R.; Kumar, R.; Minasyan, T.; Antonov, M.; Hussainova, I. Functionally Gradient Ti₆Al₄V–TiB Composite Produced by Spark Plasma Sintering. In *Materials Science and Engineering*; IOP Conference Series; IOP Publishing: Bristol, UK, 2021; Volume 1140, p. 012004.
115. Lu, Y.; Matsuda, Y.; Sagara, K.; Hao, L.; Otomitsu, T.; Yoshida, H. Fabrication and Thermoelectric Properties of Magnéli Phases by Adding Ti into TiO₂. *Adv. Mater. Res.* **2011**, *415–417*, 1291–1296. [[CrossRef](#)]
116. Gardos, M.N. Magnéli phases of anion-deficient rutile as lubricious oxides. Part I. Tribological behavior of single-crystal and polycrystalline rutile (Ti_nO_{2n–1}). *Tribol. Lett.* **2000**, *8*, 65–78. [[CrossRef](#)]
117. Franz, R.; Mitterer, C. Vanadium containing self-adaptive low-friction hard coatings for high-temperature applications: A review. *Surf. Coat. Technol.* **2013**, *228*, 1–13. [[CrossRef](#)]
118. Ouyang, J.; Murakami, T.; Sasaki, S. High-temperature tribological properties of a cathodic arc ion-plated (V,Ti)N coating. *Wear* **2007**, *263*, 1347–1353. [[CrossRef](#)]
119. Franz, R.; Neidhardt, J.; Kaindl, R.; Sartory, B.; Tessadri, R.; Lechthaler, M.; Polcik, P.; Mitterer, C. Influence of phase transition on the tribological performance of arc-evaporated AlCrVN hard coatings. *Surf. Coat. Technol.* **2009**, *203*, 1101–1105. [[CrossRef](#)]

120. Fateh, N.; Fontalvo, G.; Gassner, G.; Mitterer, C. Influence of high-temperature oxide formation on the tribological behaviour of TiN and VN coatings. *Wear* **2007**, *262*, 1152–1158. [[CrossRef](#)]
121. Wang, Y.; Lee, J.-W.; Duh, J.-G. Mechanical strengthening in self-lubricating CrAlN/VN multilayer coatings for improved high-temperature tribological characteristics. *Surf. Coat. Technol.* **2016**, *303*, 12–17. [[CrossRef](#)]
122. Fateh, N.; Fontalvo, G.A.; Gassner, G.; Mitterer, C. The Beneficial Effect of High-Temperature Oxidation on the Tribological Behaviour of V and VN Coatings. *Tribol. Lett.* **2007**, *28*, 1–7. [[CrossRef](#)]
123. Kamath, G.; Ehiasarian, A.; Purandare, Y.; Hovsepian, P. Tribological and oxidation behaviour of TiAlCN/VCN nanoscale multilayer coating deposited by the combined HIPIMS/(HIPIMS-UBM) technique. *Surf. Coat. Technol.* **2011**, *205*, 2823–2829. [[CrossRef](#)]
124. Wang, J.Y.; Shan, Y.; Guo, H.; Li, B.; Wang, W.; Jia, J. Friction and wear characteristics of Hot-pressed NiCr–Mo/MoO₃/Ag self-lubrication composites at elevated temperatures up to 900 °C. *Tribol. Lett.* **2015**, *59*, 1–16. [[CrossRef](#)]
125. Liu, E.-Y.; Wang, W.-Z.; Gao, Y.-M.; Jia, J.-H. Tribological Properties of Adaptive Ni-Based Composites with Addition of Lubricious Ag₂MoO₄ at Elevated Temperatures. *Tribol. Lett.* **2012**, *47*, 21–30. [[CrossRef](#)]
126. Liu, E.; Bai, Y.; Gao, Y.; Yi, G.; Jia, J. Tribological properties of NiAl-based composites containing Ag₃VO₄ nanoparticles at elevated temperatures. *Tribol. Int.* **2014**, *80*, 25–33. [[CrossRef](#)]
127. Liu, E.; Gao, Y.; Bai, Y.; Yi, G.; Wang, W.; Zeng, Z.; Jia, J. Tribological properties of self-lubricating NiAl/Mo-based composites containing AgVO₃ nanowires. *Mater. Charact.* **2014**, *97*, 116–124. [[CrossRef](#)]
128. Rajeswari, K.; Hareesh, U.; Subasri, R.; Chakravarty, D.; Johnson, R. Comparative evaluation of spark plasma (SPS), microwave (MWS), two stage sintering (TSS) and conventional sintering (CRH) on the densification and micro structural evolution of fully stabilized zirconia ceramics. *Sci. Sinter.* **2010**, *42*, 259–267. [[CrossRef](#)]
129. Reichardt, A.; Shapiro, A.A.; Otis, R.; Dillon, R.P.; Borgonia, J.P.; McEnerney, B.W.; Hosemann, P.; Beese, A.M. Advances in additive manufacturing of metal-based functionally graded materials. *Int. Mater. Rev.* **2020**, *66*, 1–29. [[CrossRef](#)]
130. Gladman, A.S.; Matsumoto, E.A.; Nuzzo, R.G.; Mahadevan, L.; Lewis, J.A. Biomimetic 4D printing. *Nat. Mater.* **2016**, *15*, 413–418. [[CrossRef](#)]
131. Yu, G.; Tian, P.; Ren, K.; Wu, W.; Zhang, Z.; Gong, Z.; Zhang, J. Effects of water molecules on the formation of transfer films and the occurrence of superlow friction. *Ceram. Int.* **2021**, *47*, 21325–21333. [[CrossRef](#)]
132. Bhowmick, S.; Shirzadian, S.; Alpas, A.T. High-temperature tribological behavior of Ti containing diamond-like carbon coatings with emphasis on running-in coefficient of friction. *Surf. Coat. Technol.* **2021**, *431*, 127995. [[CrossRef](#)]
133. Bhaumik, S.; Pathak, S.; Dey, S.; Datta, S. Artificial intelligence based design of multiple friction modifiers dispersed castor oil and evaluating its tribological properties. *Tribol. Int.* **2019**, *140*, 105813. [[CrossRef](#)]
134. Rosenkranz, A.; Costa, H.L.; Baykara, M.Z.; Martini, A. Synergetic effects of surface texturing and solid lubricants to tailor friction and wear—A review. *Tribol. Int.* **2021**, *155*, 106792. [[CrossRef](#)]
135. Kumar, R.; Antonov, M.; Klimczyk, P.; Mikli, V.; Gomon, D. Effect of cBN content and additives on sliding and surface fatigue wear of spark plasma sintered Al₂O₃-cBN composites. *Wear* **2022**, *494–495*, 204250. [[CrossRef](#)]
136. Rosenkranz, A.; Marian, M.; Profito, F.J.; Aragon, N.; Shah, R. The Use of Artificial Intelligence in Tribology—A Perspective. *Lubricants* **2021**, *9*, 2. [[CrossRef](#)]
137. Gong, H.; Yu, C.; Zhang, L.; Xie, G.; Guo, D.; Luo, J. Intelligent lubricating materials: A review. *Compos. Part B Eng.* **2020**, *202*, 108450. [[CrossRef](#)]

Curriculum vitae

Personal data

Name: Rahul Kumar
Date of birth: 13 September 1993
Place of birth: India
Citizenship: India

Contact data

E-mail: rahul.kumar@taltech.ee; rahulkumar0167@gmail.com

Education

2018–2022 Tallinn University of Technology – PhD
2015–2017 Manipal University – MSc
2010–2014 Manipal University – BSc

Language competence

Hindi Native
English Fluent
German Basic

Professional employment

2022– Early stage researcher, Tallinn University of Technology, Estonia
2017–2018 Lecturer, AKTU, India
2016–2017 Project assistant, Laser additive manufacturing, RRCAT, Department of Atomic Energy, India
2014–2015 Service engineer, Honda Cars India Ltd, India

Projects

ETAG 4-8/22/15 M-ERA.NET “High performance duplex ceramics for efficient machining of nickel superalloys (DuplexCER)”, Maksim Antonov; Tallinn University of Technology, School of Engineering, Department of Mechanical and Industrial Engineering.

PRG 643 “Bio-replicating Engineering Structures for Tribo-applications (BEST)” (1.01.2020–31.12.2024), Irina Hussainova; Tallinn University of Technology, School of Engineering, Department of Mechanical and Industrial Engineering.

COMET-Program InTribology, FFG-No. 872176 (05.05.2021–31.03.2022), AC2T research GmbH, Austria.

MOBERA18 “Self-lubrication systems for high-temperature tribo-applications (HOTselflub)” (1.09.2019–31.08.2021), Irina Hussainova; Tallinn University of Technology, School of Engineering, Department of Mechanical and Industrial Engineering.

ETAG18012 “Durable ceramic composites with superhard particles for wear-resistant cutting tools (DuraCER)” (1.09.2018–31.08.2021), Maksim Antonov; Tallinn University of Technology, School of Engineering, Department of Mechanical and Industrial Engineering.

Research visits

Sep. 2019 Institute of Advanced Manufacturing Technology, Łukasiewicz Research Network – Krakow Institute of Technology, Poland.

Jan.–May 2021 Austrian Center of Competence for Tribology (AC2T research), Austria.

Conference presentations

11th International Conference on the Science of Hard Materials (ICSHM11) 2019, Khao Lak, Thailand.

Modern Materials and Manufacturing (MMM) 2019, Tallinn, Estonia.

46th Leeds-Lyon Symposium on Tribology 2019, Lyon, France, 2019.

Modern Materials and Manufacturing (MMM) 2021, Tallinn, Estonia.

23rd International Conference on Wear of Materials (WOM) 2021, Online.

Nordic Tribology Symposium (NORDTRIB) 2022, Alesund, Norway.

5th Young Tribological Researcher Symposium (YTRS), Karlsruhe, Germany, (Received Full-funding by German Society of Tribology -GfT).

Elulookirjeldus

Isikuandmed

Nimi: Rahul Kumar
Sünniaeg: 13 September 1993
Sünnikoht: India Vabariik
Kodakondsus: India

Kontaktandmed

E-post: rahul.kumar@taltech.ee; rahulkumar0167@gmail.com

Hariduskäik

2018–2022 Tallinna Tehnikaülikool – PhD
2015–2017 Manipal University – MSc
2010–2014 Manipal University – BSc

Keelteoskus

Hindi keel Emakeel
Inglise keel Kõrgtase
Saksa Algtase

Teenistuskäik

2022 – Noorteadur, Tallinna Tehnikaülikool, Eesti
2017–2018 Lektor, AKTU, India
2016–2017 Projektiassistent, 3D printimine, RRCAT, Department of Atomic Energy, India
2014–2015 Teenindusinsener, Honda Cars India Ltd, India

Projektid

ETAG 4-8/22/15 M-ERA.NET “High performance duplex ceramics for efficient machining of nickel superalloys (DuplexCER)”, Maksim Antonov; Tallinna Tehnikaülikool.

PRG 643 “Bio-replicating Engineering Structures for Tribo-applications (BEST)” (1.01.2020–31.12.2024), Irina Hussainova; Tallinna Tehnikaülikool.

COMET-Program InTribology, FFG-No. 872176 (05.05.2021–31.03.2022), AC2T research GmbH, Austria.

MOBERA18 “Self-lubrication systems for high-temperature tribo-applications (HOTselflub)” (1.09.2019–31.08.2021), Irina Hussainova; Tallinna Tehnikaülikool.

ETAG18012 “Durable ceramic composites with superhard particles for wear-resistant cutting tools (DuraCER)” (1.09.2018–31.08.2021), Maksim Antonov; Tallinna Tehnikaülikool.

Teadustöö välismaal

September 2019 Institute of Advanced Manufacturing Technology, Łukasiewicz Research Network – Krakow Institute of Technology, Poland.

Jaanuar–Mai 2021 Austrian Center of Competence for Tribology (AC2T research), Austria.

Esinemine konverentsidel

11th International Conference on the Science of Hard Materials (ICSHM11) 2019, Tai.

Modern Materials and Manufacturing (MMM) 2019, Eesti.

46th Leeds-Lyon Symposium on Tribology 2019, Prantsusmaa.

Modern Materials and Manufacturing (MMM) 2021, Eesti.

23rd International Conference on Wear of Materials (WOM) 2021, veebikonverents.

Nordic Tribology Symposium (NORDTRIB) 2022, Norra.

5th Young Tribological Researcher Symposium (YTRS), Saksamaa (toetus: German Society of Tribology -GfT).

ISSN 2585-6901 (PDF)
ISBN 978-9949-83-936-0 (PDF)